INSTITUTE OF SEISMOLOGY
UNIVERSITY OF HELSINKI
REPORT S-71

LITHOSPHERE 2021

ELEVENTH SYMPOSIUM ON STRUCTURE, COMPOSITION AND EVOLUTION OF THE LITHOSPHERE

PROGRAMME AND EXTENDED ABSTRACTS

Edited by

Ilmo Kukkonen, Toni Veikkolainen, Suvi Heinonen, Fredrik Karell, Elena Kozlovskaya, Arto Luttinen, Kaisa Nikkilä, Vesa Nykänen, Markku Poutanen, Pietari Skyttä, Eija Tanskanen and Timo Tiira

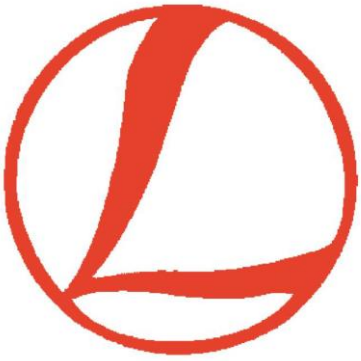

Virtual Meeting
January 19 – 20, 2021

Series Editor-in-Chief: Timo Tiira

Guest Editors: Ilmo Kukkonen, Toni Veikkolainen, Suvi Heinonen, Fredrik Karell, Elena Kozlovskaya, Arto Luttinen, Kaisa Nikkilä, Vesa Nykänen, Markku Poutanen, Pietari Skyttä, Eija Tanskanen and Timo Tiira

Publisher: Institute of Seismology
P.O. Box 68
FI-00014 University of Helsinki
Finland
Phone: +358-294-1911 (switchboard)
http://www.helsinki.fi/geo/seismo/

ISSN 0357-3060
Helsinki 2021
ISBN 978-952-10-9604-4 (pdf)

LITHOSPHERE 2021

ELEVENTH SYMPOSIUM ON STRUCTURE, COMPOSITION AND EVOLUTION OF THE LITHOSPHERE

PROGRAMME AND EXTENDED ABSTRACTS

Virtual meeting
January 19 – 20, 2021

CONTRIBUTING ORGANIZATIONS

Finnish National Committee of the International Lithosphere Programme (ILP)
Aalto University
Geological Survey of Finland (GTK)
National Land Survey of Finland, Finnish Geospatial Research Institute (FGI)
University of Helsinki
University of Turku
University of Oulu
Åbo Akademi University

ORGANIZING COMMITTEE AND EDITORS

Ilmo Kukkonen	University of Helsinki (ilmo.kukkonen@helsinki.fi)
Toni Veikkolainen	University of Helsinki (toni.veikkolainen@helsinki.fi)
Suvi Heinonen	Geological Survey of Finland (suvi.heinonen@gtk.fi)
Fredrik Karell	Geological Survey of Finland (fredrik.karell@gtk.fi)
Elena Kozlovskaya	University of Oulu (elena.kozlovskaya@oulu.fi)
Arto Luttinen	University of Helsinki (arto.luttinen@helsinki.fi)
Kaisa Nikkilä	Åbo Akademi University (kaisa.nikkila@abo.fi)
Vesa Nykänen	Geological Survey of Finland (vesa.nykanen@gtk.fi)
Markku Poutanen	Finnish Geospatial Research Institute FGI (markku.poutanen@nls.fi)
Pietari Skyttä	University of Turku (pimisk@utu.fi)
Eija Tanskanen	University of Oulu (eija.tanskanen@oulu.fi)
Timo Tiira	University of Helsinki (timo.tiira@helsinki.fi)

References of Lithosphere Symposia Publications

Pesonen, L.J., Korja, A. and Hjelt, S.-E., 2000 (Eds.). Lithosphere 2000 - A Symposium on the Structure, Composition and Evolution of the Lithosphere in Finland. Programme and Extended Abstracts, Espoo, Finland, October 4-5, 2000. Institute of Seismology, University of Helsinki, Report S-41, 192 pages.

Lahtinen, R., Korja, A., Arhe, K., Eklund, O., Hjelt, S.-E. and Pesonen, L.J., 2002 (Eds.). Lithosphere 2002 – Second Symposium on the Structure, Composition and Evolution of the Lithosphere in Finland. Programme and Extended Abstracts, Espoo, Finland, November 12-13, 2002. Institute of Seismology, University of Helsinki, Report S-42, 146 pages.

Ehlers, C., Korja A., Kruuna, A., Lahtinen, R. and Pesonen, L.J., 2004 (Eds.). Lithosphere 2004 – Third Symposium on the Structure, Composition and Evolution of the Lithosphere in Finland. Programme and Extended Abstracts, November 10-11, 2004, Turku, Finland. Institute of Seismology, University of Helsinki, Report S-45, 131 pages.

Kukkonen, I.T., Eklund, O., Korja, A., Korja, T., Pesonen, L.J. and Poutanen, M., 2006 (Eds.). Lithosphere 2006 – Fourth Symposium on the Structure, Composition and Evolution of the Lithosphere in Finland. Programme and Extended Abstracts, Espoo, Finland, November 9-10, 2006. Institute of Seismology, University of Helsinki, Report S-46, 233 pages.

Korja, T., Arhe, K., Kaikkonen, P., Korja, A., Lahtinen, R. and Lunkka, J.P., 2008 (Eds.). Lithosphere 2008 – Fifth Symposium on the Structure, Composition and Evolution of the Lithosphere in Finland. Programme and Extended Abstracts, Oulu, Finland, November 5-6, 2008. Institute of Seismology, University of Helsinki, Report S-53, 132 pages.

Heikkinen, P., Arhe, K., Korja, T., Lahtinen, R., Pesonen, L.J. and Rämö, T., 2010 (Eds.). Lithosphere 2010 – Sixth Symposium on the Structure, Composition and Evolution of the Lithosphere in Finland. Programme and Extended Abstracts, Helsinki, Finland, October 27-28, 2010. Institute of Seismology, University of Helsinki, Report S-55, 154 pages.

Kukkonen, I.T., Kosonen, E., Oinonen, K., Eklund, O., Korja, A., Korja, T., Lahtinen, R., Lunkka, J.P. and Poutanen, M., 2012 (Eds.). Lithosphere 2012 – Seventh Symposium on the Structure, Composition and Evolution of the Lithosphere in Finland. Programme and Extended Abstracts, Espoo, Finland, November 6-8, 2012. Institute of Seismology, University of Helsinki, University of Helsinki, S-56, 116 pages.

Eklund, O., Kukkonen, I.T., Skyttä, P., Sonck-Koota, P., Väisänen, M. and Whipp, D., 2014 (Eds.). Lithosphere 2014 – Eighth Symposium on the Structure, Composition and Evolution of the Lithosphere in Finland. Programme and Extended Abstracts, Turku, Finland, November 4-6, 2014. Institute of Seismology, University of Helsinki, S-62, 126 pages.

Kukkonen, I.T., Heinonen, S., Oinonen, K., Arhe, K., Eklund, O., Karell, F., Kozlovskaya, E., Luttinen, A., Lahtinen, R., Lunkka, J., Nykänen, V., Poutanen, M., Tanskanen, E. and Tiira T. (Eds.), 2016. Lithosphere 2016 – Ninth Symposium on the Structure, Composition and Evolution of the Lithosphere in Finland. Programme and Extended Abstracts, Espoo, Finland, November 9-11, 2016. Institute of Seismology, University of Helsinki, Report S-65, 156 pages.

Kukkonen, I.T., Heinonen, S., Silvennoinen, H., Karell, Kozlovskaya, E., Luttinen, A., Nikkilä, K., Nykänen, V., Poutanen, M., Skyttä, P., Tanskanen, E., Tiira, T. and Oinonen, K. (Eds.), 2018. Lithosphere 2018 – Tenth Symposium on the Structure, Composition and Evolution of the Lithosphere. Programme and Extended Abstracts, Oulu, Finland, November 14-16, 2018. Institute of Seismology, University of Helsinki, Report S-67, 134 pages.

Kukkonen, I.T., Veikkolainen, T., Heinonen, S., Karell, F., Kozlovskaya, E., Luttinen, A., Nikkilä, K., Nykänen, V., Poutanen, M., Skyttä, P., Tanskanen, E. and Tiira, T. (Eds.), 2021. Lithosphere 2021 – Eleventh Symposium on the Structure, Composition and Evolution of the Lithosphere in Finland. Programme and Extended Abstracts, January 19-20, 2021. Institute of Seismology, University of Helsinki, Report S-71, 164 pages (pdf).

Keywords (GeoRef Thesaurus, AGI): lithosphere, crust, upper mantle, Fennoscandia, Finland, Precambrian, Baltic Shield, symposia

TABLE OF CONTENTS

PREFACE

The Finnish National committee of the International Lithosphere Programme (ILP) organises every second year the LITHOSPHERE symposium, which provides a forum for lithosphere researchers to present results and reviews as well as to inspire interdisciplinary discussions. The tradition was disturbed by the Covid-19 pandemic, and the 2020 meeting was shifted to 2021. Regardless of the exceptional circumstances the symposium provides a wide selection of geological and geophysical presentations. The eleventh symposium – LITHOSPHERE 2021 – comprises 44 presentations. The extended abstracts (in this volume) provide a good overview on current research on structure and processes of solid Earth.

The two-day symposium takes place completely in the internet as a virtual meeting during January 19 – 20, 2021. The participants will present their results in oral and poster sessions. Posters prepared by graduate and postgraduate students will be evaluated and the best one will be awarded. Research Professor Peter M. Malin, Duke University, USA, will give the invited talk.

This special volume ***"LITHOSPHERE 2021"*** contains the programme and extended abstracts of the symposium in alphabetical order.

Helsinki, January 13, 2021

Ilmo Kukkonen, Toni Veikkolainen, Suvi Heinonen, Hanna Silvennoinen, Fredrik Karell, Elena Kozlovskaya, Arto Luttinen, Kaisa Nikkilä, Vesa Nykänen, Markku Poutanen, Pietari Skyttä, Eija Tanskanen, and Timo Tiira

Lithosphere 2021 Organizing Committee

LITHOSPHERE 2021 Symposium
Programme

Tuesday, Jan 19

(All times are Helsinki time, EET = GMT+2 h)
10:00 - 10:05 Opening: I. Kukkonen, Chair of the Finnish National ILP Committee
10:05 – 10:10 Address: H. Thybo, President of the International Lithosphere Program

10:10- 12:10 Session 1: Lithosphere structure and evolution from upper crust to asthenosphere
Chair: I. Kukkonen

10:10 - 1030 **F. Chopin, A. Korja, K. Nikkilä, P. Hölttä, T. Korja, M.A. Zaher, M. Kurhila, O. Eklund, O.T. Rämö, Y. Lalaye, H. O'Brien and M. Sayab**: The Vaasa migmatitic complex: new results and perspectives for the tectonic evolution of the Svecofennian orogeny

10:30 – 10:50 **K. Nikkilä, P. Skyttä, A. Saukko and O. Eklund**: Structural evolution and melt formation within the southernmost Finland migmatitic belt

10:50 – 11:10 **A. Saukko, K. Nikkilä, O. Eklund and M. Väisänen**: Granites of southernmost Finland

11:10 – 11:30 **M. Nilov, L. Bakunovich, N. Sharov and B. Belashev**: Magnetic inhomogeneities of the White Sea region crust

11:30 – 11:50 **T. Veikkolainen, T. Luhta and I.T. Kukkonen**: Modelling geotherms of the Wiborg rapakivi batholith in southeastern Finland in light of seismic data

11:50 – 12:10 **A.A. Lebedev, and N.V. Sharov:** Natural seismicity in Russian Karelia

12:10 - 13:00 Lunch break

13:00-14:20 Session 2: Lithosphere structure and evolution from upper crust to asthenosphere (cont.)
Chair: E. Kozlovskaya

13:00 – 13:20 **T. Karinen, S. Heinonen, J. Konnunaho, H. Salmirinne, I. Lahti, I. and A. Salo**: Koillismaa Deep Hole – solving the mystery of a geophysical anomaly

13:20 – 13.40 **O. Kaisko and M. Malm**: Micro earthquakes at the Olkiluoto nuclear fuel final disposal facility construction site in 2002-2018

13:40 – 14:00 **Y. Wang and D. Whipp**: Numerical modelling of oblique subduction in the Southern Andes region

14:00 – 14:20 **I.A. Yacouba and V.N. Glaznev**: The thickness of the Earth's crust in the territory of Republic of the Niger according to the stochastic interpretation of the gravity field

14:20 - 14:40 Coffee/Tea break

14:40 – 15:20 **Poster session 1** (Posters 1-6)
Chair: F. Karell

P01. L. Ylä-Mella, I. Kukkonen and D. Whipp: Forward and inverse modelling of terrestrial cosmogenic nuclides to detect past glaciations

P02. I.A. Ponomarenko and O.M. Muravina: Application of the Group Method of Data Handling for the analysis of petrophysical and geophysical data

P03. J. Nevalainen, J-P. Ranta, E. Kozlovskaya, M. Kirsch, L. Ajjabou and R. Gloaguen: Non-invasive Exploration technologies in the INFACT project: Examples from the reference sites

P04. T.-C. Lin, G. Hillers, S.-J. Lee and S.-H. Hung: Imaging the Internal Structure along the Longitudinal Valley Fault System, Taiwan, Using Fault Zone Head Waves

P05. M. Holma, P. Kuusiniemi and K. Loo: An introduction to principles of muography in continental scientific boreholes

P06. E. Lehtonen: Geology field in The Helsinki Term Bank for The Arts and Sciences (Tieteen termipankki)

P07. V. Järvinen, T. Halkoaho, J. Konnunaho, J.S. Heinonen and O.T. Rämö: Sm-Nd isotope systematics of the Precambrian mafic-ultramafic Näränkävaara intrusion.

15:20 – 16:20 Session 3: Lithosphere evolution, structures and mineral resources
Chair: E. Tanskanen

15:20 – 15:40 **V. J. Virtanen, J. S. Heinonen, N. Barber and F. Molnár**: The effects of assimilation on sulfide saturation and the formation of norite-hosted Cu-Ni deposits in the Duluth Complex, Minnesota

15:40 – 16:00 **M. Vasilopoulos, F. Molnár, H. O'Brien and Y. Lahaye**: Comparing geochemical characteristics of a gold-only and a base metal-rich orogenic mineralization from the Central Lapland Greenstone Belt, northern Finland

16:00 – 16:20 **L. Paolillo and C. Giapis**: A preliminary assessment of hydrothermal alterations in the giant Kiruna IOA deposit, Kiruna, Sweden

16:20 – 16:40 **R. Latypov, J. S. Heinonen and S. Chistyakova**: Thermodynamic constraints on assimilation of floor cumulates by superheated basaltic-andesitic melts in the Bushveld Complex, South Africa

16:20 – 17:20 **KEYNOTE TALK**: **P.M. Malin**: The Geocritical-Rock Physics and Fracture-Seismic Mapping of Permeability in the Brittle Lithosphere

Wednesday, Jan 20

09:00-10:20 Session 4: Archaean and Proterozoic lithosphere structure and evolution
Chair: S. Heinonen

9:00 – 9:20 **K. Kärenlampi, A. Kontinen, V. Kylli and Y. Lahaye**: Conglomeratic rocks fringing the Archean Iisalmi block in central Finland: Evidence for the timing and nature of the break-up of the Karelia craton

9:20 – 9:40 **S. Hietala, A. M. Hall, N. Putkinen, E. Lindsberg and M. Holma**: Impact structures as indicators of cratonic denudation

9:40 – 10:00 **S.I. Berezneva, O. M. Muravina, and T.A. Voronova**: Technology for studying the structure of the upper crust of the Voronezh Crystalline Massif by detailed density modeling data

10:00 – 10:20 **L. Bakunovich, B. Belashev, N. Sharov and M. Nilov**: Modeling the structure of the Earth's crust of the White Sea region

10:20 – 10:40 Coffee/tea break

10:40 – 12:00 **Session 6: Induced seismicity, geothermal energy**
Chair: M. Poutanen

10:40 – 11:00 **M. Holma and P. Kuusiniemi:** Cosmic-ray based geothermal exploration – A short introduction to muography

11:00 – 11:20 **G. Taylor, G. Hillers and T. A.T. Vuorinen**: Array-derived rotational motion of induced earthquakes

11:20 – 11:40 **I.T. Kukkonen, M. Pentti and P.J. Heikkinen**: St1 Deep Heat Project: Hydraulic stimulation at 5 – 6 km depth in crystalline rock

11:40 – 12:00 **A.E. Rintamäki, G. Hillers, T.A.T. Vuorinen, K. Galvin, J. Keskinen, T.-C. Lin, T. Luhta, T. Oksanen, J. Pownall, P. Seipäjärvi, G. Taylor, C. Tsarsitalidou, A. Voutilainen and D. Whipp**: A network to study the induced seismicity related to the Otaniemi deep geothermal power plant

12:00 - 12:40 Lunch break

12:40 – 13:20 **Poster session 2** (Posters 7-13)
Chair: K. Nikkilä

P08. A.A. Lebedev and I.A. Zueva: Features of explosive seismicity in the Kostomuksha ore region

P09. N. Afonin, E. Kozlovskaya and J. Okkonen: Frost quakes in northern Finland: possible source mechanisms and formation process

P10. C. Tsarsitalidou, B. Giammarinaro, G. Hillers, P. Boué and L. Stehly: Seismic surface wave focal spot imaging

P11. A.M. Rantanen, D.M. Whipp, J.S. Heinonen, L. Kaislaniemi and M. Putz: Influence of Pulsed Magmatic Activity, Latent Heat, and Partial Melting on the Strength of the Continental Crust

P12. A. Korja, N. Junno and SEISMIC RISK Working Group: SEISMIC RISK – Mitigation of induced seismic risk in urban environments

P13. M. Holma, T. Arola and P. Kuusiniemi: Finnish crustal-scale faults as a possible source of deep low-enthalpy geothermal resources

P14. T. Vehkamäki, M. Väisänen, M. Kurhila, H. O'Brien, P. Hölttä and J.-K. Syrjänen: Metamorphic zones in SW Finland: monazite and zircon U-Pb dating of leucosomes in paragneisses

13:20 – 13:30 Coffee/Tea break

13:30 – 15:20 **Session 7: Crustal structures and mineral resources**
Chair: P. Skyttä

13:30 – 13:50 **M. Etienne, I. Bacquet, D. Monteith and L.S. Lauri**: The iron oxide mineralised Matojärvi formation, Kiruna, Sweden

13:50 – 14:10 **M. Väisänen, J. Kara, H. Penttinen, Y. Lahaye, H. O'Brien and P. Skyttä**: U-Pb zircon dating of igneous rocks in the Salo area, SW Finland

14:10 – 14:30 **O. Eklund and K. Nikkilä**: Biotite as a petrogenetic tool in granite-migmatite areas

14:30 – 14:50 **S. Karvinen, A. Heinonen and C. Beier**: The trace element composition of magmatic apatite: Mineralogical and geological controls on apatite trace element chemistry in magmatic systems

14:50 – 15:10 **R. Fred, A. Heinonen and J.S. Heinonen**: Fractional crystallization of massif-type anorthosite parental magmas and equilibrium crystallization of monzodioritic residual magmas

15:10 – 15:30 **M.A. Aaltonen, C. Beier, A. Abersteiner, and A.P. Heinonen**: Trace element and platinum group element distribution in chromites: constraints on mineral chemical tracers in mafic-ultramafic host lithologies

15.30 – 15:50 Coffee/Tea break

15:50 – 16:30 Session 9: Short communications
Chair: I. Kukkonen

15:50-16:00 **A. Korja, K. Atakan, P.H. Voss, M. Roth, K. Vogfjord, E. Kozlovskaya, E.I. Tanskanen, N. Junno and Nordic EPOS Working Group:** Nordic EPOS - A FAIR Nordic EPOS Data Hub

16:00-16:10 **A. Korja, M. Poutanen, S. Mertanen, E. Kozlovskaya, T. Fordell, J. Leveinen, A. Viljanen, A. Pursula, N. Junno and FIN-EPOS Working Group:** FIN-EPOS – Finnish national node of the European Plate Observing System

16:10 – 16:20 **M. Poutanen:** United Nations and Subcommittee on Geodesy

16:20 – 16:30 **E.I. Tanskanen, J. Tammi, J. Pulliainen, H. Koivula and E2S team:** Earth-Space Research Ecosystem: scientific and industry collaboration platform

16:30 – 16:45 **Concluding remarks and poster award**

16:45 Closing of the Symposium

EXTENDED ABSTRACTS

The publication is electronically available at https://www.seismo.helsinki.fi/ilp/lito2021/.

Trace element and Platinum Group Element distribution in chromites: constraints on mineral chemical tracers in mafic-ultramafic host lithologies

M.A. Aaltonen[1], C. Beier[1], A. Abersteiner[1] and A.P. Heinonen[1]

[1]Department of Geosciences and Geography, University of Helsinki, Helsinki, Finland
E-mail: milla.aaltonen@helsinki.fi

The compositional heterogeneity of chromites in mafic-ultramafic lithologies can be used as a multifunctional petrological tool in geosciences for determining the formation and modification of ore-forming lithologies. The formation of immiscible sulfide melts, i.e. sulfide-saturation, can potentially be identified using the PGE contents in chromite grains. In this project, we investigate the distribution of trace elements in chromites through *in situ* analyses of six chromite-bearing Finnish samples from mineralized and barren lithologies. Our preliminary data show that trace elements can be sufficiently used to distinguish between primary magmatic, as well as secondary, metamorphic processes. Our new results imply that a careful consideration of the trace element distribution in chromites may make them a suitable lithochemical tracer in prospecting Ni-Cu-PGE deposits.

Keywords: Chromite, mineral chemistry, indicator mineral, sulfide saturation

1. Introduction

Igneous ore-forming processes leave unique geochemical fingerprints in the crystallizing minerals, however, distinguishing between primary magmatic and secondary, metamorphic processes remains challenging. Indicator minerals can be used as lithochemical tracers in ore deposit exploration to track and estimate the mineralization potential. Ideally, an indicator mineral is abundant across a range of compositions and is relatively resistant to alteration and weathering.

Chromite *sensu lato* is a common mineral in mafic-ultramafic rocks derived from the upper mantle (Barnes and Roeder 2001) and is often associated with Ni-Cu-PGE deposits (Papp and Lipin 2010). Compared to common primary silicates in mafic lithologies (e.g., olivine and pyroxenes) (Barnes and Roeder 2001), chromite is relatively resistant to alteration and may thus preserve the primary magmatic mineral chemistry.

Previous studies suggest that the mineral chemistry of chromites can give insights to sulfide saturation of the host magma (Fiorentini et al. 2008). Platinum group elements (PGEs; Ru, Rh, Pd, Os, Ir, and Pt) are strongly chalcophile elements and thus partition to the sulfide liquid, leaving the residual melt relatively depleted in PGEs. However, PGEs can also behave as siderophile elements in sulfide-undersaturated conditions, where Ru is compatible in chromite (Fiorentini et al. 2008). Fiorentini et al. (2008) suggested that Ru concentration in chromites could be used as a fingerprinting element to identify sulfide saturation processes in komatiitic systems. However, only a few studies have systematically investigated the mineral-scale chemical heterogeneity of trace elements (Ti, V, Mn, Co, Ni, Zn, Ru) in altered and unaltered chromites (e.g., Mukherjee et al. 2015).

This project is designed to systematically describe and analyze *in situ* core to rim profiles of the major and trace elements, including PGEs, in both unaltered and altered chromites from a range of geodynamic environments. We use existing samples from mineralized and barren lithologies to constrain how the mineral chemistry of chromites reflects the changes from

sulfide-undersaturated to sulfide-oversaturated conditions in crystal-, outcrop- and regional scale, as well as between ophiolites and greenstone belts.

2. Preliminary results

Six Finnish chromite-bearing samples from mafic-ultramafic lithologies were selected for *in situ* analyses. They cover a range of compositions from komatiitic chromites from the Archean Vaara and Kauniinlampi cumulate lenses in the Suomussalmi greenstone belt, chromite seams from the Kellojärvi ultramafic complex belonging to the Archean Kuhmo greenstone belt and chromitites from the ophiolite-related Pitkänperä and Vasarakangas localities. Samples from the greenstone belts and ophiolites represent the mineralized and barren lithologies, respectively. Representative grains of visibly zoned and unzoned chromites (Figure 1) were analyzed by quantitative high precision laser ablation inductively coupled mass spectrometry (LA-ICP-MS) at the Department of Geosciences and Geography, University of Helsinki. The following dataset has not yet been standardized with external major element data.

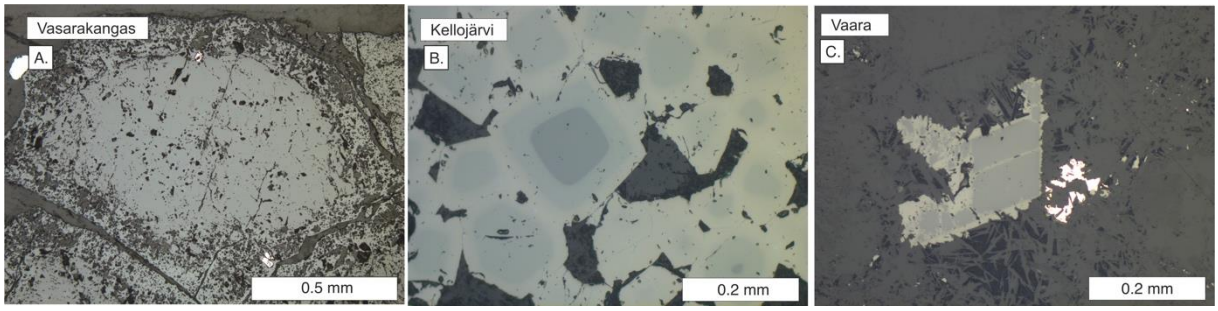

Figure 1. Chromite grains from the Finnish ophiolite related podiform chromitite (A) and greenstone belts (B and C) under reflected light. A. Brecciated chromitite from the Vasarakangas ophiolite fragment. B. Zoned chromites from Kellojärvi within the Kuhmo greenstone belt. C. Disseminated chromite from Vaara in the Suomussalmi greenstone belt.

The preliminary LA-ICP-MS results (n=145) show a clear chemical distinction both between chromites from greenstone belt and ophiolite lithologies, and between mineral cores and rims (Figures 2 and 3). The Pitkänperä and Vasarakangas ophiolite chromitites have distinctly higher Mg# [Mg/(Mg+Fe)] and lower Cr# [Cr/(Cr+Al)], Zn/Al, Ru/Al, and Mn/Al (Figures 2 and 3) compared to the greenstone belt chromites from Vaara, Kauniinlampi, and Kellojärvi. The Kauniinlampi, Kellojärvi, and Vasarakangas chromites display a systematic core-to-rim variation in Cr# and Mg#, whereas the Vaara chromites have a more scattered distribution and variation mainly in Mg# (Figure 2). Generally, the rims of the greenstone chromites show an increase in Mn/Al, V/Al, Zn/Al, and Ru/Al relative to the cores (Figure 3).

3. Discussion and proceedings

The correlations of Cr# and Mg# in individual grains from the Kauniinlampi, Kellojärvi, and Vasarakangas chromites (Figure 2) indicate normal zoning caused by fractional crystallization (Mukherjee et al. 2015). A correlation of Mn/Al, V/Al, Ru/Al, and Zn/(Al, Ti) implies that fluids may have variably influenced the composition of the chromites. However, the cores have maintained the original magmatic composition, at least partially, whilst the rims display a

systematic and stronger elemental exchange. Our preliminary findings indicate that the cores of the highly metamorphosed Finnish chromites can be used to decipher the igneous

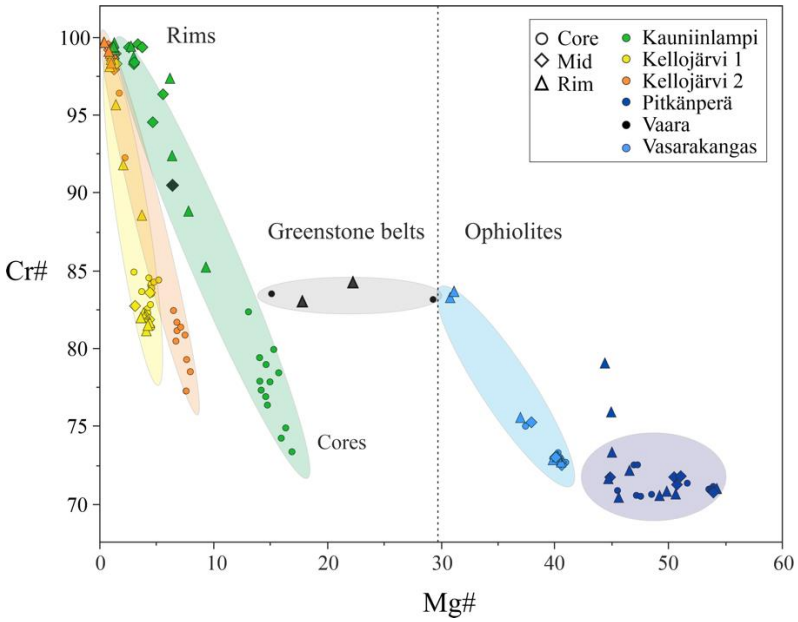

Figure 2. The calculated Mg# [Mg/(Mg+Fe)] and Cr# [Cr/(Cr+Al)] of the chromite grains from the Finnish greenstone belts (Vaara, Kauniinlampi, and Kellojärvi) and ophiolite samples (Pitkänperä and Vasarakangas).

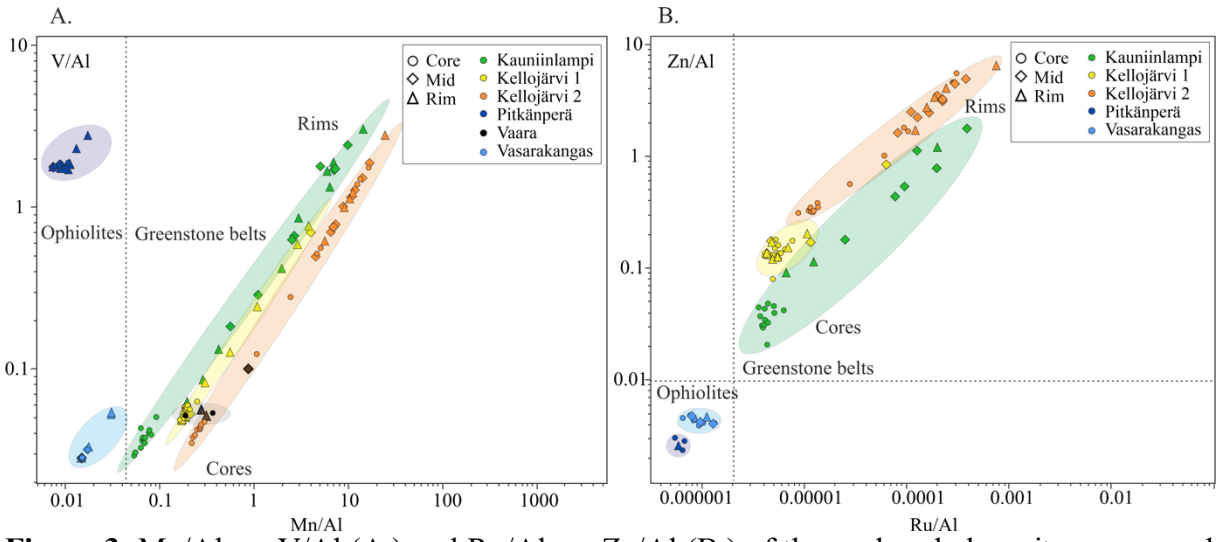

Figure 3. Mn/Al vs. V/Al (A.) and Ru/Al vs. Zn/Al (B.) of the analysed chromites expressed in logarithmic scale. The measured chromites are from the Pitkänperä and Vasarakangas ophiolites and Vaara, Kauniinlampi, and Kellojärvi greenstone belt samples. Ruthenium contents of the Vaara sample chromites are all below the limit of detection.

processes of formation whereas chromite rims yield important information related to metamorphism and possibly fluid composition.

Future aims of this study will be to expand the current sample set to cover localities worldwide, including additional chromites from Finnish mineralizations and samples from the Macquarie Island (Southwestern Pacific) and the Troodos ophiolites (Cyprus). The aim is to establish a consistent mineral chemical database of chromites, which will help in identifying potential mineralization and provide information on the magmatic, metamorphic, and hydrothermal evolution involved in Ni-Cu-PGE ore-forming processes. The fundamental application of our project will be to evaluate to which extent chromite can be used as a lithochemical tracer and what influences the compositional variability of chromites on a mineral scale.

References:

Barnes, S.J., Roeder, P.L., 2001. The Range of Spinel Compositions in Terrestrial Mafic and Ultramafic Rocks. Journal of Petrology 42, 2279–2302.

Fiorentini, M.L., Beresford, S.W., Barley, M.E., 2008. Ruthenium-Chromium variation: a new lithochemical tool in the exploration for komatiite-hosted Ni-Cu-(PGE) deposits. Economic Geology 103, 431–437.

Mukherjhee, R., Mondal, S.K., González-Jiménez, J.M., Griffin, W.L., Pearson, N.J., O'Reilly, S.Y., 2015. Trace-element fingerprints of chromite, magnetite and sulfides from the 3.1. Ga ultramafic-mafic rocks of the Nuggihalli greenstone belt, Western Dharwar craton (India). Contributions to Mineralogy and Petrology 169: 59.

Papp, J.F., Lipin, B.R., 2010. Chromium and Chromium Alloys. Kirk-Othmer Encyclopedia of Chemical Technology: 1–47.

Frost quakes in northern Finland: Possible source mechanisms and formation process

N. Afonin[1], E. Kozlovskaya[1] and J. Okkonen[1,2]

[1]Oulu Mining School, POB-3000, FIN-90014, University of Oulu
[2]Geological Survey of Finland, P.O. Box 96, FI-02151, Espoo
E-mail: nikita.afonin@oulu.fi

In our study, we describe results of investigation of source mechanisms and formation process of frost quakes in upper soils. We consider records of frost quake that occurred in Oulu on 06.01.2016 and conclude that the most possible source mechanism of this type of events is vertical fracture opening. Artificial neural network was used to analyse continuous seismic data of OUL station and detect numerous events with the same characteristics during winter, 2015-2016. The number of events per day strongly depends on variations of air temperature. Hydrological model and time series of temperature and snow thickness were used to simulate snow accumulation, melt and soil temperature at different depths beneath the snow pack and to calculate temporal variations in thermal stress in soil. The study shows that frost quakes occur when thermal stress caused by a rapid decrease in temperature exceeds fracture toughness and strength of the soil-ice mixture.

Keywords: frost quakes, upper soils, thermal stress, northern Finland

1. Introduction

Weather extremes such as rapid temperature decrease in combination with thin snow cover can result in cracking of water-saturated soil and rock when water has suddenly frozen and expanded. Such frost quakes (cryoseisms) can be hazardous for industrial and civil objects located in the near-field zone. Monitoring of frost quakes and analysis of weather conditions during which they occur is necessary to access hazard caused by them.

2. Source mechanism and magnitude of frost quake, occurred on 06.01.2016 in Oulu

As a ground-truth frost quake, we consider seismic event in Talvikangas district of Oulu on 06.06.2016 and caused damage to road surface and basements of buildings. Local citizens reported hearing a loud noise and feeling the ground shake prior to observing the ruptures (Laine, 2016). On the same day, the permanent seismic station (OUL) operated by Sodankylä Geophysical Observatory of the University of Oulu and located 14 km from Talvikangas recorded a number of unusual local seismic events, depleted in body wave energy but having large-amplitude Rayleigh waves. Large-amplitude of Rayleigh waves suggest that the seismic source was close to the surface (Aki and Richards, 2002). In the same day, a rapid decrease in air temperature was recorded (FMI, 2020), suggesting that the frost quake activity was initiated by specific weather conditions that potentially can be repeated in the future. The waveform analysis suggests that the most possible source mechanism of the event was vertical fracture opening. The local magnitude M_L = 0.705 was evaluated using equation by Uski and Tuppurainen (1996).

3. Analysis of number of frost quakes using artificial neural network detector

To access characteristics and number of cryoseisms during winter 2015-2016, we used 3-component recordings of a swarm of strong cryoseismic events with similar waveforms that was registered on 06.06.2016 by seismic station OUL. Assuming that all events in the swarm

were caused by the same mechanism (freezing of water-saturated soil), we used them as a learning sample for the neural network. Analysis of these events has shown that most of them have many similarities in selected records characteristics (central frequencies, duration etc.) with the strongest event and with each other. Application of this algorithm to the continuous seismic data recorded since the end of November, 2015 to the end of February, 2016, showed that the number of cryoseisms per day strongly correlates with variations of air temperature (Figure 1).

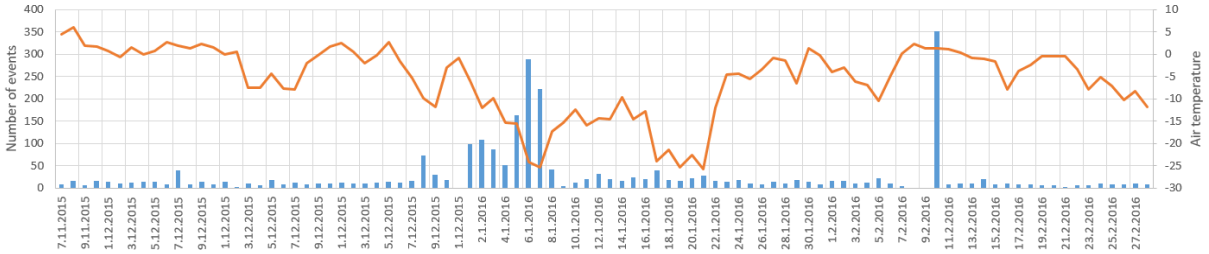

Figure 1. Dependence between air temperature and number of impulses per day

4. Formation of frost quakes by thermal stress

Thermal stresses of frozen soil were calculated for Talvikangas at depths of 5 cm, 15 cm and 30 cm using the technique described in Okkonen et al. (2020). The modelling proved that the frost quake recorded on 6 January 2016 occurred during the period of high calculated thermal stress, when the air and soil surface temperatures were below −20°C.

The air temperature dropped by as much as 9°C in the day of the frost quake (6 January 2016), and the calculated thermal stresses on the soil at a depth of 5 cm were up to 22 MPa, which was above the threshold thermal stress calculated with the critical stress intensity factor.

5. Conclusions

In our study, we show that the most probable source mechanism of frost quakes are vertical fracture opening. The magnitudes of damaging frost quakes can be as large as those of tectonic earthquakes. Using of artificial neural network detector allowed us to detect numerous seismic event with the same characteristics as the frost quake on 06.01.2016 near Oulu. Number of these events per day is modulated by air temperature.

Frost quake crack formation by a large temperature drop in air and soil is a natural phenomenon that is not well understood. Although formation of a single fracture cannot result in a seismic event comparable in magnitude with tectonic earthquakes, the ground shaking produced by frost quakes in the near-field zone can be hazardous in urban areas, as the example of Talvikangas frost quake shows. The thermal stresses in water-saturated soils due to rapid decrease of temperature, freezing and absence of thick insulating snow cover were greater than the stresses that are necessary to initiate cracking of ice and frozen soil.

References:

Uski, M., Tuppurainen, A. (1996). A new local magnitude scale for the Finnish seismic network. Tectonophysics, 261(1-3), 23-37.

Laine, K. (2016). Frost quake caused crack in house in Talvikangas—A massive boom was heard from kilometers. Kaleva. https://www.kaleva.fi/jaajaristys-halkaisi-talon-talvikankaalla-valtava/1781214

Aki, K., Richards, P. G. (2002). Quantitative seismology (2nd ed.). Sausalito, California: University science books.

FMI (2020). Open data services. Helsinki, Finland: Finnish Meteorological Institute. Accessed 2020-01-22.

Okkonen, J., Neupauer, R. M., Kozlovskaya, E., Afonin, N., Moisio, K., Taewook, K., Muurinen, E. (2020). Frost quakes: Crack formation by thermal stress. Journal of Geophysical Research: Earth Surface, 125, e2020JF005616. https://doi.org/10.1029/2020JF005616.

Modeling the structure of the Earth's crust of the White Sea region

L. Bakunovich[1], B. Belashev[1], N. Sharov[1] and M. Nilov[1]

[1]Institute of Geology, FGBUN FIC, Karelian Research Center, RAS, Petrozavodsk, Russia
E-mail: Luba5_89@mail.ru

The subject of the study is the White Sea basin and adjacent territories. Located at the junction of two large tectonic elements of the East European Craton, the Fennoscandian Shield and the Russian Plate, this region is constantly experiencing dynamic loads caused by the continuing uplift of the Fennoscandian Shield. Its original crustal structures formed in the Archean were partially transformed in the processes of Proterozoic rifting and subsequent tectonomagmatic activation. Studies of geodynamics, tectonics, and the evolution of the material composition of the lithosphere are relevant in the region. Its characteristic feature is the manifestation of kimberlite magmatism, deposits of diamonds and other minerals. It is believed that the Arkhangelsk province, which ranks second in Russia in diamond mining after Yakutia, is far from exhausting its diamond potential. The geological research recently conducted here is aimed at finding hydrocarbons. The formulation and solution of theoretical and applied problems are facilitated by the study of the deep structure of the region.

Interpretation of geological and geophysical data is usually carried out together with with the construction of 2D and 3D models using the petrological characteristics of rocks, such as density and magnetization. The many known geophysical models of the earth's crust of the White Sea are characterized by detail loss, incomplete information, uneven coverage of areas, differences in local volumes of data used. Some of them represented geophysical environment in cylindrical blocks.

The modern modeling tool is the Integro software package developed by VNIIgeosystem for solving predictive and diagnostic problems and problems of thematic regionalization of territories. This complex automates the solution of direct and inverse problems of geophysics, allowing to draw up digital maps, carry out cartographic references, process, visualize and store 3D data.

The goal of our work is to model the velocity structure of the region's earth crust based on instrumental observation data using the Integro software complex (Cheremisina et al. 2018). The objectives of the research are the construction of the velocity layers of the earth's crust, the study of their connections with density heterogeneities and geophysical fields.

The modeling of the region's lithosphere is based on the results of geophysical studies conducted along 3-AP, 1-EB, QUARTZ, AGATE and other traverses as well as geologo-geophysical summary maps and schemes (Sharov and Zhuravlev, 2019). We also used a digital map of the anomalous gravitational field in the Bouguer reduction and a topographical map on a scale 1:1,000,000. The longitudinal seismic waves velocities we recalculated in the densities of rocks by the reference velocity model (Sharov, 2017).

The method of modeling included the selection of an environmental model and its geometric framework, construction of 2D density models from seismic profiles and the transition to a 3D density model of the region's earth crust. The geometric framework and the environmental model were selected based on the block structure of the seismic profile. The

values of the block densities calculated from the reference velocity model as initial approximations. Direct problem was solved using 2D models. The values of the selected structure blocks' density varied within the specified limits, achieving a minimum difference in the values of the calculated and the profile Bouger anomaly. If it was necessary to improve the optimization, the blocks were further divided, new heterogeneities were introduced, and the block boundaries were shifted. The 3D density model was built by solving the inverse problem of gravity prospecting. The material of the mantle was considered homogeneous, and the density heterogeneities inherent in the earth's crust.

The 3D model allowed to determine the spatial position and visualized the boundaries of the velocity layers of the earth's crust of the White Sea region (Figure 1).

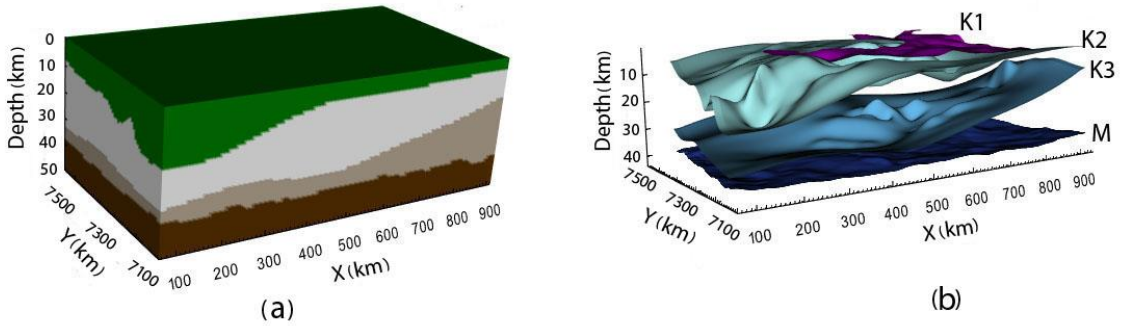

Figure 1. a: 3D model showing the density distribution of the White Sea Region's earth crust; b: the spatial representation of the boundary surfaces K1, K2, K3 and M of the velocity layers of the region's earth crust.

The proposed interpretation of the simulation results explains the absence of a sedimentary cover on part of the water area and its large capacities in the deep sea parts by raising the Fennoscandian shield, connection within the framework of the granite-metamorphic layer of the Winter Bank Uplift and the Onega Peninsula with the structures of the Terek Coast and the Karelian Megablock, respectively, large capacities of granulite-basite layer in the area of Winter Bank lifting by the intensity of it's formation, the depression of the M boundary by the existence of a subvertical structure associated with manifestations of kimberlite magmatism.

The study was conducted under the Research Project AAAA-A18-118020290086-1 funded by the Russian Foundation for Basic Research under the Research Projects 20-05-00481 «Lithospheric structure and dynamics of the White Sea Region» and 20-35-90034 «Complexing geophysical methods for 2D and 3D modelling of the earth crust of the White Sea and adjacent territories».

References:

Cheremisina E.N., Finkelstein M.Ya., Lyubimova A.V. GIS INTEGRO – an import-replacing software-technological complex for solving geologo-geophysical problems. *Geoinformatika*. 2018. No.3. pp. 8-17. (In Russian).

Sharov N. V. Lithosphere of Northern Europe, as shown by seismic data. KarRC RAS. Petrozavodsk. Russia. 2017. 173 p. (In Russian).

Sharov N.V., Zhuravlev A.V. Crustal structure of the White Sea and adjacent areas. *Arctic: ecology and economy.* 2019. No. 3 (35). pp. 62—72. DOI: 10.25283/2223-4594-2019-2-62-72. (In Russian).

Technology for studying the structure of the upper crust of the Voronezh Crystalline Massif by detailed density modeling data

S.I. Berezneva[1], O.M. Muravina[1] and T.A. Voronova[1]

[1]Voronezh State University, Voronezh, Russia
E-mail: [1]kogsveta@mail.ru

The article presents the technology for constructing detailed three-dimensional density models of the upper crust of the Voronezh Crystalline Massif (VCM). Such technology is based on the inversion of the gravity field and complex interpretation of geological, petrophysical and geophysical information. The use of the proposed technology makes it possible to obtain a 3D density model that reflects the structural features of the site.

Keywords: gravity field, density modeling, petro-density model

Voronezh Crystalline Massif (Figure 1) is located in the central part of the East European platform (Gorbatschev and Bogdanova, 1993; Chernyshov et al. 1997; Mints et al. 2010; Mints, 2011; Mints et al. 2014; Savko et al. 2017). The massif stretches in the northwest direction, in the southwest and southeast it borders to the Neoproterozoic-Phanerozoic depressions, in the west, northwest and northeast, the massif is framed by the Paleoproterozoic depressions. (Mints et al. 2014; Savko et al. 2017). The Voronezh Crystalline Massif has a linear size of about 450 by 300 km and an asymmetric elongated shape.

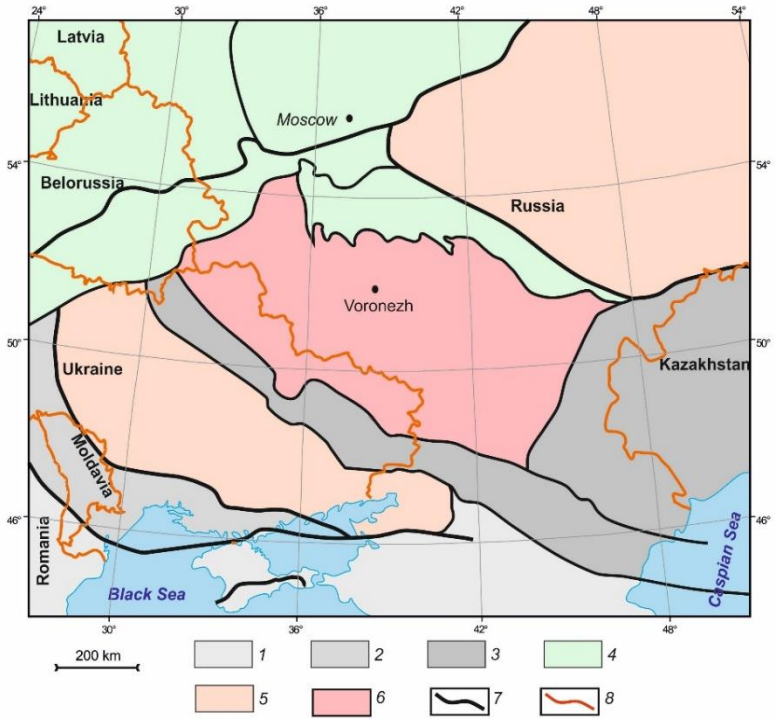

Figure 1. The main tectonic elements of the EEP (the area of density modeling of the lithosphere is shown): 1 - Scythian platform; 2 - Black Sea depression; 3 - Neoproterozoic-Phanerozoic structures; 4 - Paleoproterozoic structures; 5 - Archean structures; 6; -Voronezh Crystalline Massif; 7 - boundaries of large tectonic elements; 8 - state borders

Due to the fact that the consolidated foundation is covered by a platform cover, the thickness of which varies from several meters to hundreds of meters, and on the outskirts can reach several kilometers. The study of the deep structure of the region is based on geophysical data. The geological significance of the interpretation of geophysical fields is provided by petrophysical information. About 9000 wells were drilled within the VCM, more than half of which penetrated the crystalline basement and provided coring. The total number of core samples from sedimentary and crystalline rocks reaches 150,000. Based on the results of petrophysical determinations, a digital spatial petrophysical database was formed and a petro-density map of the Precambrian foundation was constructed (Glaznev et al. 2020). Information on the density distribution of Precambrian sediments, as well as seismic and thermal models of the Earth's crust, became the initial data for calculating a 3D regional density model (Muravina et al. 2018).

The next stage in the study of the structure of the region was a detailed density modeling of the upper crust based on the inversion of the gravity field and a comprehensive interpretation of geological, petrophysical and geophysical information, presented in this article (Figure 2). One of the important aspects of building three-dimensional density models is the formation of a starting model, which plays an important role in ensuring the geological content of the solution. This model is built on the basis of prior information, and summarizes the petrophysical and geological data related to the study area. The initial data for modeling in VCM conditions are: geological and topographic base; the values of the thickness of the «gravitational» layer obtained from the results of the statistical analysis of the anomalous field (Glaznev et al., 2014); a regional density model of the lithosphere covering the territory of the VCM (Glaznev et al. 2016; Muravina, 2016; Mints et al. 2017) and the regional gravitational field corresponding to this model; petro-density model of sedimentary cover and crystalline rocks (Muravina et al. 2013, 2019).

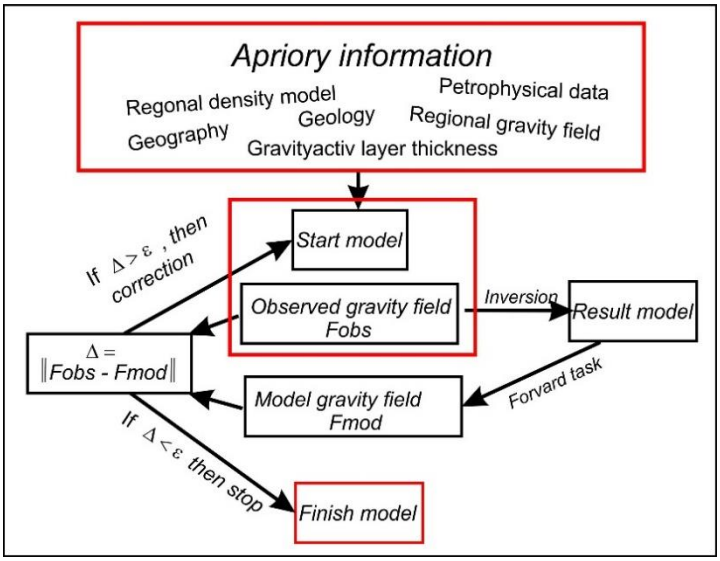

Figure 2. Block diagram of detailed density modeling technology

When constructing detailed density models of the upper part of the crystalline crust, it is also necessary to take into account the gravitational effect of the sedimentary cover, which is calculated based on the petrodensity model of sedimentary rocks (Muravina et al. 2013; Glaznev et al. 2013).

A three-dimensional model of the regional density of the central part of the East European Platform establishes the density distribution on the roof and bottom of the upper, middle and lower layers of the Earth's crust, in the transition layer and the upper mantle to a depth of 80 km. The solution of the direct problem of gravimetry for the model makes it possible to establish the regional component of the field for any territory within the region.

When creating a starting model, the features of the structure and location of each specific site are taken into account. The position of the upper edge corresponds to the depth of the crystalline surface foundation, and the lower edge corresponds to the position of the bottom of the «active gravitational» layer for the given territory. The structure of the model is set by a set of layers, at the boundaries of which, in accordance with the petrophysical data of the region, the absolute values of the density are set. The transition to excess density values is carried out by subtracting the density values of the regional model. Also, at each point of the detailed 3D model, the minimum and maximum density restrictions and the values of the weight function are set.

The solution of the inverse problem of gravimetry is a multi-stage iterative process of inverting the field residuals at each point of the surface into the density values of the equivalent horizontal layer of a given thickness, and redistributing the obtained density values to the lower layers of the medium in accordance with the weight function. The inversion of the gravitational field into density is carried out on the basis of an algorithm for the quasinormal solution of the inverse problem in a three-dimensional formulation in Cartesian coordinates. An approximation representation of the inverse operator is used in the form of a sum of transformations: calculating the vertical derivative and analytic continuation to the upper half-space to some optimal height (Glaznev et al. 2002). The effectiveness of this approach was shown on a number of simple theoretical and real examples of detailed density modeling of the structure of the upper crust (Glaznev et al. 2008, 2015; Mints et al. 2018). The results of solving the inverse problem should minimize the discrepancy between the model field and the observed field, and also satisfy the specified criteria of all the initial geological information. It is obvious that the quality of modeling based on gravity inversion depends on the quantity and quality of a priori data, which, as a rule, are probabilistic in nature with varying degrees of uncertainty. Consequently, in conditions of a complex geological structure, it is possible to improve the quality of modeling due to multistage field inversion, with the implementation of a point correction of the original model at each stage in a given range of changes in model parameters.

The proposed detailed modeling technology was tested in a number of areas located within the Voronezh Crystalline Massif (Glaznev et al. 2015; Muravina et al. 2017; Voronova et al. 2019).

The research was supported by the RFBR, grants No20-05-00190 and 19-05-00336.

References:

Chernyshov N.M., Nenakhov V.M., Lebedev I.P., Strik Yu.N. 1997. Model of geodynamic development of the Voronezh massif in the Early Precambrian. Geotectonics. 1997. No. 3. P. 21-30.

Glaznev, V.N., Raevsky, A.B., Balagansky, V.V., Manninen T., 2002. 3D model of the upper crust of the Kittilä-Sodankylä region, Finnish Lapland (north of the Baltic shield) // Collection of materials dedicated to the 40th anniversary of the Department of Geophysics, Voronezh, C. 11-20.

Glaznev, V.N, Zhirova A.M., Raevsky, A.B., 2008. New data on the deep structure of the Khibiny and Lovozersky massifs, Kola Peninsula. Reports of the Academy of Sciences, T. 422. No. 3. S. 391-393.

Glaznev, V.N., Zhavoronkin, V.I., Mints, M.V., Muravina, O.M., Khovanskiy, N.E., 2013. Petrodensity model and gravitational effect of the sedimentary cover of the Voronezh Crystalline Massif and its framing. Materials of the 40th session of the international seminar. D.G. Uspensky "Questions of theory and practice of geological interpretation of geophysical fields." Moscow: Institute of Earth Physics Russian Academy of Sciences, P. 107-112.

Glaznev, V.N., Muravina, O.M., Voronova, T.A., Kholin, V.M., 2014. Estimation of the thickness of the gravitational layer of the earth's crust of the Voronezh Crystalline Massif. Vestnik VSU. Ser. Geology, No. 4. P. 78-84.

Glaznev, V.N., Mints, M.V., Muravina, O.M., Raevsky, A.B., Osipenko, L.G., 2015. Complex geological–geophysical 3D model of the crust in the southeastern Fennoscandian Shield: Nature of density layering of the crust and the crust–mantle boundary. Geodynamics & Tectonophysics, V. 6. № 2. P. 133–170.

Glaznev, V.N., Voronova, T.A., Antonova, I.Yu., Muravina, O.M., 2015. Methodology and results of 3D density modeling in the study of the structure of the upper crust of the Voronezh Crystalline Massif // Materials of the 42nd session of the International Seminar. D.G. Uspensky "Questions of theory and practice of geological interpretation of geophysical fields." Perm: Mining Institute, Ural Branch of the Russian Academy of Sciences, P. 49-52.

Glaznev V.N., Mints M.V., Muravina O.M., 2016. Density modeling of the earth's crust in the central part of the East European platform. Bulletin of KRAUNC, Earth Sciences, Iss. 29, No. 1, P. 53-63.

Gorbatschev R., Bogdanova S., 1993. Frontiers in the Baltic Shield. Precambrian Res. V. 64. P. 3–21.

Mints M. V., Suleimanov A. K., Babayants P. S., Belousova E. A., Blokh Yu. I., Bogina M. M., Bush V. A., Dokukina K. A., Zamozhnyaya N.G., Zlobin V.L., Kaulina T.V., Konilov A.N., Mikhailov V.O., Natapov L.M., Piip V. B., Stupak V. M., Tikhotskiy S. A.A., Trusov A.A., Filippova I. B., Shur D. Yu., 2010. Deep structure, evolution and minerals of the Early Precambrian foundation of the East European Platform: Interpretation of materials from the reference profile 1-EB, profiles 4B and Tatseis. V. 1.408 s., T. 2.400 p.

Mints, M.V., 2011. 3D model of deep structure of the Early Precambrian crust in the East European Craton and paleogeodynamic implications. Geotectonics, V. 45 (4). P. 267–290.

Mints, M.V., Bush, W.A., Ageev S.N., 2014. Bryansk-Kursk-Voronezh intracontinental collisional orogen (East European craton). Geodynamics & Tectonophysics, V. 5, N 3. P. 717–742.

Mints, M.V., Sokolova, E.Yu., Vardanyants, I.L., Smirnov, M.Yu., Uspensky, N.I., Golubtsova, N.S., Kulikov, V.A., Pushkarev, P.Yu., Taran, Ya V.V., Zolotaya L.A., Kosnyreva, M.A., Yakovlev, Ya.G., Rokityansky, I.I., Ryazantsev, P.Yu., Nilov, M.Yu., Glaznev, V.N., Muravina, O.M., 2018. A volumetric model of the deep structure of the Svecofennian accretionary orogen based on the data of MOV-CDP, MTZ and density modeling. Transactions of the Karelian Scientific Center of the Russian Academy of Sciences, № 2, P. 34-61.

Muravina, O.M., 2016. Density model of the earth's crust of the Voronezh Crystalline Massif. Vestnik VSU, Ser. Geology, No. 1. P. 108-114.

Mints, M.V., Glaznev, V.N., Muravina, O.M., 2017. Deep structure of the crust in the southeast of the Voronezh Crystalline Massif according to geophysical data: geodynamic evolution in the Paleoproterozoic and the current state of the crust. Vestnik VSU. Ser. Geology, No. 4. P. 5-23.

Muravina, O.M., Glaznev, V.N., Mints, M.V. 2018. 3D-density model of the Earth crust for central part of the East-European platform / In: Surface waves propagating in the geophysical environment "lithosphere - hydrosphere - ice cover - atmosphere", P. 81-86.

Muravina, O.M., Glaznev, V.N., Zhavoronkin, V.I., Mints M.V., 2019. Reflection of the Petrophysical Basement Rocks Models in Geophysical Fields. Practical and Theoretical Aspects of Geological Interpretation of Gravitational, Magnetic and Electric Fields. Springer Proceedings in Earth and Environmental Sciences. Springer Nature Switzerland AG, P. 49-53.

Muravina, O.M., Zhavoronkin, V.I., Glaznev, V.N., 2013. Petrophysical characteristics of the sedimentary cover of the Voronezh anteclise. Vestnik Voronezh State University. Ser. Geology, No. 1, P.189-196.

Muravina, O.M., Voronova, T.A., Antonova, I.Yu., Gruzdev, V.N., 2017. Results of detailed density modeling of the upper crust of the Voronezh Crystalline Massif. Problems of natural science, 2017. – № 1 (13). – P. 67-70.

Savko, K.A., Samsonov, A.V., Kholin V.M., Bazikov, N.S., 2017. Megablock Sarmatia as a fragment of the Vaalbar supercraton: correlation of geological events at the Archean-Paleoproterozoic boundary // Stratigrafiya. Geological correlation, V. 25, № 2. C. 3–26.

Voronova, T.A., Glaznev, V.N., Muravina, O.M., Antonova, I.Y., 2019. The Density Model of the Crystalline Crust the Southwestern Part of the Lipetsk Region / Springer Proceedings in Earth and Environmental Sciences: Practical and Theoretical Aspects of Geological Interpretation of Gravitational, Magnetic and Electric Fields. Eds. D.Nurgaliev, N.Khairullina. Springer Nature Switzerland AG, 2019. P. 69-76.

The Vaasa migmatitic complex: new results and perspectives for the tectonic evolution of the Svecofennian orogen

F. Chopin[1,2], A. Korja[3], K. Nikkilä[4], P. Hölttä[5], T. Korja[6], M.A. Zaher[7], M. Kurhila[5], O. Eklund[4], O.T. Rämö[3], Y. Lalaye[5], H. O'Brien[5] and M. Sayab[7]

[1]Université de Strasbourg, CNRS, ITES UMR 7063, 1 rue Blessig, 67000 Strasbourg, France
[2]Center for Lithospheric Research, Czech Geological Survey, Klárov 3, 118 21 Prague 1, Czech Republic
[3]Department of Geosciences and Geography, P.O. Box 64, 00014 University of Helsinki, Finland
[4]Geology and Mineralogy, Åbo Akademi University, 20500 Turku, Finland
[5]Geological Survey of Finland, P.O. Box 96, 02151 Espoo, Finland
[6]Exploration Geophysics, Geosciences and Environmental Engineering, Luleå University of Technology, 97187, Luleå, Sweden
[7]Geomagnetic and Geoelectric Department, National Research Institute of Astronomy and Geophysics, Helwan, 11421, Cairo, Egypt
E-mail: f.chopin@unistra.fr

In this paper, we present briefly a tectonic model for the evolution of the Vaasa migmatitic complex (Finland) and how we believe it could be integrated into the formation of an oroclin during the Svecofennian orogeny. We finally show some results on the metamorphic gradient affecting the supracrustal rocks.

Keywords: Svecofennian orogen, Vaasa migmatitic complex, orocline, LP-HT metamorphism, pseudosection

1. Introduction

The Vaasa migmatitic complex (Finland) offer a mid-crustal horizontal section of a partially molten crust, formed by the accretion of various supra-crustal rocks within an accretionary wedge during the growth of the Svecofennian Paleoproterozoic orogen. Review and/or new sets of geophysical, structural, geochronological and petrological data have been used to propose a coherent tectonic scenario for this large magmatic complex. It includes a magmatic core made of S-Type granitoids passing to diatexite, migmatites, gneiss and schists towards its border.

2. Tectonic scenario

The model has been recently published by Chopin et al. (2020). It proposes a 3 steps tectonic scenario: accretion followed by channel flow (D1), oroclinal buckling (D2), magmatic core exhumation by mechanical instabilities within the hinge of the orocline (D3). Geophysical data, in particular seismic reflection (FIRE 3a) and new magnetotelluric profiles (MT-PE and MT-B2) are compared to geological field data. The good continuity between reflections in the seismic profiles, conductivity in the magnetotelluric profile, lithology and field schistosity permit to propose that early primary structures are prominent in most of the complex. It reflects westwards D1 stacking of the supracrsutal rock until anataxis in its core. Inverted metamorphic gradient along these structures is interpreted as a channel flow exhuming the deep-seated partially molten rocks over the mica schists in a LP-HT gradient.

D2 structures corresponds to W-E striking folds visible at all scale in the border of the complex, whereas only faint orientation of Kfs phenocryst is visible within the core. N-S shortening developing a regional orocline could be responsible for the formation of those structures, similar to what have been proposed by Lahtinen et al. (2015).

Vertical shear zones, in particular within and around the magmatic core may correspond to crustal scale vertical mass transfert of the weak and low density magma within the hinge of the orocline (D3).

3. Quantification of the metamorphism

Our work is now focused on the precise quantification of the metamorphism affecting the supracrustal rocks together with detailed microstructural observations. The results will be confronted to the above described scenario. A set of 5 mica schists and migmatites have been used to develop pseudosections in order to better understand the HP-LT metamorphic gradient in the Vaasa migmatitic complex. Preliminary results show that a slightly prograde metamorphism is preserved in the staurolite mica schists (from 5 kbar at 550 °C to 6.5 kbars at 600 °C, 550 to 600 °C) whereas small grains of kyanite, frequent in the metatexites, may reflect stacking up to 8 kars and 700 °C. These results should be compared to new U/Pb ages monazites obtained from the same metamorphic gradient.

References:

Chopin, F., Korja, A., Nikkilä, K., Hölttä, P., Korja, T., Zaher, M.A., Kurhila, M., Eklund, O., Rämö, O.T., 2020. The Vaasa migmatitic complex (Svecofennian orogen, Finland): build-up of a LP-HT dome during Nuna assembly. Tectonics, 39(3), e2019TC005583, doi: 10.1029/2019TC005583

Lahtinen, R., Johnston, S. T., & Nironen, M. (2014). The Bothnian coupled oroclines of the Svecofennian Orogen: A Palaeoproterozoic terrane wreck. Terra Nova, 26(4), 330–335. https://doi.org/10.1111/ter.12107

Biotite as a petrogenetic tool in granite-migmatite areas

O. Eklund[1] and K. Nikkilä[1]

[1]Åbo Akademi University, Faculty of Science and Technology, Geology and mineralogy
E-mail: olav.eklund@abo.fi

Partial melting of rocks that have been affected by external fluids (water-fluxed partial melting) usually lack peritectic minerals common in response to dehydration melting. Dehydration melting in upper amphibolite to granulite facies usually produce peritectic minerals like garnet, cordierite and orthopyroxene in the paleosome as well as in the leucosome from biotite bearing protoliths. In the case of water-fluxed melting of a biotite bearing protolith, the most common mineral in the leucosome is also biotite (amphiboles may appear). In migmatite areas, formed by water-fluxed melting, the biotite chemistry may contain important information about the composition of the protolith and the evolution of leucosomes and granites.

Keywords: lithosphere, migmatite, biotite, Svecofennian orogeny

General

The southernmost part of Finland extending from Bengtskär via Hanko peninsula to Jussarö is a migmatite area comprising principally a K-feldspar rich granitic metatexite with granitic leucosomes and areas of leucogranite. The granitic metatexite contains partially melted and deformed xenoliths of various compositions (igneous, volcanic, sedimentary) indicating that the chemically homogenous granitic metatexite may have formed from different protoliths.
This heterogenous appearance was reported by Saukko et al. (2018) as a felsic MASH zone. A felsic MASH zone is an area in the middle crust that has been at the protolith solidus temperature for a long period resulting in areas containing melts from different crustal sources that interact with each other, crystal mushes and restites and signs of fluid interaction with the melt as an inducing agent of anataxis are often present. (Schwindinger and Weinberg, 2017).

Although partial melting of the granitic metatexite is recognised in field, no peritectic minerals are found in response to the melting process. The major mafic mineral in all granitic rocks are biotite, indicating water induced melting.

To gain information about possible protoliths and the physical environment during the the migmatization event, biotites from granitic metatexites, leucosomes and leucogranites were analysed.

Geochemical classification of the studied rocks

The rocks on focus here are geochemically peraluminous granodiorites, monzogranites and granites (the granitic metatexite) and peraluminous leucogranite (granitic leucosome and leucogranites). See Saukko et al. (2021) (this volume).

Analytical methods

Biotites from granitic metatexites and leucosomes therein and leucogranites were analysed with a Phenom XL low vacuum SEM instrument at the Geohouse in Turku. The results (reported as 100 wt% oxides) were calculated to 95% assuming that 5% of the analyses was crystal water or other fluids not determined with the instrument. The results was recalculated to atoms per formula units using 24 O. For classifications, only biotites with $K_2O > 6$ wt% was used. In total, 104 of 272 spot analyses were used in this study. The rest were disqualified because of

chloritisation**.** We are aware of the quantitative limitations of the instrument. However, since we analysed hundreds of spots from different micas in different samples, we are able to identify important trends without 100% quantitatively reliable analyses.

Results

The general composition of all biotites is annite in the Fe/(Fe+Mg) vs. tot.Al diagram (Figure 1a). In the diagram it is seen that biotite from leucosomes (open triangels and circles) has lower Fe-index compared to granitic metatexites (filled triangles and circles). Leucogranites from two different areas (crosses and tilted crosses) have distinct compositions. The Morgonlandet area (tilted crosses) comprise of biotites with high total aluminium whereas Bengtskär (crosses) has lower total aluminium but higher Fe-index. In the FeO-10xTiO_2-MgO diagram, separating primary biotites from primary re-equilibrated and secondary biotites, the majority of the micas plot in the field of primary micas except those that are deficient in Ti and plot in the field of recrystallized biotites (Figure 1b). Majority of these biotites are from Bengtskär even-grained granite.

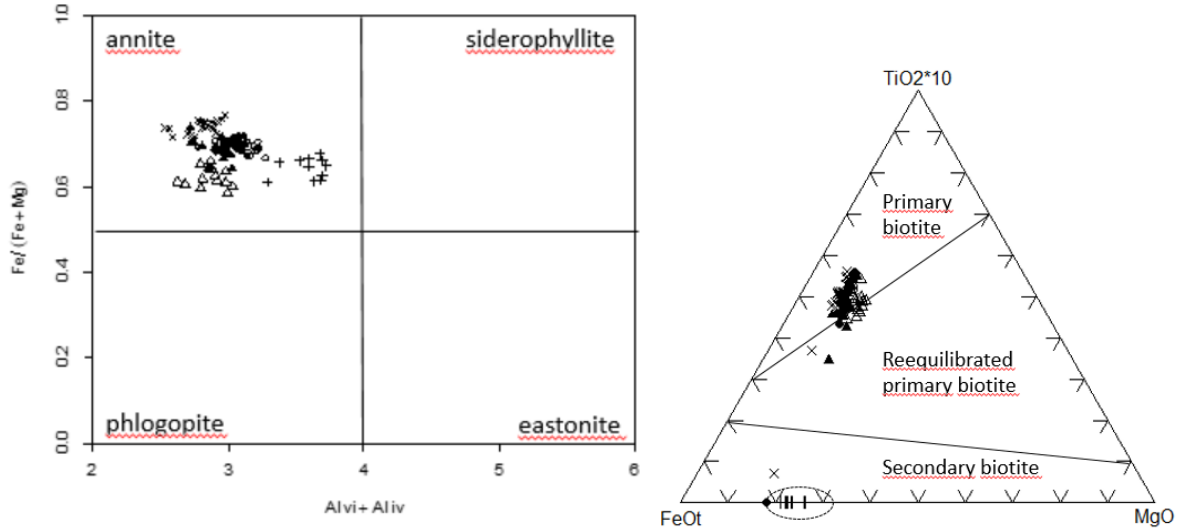

Figure 1. a). (Left). Biotites classified as primary annites according to the Fe/(Fe+Mg) vs. total Al. b) (Right) diagram separating primary biotite from reequilibrated primary biotite and secondary biotite.

It is known that the titanium content and Mg# are indicators for crystallization temperature of biotite. The higher Ti content and higher Mg#, the higher is the crystallization temperature. By using the Ti-in-biotite geothermometer by Henry et al. (2005) the majority of analysed biotites gave temperatures between 600 and 700 °C close to 650 °C (except recrystallized biotites deficient in Ti)

Several authors have developed diagrams based on the Al, Mg and Fe contents of biotites to indicate from what kind of rock series the rocks on focus stem from (Natchet et al. 1985; Abdel-Rahman, 1994; Natchet et al. 2005; Bucholz et al. 2018). Bucholz et al. (2018) constructed a diagram based on the cations Al, Mg and Fe per formula unit to separate suites for calc-alkaline, alkaline and peraluminous biotites (Figure 2). The granitic metatexites and leucosome biotites from one area (Stenskär) plot in the field of calk-alkaline (metaluminous) suites while the rest of biotites plot in the field of peraluminous suites.

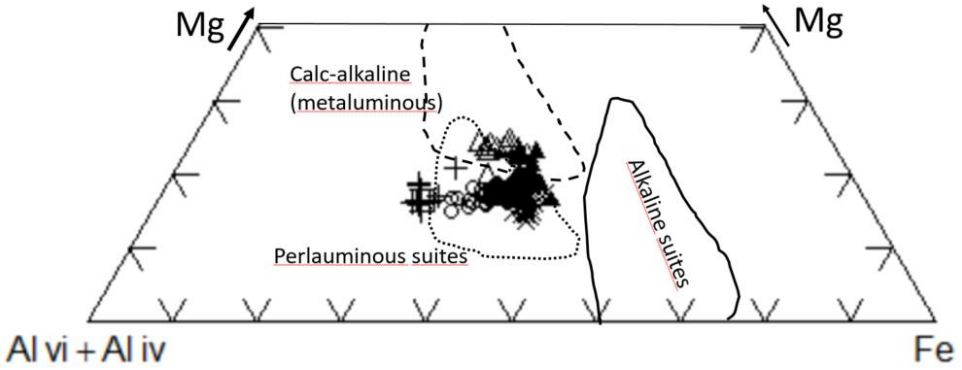

Figure 2. Diagram separating different rock suites based on cations per formula unit. Biotites from the study area plot in the fields of calc-alkaline (metaluminous) and peraluminous suites.

Discussion

Biotites are sensitive to adapt their compositions to be in equilibrium with the surrounding physiochemical environment references. For example, Bell et al. (2017) used the chemistry of biotite inclusions in zircons from Black Hills in Western Australia and Nuvvuagittuq supracrustal belt on Greenland (areas with the oldest zircons on Earth), to state that these protoarchean zircons from different areas were growing in a more reduced metaluminous melt and an oxidised peraluminous melt, respectively. Bell et al. (2017) classified their micas in a diagram taking into account fO_2 and aluminosity (Figure 3).

The relative fO_2 of the environment biotite are growing in is reflected by the FeO/MgO ratio. The higher ratio the more reduced is the environment. Bell et al. (2017) used the value 3.5 to distinguish between reduced, i.e. the ilmenite series granites by Ishihara (1977) and oxidised, i.e. the magnetite series granites by Ishihara (1977) (Figure 3). As an index for aluminosity Bell et al. (2017) used $Al_2O_3/(FeO+MgO)$ index. They used the values > 0.55 for peraluminous rocks and < 0.45 for metaluminous rocks.

Biotites from even-grained granites in southernmost Finland plot in different parts of the diagram. Biotites from Morgonlandet has a high Fe/Mg index and an aluminosity index close to 0.55. This indicate that the granite crystallised from a metaluminous to peraluminous magma in a reduced environment. Biotites from the granite of Bengtskär has a lower Fe/Mg index, but high aluminosity index indicating crystallisation from a peraluminous magma in higher fO_2 conditions. The strong peraluminosity is supported by muscovite in the analysed rock.

The biotites from leucosomes within two metatexites form a trend with decreasing fO_2 and increasing aluminosity. This reflect access to aluminium in the leucosome melts and that the fO_2 was different in the formation of metatexite biotites and leucosome biotites.

The two metatexites are separated at a Fe/Mg index about 3.5. This indicate that micas from Klovaskär metatexit (filled triangels) grew in a more reduced environment compared to metatexite micas from Stenskär (open triangles) that grew in a more oxidising environment outside the ilmenite series.

Conclusions

Our study indicate that biotite may give additional information to bulk geochemical data about protoliths and partial melting processes in migmatites.

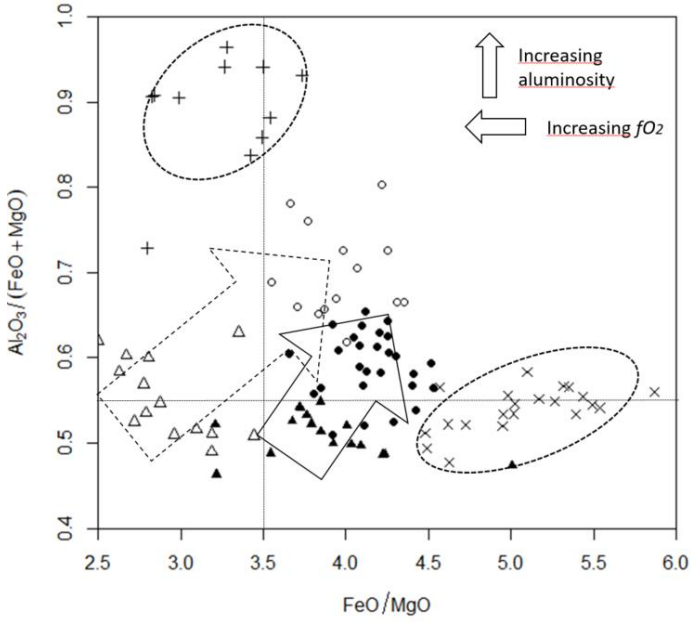

Figure 3. Diagram illustrating variations in fO_2 and aluminosity. Ellipses indicate leucogranites, arrows indicate trends from metatexites to leucosomes. See text for further explanations.
Crosses = leucogranite from Bengtskär
Tilted crosses = leucogranite from Morgonlandet
Filled triangles = metatexite from Klovakär
Filled circles = leucosomes from Klovaskär
Open triangles = metatexite from Stenskär

We have recognised two protoliths, one calk-alkaline source formed in slightly higher *fO2* compared to a peraluminous source formed in a more reduced environment. Biotites from leucosomes indicate a higher aluminosity with decreasing fO_2 compared to the metatexites. The crystallization temperature given by Ti in biotite, about 650°C, fits well with the idea of a long-lived MASH zone at wet solidus temperature for the protolith.

Our study also indicate that the term peraluminous is not strictly source related, but also process related, since the environment in our migmatite areas drives the leucosomes to form more reduced and more peraluminous melts compared to their host rocks. This can lead to serious misinterpretations for geologists that search for proper protoliths for peraluminous granites, since metaluminous calc-alkaline rocks may produce peraluminous melts.

References:

Abdel-Rahman A.F.M., 1994. Nature of biotites from alkaline, calc-alkaline, and peraluminous magmas. Journal of Petrology, 35(2):525-541.

Bell, E. A., Boehnke, P., Harrison, T. M. & Wielicki, M. M., 2017.Mineral inclusion assemblage and detrital zircon provenance. Chemical Geology 477, 151–160.

Bucholz, C.E., Stolper, E.M., Eiler, J.M., Breaks, F.W., 2018. A Comparison of Oxygen Fugacities of Strongly Peraluminous Granites across the Archean–Proterozoic Boundary. Journal of Petrology, 2018, 59(11): 2123–2156. doi: 10.1093/petrology/egy091

Henry, D.J., Guidotti, C.V., Thomson, J.A., 2005. The Ti-saturation surface for low-to-medium pressure metapelitic biotites: Implications for geothermometry and Ti-substitution mechanisms. American Mineralogist, 90: 316-328.

Nachit, H, Razafimahefa, N, Stussi, J.M., Caron, J.P., 1985. Composition chimique des Biotitesettypologiemagmatique des granitoids. C.R. Acadomic Sciences Paris, Series 2, 301: 813-818.

Nachit, H., Ibhi, A., Abia, E.H., Ben Ohoud M., 2005. Discrimination between primary magmatic biotites, reequilibrated biotites and neoformed biotites. Comptes Rendus Geoscience, 337(16):1415-1420.

Saukko,A., Nikkilä, K., Väisänen, M., Eklund. O., 2018. Southernmost Finland Felsic MASH zone. Lito-2018, abstract volume.

Saukko, A., Nikkilä, K., Eklund, O., Väisänen, M. 2021. Granites of southernmost Finland Lito-2021 (this issue)

Schwindinger, M., Weinberg, R. 2017. A felsic MASH zone of crustal magmas — Feedback between granite magma intrusion and in situ crustal anatexis Lithos 284–285: 109-121

The iron oxide mineralised Matojärvi formation, Kiruna, Sweden

M. Etienne[1], I. Bacquet[1], D. Monteith[1] and L.S. Lauri[1]

[1]EXF, LKAB, Kiruna, Sweden
E-mail: marius.etienne@lkab.com

We present new insights into the stratigraphy of the volcanosedimentary Matojärvi formation, which hosts the Per Geijer IOA mineralizations in Kiruna, Norrbotten, Sweden.

Keywords: iron oxide-apatite deposit, Kiruna, Per Geijer, magnetite, hematite, stratigraphy

1. Introduction

The Per Geijer (PG) area is located on the northern side of the Kiruna town in Norrbotten, Sweden (Figure 1). The area comprises five iron oxide-apatite (IOA) deposits that form a four-km-long semi-continuous zone on the surface. Four of these deposits (Rektorn, Haukivaara, Henry and Nukutus) have been in production by open pit mining with a total production of ~11 Mt of iron-phosphorus ore between 1925 and 1987. The Lappmalmen orebody, which is located ~500−1200 m under the surface, has not been mined.

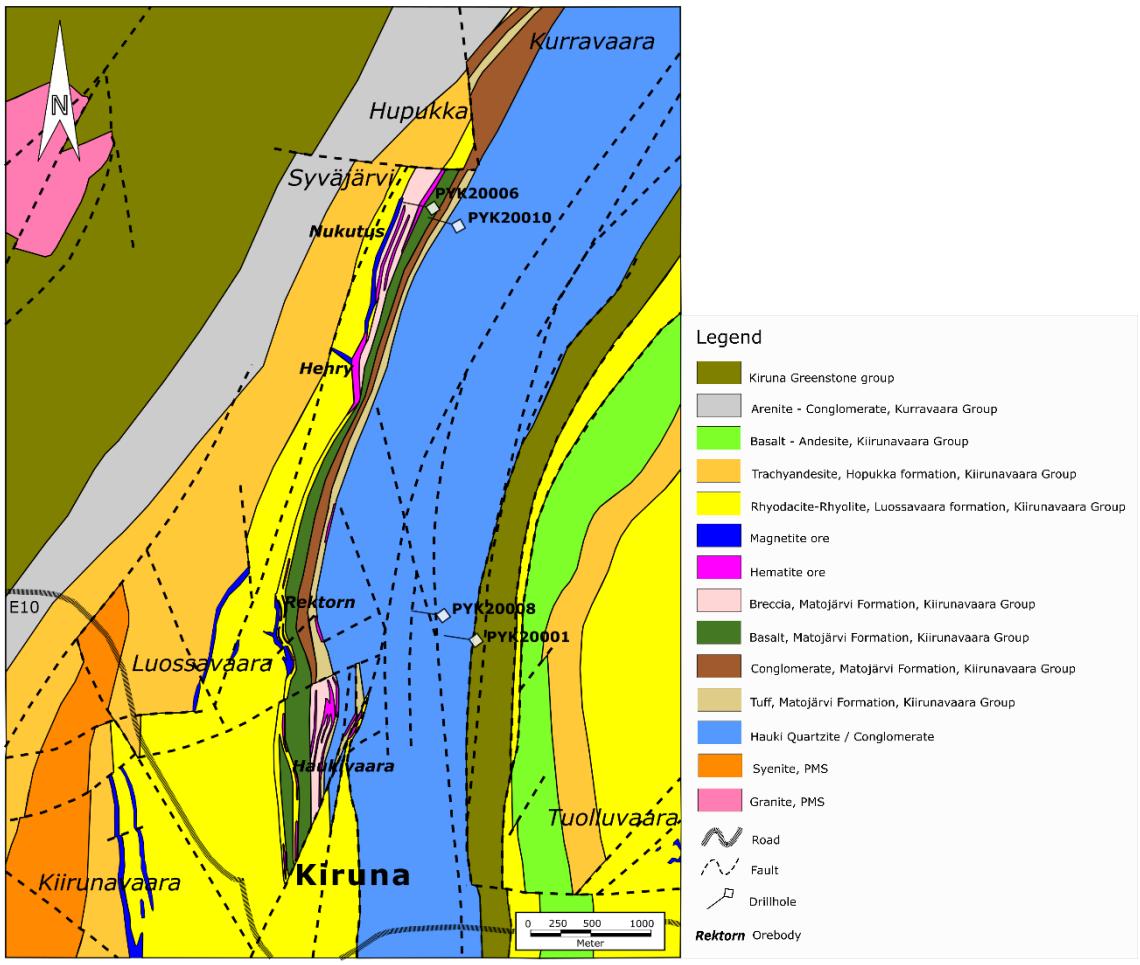

Figure. 1. Geological map of the Per Geijer area. Modified from Martinsson and Erlandsson (2009). Drill holes marked on the map are shown in detail in Figure 2.

The PG IOA deposits are emplaced at distinct levels in the volcanosedimentary stratigraphy of the upper Kiirunavaara Group: they are present in the upper part of the Luossavaara formation, at the contact of the Luossavaara formation and the overlying Matojärvi formation and within the latter (see Martinsson, 2004). Several iron oxide-rich zones are recognized, with magnetite dominating in the lower units and the amount of hematite increasing towards the upper units. Apatite is present both within the iron oxide units and as crosscutting veins.

The internal stratigraphy of the Matojärvi formation is not very well known due to limited outcrop and extensive alteration associated with the iron mineralization processes. The recent investigations by LKAB in the Per Geijer area allow us to work on a revised interpretation of the geology of the Matojärvi formation and the IOA mineralization within it based on new drillings.

2. Geology of the Matojärvi formation

The Matojärvi formation forms the uppermost part of the Kiirunavaara group, which is a Svecofennian age (~1.89-1.87 Ga) volcanosedimentary sequence that hosts the world-class Kiirunavaara deposit and several other IOA ore bodies. The stratigraphy of the Kiirunavaara group is quite well established, starting with a volcanic phase comprising the trachyandesitic Hopukka formation and the Luossavaara formation composed of porphyritic rhyodacite and rhyolite. The Kiirunavaara IOA orebody is emplaced at the contact between the abovementioned formations. The Matojärvi formation, which is the main host for the PG IOA deposits, is overlying the Luossavaara formation, and its upper contact is towards the Hauki quartzite formation that belongs to the younger Snavva-Sjöfallet group (Martinsson, 2004). The presence of iron mineralization and strong hydrothermal alteration at the contact zones makes the exact placing of particularly the lower contact of the Matojärvi formation difficult in many cases.

Overall, the Matojärvi formation is a heterogenous succession of volcanosedimentary lithologies that are commonly interbedded and may also show repetitions due to faulting. A major part of the formation is composed of tuffs and tuffites, previously considered to represent greywackes and mudstones, but basaltic lavas and sedimentary rocks such as polymictic conglomerates are also present. On the surface the thickness of the Matojärvi formation is between 250 m and 400 m. The top directions are consistently towards the east, and the whole package dips eastwards below the Hauki quartzite formation with approximately 50º dip angle. There is a lateral variation in the rock types, with basaltic lavas and agglomerates being more common in the northern part of the area and the southern parts being richer in tuffs (Figure 2). The Matojärvi formation also seems to thin out in the deeper parts under the Hauki quartzite.

The tuffs and tuffites of the Matojärvi formation are fine-grained, grey to green rocks that may appear as massive or laminated. Lithic tuffs with flattened, angular fragments are also present. The rocks can be tainted in pink probably due to hematite alteration, but they are mostly affected by calcite alteration that fills the porosity or acts as a gangue mineral in cross-cutting veins. Higher in the stratigraphy there are dark, very fine-grained, laminar phyllite intercalations that are enriched in chlorite and sericite; these are most probably ash layers that may show soft sediment deformation.

The Matojärvi formation hosts several units of polymictic conglomerate or breccia that consist of fine-grained, sandy to clayey groundmass and deformed sub-rounded clasts of redbrick altered porphyritic rhyodacite, dark to reddish fine-grained mafic rocks and phyllite-mudstone. Iron ore clasts are also occasionally found in the conglomerate. In the central and northern parts of the Matojärvi formation there are thin conglomerate units where most of the clasts consist of hematite. Units with tuff or lava clasts within a hematite matrix are also found.

The conglomerate clasts are elongated along a foliation dipping 50-60° towards the S-SE. Strong calcite alteration is commonly seen as pore filling and cross-cutting veins within the conglomeratic layers.

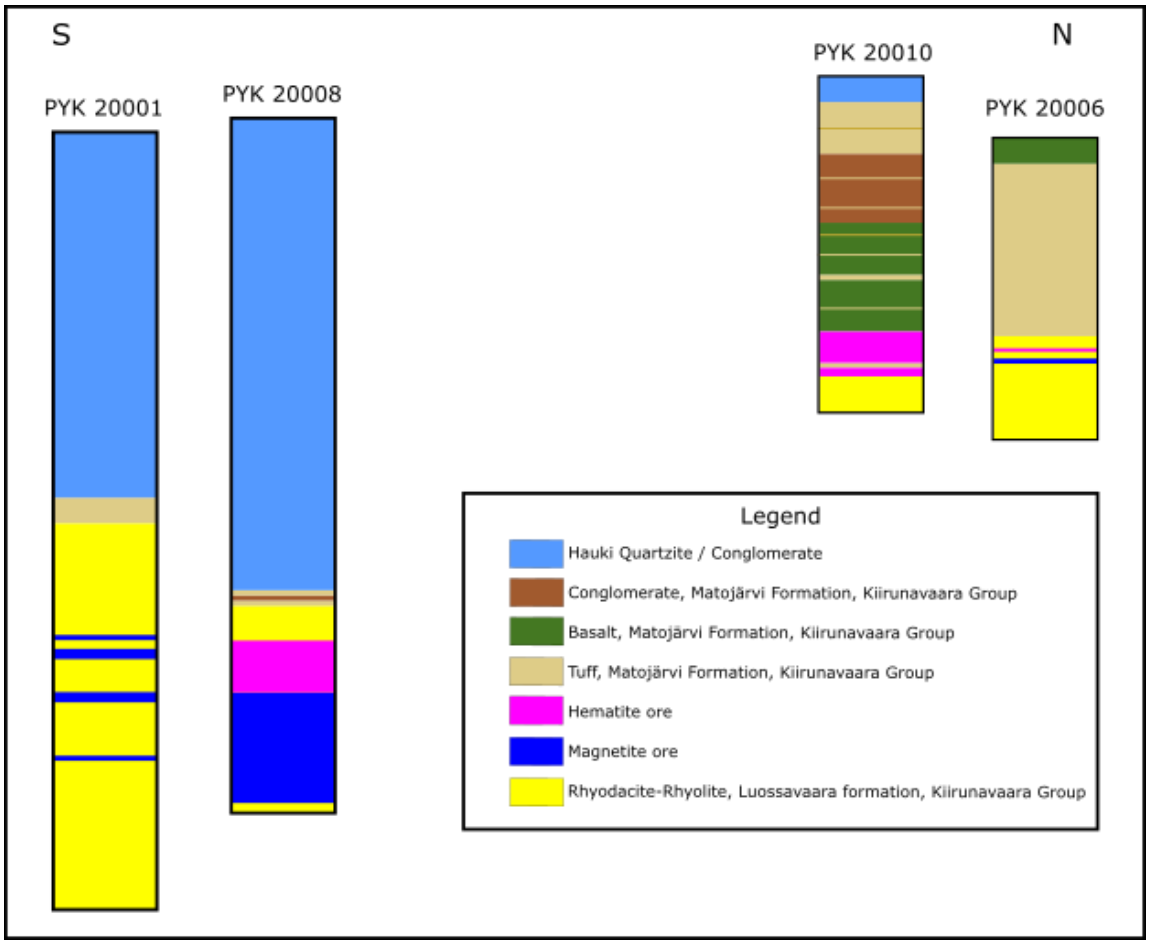

Figure 2. Schematic comparison of the thickness and stratigraphic sequence of the Matojärvi formation in some recent drill holes in the southern (PYK20001, PYK20008) and northern (PYK20006, PYK20010) parts of the Per Geijer area. The drill holes are marked in Figure 1.

The iron oxides are present as layers and lenses, located at different levels in the formation. The classical PG mineralizations are found at the contact of the Luossavaara and Matojärvi formations and higher up within the Matojärvi formation, with gradation from magnetite-dominant ore at depth to hematite dominant ore towards the top of the formation. The Lappmalmen orebody is found within the upper part of Luossavaara formation and is most probably intrusive. A difference in gangue mineralogy is visible between the two types of mineralizations: in the deep magnetite-dominated parts there are apatite veins and disseminations with minor calcite veining, whereas the hematite-dominated parts higher up in the stratigraphy are intersected by a high amount of calcite veins and specularite veinlets in addition to apatite. Sulfides are commonly seen in the calcite veins.

The dominant alteration type throughout the Matojärvi formation is the strong redbrick alteration that is associated with all types of iron oxides. This alteration type was first described in the hanging wall of the Rektorn IOA deposit, resulting in the name Rektorn Porphyry that was originally described as an altered rhyolitic unit. However, based on new logging and

geochemical data we consider the Rektorn Porphyry to be an alteration zone, which affects the wall rocks of the mineralized zones and it thus does not represent a single rock unit. The redbrick alteration is in many places so intense that it prevents visually distinguishing the lithologies that the alteration is overprinting. In the most altered zones, the textures and structures in the rocks are barely visible or unrecognizable. Trace element geochemical data is needed to ascertain the precursor of the alteration.

The whole Matojärvi formation was affected by high strain deformation that was mostly brittle (with associated slickenside faults/microfaults); the upper contact with the Hauki quartzite is generally strongly sheared, brecciated and faulted. Directly underneath the sheared contact, folds, soft sediments structures and foliations with varying orientations can also be found. More data is needed for a comprehensive structural geological interpretation of the Per Geijer area.

3. Conclusions

Considering the ore forming processes related to the PG IOA ores, understanding the building of the Matojärvi formation and the magmatic and hydrothermal alteration processes involved is crucial. We consider most of the formation to have been formed by volcanic processes and prolonged hydrothermal activity associated with them. New drilling, geochemical data and structural interpretation allow us to more precisely define lateral variations within the formation and work towards an updated stratigraphic interpretation of the Matojärvi formation, which represents the final volcanic phase in the Kiirunavaara group.

References:

Martinsson, O., 2004. Geology and Metallogeny of the Northern Norrbotten Fe-Cu-Au Province. SEG Guidebook Series, Vol. 33, 131−148.

Martinsson, O., Erlandsson, M., 2009. Fältarbete 2006-2008: objekt Lappmalmen. GeoVista Ab, Internal Consultant report GV 09018.

Fractional crystallization of massif-type anorthosite parental magmas and equilibrium crystallization of monzodioritic residual magmas

R. Fred[1], A. Heinonen[1] and J.S. Heinonen[1]

[1]Department of Geosciences and Geography, University of Helsinki, Gustaf Hällströmin katu 2, PL64, 00014 Helsinki
E-mail: Corresponding. riikka.fred@helsinki.fi

Our study describes different crystallization processes responsible for observed compositional evolution and Mg-poor mafic mineral compositions of the monzodioritic rocks related to massif-type anorthosites in the Ahvenisto complex. We suggest that the Mg-poor mafic mineral compositions were produced in equilibrium crystallization of individual monzodioritic magma batches and that the compositional evolution of the monzodioritic rocks was controlled by fractional crystallization of the anorthositic cumulates.

Keywords: Massif-type anorthosites, monzodiorites, mineral-melt equilibrium, crystallization modelling

Massif-type anorthosites (Ashwal and Bybee 2017) are igneous cumulate rocks often found in AMCG (anorthosite-magnerite-charnokite-granite) complexes with three main lithological groups: 1) anorthosites and mafic rocks, 2) monzodioritic rocks (also referred to as jotunites, ferrodiorites, ferrogabbros, and monzonorites), and 3) granitoids (Emslie et al. 1994). The source for the anorthosite parental magmas is presumed to be either the mantle (e.g., Mitchell et al. 1995, Frost and Frost 1997) or the lower crust (Duchesne et al. 1999). Regardless of the source, the anorthosite parental magmas have undergone polybaric fractional crystallization at different crustal levels until final emplacement at 5–10 km depth in the upper crust (e.g., Duchesne et al. 1999, Charlier et al. 2010, Heinonen et al. 2020). Several studies agree that the magmas have undergone significant crustal assimilation based on their isotopic signatures (Mitchell et al 1995).

Fe-Ti-P-enriched mafic to intermediate rocks (monzodiorites and oxide-apatite-gabbronorites, OAGNs) are found as small intrusions associated with the anorthositic cumulates in most AMCG suites. The OAGNs contain significant amounts of Fe-Ti-oxides, apatite, and mafic phases (pyroxenes + olivine) and are often presumed to represent fractionates of highly differentiated magmas in the evolution of the suites (McLelland 1994). The origin of the anorthosite-associated monzodioritic rocks is still debated, and several options for their origin have been proposed. Most likely they represent either anorthosite parental magmas or residual magmas left after anorthosite fractionation (Bybee et al. 2015 and references therein). Regardless of the origin of the monzodiorites, they are usually fine-grained, contain more mafic minerals compared to the anorthositic cumulates, and thus, are often presumed to represent near melt compositions (Emslie et al. 1990).

The 1.64 Ga Ahvenisto anorthosite complex, SE Finland, comprises a granitic intrusion surrounded by an anorthositic arc (Alviola et al. 1999). In the Ahvenisto complex, the monzodioritic rocks occur as minor dike-like lenses closely associated with the anorthositic rocks (e.g. Alviola et al. 1999; Fred et al. 2019). New field, petrographic, and geochemical (XRF, ICP-MS, EMPA) data for the monzodioritic rocks, apatite-oxide-gabbronorite (similar

to OAGN but referred to as apatite-oxide-gabbronorite in this study, see Fred et al. 2020), and olivine-bearing anorthositic rocks complemented with crystallization modelling [rhyolite-MELTS (Gualda et al. 2012), MAGFRAC (Morris, 1984)] provided new insight into the complicated crystallization history of the Ahvenisto complex (Fred et al. 2020). Our study suggests that the monzodioritic rocks closely represent melt compositions while the apatite-oxide-gabbronorite and olivine-bearing anorthositic rocks are cumulates (Fred et al. 2020). As presumed in previous studies (Fred et al. 2019), the monzodioritic rocks seem to form a liquid line of descent (LLD) from primitive olivine monzodiorites to more evolved monzodiorites (Figure 1; Fred et al. 2020, see also Fred et al. 2019). The mafic minerals (pyroxenes and olivine), however show remarkably low Mg/Fe ($En_{48–63}$, $Mg\#(cpx)_{60–69}$, $Fo_{25–45}$) compared to the corresponding whole-rock compositions (Mg# 42–52), although they seem to form a compositional evolution trend parallel to the LLD (Figure 2; Fred et al. 2020).

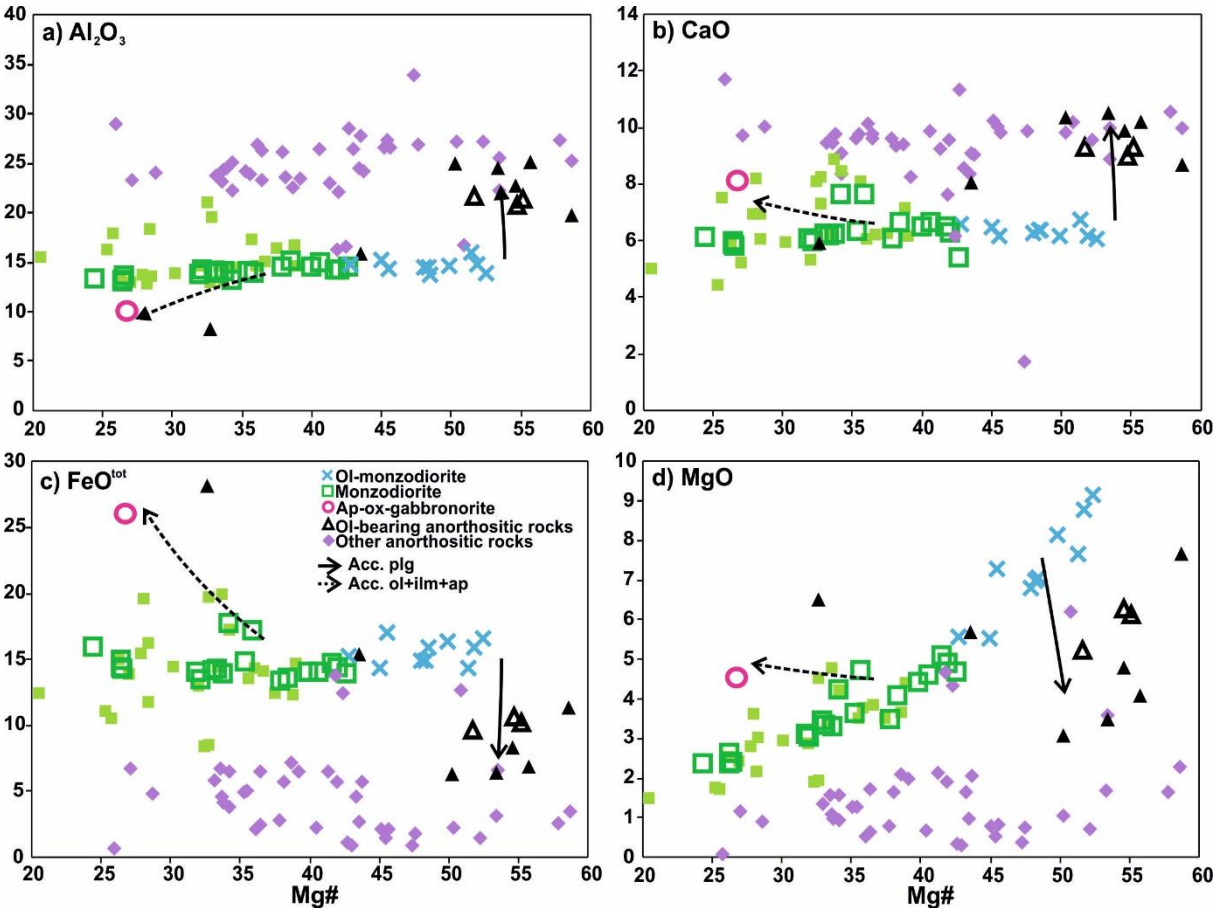

Figure 1. Major element variation diagrams of Mg# [$Mg^{2+}/(Mg^{2+}+Fe^{2+})*100$] vs. a) Al_2O_3, b) CaO, c) FeO_{tot}, and d) MgO for the Ahvenisto complex monzodioritic rocks, olivine-bearing anorthositic rocks, and apatite-oxide-gabbronorite showing the compositional evolutionary trend (liquid line of descent, LLD) of the monzodioritic rocks. The accumulation of plagioclase in anorthositic rocks is indicated with black solid arrows, and accumulation of oxide, apatite, and olivine (in 1:1:5, respectively) in apatite-oxide-gabbronorite is indicated with black dashed arrows. The other anorthositic rocks refer to anorthositic rocks without any olivine. Modified after Fred et al. (2020).

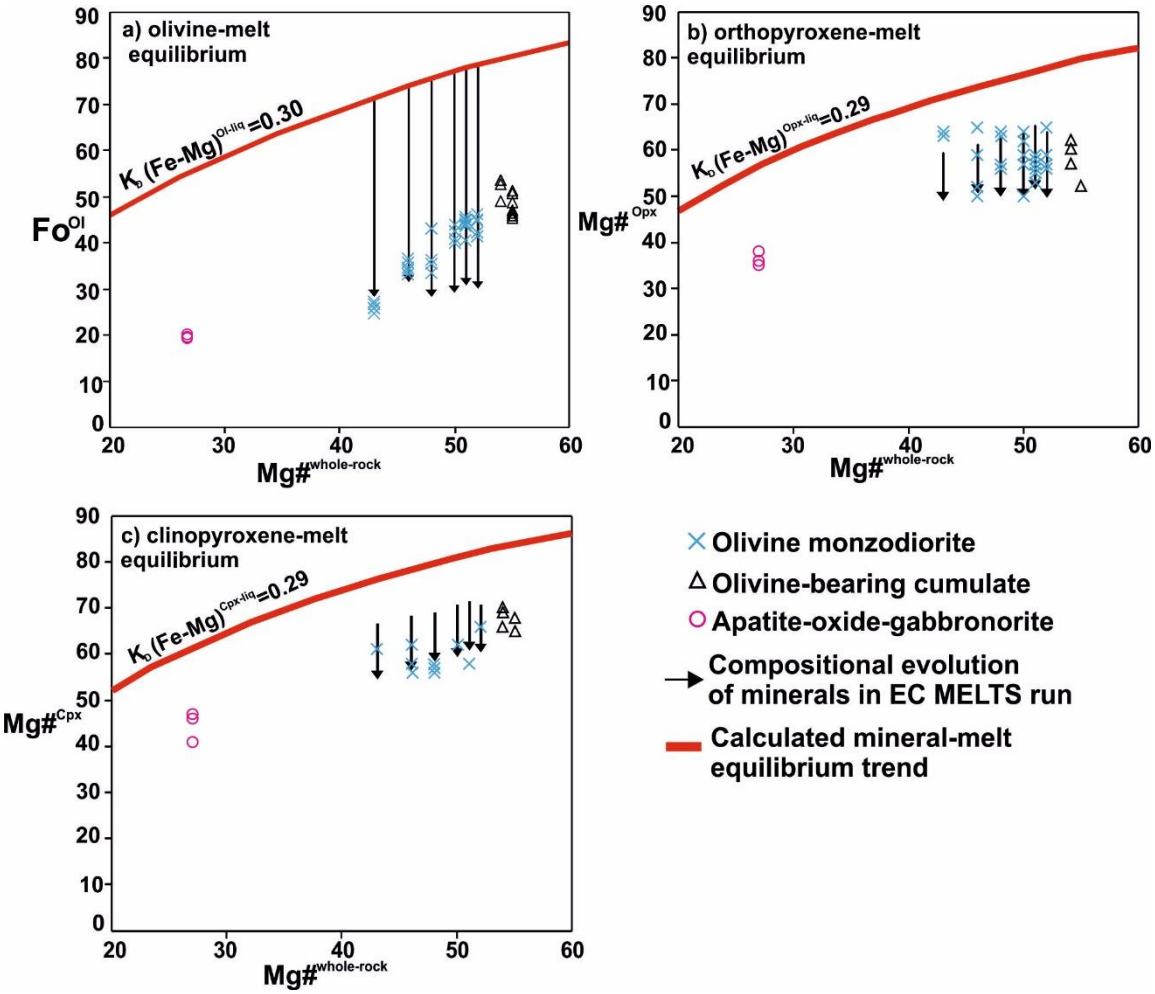

Figure 2. Mafic mineral compositions of olivine monzodiorites, olivine-bearing anorthositic rocks, and apatite-oxide gabbronorites shown in a) olivine-melt, b) orthopyroxene-melt, and c) clinopyroxene-melt Fe-Mg equilibrium diagrams (Roeder and Emslie 1970). The figures illustrate the low Fe/Mg of the minerals compared to corresponding measured whole-rock compositions. The range of evolving mineral compositions of modelled olivine-monzodiorites resulting from equilibrium crystallization models conducted with rhyolite-MELTS version 1.2.0 (Gualda et al. 2012) is indicated with black arrows. The red line indicates the calculated mineral-melt equilibrium trend. Modified after Fred et al. (2020).

Petrological modelling of the Ahvenisto complex rocks suggests that the interpreted monzodiorite LLD corresponds to a residual melt trend left after fractional crystallization (FC) and formation of the cumulate anorthositic rocks and apatite-oxide-gabbronorite in shallow magma chambers (Fred et al. 2020). Equilibrium crystallization (EC) of separate monzodioritic residual magma batches can produce the observed mineral assemblages of the observed rocks and the low Mg-numbers measured from the mafic minerals (Fred et al. 2020). The monzodioritic and anorthositic rocks and apatite-oxide-gabbronorites of the Ahvenisto complex show similar petrological and geochemical characteristics to corresponding rock types in other AMCG suites suggesting that they formed by similar crystallization processes and that the model described here could be applicable to them as well (Fred et al. 2020).

References:

Alviola, R., Johanson, B.S., Rämö, O.T., Vaasjoki, M., 1999. The Proterozoic Ahvenisto rapakivi granite-massif-type anorthosite complex, southeastern Finland; petrography and U-Pb chronology. Precambrian Research 95, 89–107.

Ashwal, L.D., Bybee, G.M., 2017. Crustal evolution and the temporality of anorthosites. Earth-Science Reviews 173, 307–330.

Bybee, G.M., Ashwal, L.D., Gover, C.F., Hamilton, M.A., 2015. Pegmatitic Pods in the Mealy Mountains Intrusive Suite, Canada: Clues to the Origin of the Olivine-Orthopyroxene Dichtomy in Proterozoic Anorthosites. Journal of Petrology 56, 845-868.

Charlier, B., Duchesne, J.C., Vander Auwera, J., Storme, J.Y., Maquil, R., Longhi, J., 2010. Polybaric Fractional Crystallization of High-Alumina Basalt Parental Magmas in the Egersund-Ogna Massif-type Aorthosite (Rogaland, SW Norway) Constrained by Plagioclase and High-alumina Orthopyroxene Megacrysts. Journal of Petrology 51, 12, 2515–2546. Duchesne, J.C., Liégeois, J.P., Vander Auwera, J., Longhi, J., 1999. The crustal tongue melting model and the origin of massif anorthosites. Terra Nova 11, 100–105.

Emslie, R.F., Hamilton, M.A., Thériault, R.J., 1994. Petrogenesis of a Mid-Proterozoic anorthosite-mangerite-charnockite-granite (AMCG) complex: isotope and geochemical evidence from the Nain Plutonic suite. Journal of Geology 102, 539–558.

Fred, R., Heinonen, A., Heikkilä, P., 2019. Tracing the styles of mafic-felsic magma interaction: A case study from the Ahvenisto igneous complex, Finland. Bulletin of the Geological Society of Finland 91, 5–33.

Fred, R., Heinonen, A., Heinonen, J.S., 2020. Equilibrium crystallization of massif-type anorthosite residual melts: a case study from the 1.64 Ga Ahvenisto complex, Southeastern Finland. Contributions to Mineralogy and Petrology 175.

Frost, C.D., Frost, B.R., 1997. Reduced rapakivi-type granites: The tholeiite connection. Geology 25, 647–650.
Gualda, G.A., Ghiorso, M.S., Lemons, R.V., Carley, T.L. 2012. Rhyolite-MELTS: a modified calibration of MELTS optimized for silica-rich, fluid-bearing magmatic systems. Journal of Petrology, 53, 875–890.

Heinonen A., Kivisaari, H., Michallik, R.M., 2020. High-aluminum orthopyroxene megacrysts (HAOM) in the Ahvenisto complex, SE Finland and the polybaric crystallization of massif-type anorthosites. Contributions to Mineralogy and Petrology 175:10.

McLelland, J., Ashwal, L., Moore, L., 1994. Composition and petrogenesis of oxide-, apatite-rich gabbronorites associated with Proterozoic anorthosite massifs: examples from the Adirondack Mountains, New York. Contributions to Mineralogy and Petrology 116, 225-238.

Mitchell, J.N., Scoates, J.S., Frost, C.D., 1995. High-Al gabbros in the Laramie Anorthosite Complex, Wyoming: implications for the composition of melts parental to Proterozoic anorthosite. Contributions to Mineralogy and Petrology 119, 166–180.

Morris, P.A., 1984. Magfrac: A basic program for least-squares approximation of fractional crystallization. Computers & Geosciences 10, 437–444.

Roeder, P.L., Emslie, R.F., 1970. Olivine-liquid equilibrium. Contributions to Mineralogy and Petrology 29, 275–289.

Impact structures as indicators of cratonic denudation

S. Hietala[1,2], A. M. Hall[3], N. Putkinen[4], E. Lindsberg[2] and M. Holma[5-7]

[1]Department of Geology, University of Tartu, Ravila 14A, 50411 Tartu, Estonia
[2]Geological Survey of Finland, P.O. Box 1237, FI-70211, Kuopio, Finland
[3]Department of Physical Geography, Stockholm University, S-10691 Stockholm, Sweden
[4]Geological Survey of Finland, P.O. Box 97, FI-67101, Kokkola, Finland
[5]Muon Solutions Oy, Rakkarinne 9, FI-96900, Saarenkylä, Finland
[6]Kerttu Saalasti Institute, University of Oulu, Pajatie 5, 85500 Nivala, Finland
[7]Arctic Planetary Science Institute, Lihtaajantie 1 E 27, 44150 Äänekoski, Finland
E-mail: satu.hietala@ut.ee

Meteorite impact structures can provide important information on long-term denudation on the Earth's cratons. Impact structures in the Fennoscandian Shield contain rocks (i.e., impactites), that have developed during the collision, and, possibly, remnants of the pre-impact sedimentary rocks. The crater depressions may also be filled with post-impact sediments. Sedimentary deposits in impact structures have not been much utilized before in studying the erosion-burial history of the Fennoscandian craton. Here, we use published data on meteorite impact structures to reconstruct the depth of erosion in southern Finland and neighboring platform areas. Post-impact erosion depths were estimated using an empirical relationship derived from well-preserved impact structures. Results support ultra-slow erosion of the basement and sedimentary cover continuing over hundreds of millions of years.

Keywords: Fennoscandian Shield, unconformity, meteorite impact structure, erosion, sedimentary rocks, denudation.

1. Introduction

Terrestrial meteorite impact cratering is an important geological process. Around ~200 impact structures (IMPs) are proven globally (Schmieder and Kring, 2020). The Fennoscandian Shield hosts ~17% of them whereas in Finland 12 structures are proven. The remarkable concentration of IMPs in Finland is mainly a result of the re-exposure of an extensive bedrock denudation surface, the Cambrian unconformity, and temporary burial of IMPs under the protective cover of sedimentary rocks.

Meteorite impact structures always contain breccias, but some of the structures include sedimentary rocks as well. Several small craters in Fennoscandia (Sääksjärvi, Lumparn, Karikkoselkä, Söderfjärden, Iso-Naakkima, Saarijärvi, Suvasvesi N, Neugrund, Kärdla, Lockne, Mishina Gora, and Jänisjärvi) hold remnants of post-impact sedimentary rocks or traces of pre-impact sedimentary cover. Most of the IMPs in Fennoscandia are <10 kilometers in diameter with Neoproterozoic to Upper Palaeozoic ages. In many cases, the inner structure has been studied by drilling and/or geophysical studies. Impact craters have suffered erosion of various intensity depending much on their size and age. We use this dataset to estimate erosion depths across southern Finland and its surroundings through the Neoproterozoic and Phanerozoic.

2. Study methods

We calculated erosion depths based on geometries and ages of proven IMPs in the region. Altogether, we used data on 21 simple and complex IMPs in Finland, Sweden, Estonia, and Russia (Figure 1). We applied the method of Degeai and Peulvast (2006) that is based on the empirical relationship between the original diameter (D) and original depth (dt) derived from

well-preserved IMPs on Earth (Figure 2). Original depth is derived from values of maximum and minimum depth, taking into account the uncertainties (>30%) that exist in estimating depth in the global dataset due to differences between terrestrial and marine target settings, target material, and impact trajectories. The total post-impact erosion depth (*ed*) since the impact is derived by subtraction of breccia base elevation below present (*dp)* from *dt*. If *dp* is unknown, the maximum depth of the rock sequence lost to erosion is constrained by *dt* only (Figure 2). The rate of erosion is averaged for the time since impact.

3. Results

The large Keurusselkä IMP in south-central Finland has a $^{40}Ar/^{39}Ar$ date of 1150 ± 10 Ma (Schmieder et al. 2016). The original diameter has been between 14 and 36 km (Hietala and Moilanen, 2007; Osinski and Ferriére, 2016; Raiskila et al. 2011). Today, the crater is eroded close to the base of its former breccia layer (Raiskila et al. 2013), indicating a post-impact erosion depth of 0.80–1.23 km. Thus, the long-time erosion rate is, considering the age, very low (<1 m/Ma).

The absence of small Mesoproterozoic IMPs likely reflects the protection of the basement beneath the sedimentary cover. Iso-Naakkima, only 130 km E of Keurusselkä (Figure 1), has a palaeomagnetic age of 1200–900 Ma (Pesonen et al. 1996). Considering the above erosion rate, the survival of this small (D = 2.5 km) crater is incompatible with erosion and the palaeomagnetic age is most likely overestimated. Microfossil evidence from the sediment sequence prefers rather the early Ediacaran age (Elo et al., 1993), and erosion depth can be explained if the youngest sediment is of post-impact age. Existence of this small crater can be accounted for by slow erosion in the Ediacaran and later burial. Also, the survival of the small (D = 3.8 km) IMP at Suvasvesi North dated to >710 Ma (Schmieder et al. 2016b) implies limited basement erosion during or since the Neoproterozoic.

Jänisjärvi is dated to 687 ± 5 Ma and it retains fragments of Neoproterozoic siltstone in breccias (Jourdan et al. 2012). Its *dp* is uncertain, but *dt* provides a maximum depth of erosion of 650 m. Söderfjärden (550–520 Ma) and Kärdla (455 Ma) have been buried since the formation and preserve original crater forms (Puura and Plado, 2005). Söderfjärden (D = 6.6 km) provides an estimate for *dt* of 390 m that compares to a drilled depth of 320 m (Lehtovaara, 1982; Öhman and Preeden, 2013) and recent seismic studies between 330–410 m of depth (Fennvik, 2018). At Kärdla (D = 4 km), the estimated *dt* is 290 m and the drilled depth of impact breccias is 220 m (Suuroja et al., 2002). At Söderfjärden the fine state of preservation of the crater rim indicates that this crater has been exhumed recently.

Two IMPs of the Triassic age, Karikkoselkä (Schmieder et al. 2010; Schwarz et al. 2015) and Paasselkä (Schwarz et al. 2015), show that the original depths of these structures constrain the maximum remaining depths of Palaeozoic sedimentary rock at the time of impact to 170–490 m. Lappajärvi 170 m of the sedimentary cover has been removed since 78 Ma, providing an average erosion rate of 2.2 m/Ma since impact. Results show also that Cenozoic erosion rates remained low.

4. Discussion and conclusions

Meteorite impact structures provide important evidence of burial and post-impact erosional histories (e.g., Masaitis, 2005; Puura and Plado, 2005) potentially spanning a prolonged period of time since they are not an immediate consequence of plate tectonic movements and subsequent thickening or thinning of the crust. In Finland, the sedimentary rocks preserved in IMPs indicate that (i) W and S Finland retained Early Palaeozoic cover through the Mesozoic, whereas (ii) in E Finland, Early Palaeozoic cover persisted in the Triassic, but the basement was re-exposed by the Late Cretaceous.

The absence of IMPs dated between 1150 and 710 Ma supports the former existence of protective sedimentary cover(s); perhaps including transient sedimentary cover derived from the Sveconorwegian orogenic belt. However, this cover may not have been thick: thickness of ≥640 m has been sufficient to protect the basement from any crater with $D \geq 10$ km. We note that the survival of small IMPs ($D \leq 5$ km) permits only limited depths of erosion ($dt \leq 300$ m). Altogether, the IMPs show that the Fennoscandian Shield has suffered ultra-slow erosion in the basement and sedimentary cover with rates to <2.5 m/Ma. This value is one of the lowest reported on Earth (see Hall et al. 2020).

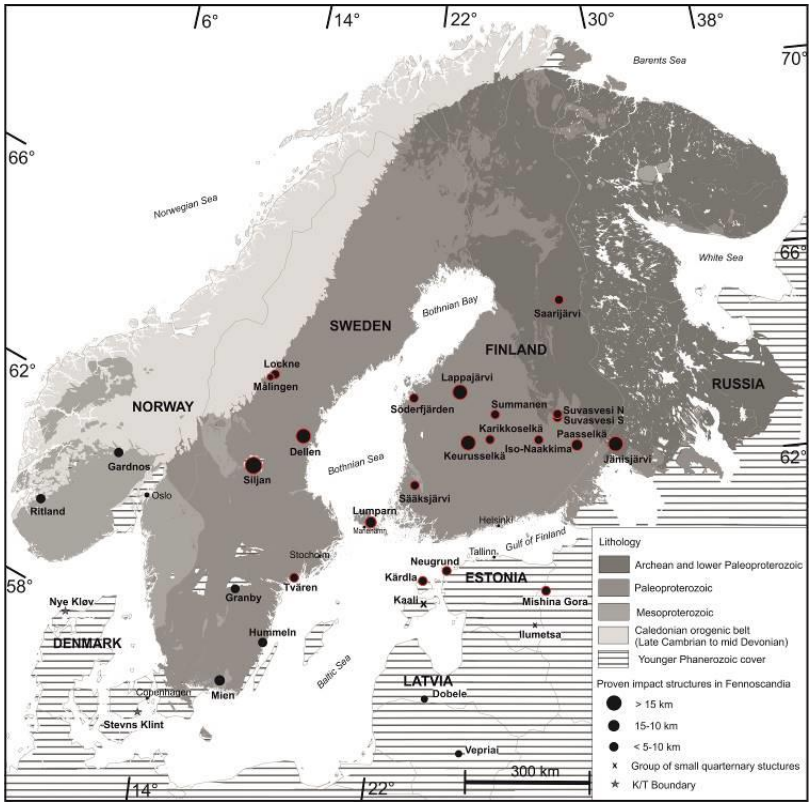

Figure 1. Bedrock map of the Fennoscandian Shield and proven impact structures. The studied impact structures are surrounded by red circles. Modified after Koistinen et al. (2001) and Plado & Pesonen (2002).

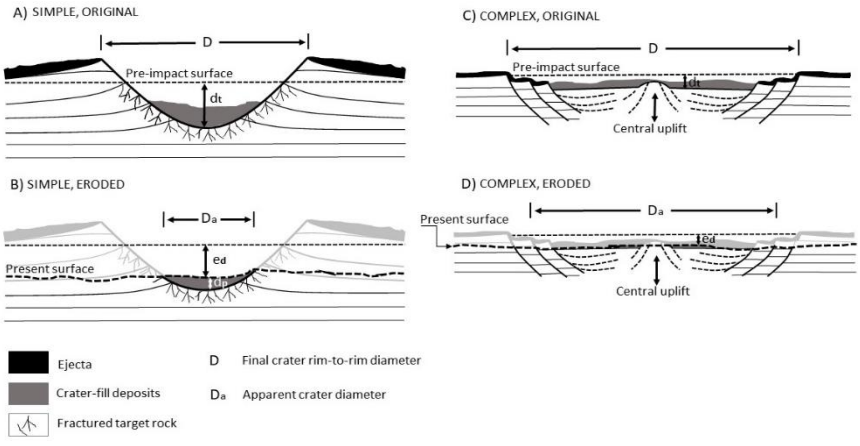

Figure 2. Models for simple and complex impact structures used to estimate post-impact erosion depths. Adapted from Degeai & Peulvast (2006), Osinski et al. (2018), Peulvast et al. (2009), and Turtle et al. (2005).

References:

Degeai, J.-P., Peulvast, J.-P., 2006. Calcul de l'érosion à long terme en région de socle autour de grands astroblèmes du Québec et de France. Géographie physique et Quaternaire 60, 131-148.

Elo, S., Kuivasaari, T., Lehtinen, M., Sarapää, O., Uutela, A., 1993. Iso-Naakkima, a circular structure filled with Neoproterozoic sediments, Pieksämäki, south-eastern Finland. Bulletin of the Geological Society of Finland 65, 3-30.

Fennvik, E., 2018. A shallow reflection seismic investigation and depth determination of Söderfjärden, an impact crater in western Finland. Master Thesis. University of Gothenburg. 34p.

Hall, A.M., Putkinen N., Hietala, S., Lindsberg, E., Holma, M., 2020. Ultra-slow cratonic denudation in Finland since 1.5 Ga indicated by tiered unconformities and impact structures, Precambrian Research (2020), doi: https://doi.org/10.1016/j.precamres.2020.106000 (*in press*)

Hietala, S., Moilanen, J., 2007. Keurusselkä-Distribution of shatter cones. Lunar and Planetary Science Conference, p. 1762.

Koistinen, T., Stephens, M., Bogatchev, V., Nordgulen, Ø., Wennerström, M., Korhonen, J., 2001. Geological map of the Fennoscandian Shield 1: 2 000 000, Espoo, Trondheim, Uppsala, Moscow. Geol surveys of Finland, Norway, Sweden, Ministry of Natural Resources, Russia.

Lehtovaara, J.J., 1982. Stratigraphical section through Lower Cambrian at Söderfjärden, Vaasa, western Finland. Bulletin of the Geological Society of Finland 54, 35-43.

Masaitis, V., 2005. Morphological, structural and lithological records of terrestrial impacts: an overview. Australian Journal of Earth Sciences 52, 509-528.

Osinski, G.R., Ferrière, L., 2016. Shatter cones:(Mis) understood? Science Advances 2, e1600616.

Osinski, G.R., Grieve, R.A., Bleacher, J.E., Neish, C.D., Pilles, E.A., Tornabene, L.L., 2018. Igneous rocks formed by hypervelocity impact. Journal of Volcanology and Geothermal Research 353, 25-54.

Pesonen, L.J., Järvelä, J., Sarapää, O., Pietarinen, H., 1996. The Iso-Naakkima meteorite impact structure: physical properties and paleomagnetism of a drill core. Meteorit. Planet. Sci. Suppl. 31, 105–106.

Peulvast, J.-P., Claudino Sales, V., Bétard, F., Gunnell, Y., 2008. Low post-Cenomanian denudation depths across the Brazilian Northeast: Implications for long-term landscape evolution at a transform continental margin. Global and Planetary Change 62, 39-60.

Plado, J., Pesonen, L. J. (Eds)., 2002. Impacts in Precambrian Shields.: Impact Studies Series. xiii + 336 pp. Berlin, Heidelberg, New York: Springer-Verlag.

Puura, V., Plado, J., 2005. Settings of meteorite impact structures in the Svecofennian crustal domain, in: Koeberl, C., Henkel, H. (Eds.), Impact tectonics. Springer, pp. 211-245.

Raiskila, S., Plado, J., Ruotsalainen, H., Pesonen, L., 2013. Geophysical Signatures of the Keurusselkä. Meteorite Impact Structure-Implications for Crater Dimensions. Geophysica 49.

Raiskila, S., Salminen, J., Elbra, T., Pesonen, L.J., 2011. Rock magnetic and paleomagnetic study of the Keurusselkä impact structure, central Finland. Meteoritics & Planetary Science 46, 1670–1687.

Schmieder, M., Kring, D.A., 2020. Earth's Impact Events Through Geologic Time: A List of Recommended Ages for Terrestrial Impact Structures and Deposits. Astrobiology 20, 91-141.

Schmieder, M., Jourdan, F., Moilanen, J., Buchner, E., Öhman, T., 2016. A Late Mesoproterozoic 40Ar/39Ar age for a melt breccia from the Keurusselkä impact structure, Finland. Meteoritics & Planetary Science 51, 303-322.

Schmieder, M., Schwarz, W.H., Buchner, E., Trieloff, M., Moilanen, J., Öhman, T., 2010. A Middle-Late Triassic 40Ar/39Ar age for the Paasselkä impact structure (SE Finland). Meteorit. Planet. Sci. 45, 572–582.

Schmieder, M., Schwarz, W.H., Trieloff, M., Buchner, E., Hopp, J., Tohver, E., Pesonen, L. J., Lehtinen, M., Moilanen, J., Werner, S.C., Öhman, T., 2016b. The two Suvasvesi impact structures, Finland: Argon isotopic evidence for a "false" impact crater doublet. Meteorit. Planet. Sci. 51, 966–980.

Suuroja, K., Suuroja, S., All, T., Floden, T., 2002. Kärdla (Hiiumaa Island, Estonia)—the buried and well preserved Ordovician marine impact structure. Deep Sea Research Part II: Topical Studies in Oceanography 49, 1121-1144.

Schwarz, W.H., Schmieder, M., Buchner, E., Trieloff, M., Moilanen, J., Öhman, T., 2015. A Carnian 40Ar/39Ar age for the Paasselkä impact structure (SE Finland)—an update. Meteorit. Planet. Sci. 50, 135–140.

Turtle, E., Pierazzo, E., Collins, G., Osinski, G., Melosh, H., Morgan, J., Reimold, W., 2005. Impact structures: What does crater diameter mean? Geological Society of America Special Papers 384, 1-24.

Öhman, T., Preeden, U., 2013. Shock metamorphic features in quartz grains from the Saarijärvi and Söderfjärden impact structures, Finland. Meteoritics & Planetary Science 48, 955–975.

Finnish crustal-scale faults as a possible source of deep low-enthalpy geothermal resources

M. Holma[1,2,3], T. Arola[4] and P. Kuusiniemi[3]

[1]Kerttu Saalasti Institute, University of Oulu, Nivala, Finland
[2]Arctic Planetary Science Institute, Äänekoski, Finland
[3]Muon Solutions Oy, Saarenkylä, Finland
[4]Geological Survey of Finland, Espoo, Finland
E-mail: marko.holma@oulu.fi

Crustal-scale faults deserve more attention as potential deep low-enthalpy geothermal energy sources in Finland. As well known, major structures may behave as favourable permeability channels for meteoric waters. They may also be characterised by elevated geothermal gradients, although the opposite is also possible. For Enhanced Geothermal System (EGS) exploration projects, major faults may offer an alternative target potentially requiring much less hydraulic stimulation than conventional EGS projects.

Keywords: crust, faults, geothermal energy, geothermal exploration, heat storage, muography

1. Introduction

The advantages of geothermal energy compared to many other renewable energy sources (e.g., wind and solar) are numerous and support attempts to decarbonate the world's energy production. This natural energy source has a great and yet only marginally developed potential. In addition, it is available around the clock ubiquitously and in an environmentally friendly manner. It is also economically rewarding energy. There are three types of deep geothermal systems: (1) hydrothermal convective systems; (2) enhanced geothermal systems (also referred to as 'hot dry rock' systems); and (3) hot aquifers. Furthermore, geothermal systems are classified as high (above 150°C) or low (less than 150°C) enthalpy. The thermal energy extracted from the high-enthalpy systems allows direct production of electricity, but the low-enthalpy systems are inefficient in this conversion and that is why they are mainly used for direct heating.

Conventional geothermal systems are hydrothermal convective systems characterised by surface geothermal features such as fumaroles, hot springs, steaming ground, mud pools, and geysers, or just known thermal anomalies. Unfortunately, the Precambrian crystalline cratonic lithosphere of Finland is cold and hence totally unattractive from the viewpoint of conventional high-enthalpy geothermal exploration. Instead, bedrock of Finland is far from active volcanoes, tectonic plate boundaries, and other regions of high crustal heat flow. The metamorphically recrystallised bedrock is also dry, hard and has a low porosity (i.e., rocks are characterised by low fluid permeability, which is unfavourable for geothermal systems).

The current solution in Finland is to go deeper. Several deep geothermal projects are in the planning phase in Finland. For example, the St1 Deep Heat project has achieved to drill two boreholes over 6 km depth and managed to perform successful enhanced (or engineer) geothermal system (EGS) stimulation test (Kwiatek et al. 2019). In an EGS (Olasolo et al. 2016) project at crystalline bedrock, natural fracture network is stimulated to increase the permeability. However, the attempt is not to create new fractures to crystalline basement rock.

In this contribution, the focus is on the crustal-scale faults in Finland and their potential to host deep low-enthalpy geothermal resources. In the literature, these are often referred as hot

aquifer geothermal systems. Sadly, bedrock in Finland is cold and topography of the typical Finnish landscape is subdued and thus advective geothermal cells where groundwater can circulate and become heated are hard to come by (Kukkonen, 2000). Nevertheless, geothermal heat is available even in these conditions if one only knows where to look for and has the technical capabilities (and a budget) to reach for it. We propose that faults as potential aquifers deserve more attention in Finland.

2. Conventional methods used in geothermal exploration

Like in mineral exploration, oil & gas exploration and water exploration, exploration of active geothermal systems essentially involves applications from of a number of geological, geochemical, and geophysical techniques. Geological studies may include, for example, surface geological mapping, structural geological modelling, stress field analysis, geomechanical studies, and test drilling. Different geochemical and geophysical methods are reviewed, for example, in the "Best practices guide for geothermal exploration" (IGA Service GmbH, 2014). Holma et al. (2021) introduces a new technique called muography to the geothermal community in Finland. In certain circumstances, this novel density-variation sensitive method has potential in this field of research, as already demonstrated by Tanaka et al. (2011) and Tanaka and Sannomiya (2013). It is noteworthy, however, that many of these methods are not necessarily suitable for areas having similar 'cold' geology as Finland.

3. Structural controls on underground flow of meteoric water

Favourable geothermal reservoirs are often characterised by interactions of fluids moving along fractures in bedrock like, for example, in Menderes Graben in Western Turkey (Faulds et al. 2009). Wherever the faults intersect, thermally heated meteoric water can migrate either vertically or laterally, or both. At locations of increased permeability, hot springs occur as a manifestation of the underlying high-enthalpy geothermal field (the famous Pamukkale is one of these). However, in most places there is no evidence of the underlying geothermal deposit on the surface. In Finland, all geothermal resources are blind and of low enthalpy (i.e., they lack surface expression) due to low contemporaneous heat flow.

Concerning crustal-scale fault zones, evidence from other parts of the world indicates that major structures are often favourable for high-enthalpy geothermal heat energy (e.g., Bächler et al. 2003; Garibaldi et al. 2010). There are many reasons for this. First, faults and fracture zones crosscutting crystalline bedrock have an enhanced permeability comparing to their less deformed surrounding lithologies. Indeed, faults and fractures accelerate introduction of surficial waters to depth, as well known by underground miners that have to pump water constantly to prevent flooding of their tunnels. Hence, major fault zones favour development of the deep (bedrock) aquifers. Second, the water is heated to the temperature of the surrounding heat gradient. This happens regardless how the water is introduced to its site of residence in the crust (i.e., actively by industrial-scale pump station or passively by natural drainage of surface water along structural failures in rocks). In the Rhine Graben, for example, contemporaneous water temperatures at the depths of 500 m and 1000 m are 20-40°C higher than expected, suggesting that the given fault zone reaches at least 3 km depth and controls a major convective vertical fluid flow system (Bächler et al. 2003). Younger et al. (2012) report a nearly 1 km deep geothermal energy exploration borehole drilled in the UK in 2004 deliberately to a large fault zone. This new approach was in a drastic contrast with the earlier investigations based on the EGS concept. However, the result was a success as the borehole discovered permeability levels Younger et al. (2012) believed to be the highest natural permeabilities ever found in granite anywhere in the world. The bottom-hole water temperature at 995 m was 46.2°C yielding a

geothermal gradient estimate of around 3.88°C per 100 m. The heat flux (heat-flow density) from the granite was calculated to be 115 mW/m^2. In Finland, the measured heat flux in the uppermost 1 km of bedrock range from very low values of <15 mW/m^2 to 69 mW/m^2, while temperatures vary between 14 to 22°C at 1 km depth (Kukkonen, 2000). Based on extrapolated data and thermal modelling, temperatures exceeding 40ºC should be encountered at 1-1.5 km depth in Finland. Due to the fact that these numbers are far from those encountered at ~1 km depth in the project area described by Younger et al. (2012), we propose that the best project areas are likely there where the targeted fault zone is covered by a sequence of rocks of poor thermal conductivity forming an elevated geothermal gradient below. The Muhos Graben, delineated by fracture and fault zones (Kohonen and Rämö, 2005), is an example of such geological domains in Finland.

4. Concluding remarks

Finland is located in an ancient cratonic shield area where geothermal energy is not as readily available as it is in countries like Iceland, Italy, Turkey, and New Zealand, where high-enthalpy geothermal systems are a well-known source of energy, including electricity production. Geothermal energy can nevertheless be harnessed in various ways and one of them is to tap into an enormous low-enthalpy heat source of the shallow crust. This is done in projects following the EGS concept. Some of the typical problems of EGS projects include microseismic events triggered by active hydraulic stimulation, which some people consider disturbing, especially if they occur during nights. Induced seismicity has been the cause of delays and threatened cancellation of several EGS projects worldwide (Majer et al. 2007). Normally, in EGS projects, the exploration and production heat wells are directed towards structurally relatively simple bedrock volumes in an effort to avoid technical problems in drilling. We propose, as summarised below, a tweak to this standard project outline.

Geothermal energy is not suffering from the intermittency issues associated with variable renewables like wind and solar energy. Hence it is an ideal renewable resource for power production and especially for heating. We believe that there is a need in Finland for conceptual modelling, numeric simulations, and field testing of a geothermal EGS project in which the target for deep low-enthalpy geothermal energy is deliberately chosen to be a major structurally broken zone, instead the currently favoured model in which the target is relatively non-fractured. This concept mixes warm aquifer (or, ideally, hot aquifers) and EGS concepts in an attempt to generate district heat (and possibly to provide heat storage opportunities) and to diminish the need for prolonged hydraulic stimulation. The first step in testing this concept could be done by investigating the concept with a small-scale pilot. On a larger scale, the target could be a known major structure that crosscuts nearby a settlement interested in geothermal energy and potentially also in heat storage. The directional drilling method could be used at the test drilling stage to locate the targeted structure(s) at depth. This way, theoretically speaking, the problem relating to low permeability could be lessened, and the time and resources put to stimulation of pre-existing fractures (potentially) cut.

We naturally recognise many inherited problems in the above-described concept. These include higher risk for induced seismicity than those in the areas of solid rock and that there may be too much of the heat-transferring water lost to a major fault zone due to uncontrolled dimensions of the natural fracture network. In Finland, however, this may not be as significant a problem as in some other, less water-blessed countries. There are also other challenges, such as technical problems with drilling itself and potential unwanted impurities in water that interacts with faulted rocks at depth. In addition, resource cooling due to cool meteoric water may also result in problems for long-term heating energy production. This risk may be notable

where active hydrothermal systems do not occur (like in Finland). Owing to these problems and challenges, more conceptual work with multidisciplinary approach is needed (e.g., numeric simulations). In practical tests, geophysical methods are useful in selecting fault zones that are mid-sized (to lessen likelihood of severe water loss) and also otherwise favourable (e.g., located far from intersections of major structures to avoid uncontrollable fluid loss, and well oriented with respect to stress field). If possible, attention must also be paid for structural geological, microfabric, and seismic analysis to find out if any of the faults in a given region of interest contain evidence of geologically young activity. This may be important as the fault reactivation (Sibson, 1989) may have increased the permeability by re-opening ancient, sealed fractures (Laubach et al. 2014). Bense et al. (2013) discuss in detail about fault zone hydrogeology and fault zone processes that either increase or reduce permeability. We further propose that the novel geophysical method called muography could be used in geothermal resource assessment and aiding drilling to the most desirable structures in depth (for details, see Holma et al. 2021).

References:

Bächler, D., Kohl, T., Rybach, L., 2003. Impact of graben-parallel faults on hydrothermal convection - Rhine Graben case study. Physics and Chemistry of the Earth 28(9-11), 431-441.

Bense, V.F., Gleeson, T., Loveless, S.E., Bour, O., Scibek, J., 2013. Fault zone hydrogeology. Earth-Science Reviews 127, 171-192.

Faulds, J.E, Bouchot, V., Moeck, I., Oĝuz, K., 2009. Structural Controls on Geothermal Systems in Western Turkey: A Preliminary Report. GRC Transactions 33, 375-382.

Garibaldi, C., Guillou-Frottier, L., Lardeaux, J.-M., Bonte, D., Lopez, S., Bouchot, V., Ledru, P., 2010. Thermal anomalies and geological structures in the Provence basin: Implications for hydrothermal circulations at depth. Bulletin de La Societe Geologique de France 181(4), 363-376.

Holma, M. & Kuusiniemi, T., 2021. Cosmic-ray based geothermal exploration - A short introduction to muography. Lithosphere 2018 – Eleventh Symposium on the Structure, Composition and Evolution of the Lithosphere. Programme and Extended Abstracts. Institute of Seismology, University of Helsinki. *This publication.*

IGA Service GmbH, 2014. Best practices guide for geothermal exploration. IGA Service GmbH, c/o Bochum University of Applied Sciences (Hochschule Bochum), 196 p.

Kohonen, J., Rämö, O.T., 2005. Sedimentary rocks, diabases, and late cratonic evolution. Developments in Precambrian Geology 14. Elsevier B.V., Amsterdam, 563-604.

Kukkonen, I.T, 2000. Geothermal energy in Finland. Proceedings World Geothermal Congress 2000, Kyushu - Tohoku, Japan, May 28 - June 10, 2000, 277-282.

Kwiatek, G., Saarno, T., Ader, T., Bluemle, F., Bohnhoff, M., Chendorain, M. et al., 2019. Controlling fluid-induced seismicity during a 6.1-km-deep geothermal stimulation in Finland. Science Advances 5(5), eaav7224.

Laubach, S.E., Eichhubl, P., Hargrove, P., Ellis, M.A. & Hooker, J.N., 2014. Fault core and damage zone fracture attributes vary along strike owing to interaction of fracture growth, quartz accumulation, and differing sandstone composition. Journal of Structural Geology 68, 207-226.

Majer, E.L., Baria, R., Stark, M., Oates, S., Bommer, J., Smith, B., Asanuma, H., 2007. Induced seismicity associated with Enhanced Geothermal Systems. Geothermics 36(3), 185-222.

Olasolo, P., Juárez, M.C., Morales, M.P., D´Amico, S., Liarte, I.A., 2016. Enhanced geothermal systems (EGS): A review. Renewable and Sustainable Energy Reviews 56, 133-144.

Sibson, R.H., 1989. Earthquake faulting as a structural process. Journal of Structural Geology 11(1-2), 1-14.

Tanaka, H.K.M., Miyajima, H., Kusagaya, T., Taketa, A., Uchida, T., Tanaka, M., 2011. Cosmic muon imaging of hidden seismic fault zones: Rainwater permeation into the mechanical fractured zones in Itoigawa-Shizuoka Tectonic Line, Japan. Earth and Planetary Science Letters 306, 156-162.

Tanaka, H.K.M., Sannomiya, A., 2013. Development and operation of a muon detection system under extremely high humidity environment for monitoring underground water table. Geoscientific Instrumentation Methods and Data Systems 2, 29-34.

Younger, P.L., Gluyas, J.G., Stephens, W.E., 2012. Development of deep geothermal energy resources in the UK. Proceedings of the Institution of Civil Engineers - Energy 165(1), 19-32.

Cosmic-ray based geothermal exploration – A short introduction to muography

M. Holma[1,2,3] and P. Kuusiniemi[2,3]

[1]Muon Solutions Oy, Saarenkylä, Finland
[2]Kerttu Saalasti Institute, University of Oulu, Nivala, Finland
[3]Arctic Planetary Science Institute, Äänekoski, Finland
E-mail: marko.holma@oulu.fi

Muography is a novel geophysical imaging method for large solid objects and it maps relative density variations in 2D, 3D or 4D (density data + time analysis). In geothermal exploration, muography can be used, for example, for remote detection of faults and estimation of associated permeabilities. In the best-case scenarios, muography can be used to direct further geothermal exploration drilling and mitigating exploration risks associated with permeability models. The method is feasible for the 1-2 km in the vertical direction or, if applied at the ground surface level, up to 2-3 km in horizontal and near-horizontal directions.

Keywords: geothermal energy, geothermal exploration, muography

1. Introduction

Even in countries with active high-enthalpy geothermal systems, like Iceland, Italy, New Zealand and Turkey, discovery and characterisation of a geothermal resource is often challenging. This is particularly true if the resource lacks obvious surface expressions like hot springs or geysers. In those cases, the geothermal resource may be hiding, for example, under a blanket of impermeable rocks preventing transportation of fluids and gases from deep-seated thermally heated sources to the surface (Hanson et al. 2014). These types of geothermal resources are often called as blind or hidden geothermal systems (Hanson et al. 2014). In contrast, heat flows in ancient cratonic shield areas are low and classical surface expressions associated with convective hydrothermal systems simply do not occur as there are no convective hydrothermal systems. In brief, exploration of economically feasible geothermal resources is often challenging, and the challenges are not the same everywhere. Developments in methods and techniques in geothermal exploration are thus important. We introduce herein a new technique that may be useful in geothermal energy exploration in the future. This technique is called muography.

2. Principles of muography

Muography is based on the utilisation of cosmic-ray induced atmospheric muon particles as probes to image density variations in solid (and liquid) materials. In geology, this novel geophysical imaging method can be used for density characterisation and monitoring of soil and rock formations of any kind, as long as there are adequately large density variations present (e.g., lithological boundaries, ore bodies, major alteration zones, and major damage zones). So far, density imaging of interiors of volcanoes is the most widespread application. Muographic imaging in geology and engineering (Zhang et al. 2020) is based on variable attenuation of muon flux in different directions (less muons are detected from the direction of denser materials). It can be performed as 2D muon radiography (e.g., Lesparre et al. 2012), 3D muon tomography (e.g., Guardincerri et al. 2017), and time-lapse (time-sequential) muography (e.g., Tanaka, 2020). Furthermore, depending on the need and availability of muon detectors, the

latter can be performed in 2D or 3D. Time-sequential muography has been used, for example, to visualise and analyse magma movements in a volcano (Lesparre et al. 2012) or groundwater movements in faults (Tanaka et al. 2011). Densities are visualised as variations in the mean density of a soil or rock volume (i.e., as pixels in 2D, voxels in 3D, and time-referenced pixels or voxels in time-lapse muography).

Muography surveys can be conducted by a variety of detector types. Without going into technical details, the detectors can be divided into two classes based on the mobility and place of emplacement: cylindrical borehole probes and 'telescopes' (a common term used in the literature for these kinds of instruments, but rather vague in content as a telescope can be actualised with a number of different techniques). In general, telescopes are small enough to be mobile (e.g., 1 m^3) but still way too large to fit into the borehole. Telescopes are the best option for density imaging wherever there is a need for particularly high resolution and enough room for this detector type (e.g., underground tunnels, caves, or mountainous areas where a telescope can be positioned directly on the ground to image a mountain or volcano). However, as is well known, such underground spaces are not in abundance in most landscapes and many terrains are relatively flat. Boreholes, on the other hand, are more numerous. In Finland alone, way more than 37 000 deep boreholes have been drilled so far, as based on the database of the National Drill Core Archive in Finland (GTK, 2020a,b). These boreholes equal to over 3500 km of drill core. As a comparison, Sweden's National Drill Core collection consists of more than 3000 km of drill core from more than 18 000 boreholes (SGU, 2020). Norway's National Drill Core and Sample Centre contains 750 km drill core in total (NGU, 2019). It is worth noting that the actual total number of boreholes in these three countries is considerably larger than those inferred from the official sources as many companies have also their own drill core storage facilities. It can nevertheless be estimated that only a fraction of boreholes is truly available for borehole muography due to decrease in numbers owing to borehole collapse, destruction of rock sequences (e.g., due to mining), and a lack of access licence. Yet, borehole muography offers more possible locations for muography than telescope-based muography.

The lowest density variations that may be observed by muography with a significance level of 3σ are around 2% at 150 m of depth, 4% at 300 m, and 10% at 700 m (Hivert et al. 2017). The 1% difference in a mean rock density translates into approximately 3% difference in the measured muon flux. Moreover, if a rock having a porosity of 10% is saturated with water, measured muon flux is reduced by 10% (Tanaka and Sannomiya, 2013). Due to these reasons muography has potential as a tool for detection and monitoring of natural bedrock aquifers, or at least those associated with high-porosity faults and fracture zones.

As a geophysical method, muography can be combined with other geophysical methods. In these regards, Pasquet et al. (2019) discusses about pairing of muography with seismics and electrical resistivities, and Holma et al. (2019) with microseismic monitoring. Muography data has also been jointly inverted with gravity data (e.g., Barnoud et al. 2019), while Lesparre et al. (2012) compares muography data with electrical resistivity and gravity data.

3. Applications of muography in geothermal exploration

Deep geothermal systems can be classified into: (1) hydrothermal (convective) systems; (2) enhanced geothermal systems (EGS) (also called as hot dry rock systems); and hot aquifers. Classification can also be based on temperature; in which case the geothermal systems fall either to high enthalpy (above 150°C) or low enthalpy (less than 150°C) systems. In some cases, the terms 'medium enthalpy' and 'ultra-high enthalpy' have been found to be more appropriate. As an example of the latter, the Japan Beyond-Brittle Project targets supercritical geothermal resources in an EGS reservoir in ~400-500°C rocks (Asanuma et al. 2019). Borehole

muography is not applicable in high-temperatures due to detector-related technical limits (we estimate T_{max} to be close to 50°C).

Favourable geothermal reservoir settings are often characterised by interactions of fluids flowing along fractures in the bedrock. As (1) muon detectors reveal density changes with a reasonably high resolution (at least at depths above 1 km) and (2) fractures typically have lower bulk densities than non-fractured rocks, major faults are visible by both muon telescopes and borehole muon probes as low-density features. While muography can be used in exploration of geothermal deposits that are related to fractures, it may not be effective in exploration of non-fracture related geothermal deposits, unless there occur associated density contrasts. Other constraints include telescopes that can be used only if there are tunnels or caves where they can be installed, or there is enough topography so that telescopes can be installed on the side of the object of interest, such as a mountain or similar steep landform. Telescopes set up on the ground can be applied for the detection of density contrasts in solid materials up to 2-3 km thick in a horizontal or near-horizontal direction (e.g., Tanaka et al., 2014). This enables telescopes for geothermal exploration in mountainous areas. Borehole probes, in contrary, can be used anywhere there are available boreholes. However, as the muon flux diminishes substantially with increasing depth, the maximum depth borehole detectors can be used effectively is likely somewhere between 1-2 km. The gradually increasing geothermal gradient is another constrain for borehole muon detectors. Hence, the method works best in detection and monitoring of permeable fault zones in the uppermost 1-2 km. Nevertheless, as sub-vertical fault zones are typically rooted to much greater depths, sub-vertical structures inferred from muographic data may, at least in some instances, be extrapolated to continue with reasonable reliability to greater depths.

Major changes in water table levels in permeable beds and fractures in bedrock are typically related to seasonal recharge and discharge events, or occasional storms or droughts. If the water level of a bedrock aquifer changes, the bulk density of the affected rock volume changes and, if the change is strong enough, is hence observable by muography. Indeed, Tanaka et al. (2011) have demonstrated that muography can detect time-dependent density changes in rock volumes caused by fluctuation of water levels in major structures. Hence, long-term muography measurements can be used in the detection and monitoring of natural bedrock aquifers associated with faults and fracture zones.

Major fault zones have a capacity to be hydraulic conduits connecting shallow and deep geological environments, even though some segments of these structures may form effective barriers for fluid flow (Bense et al. 2013). In the areas of high heat flow, large faults may enhance permeability anisotropy and control the fluid velocities and hydrothermal convection. In such cases the regional heat flux distribution can change, as shown by Bächler et al. (2003) in their study of the Rhine Graben, Germany. The authors report temperature undulations along one of the studied faults reaching ±8°C at 500 m depth and ±12°C at 1 km depth. Moreover, the temperatures were 20–40°C higher than expected in both depths. The highest measured temperature at 1 km depth (98°C) was interpreted as a clear evidence that the fluid source must be at least at the depth of 3 km and possibly deeper. Bächler et al. (2003) also conclude that as the minimum horizontal stress is typically perpendicular to the strike of a graben, fracturing along graben-parallel structures stimulates fluid flow. In brief, the graben-controlling master faults are important as permeability structures and temperature anomalies. Muography can be used to map these faults in detail and for collecting time-dependent density change data of the hydraulic behaviour of the fault over time.

4. Concluding remarks

Temperature, permeability, and volume are the three subsurface parameters that are most critical to constrain a geothermal resource (Witter et al. 2019). Muography can be used to increase knowledge of permeability by remote detection of faults and determination of their direction and widths. Muography may also proof useful for improving geological working models in geothermal exploration and, by doing so, it may guide drilling and mitigate exploration risks.

References:

Asanuma, H., Mogi, T., Tsuchiya, N., Watanabe, N., Naganawa, S., Ogawa, Y. et al., 2019. Status of Japanese Supercritical Geothermal Project in FY2018. GRC Transactions 43, 2019.

Bächler, D., Kohl, T. & Rybach, L., 2003. Impact of graben-parallel faults on hydrothermal convection - Rhine Graben case study. Physics and Chemistry of the Earth 28(9-11), 431-441.

Barnoud, A., Cayol, V., Niess, V., Cârloganu, C., Lelièvre, P., Labazuy, P. & Le Ménédeu, E., 2019. Bayesian joint muographic and gravimetric inversion applied to volcanoes. Geophysical Journal International 218, 2179-2194.

Bense, V.F., Gleeson, T., Loveless, S.E., Bour, O. & Scibek, J., 2013. Fault zone hydrogeology. Earth-Science Reviews 127, 171-192.

NGU, 2019. A Jigsaw. Annual Report 2018. Retrieved from https://bit.ly/39P6nBE. (December 4 2020)

Guardincerri, E., Rowe, C., Schultz-Fellenz, E., Roy, M. George, N., Morris, C. et al., 2017. 3D Cosmic Ray Muon Tomography from an Underground Tunnel. Pure and Applied Geophysics 174, 2133-2141.

GTK, 2020a. National drill core archive. Retrieved from https://bit.ly/37BOkw3. (December 4 2020)

GTK, 2020b. Drill cores from deep drilling (Drill Core Archive). Retrieved from https://bit.ly/2VDMeX0. (December 4 2020)

Hanson, M.C., Oze, C. & Horton, T.W., 2014. Identifying blind geothermal systems with soil CO_2 surveys. Applied Geochemistry 50, 106-114.

Hivert, F., Lázaro, I., Decitre, J.B., Brunner, J., Busto, J. & Gaffet, S., 2017. Muography sensitivity to hydrogeological rock density perturbation: Roles of the absorption and scattering on the muon flux measurement reliability. Near Surface Geophysics 15, 121-129.

Holma, M., Kuusiniemi, P., Kozlovskaya, E. & Zhang, Z.-X., 2019. Cosmic-ray muography and microseismic monitoring - a potential pair for enhancing characterisation, analysis and 3D modelling of underground facilities. Sovelletun geofysiikan XXII neuvottelupäivät, 19.-20.11.2019, Rovaniemi. Vuorimiesyhdistys ry.

Lesparre, N., Gibert, D., Marteau, J., Komorowski, J.-C., Nicollin, F. & Coutant, O., 2012. Density muon radiography of La Soufrière of Guadeloupe volcano: comparison with geological, electrical resistivity and gravity data. Geophysical Journal International 190, 1008-1019.

Pasquet, S., Rosas-Carbajal, M., Marteau, J., Ianigro, J.-C., Chalikakis, K., Mazzilli, N., Tramontini, M. & Champollion, C., 2019. Combined Muon, Seismic and Electrical Resistivity Measurements to Characterize a Karstic Unsaturated Zone (LSBB, France). NS43B-0837, AGU 100 Fall Meeting, 9-13 December 2019, San Francisco, CA, USA.

SGU, 2020. Drill core collection. Retrieved from https://bit.ly/3lH5D3O. (December 4 2020)

Tanaka, H.K.M., 2020. Development of the muographic tephra deposit monitoring system. Scientific Reports 10, 14820.

Tanaka, H.K.M., Miyajima, H., Kusagaya, T., Taketa, A., Uchida, T. & Tanaka, M., 2011. Cosmic muon imaging of hidden seismic fault zones: Rainwater permeation into the mechanical fractured zones in Itoigawa-Shizuoka Tectonic Line, Japan. Earth and Planetary Science Letters 306, 156-162.

Tanaka, H.K.M., Kusagaya, T. & Shinohara, H., 2014. Radiographic visualization of magma dynamics in an erupting volcano. Nature Communications 5, 3381.

Tanaka, H.K.M. & Sannomiya, A., 2013. Development and operation of a muon detection system under extremely high humidity environment for monitoring underground water table. Geoscientific Instrumentation Methods and Data Systems 2, 29-34.

Witter, J.B., Trainor-Guitton, W.J. & Siler, D.L., 2019. Uncertainty and risk evaluation during the exploration stage of geothermal development: A review. Geothermics 78, 233-242.

Zhang, Z.-X., Enqvist, T., Holma, M. & Kuusiniemi, P., 2020. Muography and its potential applications to mining and rock engineering. Rock Mechanics and Rock Engineering 53, 4893-4907.

An introduction to principles of muography in continental scientific boreholes

M. Holma[1,2,3], P. Kuusiniemi[1,3] and K. Loo[1]

[1]Muon Solutions Oy, Saarenkylä, Finland
[2]Kerttu Saalasti Institute, University of Oulu, Nivala, Finland
[3]Arctic Planetary Science Institute, Äänekoski, Finland
E-mail: marko.holma@muon-solutions.com

In the present study, the novel geophysical imaging method of muography is introduced for the studies of rocks around scientific boreholes drilled into continental crust (or oceanic crust thrust over continental crust). In this application, the method can be used for detecting density variations in rocks intersected by the borehole. The present study also explains what are the lowest density variations observable by muography, what are the principles governing the volume the density data is extracted from, and what are the likely practical limits for borehole muography.

Keywords: crust, scientific drilling, density, geophysics, muography, muon angular distribution, downhole geophysics

1. Introduction

Scientific boreholes are drilled to sample, characterise, and understand rocks, deep fluids, and even microbial life in the shallow crust for a variety of purposes. While they can be drilled both into the continental and oceanic crust, we focus herein into scientific boreholes drilled on dry land. Boreholes drilled into the present seafloor are hence excluded, while boreholes drilled into obducted oceanic crust are included. As continental scientific drill holes are typically far deeper than most technical and mineral exploration boreholes, it is a common practise to examine both the drill core and its borehole with as many different techniques as possible to gain as much information of the subsurface structure, stratigraphy, chemistry and physical mechanisms and processes of the deep realm as possible. In some cases, the scientific boreholes are maintained long after the actual drilling in order to support further studies in the upcoming years. These types of boreholes are practically laboratories where new techniques and methods can be tested not only to collect new data, but to develop these new techniques/methods to the needs of the future. The present work introduces what one can learn from the rocks surrounding scientific boreholes by measuring cosmic-ray induced atmospheric muon particles employing one or more borehole probes designed for this purpose. In addition, we discuss the practical limits for this method.

2. Muography: a method to detect density variations in large solid objects

Underground muography is based on measurements of atmospheric muon particles by detectors positioned in caves, tunnels, or boreholes (Holma and Kuusiniemi, 2018). In this work our emphasis is on the latter and how they could be used in geophysical probing through continental scientific drill holes. However, the technical details of the probes are beyond the scope of the present work.

Borehole muography provides information on mean density variations in large objects in 2D, 3D or 4D (2D or 3D + time series analyses). Imaging in 2D and 3D generates two- to three-dimensional density images in which individual pixels and voxels have different density values,

respectively. The 4D imaging can be based either on 2D or 3D imaging, but in this case the images also contain time stamps allowing monitoring of time-dependent density-changing processes. Densities are typically visualised as variations in the mean density of a rock volume (representative examples are shown, for example, in Tanaka, 2020). According to the numeric simulations of Hivert et al. (2017), the lowest density variations observable by muography with a significance level of 3σ are around 2% at 150 m of depth, 4% at 300 m, and 10% at 700 m. Interestingly, the 1% difference in a mean rock density results approximately in 3% difference in the muon flux.

3. Muon simulations

The initial cosmic-ray induced muon distributions are often obtained using particle transportation codes such as CORSIKA (Heck et al. 1998). They are designed for simulations of the development of extensive air showers, including processes resulting in cosmic-ray muons. Interactions and transport of muons through the rock overburden are usually simulated utilising toolkits such as Geant4 (Allison et al. 2016) or FLUKA (Ferrari et al. 2005). Often this includes the response of the foreseen detector setup which is simulated in subsequent steps. The full simulation chain from the primary cosmic-ray particle to the detection of a muon in the detector is typically a very computing-intensive task. However, in simple rate estimates or illustrations, simplifications based on the parametrisation of sea-level muon flux distributions or muon losses in overburdens are reasonably reliable and can be used to speed up the simulation procedure.

In the present work the muon angular distributions were simulated using the approach by Chirkin and Rhode (2016). The simulation takes into account the muon energy and angular distributions of atmospheric muons and those passing through rock at different depths. This is important because it has effects on the detected muon distributions at the given depth. Furthermore, we adjusted the simulations for the average chemical composition of 2.5-1.8 Ga juvenile upper continental crust of Condie (1993).

Figure 1 illustrates the volumetric coverage of the muography measurement conducted at different depths. For clarity, these are placed at three different positions in the horizontal plane. Similar distributions are obviously produced even if the three positions are vertically aligned, like they were if the measurements are conducted in a vertical borehole at three depths. However, that is not the case if muons are detected in an inclined borehole as in this case the 'data cones' (this is an informal reference to the volume from where density data can be extracted at the given underground position) become only partially overlapped. This is an important feature while planning muographic surveys as it allows the mapping of the overburden in different ways if boreholes of different inclinations are available. It must be emphasised, however, that many scientific boreholes are drilled with steep to vertical angles to reach the maximum depth with the minimised drill metres. The muon rate (flux) and angular distributions change according to the depth of observation. In brief, a detector at 200 m depth collects less muons than that at 100 m within the same period of time, but more than any similar-size detector positioned deeper (assuming that the material is homogeneous). Furthermore, the data cones are of approximately similar shape down to several hundred meters after which they are tapering rapidly. Note also that the deeper the detector is, the larger volume of rocks it ‘sees’, i.e., its data cone is larger. A simple approximation is that the diameter of the data cone at the ground surface is about twice the depth of the detector.

4. Maximum depth of muography in a borehole

The intensity of muon flux exponentially diminishes the deeper in rocks one goes, until even the most energetic atmospheric muons are attenuated, and none (or very few) remains to be

detected. How deep this happens depends on the mean density of the rocks the muons have to pass through before reaching the detector, the size of the detector (or the total volume of the available detectors) and the time available for muon detection. As muography is a statistical imaging method, one parameter affecting the image sharpness is the total measuring time (just like in the early years of photography, images get "better" with longer exposure times) as more time yields more detected muons. However, given the limited space available even in the widest of boreholes, it is likely that borehole muography is not viable vertically from the ground surface deeper than 1-2 km. Technically atmospheric muons can be detected even deeper, but their flux is so diminished that muographic surveys are likely taking years rather than months. In any depth, the duration of the measurement can be reduced using larger detectors or increase their number. In a borehole, this can be accomplished by a downhole passive muographic array containing more than one probe, each detecting muons independently and simultaneously.

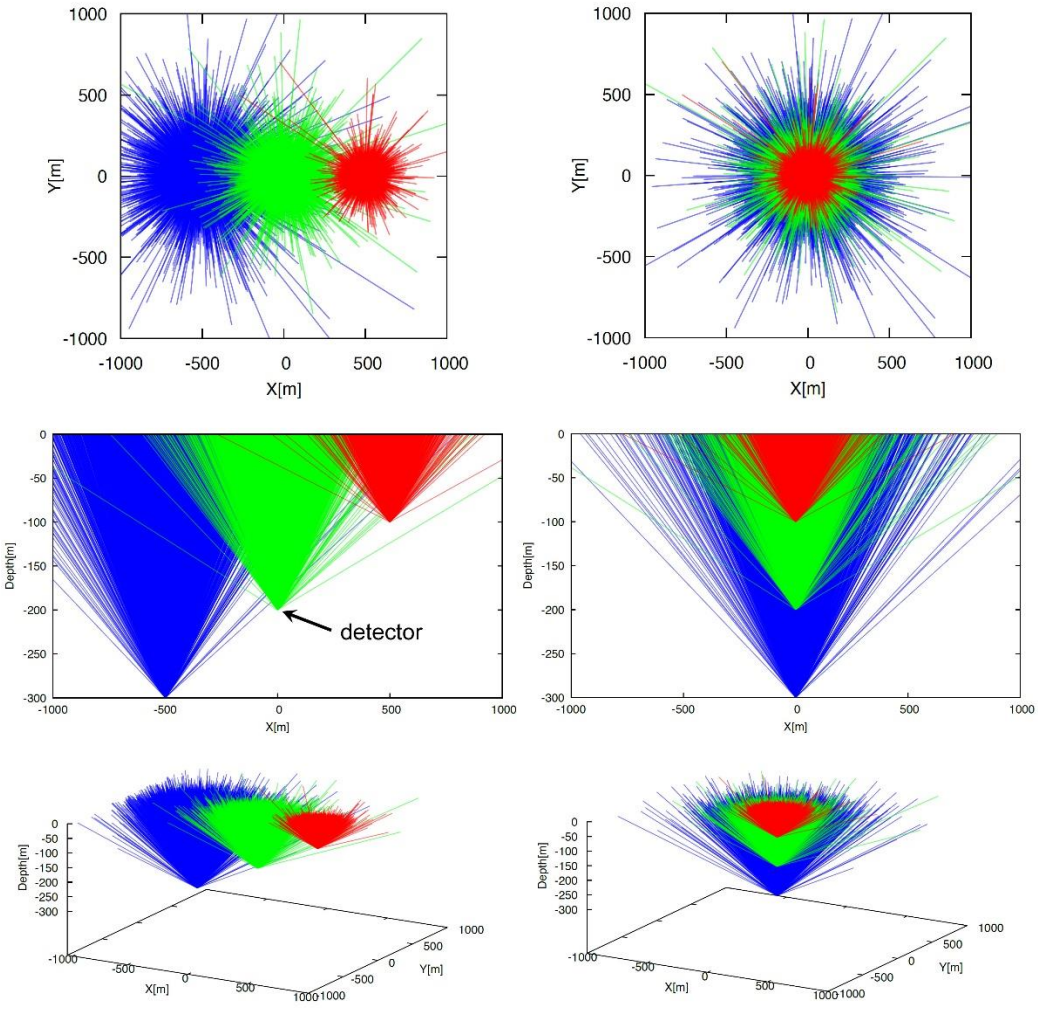

Figure 1. Simulated muons observed using three borehole muon detectors at 300 m (blue), 200 m (green) and 100 m (red) underground. Each line represents a flight path of a single muon. In all three simulations the number of muons is one million. The upper images represent a top view. The middle image pair represents the 'data cones' as a side view of the respective images above. The lower image pair represents 3D visualisation of the images above. Note that on the right side the detectors are vertically aligned, while those on the left are 500 m apart. In both cases the data cones partially overlap, but this is greater in the right-hand arrangement of detectors.

5. Concluding remarks

Deep scientific boreholes provide a unique opportunity to learn more about the physical properties of the upper crust and hence are favoured targets for implementation of downhole geophysical surveys. Borehole muon detectors utilised in these boreholes would deliver density contrast maps of the surrounding volume of rocks. As there commonly is only one borehole in any given continental deep scientific borehole site, muon collection and data analysis differ from some other applications of borehole muography where there often are multiple boreholes available. Muon detection in a scientific borehole will likely provide better results if utilised in multiple depths. Furthermore, as collecting statistically meaningful numbers of muons takes significantly more time (e.g., months) than conventional borehole geophysical surveys (e.g., few hours), muography is best suited for boreholes from which other data sets have already been collected. We believe that borehole muography is not viable deeper than 1-2 km from the ground surface. This, alas, limits the usability of muography for the relatively shallow parts of continental scientific boreholes.

In summary, muography is a suited method to investigate rock density variations around continental scientific boreholes if there are reasonable density variations in the uppermost 1-2 km of drill core. These density inhomogeneities can be either between rock types or in the form of major structural breaks (e.g., a major zone of core loss would probably be detectable as a low-density fault in muography data). Inversion of geophysical data is inherently non-unique and benefits from additional information. Both hold true also for muography data. Hence, if other geophysical data are already available, those and the muography data can be jointly inversed to reach the best combined results.

References:

Allison, J., Amako, K., Apostolakis, J., Arce, P., Asai, M., Aso, T. et al., 2016. Recent Developments in Geant4. Nuclear Instruments and Methods in Physics Research Section A: Accelerators, Spectrometers, Detectors and Associated Equipment 835, 186-225.

Chirkin, D. & Rhode, W., 2016. Propagating leptons through matter with Muon Monte Carlo (MMC). arXiv:hep-ph/0407075v3 3 Aug 2016.

Condie, K.C., 1993. Chemical composition and evolution of the upper continental crust: Contrasting results from surface samples and shales. Chemical Geology 104, 1-37.

Ferrari, A., Sala, P.R., Fasso, A. & Ranft, J., 2005. FLUKA: a multi-particle transport code. CERN-2005-010, INFN TC_05/11, SLAC-R-773.

Heck, D., Knapp, J., Capdevielle, J.N., Schatz, G. & Thouw, T., 1998. CORSIKA: A Monte Carlo Code to Simulate Extensive Air Showers. Forschungszentrum Karlsruhe, Technik und Umwelt, Wissenschaftliche Berichte, Report FZKA 6019, 90 p.

Hivert, F., Lázaro, I., Decitre, J.B., Brunner, J., Busto, J. & Gaffet, S., 2017. Muography sensitivity to hydrogeological rock density perturbation: Roles of the absorption and scattering on the muon flux measurement reliability. Near Surface Geophysics 15, 121-129.

Holma, M. & Kuusiniemi, P., 2018. Underground muography: The raise of geoparticle physics as a soil, orebody and rock realm imaging method. Lithosphere 2018 – Tenth Symposium on the Structure, Composition and Evolution of the Lithosphere. Programme and Extended Abstracts, Oulu, Finland, November 14-16, 2018. Institute of Seismology, University of Helsinki, Report S-67, 27-30, 136 p.

Tanaka, H.K.M., 2020. Development of the muographic tephra deposit monitoring system. Scientific Reports 10, 14820.

Sm-Nd isotope systematics of the Precambrian mafic-ultramafic Näränkävaara intrusion

V. Järvinen[1], T. Halkoaho[2], J. Konnunaho[2], J.S. Heinonen[1], and O.T. Rämö[1]
[1]University of Helsinki
[2]Geological Survey of Finland
E-mail: ville.jarvinen@helsinki.fi

The Precambrian mafic-ultramafic Näränkävaara intrusion contains a 1.5-2 km thick basal dunite, mostly composed of low-porosity olivine adcumulates, and a ~1.3 km thick peridotitic-pyroxenitic-gabbronoritic layered series. The basal dunite exhibits lithological features typically found in high-volume open-system komatiite flows, and its location between two Archean komatiite-hosting greenstone belts has led to the hypothesis that it may represent an Archean komatiitic wall-rock to the Paleoproterozoic layered intrusion magmatism. Results from six new whole-rock Sm-Nd isotope analyses show similar isotopic ratios for both the layered series and basal dunite, with εNd from −3.5 to −1.5 at 2440 Ma, which supports a cogenetic relationship instead. The open-system lithological features suggest that the basal dunite may have formed (at least partly) as a magmatic feeder channel, possibly connected to the geophysical Koillismaa "hidden dyke".

Keywords: Näränkävaara, layered series, dunite, Sm-Nd isotopes

1. Introduction and geological setting

Several mafic layered intrusions were emplaced in northern Fennoscandia at 2.5−2.4 Ga during a long-lived (~80 Ma) Large Igneous Province (LIP) related mantle plume event. The mafic-ultramafic Näränkävaara intrusion is the easternmost member of the Finnish Tornio-Näränkävaara belt (Fig. 1), and belongs to the younger ~2.44 Ga age group of the plume magmatism (Alapieti 1982). The Fennoscandian intrusions were mostly intruded between the Archean granitoid basement complex and plume-induced continental rifting related volcanic-sedimentary supracrustal rocks; however, the Näränkävaara and Burakovsky intrusions are completely surrounded by granitoid basement (e.g. Amelin & Semenov 1996). The parental magmas of these intrusions can be classified as komatiitic or High-Mg basalts contaminated with Archean crust (average ε_{Nd} approximately −2, 9−18 wt% MgO, 0.5−1.0 wt% TiO_2; Kulikov et al. 2010).

The ~3 km thick Näränkävaara intrusion (Fig. 1) contains a 1.5-2 km thick 'basal dunite' series, primarily composed of olivine adcumulates with minor meso- and orthocumulates, and a ~1.2 km thick layered series, composed of pyroxenites-gabbronorites and lesser peridotites. The intrusion has two structural blocks with opposing dip-directions (~10-25°), divided by a major NE-trending fault. The SE-block contains a marginal series gabbronorite along the (tectonized) basal dunite−layered series contact, with the marginal series grading into the layered series, suggesting an age gap between the two series; contact along the NE-block is an ambiguous strongly altered olivine to olivine-bronzite cumulate (Järvinen et al. 2020a).

The Näränkävaara intrusion belongs to the Koillismaa Layered Intrusion Complex (KLIC), partly because of a prominent linear geophysical anomaly that connects the Näränkävaara intrusion to the Western Intrusions of the KLIC – this anomaly has been hypothesized to be related to a concealed dyke that fed the KLIC (Alapieti 1982). The small Takanen greenstone belt (GSB) also overlaps with this anomaly just NE of Näränkävaara (Fig. 1) and the Suomussalmi GSB also terminates ~10 km to the south, with both hosting komatiitic olivine accumulate units. As the basal dunite exhibits lithological features typical of fast-flowing

komatiite systems – abundant 'extreme' olivine accumulates with back-and-forth variations in olivine compositions with depth ($Fo_{87.5-90}$), bi-modal olivine, and poikilitic chromite (Järvinen et al. 2020b) – this led to the hypothesis that the Näränkävaara basal dunite could represent an Archean komatiite wall-rock to the Proterozoic layered intrusion magmatism.

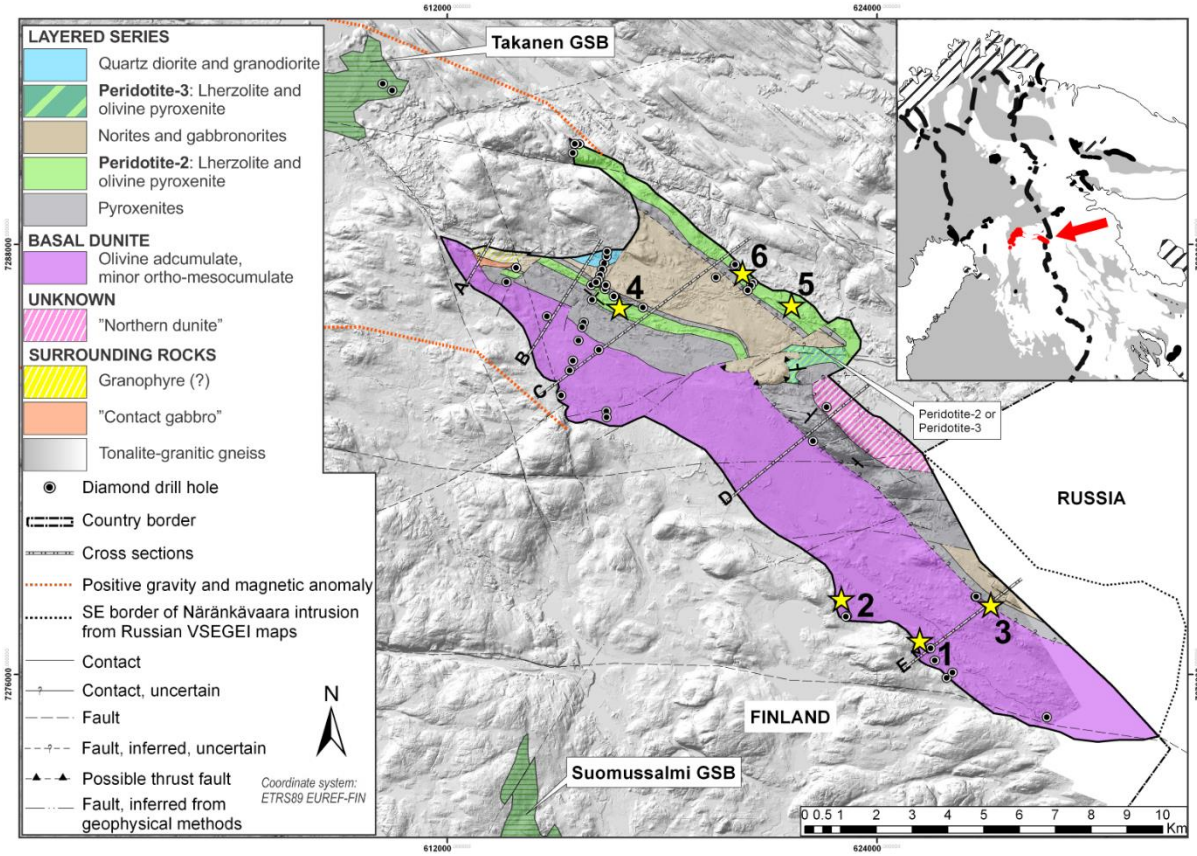

Figure 1. Simplified geological map of the Näränkävaara intrusion overlain on a digital elevation model. Stars show locations of numbered whole-rock Sm-Nd isotope samples. Inset shows locations of the 2.5–2.4 Ga mafic intrusions in Fennoscandia (black) with Näränkävaara and Koillismaa intrusions pointed out in red (white = Archean; gray = Proterozoic; hatched = Phanerozoic). Full version of the map with stratigraphy and cross-sections available from corresponding author.

We present six new Sm-Nd isotope analyses, and argue for a comagmatic Paleoproterozoic plume-related origin for both the Näränkävaara basal dunite and the layered series. The results agree with the idea that the Näränkävaara intrusion may (at least partly) represent a magmatic feeder-channel system related to the 2440 Ga event, as originally suggested by Alapieti (1982).

2. New whole-rock Sm-Nd results

Nd isotope composition of six whole-rock samples were analysed by TIMS at the University of Texas (Table 1). Initial εNd-values calculated at the age of the Näränkävaara intrusion (2436 Ma; Alapieti 1982) decrease from the basal dunite (-1.7 – -1.8) to the layered series (-2.1 – -2.4) with the marginal series being the most unradiogenic (-3.5). Figure 2A shows that the basal dunite ε_{Nd} values also overlap with Archean komatiites and komatiitic basalts from the Kuhmo

GSB at depleted mantle (DM) values (+1.2 – +1.6) with initial ratios calculated back to 2800 Ma. An Archean origin for the basal dunite is unlikely, however, as the

Table 1. Results of Sm-Nd isotope analyses from the Näränkävaara intrusion (see Fig. 1 for sample locations). All errors are 2σ.

Sample #	Series[a]	Sm ppm	Nd ppm	$^{147}Sm/^{144}Nd$ ±0.00007	$^{143}Nd/^{144}Nd$[b]	ε_{Nd} (2436Ma)
1	basal dunite	0.66	3.20	0.1255	0.511408 ± 5	−1.73
2	basal dunite	0.46	2.14	0.1295	0.511468 ± 9	−1.82
3	marginal series	1.98	9.77	0.1227	0.511271 ± 7	−3.53
4	layered series	0.61	2.99	0.1226	0.511328 ± 11	−2.39
5	layered series	0.42	1.99	0.1274	0.511421 ± 8	−2.07
6	layered series	0.66	3.22	0.1231	0.511352 ± 6	−2.07

[a] Marginal series is a melt-representative gabbronorite in contact with the basal dunite and layered series. Sample #4 is an olivine-bronzite cumulate, rest are olivine ortho-/mesocumulates. [b] Errors in isotope ratios based on within-run statistics; external uncertainty was 0.000013 based on repeated standard measurements.

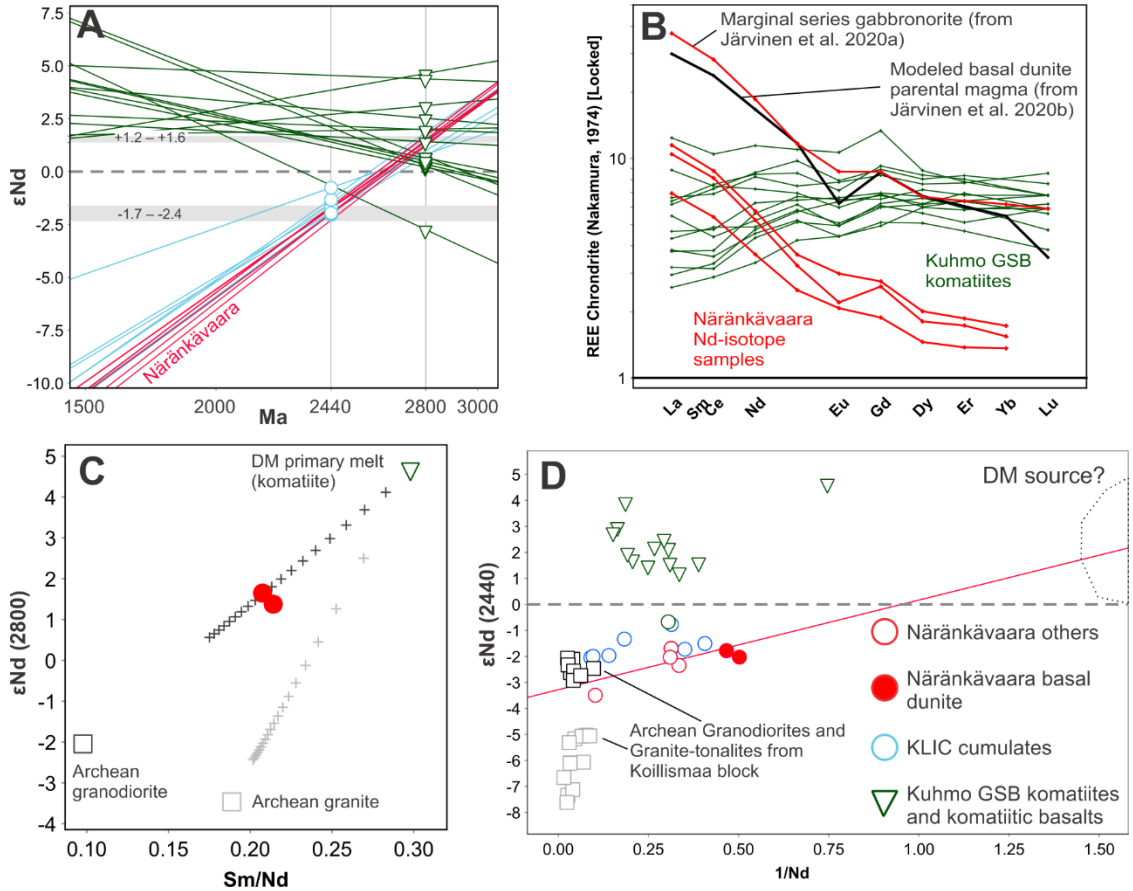

Figure 2. New isotope results from the Näränkävaara intrusion on whole-rock compositional plots; legend in lower right; other data from Hölttä et al. (2012). **A** ε_{Nd} vs. Age plot with two possible interpretations for the new results (sample #3 excluded) - 2440 Ma mafic intrusion or 2800 Ma komatiite. **B** REE-diagram comparing Näränkävaara rocks to Kuhmo samples from 2A **C** Results of AFC modelling, tick mark is cumulative 5% assimilation+fractionation. **D** εNd vs. 1/Nd plot at 2440 Ma, with trend line through new samples interpreted as a mixing line between parental (primary?) magma and Archean crustal contaminants.

Näränkävaara rocks (and parental magmas, see Fig. 2B) are strongly LREE-enriched with Sm/Nd of ~0.2, as compared to the LREE-depleted Archean komatiites with Sm/Nd of ~0.3−0.4. To maintain an Archean origin for the basal dunite, a process would be required that simultaneously produced both the low Sm/Nd, high ε_{Nd} at 2800 Ma, and the low measured $^{143}Nd/^{144}Nd$ at present. This would require either 1) extremely low-degree partial melting of the DM source (~1%, i.e. kimberlitic magma); 2) a DM source that was enriched in LREE by some metasomatic mantle processes just before production of the primary melt (i.e. not affecting ε_{Nd} but enriching LREE); or 3) a relatively highly depleted DM source having assimilated unradiogenic enriched crust. While option 2 is theoretically possible, constrained modelling parameters to investigate it further are not available, and therefore only option 3 has been investigated in more detail with simple AFC modelling (DePaolo 1981). Using the most depleted Kuhmo komatiite composition (ε_{Nd} = +4.6, Sm/Nd = 0.30) and the most LREE-enriched unradiogenic granitoids from the Koillismaa block (ε_{Nd} from −3.5 to −2.0, Sm/Nd = 0.10–0.19; Hölttä et al. 2012), an addition of 15−60% of local crust would roughly reproduce the basal dunite compositions at 2800 Ma (Fig. 2C). The prohibitively high amounts of assimilation indicated (>30-40 %) could be lessened by the presence of more unradiogenic Mesoarchean crust at a deeper level (ε_{Nd} ~-10) and by more in-depth modelling taking into account wall-rock partial melting.

Model in Fig. 2C is a rough estimate highlighting the problems related to producing both the observed initial isotope *and* trace element ratios by contamination. In addition, options 2 and 3 above are unsatisfactory in that no similar Sm/Nd and Nd-isotope systematics are found in 2800 Ma rocks elsewhere in the KLIC or nearby GSB's. A simpler interpretation is presented in Fig. 2D with the Näränkävaara basal dunite being a part of the same Proterozoic plume magmatism as the layered series, having assimilated the local Neoarchean crust.

4. Conclusions and implications

The Näränkävaara intrusion, including the basal dunite series, is part of the Fennoscandian plume magmatism. While the layered series is dated at 2436 Ma, the basal dunite may be somewhat older. The high-volume open-system features found in the basal dunite suggest it may have (at some point) acted as a magmatic feeder channel, and may well be connected to the concealed geophysical anomaly extending through Näränkävaara.

References:

Alapieti TT (1982) The Koillismaa layered igneous complex, Finland—its structure, mineralogy and geochemistry, with particular emphasis on distribution of chromium. Geol Surv Fin Bull 319:1—116

Amelin YV, Semenov VS (1996) Nd and Sr isotopic geochemistry of mafic layered intrusions in the eastern Baltic shield: implications for the evolution of Paleoproterozoic continental mafic magmas. Contrib Mineral Petrol 124:255—272

DePaolo DJ (1981) Trace element and isotopic effects of combined wallrock assimilation and fractional crystallization. Earth Planet Sci Lett 52:177—184

Hölttä P, Heilimo E, Huhma H et al (2012) Archaean complexes of the Karelia Province in 946 Finland. Geol Surv Finl, Spec Paper 54:9–20

Järvinen V, Halkoaho T, Konnunaho J et al (2020a) Parental magma, magmatic stratigraphy, and reef-type PGE enrichment of the 2.44 Ga mafic-ultramafic Näränkävaara layered intrusion, northern Finland. Miner Depos 55:1535—1560

Järvinen V, Halkoaho T, Konnunaho J et al (2020b) The basal dunite of the Precambrian mafic-ultramafic Näränkävaara intrusion: Petrogenetic considerations and implications to exploration. Miner Petrol (online) doi:10.1007/s00710-020-00725-9

Kulikov VS, Bychkova YV, Kulikova VV et al (2010) The Vetreny Poyas (Windy Belt) subprovince of southeastern Fennoscandia: An essential component of the ca. 2.5–2.4 Ga Sumian large igneous province. Precam Res 183(3):589–601.

Microearthquakes at the Olkiluoto nuclear fuel final disposal facility construction site in 2002-2018

O. Kaisko[1] and M. Malm[1]

[1]AFRY Finland Oy, Jaakonkatu 3, 01620 Vantaa
E-mail: outi.kaisko@afry.com

Posiva Oy is constructing an underground repository for spent nuclear fuel in Olkiluoto island in south-western Finland. Posiva has been monitoring seismicity at the site since 2002, and altogether 412 microearthquakes were observed in 2002 - 2018. An updated spectral source model and the associated source parameters were computed for the earthquakes in 2014 – 2018, and reliable moment tensor solutions were derived for 51 of them (Kaisko and Malm, 2019). The majority of the moment tensor solutions with subvertical pressure axes indicate that the microearthquakes are mostly adjusting the perturbed stress field caused by the excavated openings. However, the moment tensor solutions of three microearthquakes induced by pre-grouting within otherwise undisturbed bedrock are concluded to reflect natural stress field, yet not being of natural origin. The events occurred on the brittle fault zone OL-BFZ020a, with nodal planes corresponding to the fault plane in the geological structural model. Also, several other microearthquakes can be associated with the modelled brittle fault zones but based on the results of the study it can be stated that these structures have not been reactivated in the sense of releasing continuously stresses through natural mechanisms. Some of the zones have hosted microearthquakes not only beside the tunnels but also within the bedrock, which could indicate their ability for future reactivation.

Keywords: induced seismicity, microearthquake, source parameters, moment tensor solution

1. Introduction

Posiva Oy is constructing an underground disposal facility for spent nuclear fuel in Olkiluoto island, Eurajoki municipality, in the south-western coast of Finland (Figure 1A). Posiva has been monitoring the natural background seismicity in order to characterize the baseline conditions at the site since 2002 (Saari, 2003). In addition, the monitoring has focused on changes in stability of the bedrock and safeguarding the facility during the excavation since 2004 (Saari, 2005). In the end of 2018, the repository area with its surroundings was monitored with 18 permanent seismic stations equipped with accelerometers and/or geophones (Figure 1B).

The Olkiluoto area has distinctly low seismicity with no observations of natural earthquakes within 5 km radius from the site (Figure 1A; Ahjos and Uski, 1992; ISUH, 2018). Also, induced microearthquakes were only rarely recorded during the years 2003 – 2016 (Haapalehto et al. 2017). Seismicity related to the final disposal facility construction became more intense in 2017, when the excavation was conducted simultaneously in several locations at the repository level (Haapalehto et al. 2018). Since that, the number of probable microearthquakes has shown correlation with excavation intensity by decreasing significantly together with ceased blasting in the end of 2018 (Haapalehto et al. 2019).

In the following sections the microearthquake observations at the Olkiluoto site during the years 2002-2018 are presented after Kaisko and Malm (2019). Altogether 412 probable microearthquakes were detected and analysed with Posiva Oy's local microseismic network during this period. The earthquakes and rockfalls occurring in 2002-2016 were reidentified and the reported microearthquakes lacking location were reanalysed. An improved spectral source model with an ω^3-fit with the associated source parameters were computed for the 400

microearthquakes occurring after the network renewal in 2014 – 2018, and reliable moment tensor solutions could be derived for 51 of them (cf. Kaisko and Malm, 2019 for more details).

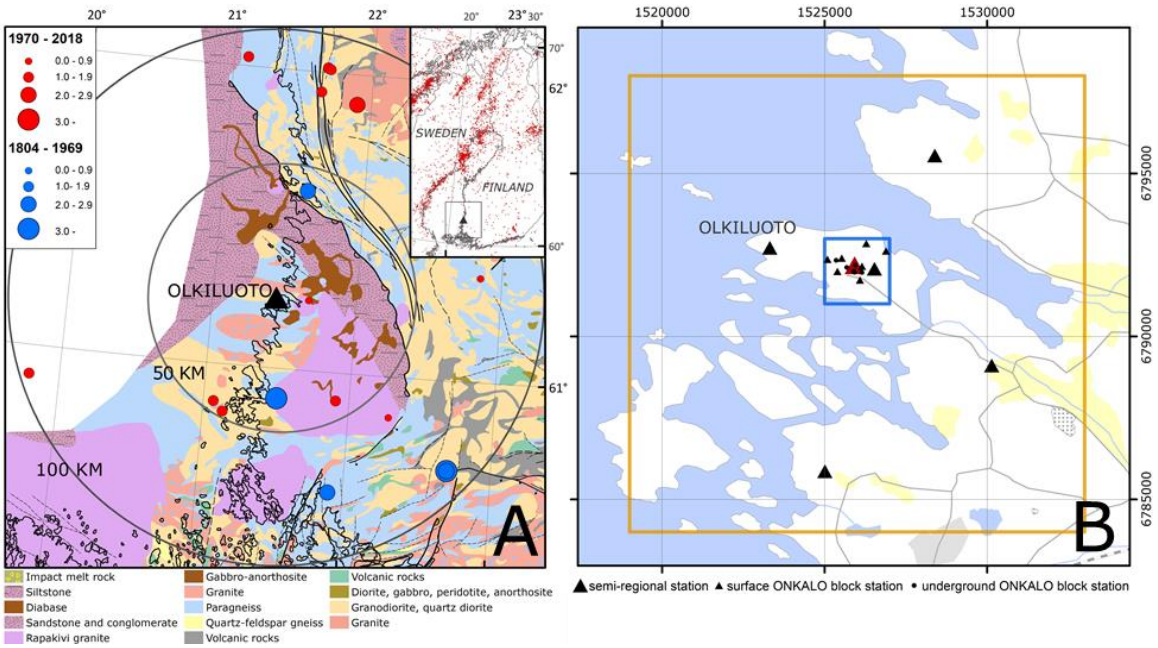

Figure 1. A: Earthquakes observed within 100 km from the Olkiluoto site (ISUH, 2018) on a map of generalized lithology (Nironen et al., 2016). On the locator map, the site is denoted with a black triangle and earthquakes with red (Ahjos and Uski, 1992). **B:** The extent of the 2 km x 2 km (blue) and 14 km x 14 km (amber) seismic monitoring areas and the locations of the seismic stations (black symbols). The final disposal facility is denoted with a red triangle (Background map: MML, 2019). (Figures: Kaisko and Malm, 2019)

2. Earthquake source parameters

Based on the adjusted spectral source model with the ω^3-fit, the 400 microearthquakes (M_L = -3.2 - M_L = -0.5) were estimated to have average source radii from 2 to 69 m, and displacements from 0.1 to 123 µm. The static and dynamic stress drops were from $3.7 \cdot 10^{-4}$ to $8.4 \cdot 10^{-1}$ MPa and $2.4 \cdot 10^{-4}$ to $9.6 \cdot 10^{-1}$ MPa. Energy released as seismic waves during an event was estimated to be from $3.7 \cdot 10^{-4}$ to $1.5 \cdot 10^{2}$ J and seismic potency and moment from $4.9 \cdot 10^{-6}$ to $4.1 \cdot 10^{-2}$ m^3 and from $1.6 \cdot 10^{5}$ to $1.4 \cdot 10^{9}$ Nm, respectively.

The events occurring within the bedrock further away from the excavated volumes had generally smaller source radii, relatively larger displacements on the source, larger stress drops and higher radiated energy especially on the P-wave than the events close to free surfaces at tunnel and shaft openings.

3. Moment tensor solutions and stress field

Seismic moment tensor solutions were computed for all the 400 events identified as probable microearthquakes in 2014 - 2018 using P- and S-wave polarities and amplitudes with the IMS Trace software (IMS, 2019). The quality of the solutions was analysed, and finally 51 of the derived solutions satisfied the predefined criteria and were accepted for further analysis (Figure 2A).

Most of the moment tensors had subvertical pressure axes, which indicates that the microearthquakes occurred mainly close to or at the tunnel walls and were adjusting the perturbed stress field caused by the bedrock openings (Figures 2B & 3A1-A3). On the other

hand, also some earthquakes within undisturbed bedrock were induced by pre-grouting. Moment tensor solutions could be derived for three of them (Figures 2C & 3B1-B3). The derived fault planes are aligned with the brittle fault zone OL-BFZ020a, and the source mechanisms are explained by the combination of the mechanism expected under natural stress field within the uppermost crust (reverse) affected by increased pore pressure (explosive). Based on the analysis of these three events, the natural pressure, tension and intermediate stress axes have trend/plunge values of 294º/16º, 56º/63º and 198º/23º at the site (Kaisko & Malm, 2019) and the stress field approximately corresponds to the direction of natural stress field at the site (Posiva Oy, 2021).

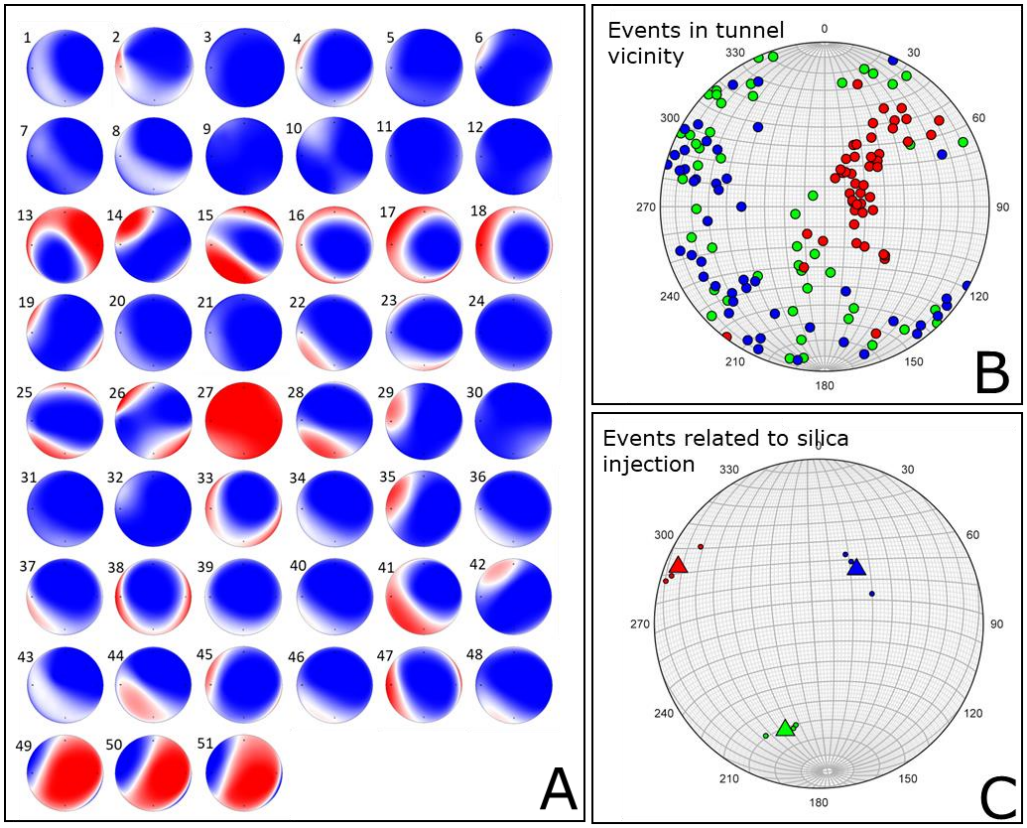

Figure 2. A: The derived 51 moment tensor solutions presented as beach balls on lower hemisphere projection. Blue indicates dilatational and red compressive according to 1% best solutions in Monte Carlo simulations. Beach balls processed with IMS Trace (IMS, 2019). **B & C:** The maximum (P, red), minimum (T, blue) and intermediate (B, green) principal axes defining the stress field orientation estimated with the moment tensor solutions are plotted with spheres. The stress field for the events in tunnel vicinity are presented in **B,** and the pre-grouting induced events within undisturbed bedrock in **C**. Computed maximum eigenvectors for the axes are presented with triangles. (Figures: Kaisko & Malm, 2019)

4. Fault reactivation

Majority of the events occurred when the excavation passed a known brittle fault zone but based on the results of the study it can be stated that these structures have not been reactivated in the sense of releasing continuously stresses through natural mechanisms. Some of the zones have hosted sporadic microearthquakes not only beside the tunnels but also within the bedrock, which could indicate their ability for future reactivation.

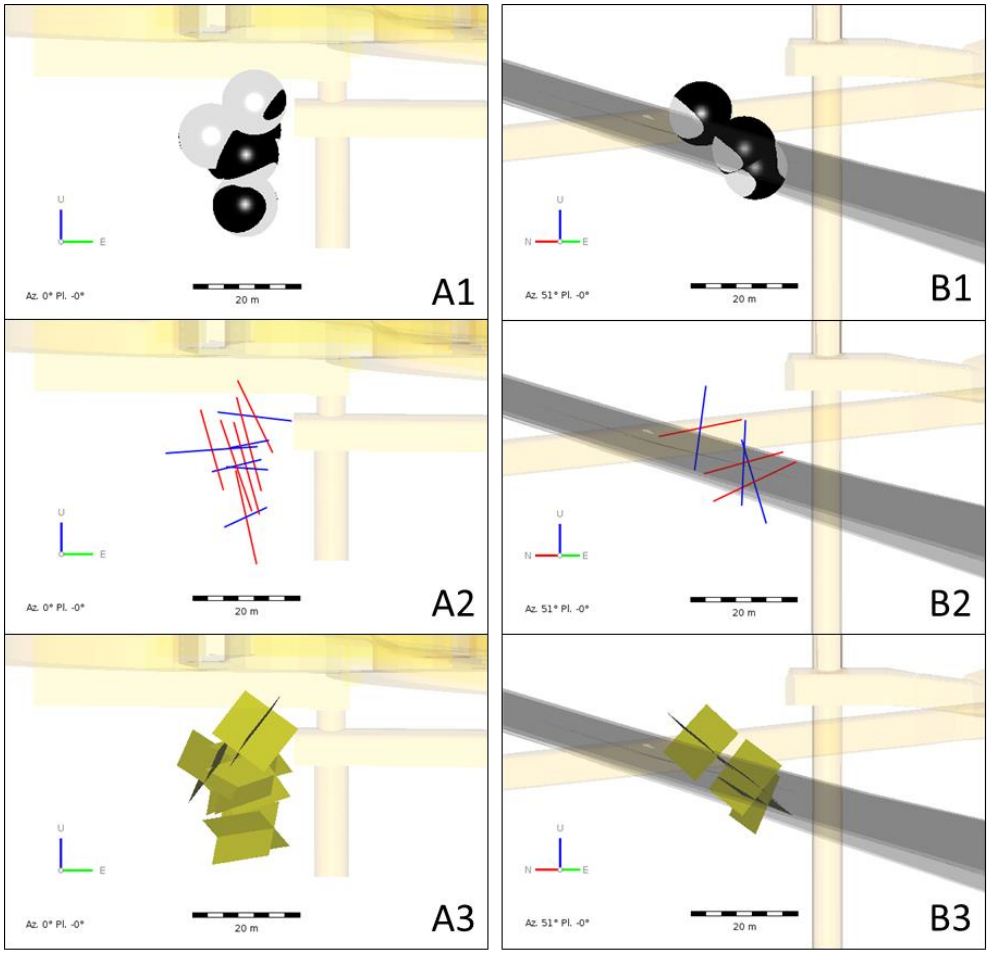

Figure 3. Examples of moment tensor solutions derived for microearthquakes occurring at the canister receiving station opening (A) and on the brittle fault zone OL-BFZ020a (B). The solutions are presented as beach balls (A1 & B1), pressure (red) and tension (blue) axes (A2 & B2), and nodal plane pairs (A3 & B3) for each event. (Figures: Kaisko & Malm, 2019)

References:

Ahjos, T. & Uski, M., 1992. Earthquakes in northern Europe in 1375-1989. Tectonophysics, 207:1-23.

Haapalehto, S. (ed.), Malm, M, Saari, J., Lahtinen, S., Saaranen, V., 2017. Results of Monitoring at Olkiluoto in 2016, Rock Mechanics, Working report 2017-47, 98 pp.

Haapalehto, S. (ed.), Malm, M., Kaisko, O., Lahtinen, S., & Saaranen, V., 2018. Results of Monitoring at Olkiluoto in 2017, Rock Mechanics, Posiva Working report 2018-4, Posiva Oy, Eurajoki, Finland, 86 pp.

Haapalehto, S. (ed.), Malm, M., Kaisko, O., Lahtinen, S., & Saaranen, V., 2019. Results of Monitoring at Olkiluoto in 2018, Rock Mechanics, Posiva Working report 2019-47, Posiva Oy, Eurajoki, Finland, 126

IMS (the Institute of Mine Seismology), 2019. The manual for IMS Trace and Vantage software.

ISUH (Institute of Seismology, University of Helsinki), 2018. Preliminary determinations of local and regional earthquakes recorded by the Finnish seismic network, http://www.seismo.helsinki.fi/bulletin/list/catalog/earthquakes.html, accessed 1.10.2018

Kaisko, O. & Malm M., 2019. Microearthquakes During the Construction and Excavation of the Final Repository for the Spent Nuclear Fuel at Olkiluoto in 2002-2018. Working Report 2019-05, Posiva Oy, Olkiluoto, Finland.

MML, 2019. Background map series. https://tiedostopalvelu.maanmittauslaitos.fi/ accessed 20.9.2019

Nironen, M., Kousa, J., Luukas, J. & Lahtinen, R., 2016. Geological map of Finland – Bedrock, GTK, Espoo.

Posiva Oy. 2021. Olkiluoto Site Description 2018. *In Preparation*. Posiva Oy, Eurajoki, Finland

Saari, J., 2003. Seismic Network at the Olkiluoto Site, Working Report 2003-37. Posiva Oy, Eurajoki, Finland,

Saari, J., 2005. Local Seismic Network at the Olkiluoto Site. Annual Report for 2002-2004, Posiva Workreport 2005-48, Posiva Oy, Eurajoki, Finland. 37 pp.

Conglomeratic rocks fringing the Archean Iisalmi block in central Finland: Evidence for the timing and nature of the break-up of the Karelia craton

K. Kärenlampi[1], A. Kontinen[2], V. Kylli[1] and Y. Lahaye[3]

[1]Oulu Mining School, P.O. Box 3000, 90014 University of Oulu, Finland
[2]Geological Survey of Finland, P.O. Box 1237, 70211 Kuopio, Finland
[3]Geological Survey of Finland, P.O. Box 96, 02151 Espoo, Finland
E-mail: kimmo.karenlampi@oulu.fi

The evolution of the Svecofennia-Karelia boundary zone is usually interpreted in terms of continental break-up at ca. 2.05 Ga and subsequent oblique protocontinent (Svecofennia)–continent (Karelia) collision at ca. 1.90 Ga. However, only scarce rock formations occure in the rock record of the boundary zone that can potentially be linked to the break-up event(s). We are currently studying four occurrences of conglomeratic rocks at the northern and western edges of the Archean Iisalmi block in central Finland. These conglomerates contain phenoclasts, which can give information on the nature of their provenance and depositional environments and processes and could be linked to the assumed 2.05 Ga break-up. For example, our first U-Pb zircon dating results show that the phenoclasts record a previously unrecognised 2.03–2.05 Ga felsic volcanic-sedimentary event.

Keywords: conglomerate, continental break-up, Paleoproterozoic, Karelia craton, Iisalmi, Finland

1. Introduction

The evolution of the Svecofennia–Karelia boundary zone is usually interpreted in terms of continental break-up at ca. 2.05 Ga and subsequent oblique protocontinent (Svecofennia)–continent (Karelia) collision at ca. 1.90 Ga. Some of the proposed models of the 2.05–1.90 Ga evolution are complex, including not only the ca. 2.05 Ga break-up, but also a later break-up-scale within margin extensional event at ca. 1.95 Ga (Lahtinen et al. 2015). A problem in this model is that only scarce rock formations occur in the rock record of the boundary zone that can potentially be linked to the break-up event(s).

We are currently studying four occurrences of conglomeratic rocks (Figure 1), which can potentially be linked to the above-above mentioned break-up event and include: 1) the conglomerates in association with the ca. 2.05 Ga Otanmäki suite A-type granites in the Otanmäki–Kuluntalahti nappe (Kärenlampi et al. 2019); 2) the conglomerates in the Itämäki schist belt located 10 km to the west from Otanmäki (Luukas, 1991); 3) the Haajainen conglomerates along the eastern margin of the Salahmi belt (Korkiakoski and Laajoki, 1988); and 4) the conglomerates fringing the Archaean Pirttimäki complex at Kukkomäki (Savolahti, 1964). In addition to obviously locally derived phenoclasts, the conglomerates also contain exotic phenoclasts that lack obvious source in the surrounding bedrock. Many of the phenoclasts are such that they can be deemed to carry significant information on the timing and geological processes related to the break-up of the Karelia craton. The conglomerate occurrences will be studied with respect to their geological setting, phenoclast rock types, chemical composition and age (zircon U-Pb dating) in order to obtain insights to their formative setting and provenance.

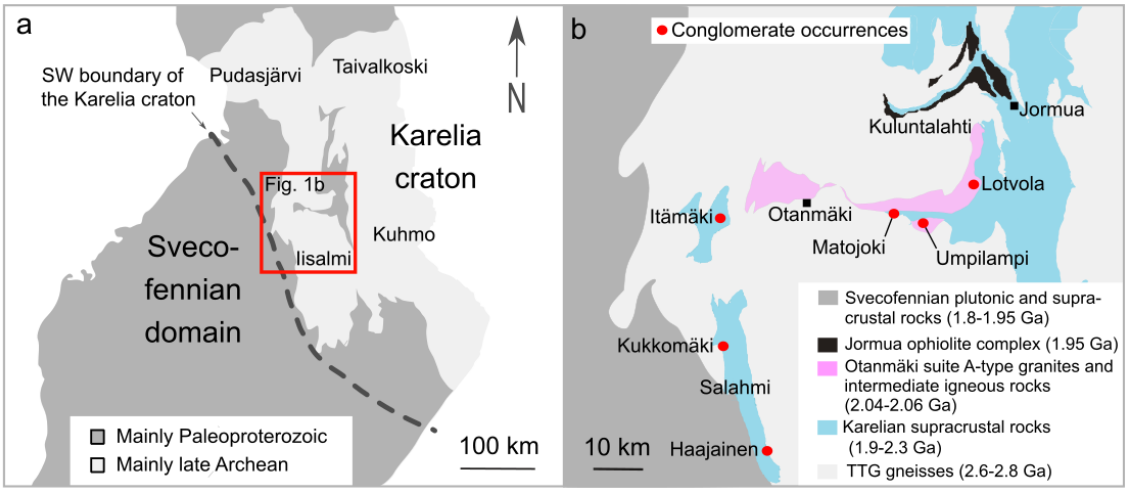

Figure 1. (a) Location of the study area (red rectangle) close to the SW margin of the Archean Karelia craton. b) Map showing the geological setting of the conglomerate occurrences at the northern and western edges of the Archaean Iisalmi block in central Finland (modified after Bedrock of Finland – DigiKP and Kärenlampi et al., 2019).

2. Geological descriptions of the conglomerate occurrences

The conglomerates from the Otanmäki-Kuluntalahti nappe constitute three formations Lotvola, Umpilampi and Matojoki (Figure 1b). The first two occur as inliers enclosed by the Otanmäki suite A-type granite in the nappe (Kärenlampi et al., 2019), whereas the last mentioned one is located in a tectonic lens lining the nappe. At Lotvola and Umpilampi, the pebble- to boulder-sized phenoclasts are of mainly composed of intermediate and felsic plutonic and volcanic rocks and occur in an intraclast matrix metamorphosed of materials formed by mafic volcanic and sedimentary carbonate materials (Figure 2a–b). The 1x2-km-sized Matojoki lens contains clast supported, mostly rock fall avalanche conglomerates mostly with gabbroic boulders but locally felsic subvolcanic-volcanic rock and mica schist boulders as well (Figure 2c–d).

The conglomerates in the Itämäki belt occur as intercalations in <100-m-thick quartz wacke formation within metagreywacke (Figure 2e–f). They contain mainly cobble-sized clasts of mature feldspar quartzite and orthoquartzite, but also boulders–cobbles of gabbro and other mafic rocks, felsic volcanic rocks and mica and black schist.

The strongly deformed Haajainen conglomerates fringing the southeastern margin of the Salahmi belt as a 100- to 1000-m-wide sheet, contain phenoclasts of mainly granodioritic to trondhjemitic plutonic and heavily altered mafic volcanic rocks, but also pebbles–cobbles of intermediate and felsic alkaline plutonic and volcanic rocks (Figure 2g–h). The Kukkomäki conglomerates are also strongly deformed and mainly comprise leucogranite–granodiorite pebbles–cobbles, but usually also some mica schist clasts.

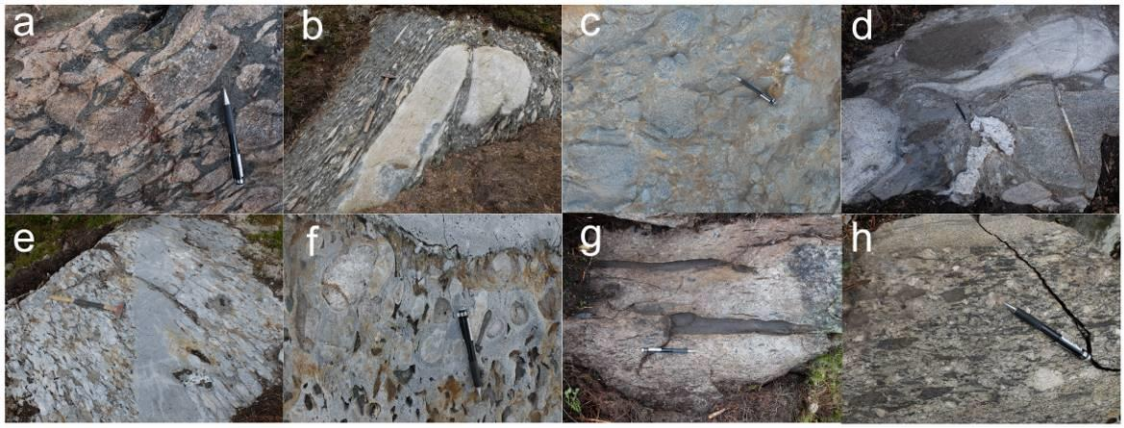

Figure 2. Outcrop photographs. Conglomerate composed mostly of boulders–cobbles of felsic volcanic rocks (light-grey) and calc-silicate matrix (dark-green) at (a) Umpilampi and (b) Lotvola. Psephitic slump/debris avalanche deposits composed mainly of metagabbroic-basaltic boulders (c) and metagabbroic, felsic volcanic rock and mica schist boulders and cobbles at Matojoki. (e–f) Quartz wacke intercalated conglomerates composed of mainly quartzite and felsic volcanic rock cobbles at Itämäki. (g) Heavily altered mafic volcanic rock phenoclasts and (h) pebbles–cobbles of intermediate and felsic alkaline plutonic and volcanic rocks at Haajainen.

3. First U-Pb zircon dating results

The emphasis in the study will be in geochemistry and geochronology of the phenoclasts. In the present early stage of the study, we mainly have semi-quantitative major and trace element data generated by portable X-ray fluorescence spectrometry (pXRF), which we have used in classification and selection of samples for future quantitative chemical analysis and age determination. We have already obtained U-Pb zircon age data for felsic volcanic phenoclasts from the Umpilampi, Lotvola, and Matojoki conglomerates (Figs. 1 and 3). Mineral separation yielded abundant euhedral zircon grains from all three samples. After standard sample preparation procedures, in-situ spot analysis were performed at the Geological Survey of Finland in Espoo using a Nu Plasma AttoM single collector ICPMS connected to a Photon Machine Excite laser ablation system (Huhma et al. 2018).

Obviously magmatic zircon grains from the Umpilampi sample plot on the concordia, giving an age of 2038±9 Ma (Figure 3a). The isotope compositions from the Lotvola sample are slightly discordant and yield a somewhat imprecise upper intercept age of 2053±31 Ma (Figure 3b). Still this age is interpreted to represent the timing of magmatic crystallization. The obtained ages are within the age limits of the Otanmäki suite A-type magmatism (ca. 2.04–2.06 Ga), indicating that in addition to felsic plutonism, this magmatic stage also included previously unrecognized volcanic activity. Analyses of zircon grains from the Matojoki sample produce slightly younger results, a concordia age of 2026±11 Ma (Figure 3c) and a similar upper intercept age of 2031±12 Ma, indicating that the age of the volcanic source of the dated phenoclasts and the maximum depositional age of the host conglomerate is approximately 2.03 Ga.

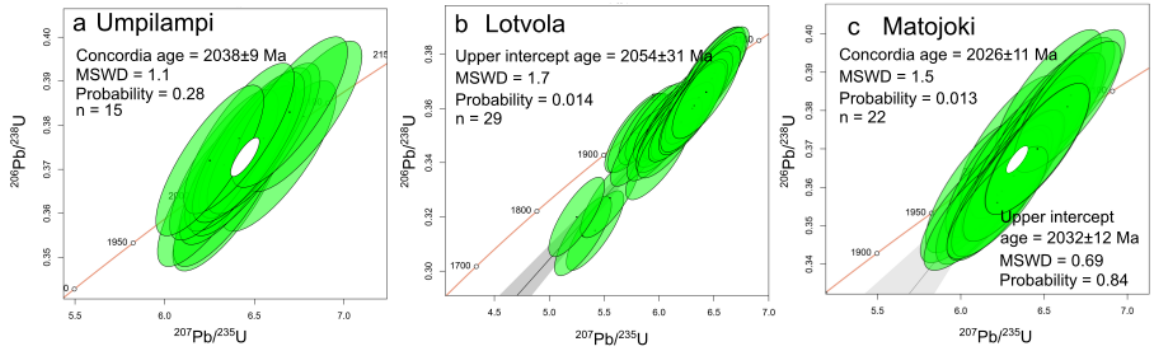

Figure 3. Concordia plots of U–Pb zircon data obtained for the felsic volcanic phenoclasts from (a) Umpilampi (b) Lotvola and (c) Matojoki conglomerate occurrences. The age calculations and concordia diagrams were made using IsoplotR (Vermeesch, 2018).

4. Discussion and closing remarks

The research we have already conducted has revealed that the craton margin conglomerates display a surprisingly large variation in the rock types of their phenoclasts, which include alkaline felsic volcanic rocks, gabbroic rocks, and black schists, providing much new information on the nature of their source and depositional environment and processes.

Our first geochronological results show that the Otanmäki stage of magmatism, which generated the Otanmäki suite evolved plutonic rocks, also includes previously unrecognized, 2.03–2.05 Ga felsic volcanic-sedimentary activity, for which there is, similarly as for the concurrent plutonism, no obvious manifestation in the regional rock record outside the Otanmäki-Kuluntalahti nappe. This finding further supports the idea that the Otanmäki-Kuluntalahti nappe is an exotic allochtonous unit (Kärenlampi et al., 2019), which was thrust on the Karelia craton from a root located west of the present craton margin, similarly to the Jormua ophiolite-bearing allochton, which was obducted possibly from even further from "the lost or hidden west".

Our observations clearly demonstrate that valuable information of the evolution of the western margin of the Karelia craton can be obtained by studying craton-fringing conglomerate occurrences, though it is possible that some of these conglomerates are not related to the assumed 2.05 Ga break-up. Especially the Haajainen conglomerate may be significantly younger.

6. References:

Huhma, H., Hanski, E., Kontinen, A., Vuollo, J., Mänttäri, I., Lahaye, Y., 2018. Sm–Nd and U–Pb isotope geochemistry of the Paleoproterozoic mafic magmatism in eastern and northern Finland. Geol. Surv. Finl., Bull. 405, 150 p.

Lahtinen, R., Huhma, H., Lahaye, Y., Kousa, J., Luukas, J., 2015. Archean–Proterozoic collision boundary i central Fennoscandia: Revisited. Precambrian Res. 261, 127−165.

Luukas, J., 1991. Salahmin-Pyhännän alueen stratigrafia ja rakennegeologia. Abstract: Stratigraphy and structure of the Early Proterozoic Salahmi-Pyhäntä area, central Finland. Res Terrae. Ser. B 16. 131 p.

Kärenlampi, K., Kontinen, A., Huhma, H., Hanski, E., 2019. Geology, geochronology and geochemistry of the 2.05 Ga gneissic A1-type granites and related intermediate rocks in central Finland: implication for the tectonic evolution of the Karelia craton margin. Bull. Geol. Soc. Finl. 91, 35–73.

Korkiakoski, E., Laajoki, K., 1988. The paleosedimentology of the early Proterozoic Salahmi Schist Belt, Central Finland. Geol. Surv. Finl., Spec. Pap. 5, 49-73.

Savolahti, A., 1964. On the schists and associated intrusive rocks of the Vieremä-Kiuruvesi region. Bull. Comm. Géol. Finl., 218, 1–83.

Vermeesch, P., 2018, IsoplotR: a free and open toolbox for geochronology. Geosci. Front. 9, 1479-1493.

Koillismaa Deep Hole – Solving the mystery of a geophysical anomaly

T. Karinen[1], S. Heinonen[2], J. Konnunaho[1], H. Salmirinne[1], I. Lahti[1] and A. Salo[3]

[1]Geological Survey of Finland, P.O. Box 77, FI-96101 Rovaniemi, Finland
[2]Geological Survey of Finland, P.O. Box 96, FI-02151 Espoo, Finland
[3]Geological Survey of Finland, P.O. Box 1237, FI-70211 Kuopio, Finland
E-mail: tuomo.karinen@gtk.fi

Geological Survey of Finland is drilling a 3000 m long hole into the geophysically anomalous zone in the Koillismaa area. Drilling has been preceded by gravity and magnetic measurement, seismic reflection soundings and AMT measurements showing anomalous feature in depth. The aim of drilling is to find out the source of the anomaly.

Keywords: deep drilling, seismic reflection, gravity, mineral potential, Koillismaa

1. Introduction

Koillismaa area in Finland has been a geological mystery for several decades. Magnetic and gravimetric measurements show anomalous values caused by a deep unknown geological origin. In LITHOSPHERE 2018 Symposium, Gislason et al. (2018) presented preliminary results from Koillismaa Seismic Exploration Survey (KOSE) project. The KOSE seismic reflection profile revealed prominent reflectivity of the subsurface and provided new information about the deep gravimetric and magnetic anomaly zone known at the Koillismaa area. These geophysical data have motivated the ongoing ambitious drilling project that attempts to solve a mystery which has been struggling the curious minds of geoscientists already for many decades. GTK started to drill a 3000 m long drill hole in the heart of the anomaly in September 2020, to finally collect rock samples from the source of the anomalous zone. In this abstract we briefly describe the background, geophysical studies, modelling and present stage of the ongoing drilling. We also describe the specific drilling technique used in order to reach the intended target inside the Archean basement of Koillismaa area.

2. Geological framework

The Koillismaa deep anomaly is ca. 50 km long zone which connects the distant parts of the 2.45 Ga layered intrusion blocks of the Koillismaa (Alapieti 1982; Karinen 2010) and mafic-ultramafic Näränkävaara intrusion (Alapieti 1982; Järvinen et al. 2020) (Figure 1). The zone is also partly traceable by a zone of breccia outcrops (Figure 2), but the relationship of the gravimetric anomaly and the breccia is unclear, although it is known that the breccia is not the source of the anomaly and no other possible causes are noticeable on the surface either. For this reason, the anomaly has been interpreted to reflect the location of a chonolith-like feeder zone for the magmas of the exposed mafic-ultramafic intrusions in the Koillismaa. Alternatively, the anomaly could reflect the presence of mafic-ultramafic rocks representing some other magmatic episode than the 2.45 Ga intrusions, for example, the Archaean greenstone belts near the Koillismaa area. This kind of voluminous mafic-ultramafic systems are globally rare, and therefore, the target is very likely an interesting example of plume derived magmatism of Fennoscandian shield. Mafic-ultramafic rocks are very potential for several commodities such as orthomagmatic Ni-Cu-Co-PGE and Cr-V-Ti-Fe.

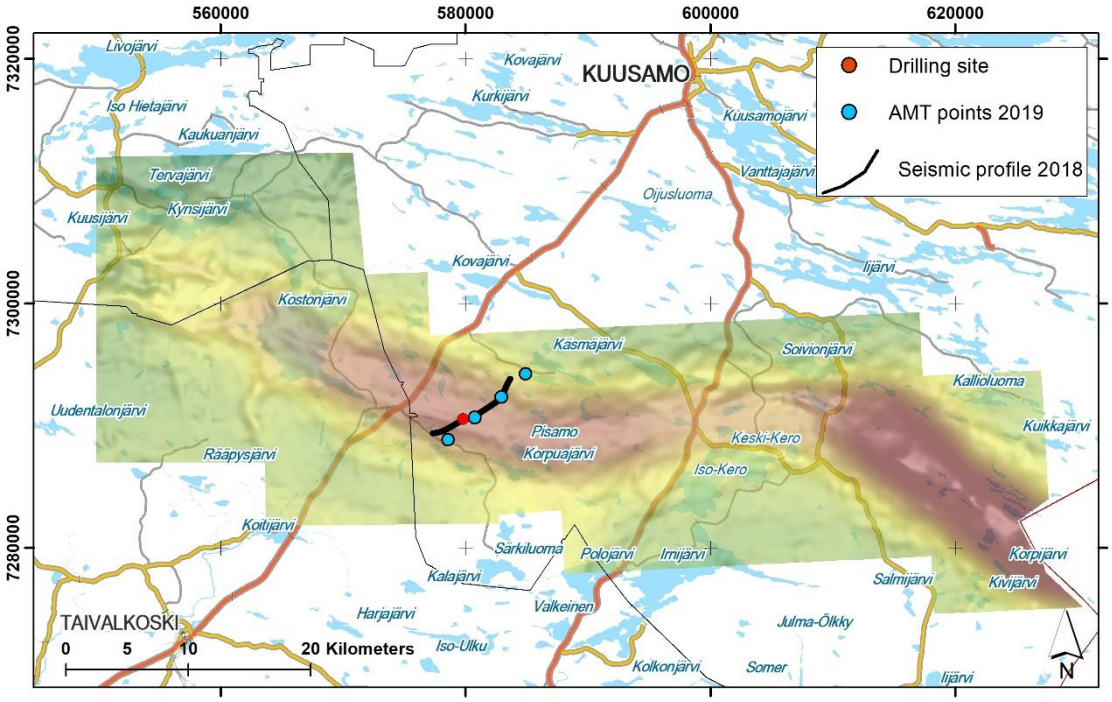

Figure 1. Drilling site on the regional gravity map. Locations of seismic profile 2018 and AMT surveys 2019 are plotted also.

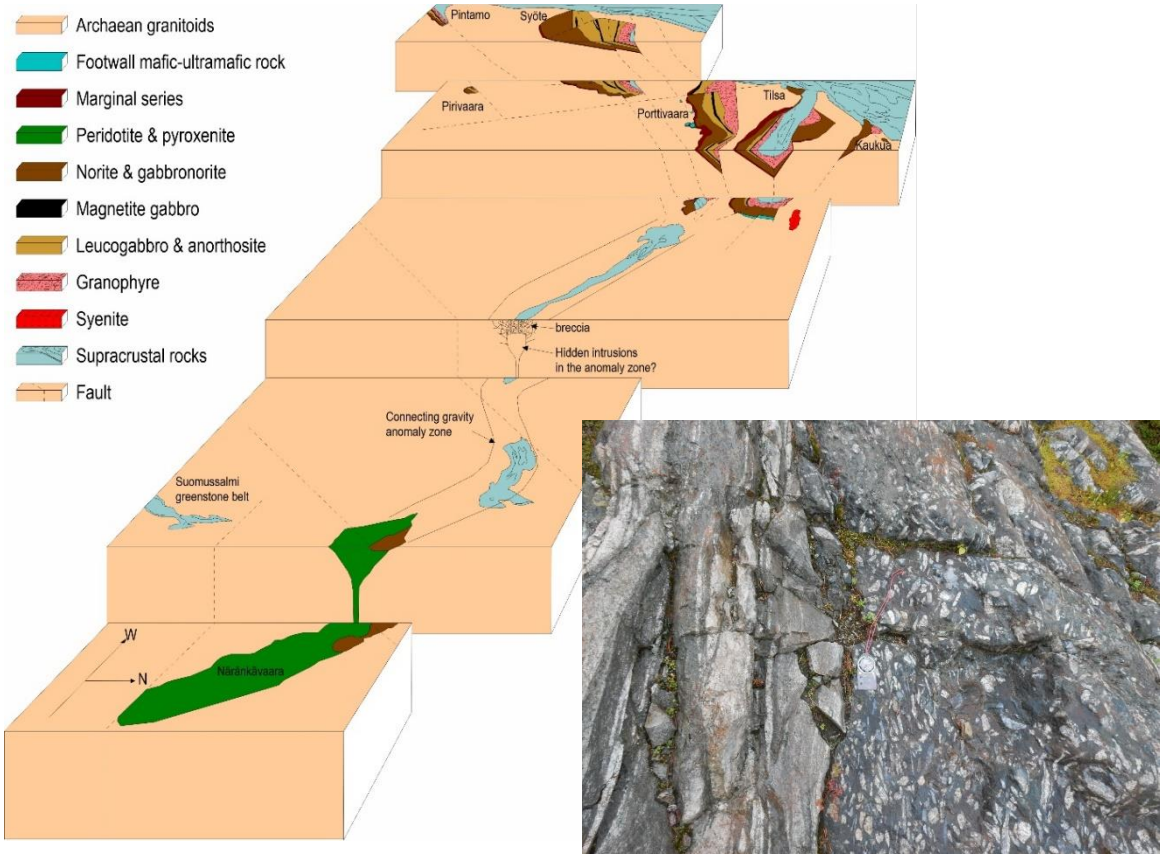

Figure 2. Geological framework of the Koillismaa area shown as exploded blocks. Photo shows outcrop containing breccia and paragneissic basement rock from Poroperä area near Lake Kostonjärvi.

3. Geophysical studies

The anomaly zone is most clearly observed by gravity and magnetic measurements, which were performed already as early as 1950s. Last geophysical surveys carried out by GTK were a seismic survey in 2018 and an audiomagnetotelluric survey (AMT) 2019.

All previous interpretation of the gravity anomaly indicate that the unexposed source is about 2.5-5 km wide and that the depth of the upper surface is between 1 and 2 km below the present erosion level depending on the location along the anomaly (Piirainen et al. 1978; Saviaro 1976). Interpretation of earliest AMT-surveys in 1970s brought up a weak conductivity anomaly located in the same area than gravity anomaly (Saviaro, 1976). The AMT surveys made in 2019 confirmed the existence of this conductivity contrast.

The KOSE seismic reflection data was acquired along the road close to the drilling site with 90 wireless geophones and explosive sources (Gislason et al. 2019). The resulting seismic reflection cross-sections show prominent reflectors that will be penetrated by the drill hole (Figure 3). These reflectors are expected to be lithological contacts or fracture zones that cause abrupt change of acoustic impedance within the subsurface. The upper boundary of the source of the gravity anomaly is expected to be at approximately 1.5 km depth based on changes in reflectivity.

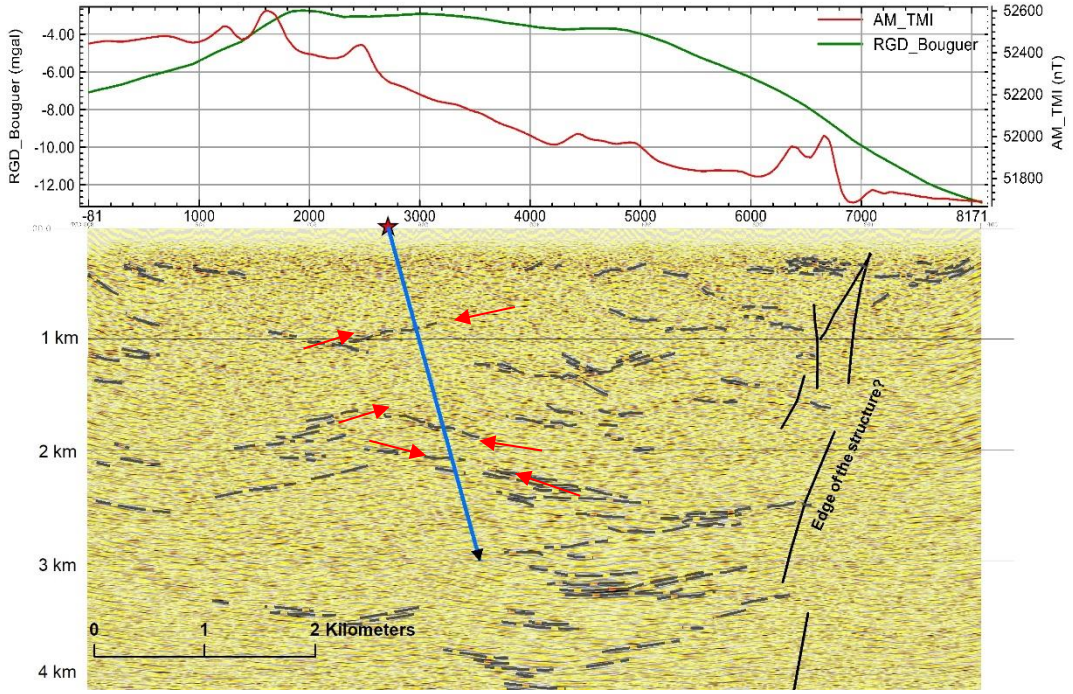

Figure 3. Planned drill hole projected to the KOSE seismic reflection profile. Red arrows are pointing to the most prominent reflectors drill hole will penetrate. Gravity (RGD_Bouguer) and airborne magnetic (AM_TMI) profiles are plotted above the seismic section.

4. Drilling technique

According to the original plan, the drilling is conducted within 5 months. The contractor to perform the drilling is Arctic Drilling Company Ltd (ADC) from Rovaniemi, who uses diamond drill rigs of their own design and manufacturing. The contractor uses best available techniques designated to these rock types based on their previous experiences in deep hole (>1500m) drilling projects. The rig has been anchored to the bedrock with a 30 m cemented anchoring

hole (diameter 96 mm). This anchoring is to prevent resonation of the rig once the core reaches a certain depth. At the beginning of the drilling campaign, a fractured bedrock down to 300 m caused serious technical challenges, which showed up mostly as continuous losses of water pressure. Therefore, a decision was eventually made to use 96 mm rods as a casing for the first 300 m. If these poor rock conditions were known beforehand, the drilling could have been started with this rod size already at the beginning of the drilling campaign. The rig was changed to a more efficient version when the first half, i.e., 1500 m of the planned 3000 m length was reached in early December 2020. The change to a more powerful drill rig, to ADC's K10, ensures that project reaches the targeted 3000 m depth. The K10 is the flagship of ADC´s fleet, and in theory, with this diamond drill rig it is possible to reach depths of 3500 m. Towards the end of drilling campaign, the rods themself will eventually weigh over 20 tonnes at the depth of 3000 m. At this length of drilling, the strength of the rod will be put to a test in which their breaking strength is the limit of drilling.

5. Discussion

In addition to increased geological understanding and unique rock samples from depth, this research has impact on providing scientific platform and testing environments for future studies. These are, for example, development of survey technology, 3D modelling, studies of geothermal energy, deep groundwater and bedrock stability.

6. Conclusions and future work

Koillismaa Deep Hole is expected to shed light into the mystery of geophysical anomaly by proving rock samples from the core of the anomaly. In addition to the study of age and composition of these samples, the future work will include several different geophysical surveys, including (1) semi-passive seismic experiment where drilling noise is utilized for retrieving a model of seismic velocity in the drill hole vicinity, (2) crossing seismic reflection profile to the KOSE profile, (3) densification of AMT measurements and testing different drill hole geophysics methods.

References:

Alapieti, T., 1982. The Koillismaa layered igneous cornplex, Finland - its structure, mineralogy and i geochemistry, with ernphasis on the distrubution of chromium. Geological Survey of Finland, Bulletin 319. 116 p.

Gislason, G., Heinonen, S., Konnunaho, J., Moisio, K., Nevalainen, J., Salmirinne, H., 2018. KOSE - Koillismaa Seismix Exploration survey: Details and first results, 11-14. In: Kukkonen et al. (Eds.), 2018. Lithosphere 2018 – Tenth Symposium on the Structure, Composition and Evolution of the Lithosphere. Programme and Extended Abstracts, Oulu, Finland, November 14-16, 2018. Institute of Seismology, University of Helsinki, Report S-67, 134 p.

Gislason, G., Heinonen, S., Salmirinne, H., Konnunaho, J. and Karinen, T., 2019. KOSE - Koillismaa Seismic Exploration survey: Acquisition, processing and interpretation. GTK:n työraportti - GTK Open File Work Report, 26 p.

Järvinen, V., Halkoaho, T., Konnunaho, J., Heinonen, J., Rämö T., 2020. Parental magma, magmatic stratigraphy, and reef-type PGE enrichment of the 2.44-Ga mafic-ultramafic Näränkävaara layered intrusion, Northern Finland. Mineralium Deposita 55, p. 1535-1560.

Karinen T., 2010. The Koillismaa Intrusion, northeastern Finland – evidence for PGE reef forming processes in the layered series. Geological Survey of Finland, Bulletin 404, 176 p.

Piirainen, T., Hugg, R, Aario, R., Forsström, L., Ruotsalainen, A., Koivumaa, S., 1978. Koillismaan malmikriittisten alueiden tutkimusprojektin loppuraportti 1976. Summary: The Report of the Koillismaa Research Project. Geologinen tutkimuslaitos. Tutkimusraportti n:o 18. 51 p.

Saviaro, K., 1976. Geofysikaalisia tutkimuksia Koillismaan gabrointruusioiden alueella. Lisensiaattityö, Oulun yliopiston geofysiikan laitos. 72 S. PSMTPl/3-76-6.

The trace element composition of magmatic apatite: Mineralogical and geological controls on apatite trace element chemistry in magmatic systems

S. Karvinen[1], A. Heinonen[1] and C. Beier[1]

[1]P.O. Box 64 (Gustaf Hällströmin katu 2)
FI-00014 University of Helsinki
Finland
E-mail: seppo.karvinen@helsinki.fi

This project focuses on the trace element composition of apatite minerals in a variety of magmatic systems: carbonatites, mafic-ultramafic intrusions, and rapakivi granites. The main aim is to study the trace element characteristics of apatite in these magmatic systems and to gain a better understanding on how apatite affects their magmatic trace element budget. The chemical compositions of the apatite are studied with *in situ* analytical techniques and the results will form a consistent chemical database of igneous apatite in various rock types in Finland.

Keywords: apatite, mineral chemistry, trace elements

1. Introduction

Apatite minerals form a supergroup of structurally similar but chemically diverse minerals (Pasero et al. 2010). Calcium phosphate apatite [Ca-P apatite group i.e. $Ca_{10}(PO_4)_6(Cl,F,OH)_2$] is a common accessory mineral in a variety of rock types in igneous, metamorphic, and sedimentary rocks (e.g. Piccoli and Candela, 2002, Hughes and Rakovan, 2015). Although only an accessory phase, apatite fundamentally controls the P budget of crustal rocks as it is usually the main phase that incorporates phosphorus (e.g., Filippelli, 2008). Apatite also accommodates a wide variety of other elements, e.g. rare earth elements (REE), actinides (Th, U), and volatiles (H_2O, C, halogens, S; e.g., Pan and Fleet, 2002; Hughes and Rakovan, 2015). The composition and structure of apatite can thus be used to trace a variety of petrogenetic processes (e.g. Mao et al. 2016, Bruand et al. 2017). Apatite is also a valuable industrial mineral as different kinds of exploitable phosphate rock deposits are composed of apatite minerals (Filippelli 2008). Some of these deposits can possibly be mined for REE as well (Emsbo et al. 2015). This project will concentrate on the geochemical control on coupled trace element substitution mechanisms of apatite (e.g. Pan and Fleet, 2002) especially in CO_3, Cl-, and F-enriched magmatic systems.

2. Research methods

The quantitative *in situ* analytical methods utilized in the project are electron microprobe (EPMA) and laser ablation inductively coupled plasma mass spectrometry (LA-ICP-MS). Imaging techniques such as back-scattering electron (BSE) and cathodoluminescence (CL) scanning electron microscopy (SEM) will be used to document mineral zoning patterns. Using these techniques prior to quantitative analysis methods aids in the planning of analysis spots and avoiding inclusions, and permits the distinction of possible zoning patterns. The combined use of EPMA and LA-ICP-MS analyses allows full quantification of mineral chemistry from major elements and halogens to trace elements.

3. Study areas

The main study area of the carbonatite sub-project is the Archean Siilinjärvi glimmerite-carbonatite complex in Eastern Finland, which is one of the oldest carbonatites (2610±4 Ma; O'Brien et al. 2015) in the world. All of the glimmerite-carbonatite rock types typically contain around 10 vol%, but up to 30 vol% apatite. The rocks are very heterogenous and are basically a mix between the two primary rock types.

The Siilinjärvi apatite is commonly a few millimetres up to several centimeters in length, subhedral to euhedral and may contain multiphase inclusions. The few published analyses of the trace element concentrations of Siilinjärvi apatites are all made of bulk chemical analyses of mineral separates and thus do not represent the composition of just the apatites, but also of the possible inclusion phases (e.g., monazite, zircon, pyrochlore, or carbonates; Al-Ani, 2013). The possible chemical zoning characteristics of the apatites is also not known.

In the other two sub-projects apatite in massif-type anorthosites, layered intrusions, and rapakivi granites will be studied. Oxide- and apatite-enriched rock types (nelsonites and oxide-apatite gabbronorites), often associated with massif-type anorthosites (McLelland, 1994; Dymek and Owens, 2001) have recently been reported from the Ahvenisto Complex in Southeastern Finland (Fred et al. 2020). Rapakivi granites are enriched in fluorine and commonly contain apatite as an accessory phase but also other phosphate and fluorine-bearing phases (e.g., monazite, fluorite; e.g., Rämö and Haapala 2005).

The study of apatite in these compositionally different magmatic environments allows us to establish a model of trace element substitution mechanisms and to gain an understanding of the geological and mineralogical controls that influence them.

References:

Al-Ani, T. 2013. Mineralogy and petrography of Siilinjärvi carbonatite and glimmerite rocks, eastern Finland. Geological Survey of Finland Report, 164.

Bruand, E., Fowler, M., Storey, C., Darling, J. 2017. Apatite trace element and isotope applications to petrogenesis and provenance. American Mineralogist, 102, 75–84.

Chakhmouradian, A.R., Reguir, E.P., Zaitsev, A.N., Couëslan, C., Xu, C., Kynický, J., Hamid Munin, A., Yang, P. 2017. Apatite in carbonatitic rocks: Compositional variation, zoning, element partitioning and petrogenetic significance. Lithos, 274, 188–213.

Emsbo, P., McLaughlin, P.I., Breit, G.N., du Bray, E.A., Koenig, A.E. 2015. Rare earth elements in sedimentary phosphate deposits: solution to the global REE crisis? Gondwana Research, 27, 776–785.

Filippelli, G.M. 2008. The global phosphorus cycle: past, present, and future. Elements, 4, 89–95.

Fred, R., Heinonen, A., Heinonen, J.S. 2020. Equilibrium crystallization of massif-type anorthosite residual melts: a case study from the 1.64 Ga Ahvenisto complex, Southeastern Finland. Contributions to Mineralogy and Petrology, 175, 1–23.

Hughes, J.M., Rakovan, J.F. 2015. Structurally robust, chemically diverse: apatite and apatite supergroup minerals. Elements, 11, 165–170.

Mao, M., Rukhlov, A.S., Rowins, S.M., Spence, J., Coogan, L.A. 2016. Apatite trace element compositions: a robust new tool for mineral exploration. Economic Geology, 111.

O'Brien, H., Heilimo, E., Heino, P. 2015. The Archean Siilinjärvi carbonatite complex. In Mineral deposits of Finland, pp. 327–343.

Pan, Y., Fleet, M.E. 2002. Compositions of the apatite-group minerals: substitution mechanisms and controlling factors. Reviews in Mineralogy and Geochemistry, 48, 13–49.

Pasero, M., Kampf, A.R., Ferraris, C., Pekov, I.V., Rakovan, J., White, T.J. 2010. Nomenclature of the apatite supergroup minerals. European Journal of Mineralogy, 22, 163–179.

Piccoli, P.M., Candela, P.A. 2002. Apatite in igneous systems. Reviews in Mineralogy and Geochemistry, 48, 255–292.

Rämö, O.T., Haapala, I. 2005. Rapakivi granites. In: Developments in Precambrian Geology 14, 533–562.

SEISMIC RISK – Mitigation of induced seismic risk in urban environments

A. Korja[1], N. Junno[1] and SEISMIC RISK Working Group[1]

[1]Department of Geosciences and Geography, P.O. Box 64, FIN-00014 University of Helsinki
E-mail: annakaisa.korja@helsinki.fi

In the SEISMIC RISK - Mitigation of induced seismic risk in urban environments - project, the research consortium consisting of University of Helsinki, VTT Technical Research Centre of Finland and Geological Survey of Finland is studying how to mitigate induced seismic risk associated with deep geothermal power stations in Finland. Small-magnitude earthquakes pose a risk to critical sensitive infrastructure such as hospitals, data centres and underground construction. Risk can be mitigated with transparent permitting, seismic monitoring and regional planning. The project will publish a set of seismic hazard maps of Finland and especially of the Helsinki Capital Region and assess the potential impact of seismic waves on different parts of the capital area via 3D models: shear wave tomography, conceptual soil and bedrock model. The project will study the different roles the national, regional and municipal governance in the "wicked" permitting processes. It will assess what information on induced seismicity and associated risks and at what level of detail the authorities need it.

Keywords: seismicity, induced seismicity, risk, hazard, geothermal power plant, GMPE, 3D structural model, tomography, soil properties, urban areas, regulators

1. Introduction

Deep geothermal energy has huge potential as environmentally friendly CO_2-free district heat source in urban centres. A drawback is that geothermal systems can induce earthquakes that pose seismic risk to critical sensitive infrastructure such as hospitals, data centres and underground construction. Risk can be mitigated with implementing transparent regulatory processes, defining adequate seismic monitoring plans and regional planning. The SEISMIC RISK project focuses on how to evaluate, mitigate and communicate seismic hazard and risk in an urban environment. One of the associated challenges is the unclear regulatory process and unclear roles of the different actors in Finland. It is also necessary to clarify what sort of information and at what level of detail the authorities need information on induced seismicity and associated risks.

A research consortium consisting of the University of Helsinki, VTT Technical Research Centre and the Geological Survey of Finland, initiated a project centred around the Otaniemi deep geothermal system, using and creating high quality datasets on induced seismicity as well as geological background data. As both scientific and societal impact is targeted, the work is organized into nine work packages each focusing on different but interrelated challenges. The work packages are 1) Intra-plate hazard, 2) Induced seismicity and its effect on urban hazard, 3) Tomography model of the Helsinki capital region, 4) Regional geological 3D model for the Helsinki capital region, 5) Vulnerabilities and risks of building infrastructure, 6) Controlling factors of disturbing sound patterns for induced earthquakes, 7) Data management, 8) Managing wicked problems in governance of geothermal energy, and 9) Dissemination and outreach.

[1] **SEISMIC RISK Working Group**: Arhe K., Arola T., Bäcklund P., Fülöp L., Hillers G., Hornborg N., Huotari T., Junno N., Jussila V., Keto L., Kosonen E., Lahtinen R., Lindqvist T., Mäntyniemi P., Oinonen K., Ojala A., Putkinen N., Rintamäki A., Tiira T., Tuomisaari J., Uski M., Veikkolainen T., Voutilainen A., Vuorinen T.

2. Project research question and objectives

The project targets the potential of Enhanced Geothermal Systems (EGSs) to induce earthquakes and the associated risks to urban environments. The research hypotheses are that 1) induced earthquakes represent a previously non-existing seismic hazard in the Helsinki capital region, the level of which may exceed that posed by natural seismicity there, and 2) future induced earthquakes have the potential to severely impact today's sensitive societal infrastructures and operations. The key to understanding the consequences of induced earthquake events lies in the combination of field data from the Otaniemi EGS and buildings, exploring the subsurface and surface conditions of the target region, and analysis of available seismicity data, as well as how risk management is understood and governed. The project applies an interdisciplinary approach to the problem, with different expert groups collaborating closely to fully exploit their expertise. The research questions are addressed through the following steps, which are associated with the nine work packages:

1) Preparing the best possible seismic hazard map for the national needs. This is a prerequisite for an analysis of seismic risk. Natural seismicity is addressed at this point.
2) Developing a general scheme for separating the seismic hazard related to induced seismicity and natural seismicity
3) Constructing a 3D tomography image of the subsurface structures of the target region
4) Preparing a 3D geological model of the target region
5) Collecting data to assess the vulnerabilities of the building stock
6) Investigating the factors that control disturbing earthquake-related sound patterns during stimulations
7) Managing the various datasets created during the project
8) Highlighting the gaps in governing geothermal energy processes and how this phenomenon should be governed to foster sustainable and societally acceptable development.

3. Expected Project Results

The expected scientific project results are Open Access seismic hazard maps of Finland and ground-motion prediction equations (GMPE) for magnitude levels >M2 tailored for the Finnish bedrock conditions. The hazard values will be useful for evaluating risks to shaking-sensitive systems or constructions, helping in risk informed decision of planning by supervising authorities. Moreover, they can be used for defining new guidelines on construction of critical infrastructure. It will produce induced seismic risk assessment and 3D tomographic velocity and geological models of the capital region. The 3D sub-surface model of the city area can be used to evaluate soil and bedrock properties for urban planning and construction, outline tremor and noise sensitive areas, and identify areas where deep geothermal plants are possibly less risky.

The surveys and interviews on the planning and regulating processes will give us information on 1) the extent to which different actors have a common understanding of the current situation and potential risks, 2) who should be responsible for coordinating risk management, and 3) how citizens should be informed of potential risks and whether they should also be able to participate in location decisions. The project will produce education material for the governmental and municipal decision makers, politicians and the general public on the concepts of seismic hazard and risk and induced seismicity and its hazard and risk to the urban societies.

Acknowledgements: The SEISMIC RISK –project number 337913 is funded through the Academy of Finland's special funding for Crisis preparedness and security of supply during 8/2020-11/2023.

Nordic EPOS - A FAIR Nordic EPOS Data Hub

A. Korja[1], K. Atakan[2], P.H. Voss[3], M. Roth[4], K. Vogfjord[5], E. Kozlovskaya[6], E.I. Tanskanen[7], N. Junno[1] and Nordic EPOS Working Group[2]

[1]Department of Geosciences and Geography, P.O. Box 64, FIN-00014 University of Helsinki
[2]University of Bergen
[3]Geological Survey of Denmark and Greenland (GEUS)
[4]Uppsala University
[5]Icelandic Meteorological Office (IMO)
[6]Oulu Mining School, University of Oulu
[7]Sodankylä Geophysical Observatory, University of Oulu
E-mail: Annakaisa.korja@helsinki.fi

Nordic EPOS - A FAIR Nordic EPOS Data Hub – is a consortium of the Nordic geophysical observatories delivering on-line data to EPOS Thematic Core Services. It will promote common Nordic interests in EPOS, and promote and build data services beneficial for the Nordic community. It will offer joint workshops and training in FAIR data collection, usage and management in monitoring of seismicity and induced seismicity, ash and gas eruptions, geomagnetic hazards. It will also disseminate related tutorials, demos and actual and virtual training sessions.

Keywords: EPOS (European Plate Observing System), Nordic countries, collaboration, FAIR (Findable, Accessible, Interoperable and Re-usable), data

1. Overview

Many of the grand challenges such as global change and sustainable use of Earth's resources in urbanizing societies strongly involve the solid Earth. This includes assessing and mitigating risks from various natural and anthropogenic hazards, natural and induced seismicity, volcanic activity, and geomagnetic storms. EPOS-ERIC (European Plate Observing System – European Research Infrastructure Consortium) builds an e-platform providing access to large quantities of European georeferenced data relating to the solid Earth. Nordic EPOS enhances and stimulates the ongoing active Nordic interactions related to Solid Earth RI in general and EPOS in particular. Together we can address global challenges in Norden and with Nordic data. We develop expertise and tools designed to integrate Nordic RI data and to enhance their accessibility and usefulness to the Nordic research community.

Nordic EPOS - A FAIR Nordic EPOS Data Hub – is a consortium of the Nordic geophysical observatories delivering on-line data to EPOS Thematic Core Services. Nordic EPOS consortium comprises the Universities of Helsinki (UH), Bergen (UiB), Uppsala (UU), Oulu (UOULU) and Geological Survey of Denmark and Greenland (GEUS) and Icelandic Meteorological Office (IMO). The hubs' main tasks are to advance the usage of multi-disciplinary Solid Earth data sets on scientific and societal problem solving (Figure 2), increase the amount of open, shared homogenized data sets, and increase the scientific expertise in creating sustainable societies in Nordic countries and especially in the Arctic region. In addition to developing services better suited for Nordic interest for EPOS, it will also try to bring forward

[2] **Nordic EPOS working group:** Barsotti S., Dahl-Jensen T., Funck T., Hillers G., Indrøy H.K.S., Keiding M., Kukkonen I., Larsen T.B., Lund B., Michalek J., Oladottir B., Pfeffer M.A., Rinds N., Rønnevik C., Tellefsen K., Vuorinen T., etc.

Nordic research interest, such as research of Arctic areas in TCS and EPOS-ERIC governance and scientific boards.

2. Nordic EPOS Objectives

The hub has three main objectives. First is to increase awareness and usage of multi-disciplinary Nordic EPOS data, data products, software and service for scientific and societal problem solving. Second is to increase the amount of, and access to, Nordic FAIR data, and third to support data management of new data types and scientific expertise needed for safe and sustainable societies in Nordic countries and especially in the Arctic region. For the comprehensive list of objectives, see Figure 1.

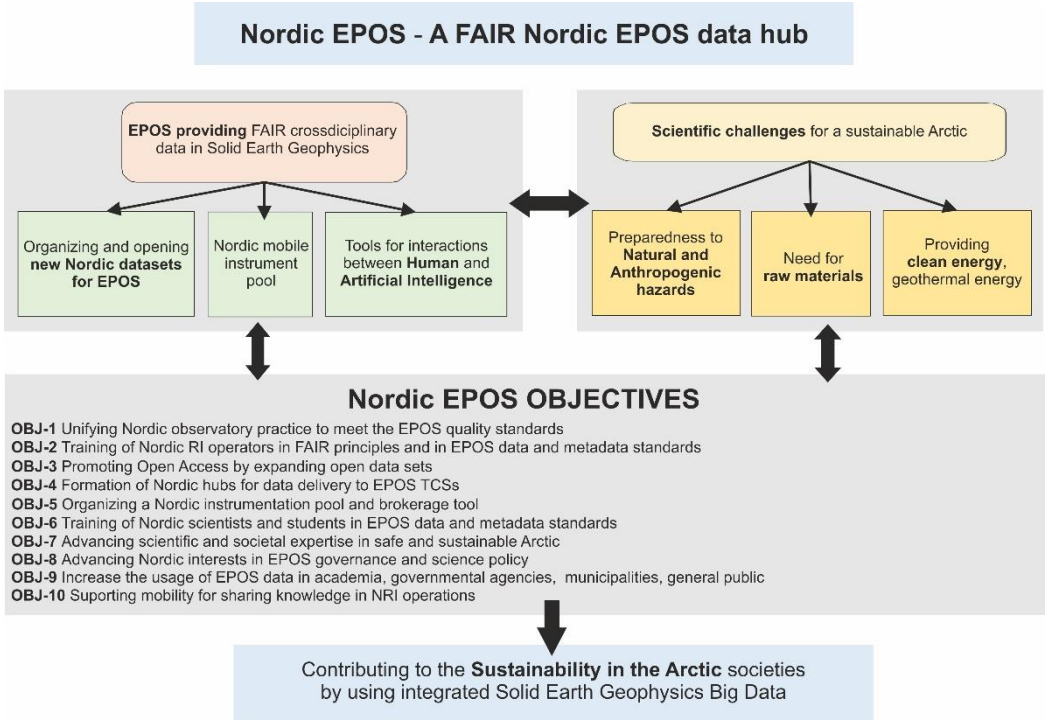

Figure 1. Mission and goals of Nordic EPOS.

3. Nordic EPOS TASKs and Activities

To reach the objectives, the Nordic EPOS is organized into Tasks and Activities**.** The project has six main infrastructure TASKs I-VI and one transversal TASK VII on communication and dissemination. Many of the tasks are addressing several objectives. The TASKs are I - Training in usage of EPOS-RI data and services; II - Nordic data integration and FAIRness; III - Nordic station management of seismological networks, IV - Induced seismicity, safe society; V - Ash and gas monitoring; VI- Geomagnetic hazards; VII - Communication and dissemination. Each of the main partners is responsible for several Activities in one or several TASKs. The activities within the TASKs are workshops, tutorials, demos and actual and virtual training sessions, website and communication and dissemination of EPOS data and metadata information at local, national and international workshops, meetings, conferences. For the comprehensive list of upcoming events, see the Nordic EPOS webpages (https://www.helsinki.fi/en/infrastructures/nordic-epos).

Acknowledgements
The Nordic EPOS is funded through the NordForsk's call for Nordic Research Infrastructure (RI) Hubs for 2020-2023.

FIN-EPOS – Finnish national node of the European Plate Observing System

A. Korja[1], M. Poutanen[2], S. Mertanen[3], E. Kozlovskaya[4], T. Fordell[5], J. Leveinen[6], A. Viljanen[7], A. Pursula[8], N. Junno[1] and FIN-EPOS Working Group

[1]Department of Geosciences and Geography, P.O. Box 64, FIN-00014 University of Helsinki
[2]National Land Survey of Finland, Finnish Geospatial Research Institute
[3]Geological Survey of Finland
[4]Oulu Mining School, University of Oulu
[5]VTT – Technical Research Centre of Finland Ltd.
[6]Aalto University
[7]Finnish Meteorological Institute
[8]CSC – IT Centre for Science Ltd.
E-mail: Annakaisa.korja@helsinki.fi

FIN-EPOS is a Finnish national node of the European Plate Observing System (EPOS). The consortium consists of Universities of Helsinki (host organization), Oulu, and Aalto, National Land Survey of Finland, Finnish Meteorological Institute, Geological Survey of Finland, VTT and CSC. These organization own and operate geophysical observatories and laboratories in Finland and deliver metadata and data to Thematic Core Services (TCS) of EPOS either through national nodes or though international data centres and global scientific programs, where they are members. FIN-EPOS RI has been accepted on the FIRI roadmap 2021-2024.

Keywords: EPOS, national node, research infrastructure consortium, data management, databases, seismology, geodesy, geomagnetism, geophysical laboratories, observatory network

1. General

The European Plate Observing System - EPOS-ERIC (http://www.epos-eu.org/; Figure 1) is distributed research infrastructure (RI) providing an integrated e-science platform for Solid Earth geoscience national networks, observatories and laboratories as well as for international science organizations in Europe. It aims to be the principal source of geoscientific data, metadata and tools in Europe. National governments, funding agencies and institutes are responsible for the funding and operation of instrumentation and data management in each country. EPOS-ERIC integrates the National Research Infrastructures (NRIs) into Thematic Core Services (TCS), which represent dedicated services (data archiving and mining, access to data products, etc.) for each special discipline. The TCS are further joined through a compatibility layer to the Integrated Core Services (ICS), consisting of a variety of multi-disciplinary services. ICS enables access to data, data products, processing and visualization tools and computational codes and resources for different stakeholders. EPOS-ERIC also holds workshops, summer and winter schools and in-house training courses, and operates a mobile instrumentation pool and transnational access program.

2. FIN-EPOS – Finnish national node of EPOS

FIN-EPOS (https://www.helsinki.fi/en/infrastructures/fin-epos) is a coordination consortium and the Finnish national node of EPOS. FIN-EPOS consists of Universities of Helsinki (host organization), Oulu, and Aalto, National Land Survey of Finland, Finnish Meteorological Institute, Geological Survey of Finland, VTT Technical Research Center for Finland Ltd. and CSC – IT Center for Science Ltd. The FIN-EPOS partners own and operate the geophysical and

geodetic national research infrastructures (NRIs) including permanent databases and data services in Finland. NRIs consist of the physical measurement instrumentation, associated data centers and personnel. The permanent seismic, geodetic and magnetic observatory networks are distributed around Finland, whereas the geodynamic and rock physical laboratories are located at host institutions. FIN-EPOS partners deliver metadata and data to Thematic Core Services (TCS) of EPOS either through national nodes or though international data centers and global scientific programs, where they are members (Figure 2). FIN-EPOS is building a national portal for finding national data sets, for brokerage of the joint mobile instrument pool and for distributing information of EPOS activities interesting for the Finnish scientific community and society. In addition, FIN-EPOS gives scientific advice to government representatives in the EPOS-ERIC General Assembly.

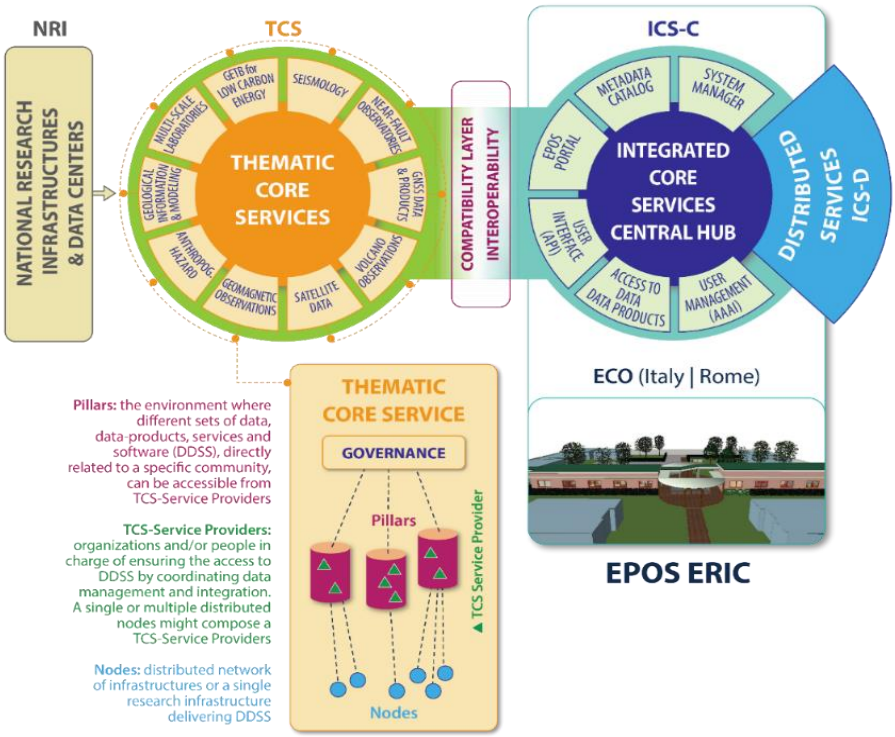

Figure 1. EPOS functional architecture. EPOS-ERIC comprises the e-infrastructure called Integrated Core Services (ICS) and EPOS Central Office (ECO). FIN-EPOS partners are examples of National Research Infrastructures (NRI) that serve as Nodes or Service Providers for individual Thematic Core Services (TCS), which represent dedicated services (data archiving and mining, access to data products, etc.) for each special discipline. NRI) deliver data to the TCSs. The ICS enables access to data, data products, software, and services (DDSS), processing and visualization tools, and computational codes and resources for different stakeholders.

The FIN-EPOS partners own and operate the geophysical and geodetic RIs and data in Finland. NRIs consist of the physical measurement instrumentation as well as associated data centers and personnel. Each NRI is financed by their host organizations that in turn are government research organizations financed by five ministries: Ministries of Education and Culture, Agriculture and Forestry, Employment and the Economy, Transport and Communications, and Foreign Affairs. In addition, FIN-EPOS has had competitive AoF FIRI funding for upgrading of the measurement stations of the NRIs. The projects (Figure 2) are *FIN-EPOS-Seismology*

upgrading Finnish national seismological network FNSN; *G-EPOS* upgrading geophysical infrastructure of geomagnetic observatories, geothermal laboratory facilities and time transfer in geodetic infrastructure; and *FLEX-EPOS* creating a national pool of geophysical instruments and multi-disciplinary geophysical superstations to solve fundamental research questions in seismology, geomagnetism and geodesy. *OpenFIRE* project gathering metadata on national legacy data and for developing open e-infrastructure and permanent IDA storage services at CSC has had funding through OpenScience and Research campaign of the Ministry of Education and Culture. The data are included in EPOS initiated SERA project developing a module for TCS - Geological information and modelling. Two of the FIN-EPOS partners participate in *Nordic EPOS - A FAIR Nordic EPOS Data Hub* that is a consortium of the Nordic geophysical observatories delivering on-line data to EPOS ERIC. Nordic EPOS is funded through NordForsk's Nordic Research Infrastructure Hubs (2020-2022). Three of the FIN-EPOS partners have been partners in H2020 Infra-dev funding for EPOS-IP project. The current national FIN-EPOS collaboration is funded through FIRI2019 and partner organizations. The FIN-EPOS consortium has proposed that Finland will apply for the full membership in the EPOS ERIC from the beginning of 2022.

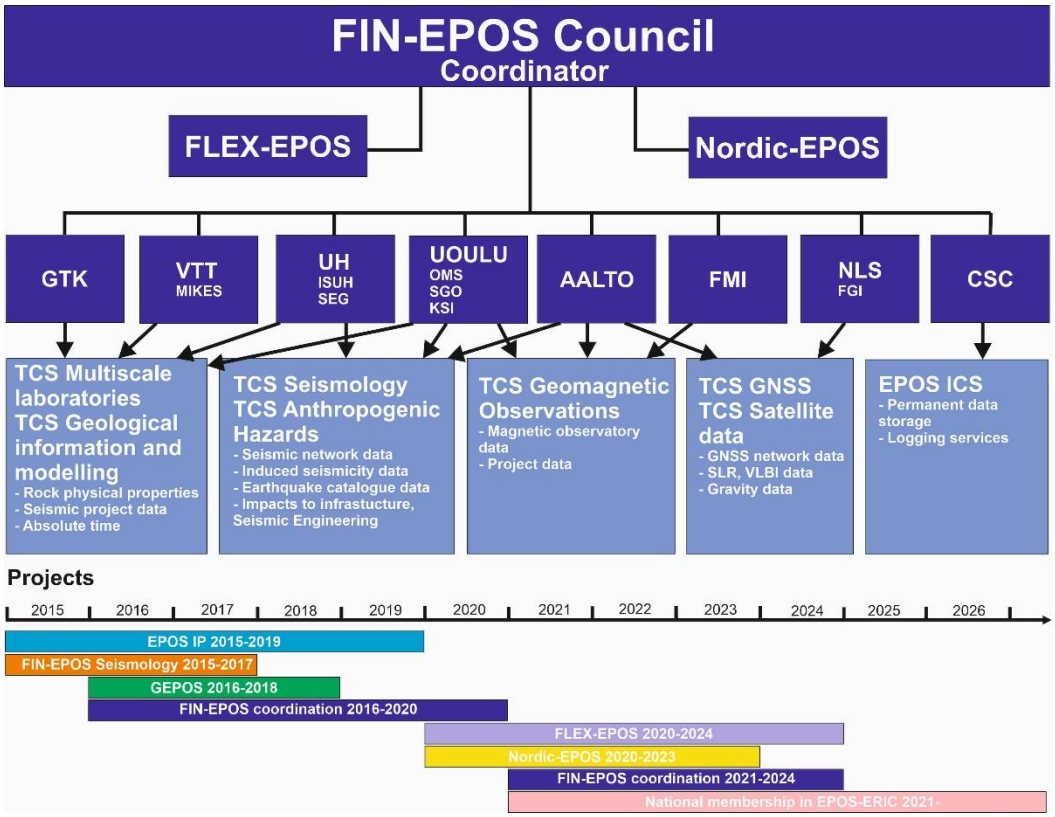

Figure 2. FIN-EPOS organization, projects and data transfer to EPOS TCSs (i.e., national and international data centers).

3. FIN-EPOS on the FIRI roadmap 2021-2024

The Finnish Research Infrastructure Committee (FIRI Committee) granted in December 2020 roadmap status to 29 research infrastructures including FIN-EPOS RI. The selected infrastructures will be included in the national roadmap for research infrastructures covering the years 2021–2024. The roadmap for national research infrastructures in Finland is a list of strategically significant research infrastructure services needed over the next 10–15 years in the Finnish research, development and innovation system.

FIN-EPOS scientific goals are aligned with EPOS's main scientific goals. The goals are 1) to boost our understanding of the complex physical and chemical processes at play in the geosphere through data-driven science; 2) to increase the resilience of Europe in the face of disaster threats posed by geologic hazards; and 3) to support a leading role of Europe in the sustainable, safe and equitable provision of geo-resources, which are critical to human well-being. FIN-EPOS emphasizes the understanding of processes in the geosphere as well as their complex interaction with hydrosphere-biosphere-atmosphere processes, provision of safe and sustainable raw materials and clean energy, and mitigation of natural and anthropogenic hazards.

FIN-EPOS is planning to enhance internal FIN-EPOS station site collaboration. Sharing station infrastructure and deploying several independent measurement instruments on a single site enables not only new studies on the interdependencies of the seismic, geomagnetic and geodetic processes but also usage as reference stations, ground truth stations for mobile instruments and airborne measurements. These so-called superstations will be developed around already existing geophysical observatories and their station networks and biological stations hosted by the FIN-EPOS partners (Figure 3; Metsähovi, Sodankylä, Kilpisjärvi). Metsähovi Geodetic Research Station is a Core Station in the network of Global Geodetic Observing System (GGOS), and it will be further developed as a FIN-EPOS superstation. To further facilitate studies of the mutual dependencies of the biosphere, atmosphere and geosphere processes, FIN-EPOS will collaborate with INAR-RI by diversifying the SMEAR (Station for Measuring Ecosystem Atmosphere relations) –station network with solid earth geophysical measurements in Värriö, Hyytiälä and Tvärminne stations. Sodankylä observatory is already a globally important geophysical observatory, with tight connections to atmosphere and biosphere studies through Sodankylä-Pallas Global Atmosphere Watch (GAW) status, SMEAR and Radar Receiving Site of EISCAT stations.

National laboratory collaboration is enhanced at Otaniemi campus, where Aalto, VTT and GTK have pooled laboratories under the *Circular Raw Materials Hub*. The cooperation enables mutual usage of the equipment, strengthens the scientific and societal impacts of the results and promotes new ideas and information for the latest technology. The hub provides also measurement services for FINMARI.

	Superstations	Current instrumentation	Instrumentation planned in 5, 10 years	RIs
MET	Metsähovi (FGI, Aalto)	FGI geodetic research station (GNSS, VLBI, SLR, absolute gravimeter, superconducting gravimeter, local tie network between instruments), groundwater monitoring, weather station, Seismometer (UH), magnetometer (AALTO)	Atomic gravimeter (FGI), SAR reflector (FGI), Hydrogen maser (FGI), Upgrading of SLR and VLBI systems (FGI), Borehole(s) for thermal and hydrological monitoring (UH)	EUREF, GGOS
KIF	Kilpisjärvi (UH)	Seismometer (UH), biological research station (UH), IMAGE station (FMI), pulsation magnetometer (SGO), gravity pillar (FGI, not measuring currently), GNSS (FGI), subalpine forest	SAR reflector (FGI), infrasound station (UH), Borehole(s) for thermal and hydrological monitoring (UH)	LTER, ICOS, EUREF
SOD	Sodankylä (SGO, UOULU)	SGO Geomagnetic observatory (IMAGE, pulsation magnetometer), Seismometer (SGO), gravity pillar and GNSS (FGI), northern boreal, Sodankylä-Palllas (GAW) Global Atmosphere Watch	SAR reflector (FGI), Time/Frequency link to VTT-MIKES (FGI, VTT-MIKES), Borehole(s) for thermal and hydrological monitoring (UH)	LTER, ICOS, ACTRIS, EISCAT, EUREF, GGOS
VRF	Värriö (UH)	SMEAR I (UH), subarctic research station (UH); Seismometer (UH), gravity pillar (Savukoski, FGI), GNSS (Savukoski, FGI)	Borehole(s) for thermal and hydrological monitoring (UH)	LTER, ICOS, ACTRIS, EUREF
FI-HYY	Hyytiälä (UH)	SMEAR II (UH), sothern boreal forestry field station (UH), Gravity pillar (Orivesi, FGI), GNSS (FGI)	Seismometer (UH), Borehole(s) for thermal and hydrological monitoring (UH)	LTER, ICOS, ACTRIS
TVF	Tvärminne (UH)	SMEAR V (UH) Seismometer (UH), marine zoological research station (UH)	Borehole(s) for thermal and hydrological monitoring (UH)	LTER, ICOS, ACTRIS
OLKF	Oulanka (SGO, UOULU)	Seismometer (UOULU, SGO), biological station (UOULU), weather station, hydrological station	Borehole(s) for thermal and hydrological monitoring (UH)	LTER

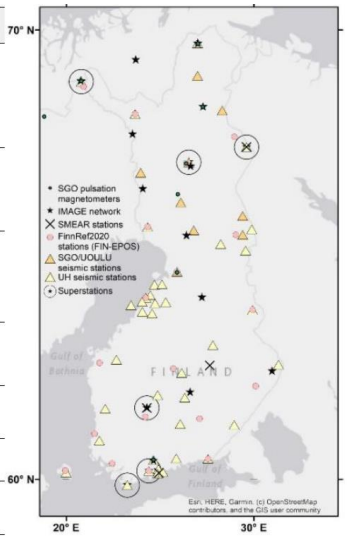

Figure 3. Geophysical observatories and station network in Finland and a preliminary plan for geophysical superstation locations.

St1 Deep Heat Project: Hydraulic stimulation at 5 – 6 km depth in crystalline rock

I.T. Kukkonen[1], M. Pentti[2] and P.J. Heikkinen[2,1]

[1]University of Helsinki, Dept. of Geosciences and Geography, Finland
[2]St1 Oy, Helsinki, Finland
E-mail: ilmo.kukkonen@helsinki.fi

St1 Deep Heat Project with its two deep wells extending to 6.2 - 6.4 km depth is the world's deepest industrial geothermal energy project. The aim is to build an EGS (enhanced geothermal system) at the depth of about 5 - 6 km. The project is a pilot aiming at exploring the technical and economic feasibility of geothermal energy in the crystalline rock conditions of Finland for production of thermal power to a district heating network. In the presentation we provide an insight to the project and its major achievements with a focus on hydraulic properties of the crystalline rock.

Keywords: geothermal, temperature, hydraulic stimulation, hydraulic conductivity, crust, Precambrian

1. Introduction

St1 Deep Heat Project started in 2014. With its two deep wells extending to 6.2 - 6.4 km depth, located in Espoo, southern Finland, it is the world's deepest industrial geothermal energy project. The aim is to build an EGS (enhanced geothermal system) at the depth of about 5 - 6 km. The project is a pilot aiming at exploring the technical and economic feasibility of geothermal energy in the crystalline rock conditions of Finland for production of thermal power to a district heating network. Due to the demands of the district heating, the aim is to produce hot fluid at about 100°C and re-inject it to the formation at 50°C. The 100°C temperature goal requires drilling to about 6 km depth. The extreme depth level sets significant challenges for drilling and hydraulic stimulation, as well as controlling of induced seismicity. So far (2021) the project has drilled a 2 km deep completely cored pilot hole (OTN-1), and two deep wells, OTN-2 to 6.2 km and OTN-3 to 6.4 km.

The extreme depth of the planned EGS is due to low geothermal gradient in the study area (ancient Precambrian bedrock) and the technical requirements of the district heating system. The reservoir temperature should be at least 100°C, and the re-injected fluid should be about 40 – 50 °C. The project aims in production of space heating energy only, and no power (electricity) production is planned. With a typical geothermal gradient of about 15-17 °C/km, the 100°C temperatures require drilling to about 6 km depth.

In EGS heat is 'mined' by circulating water as a heat transfer fluid in the formation between two deep boreholes. Natural level of hydraulic conductivity is very low at depths of several km, and provided by natural fractures of the rock. In most cases, the natural hydraulic conductivity is too low for EGS production and must be improved. It is done by hydraulic stimulation.

2. Drill site geology and geothermal conditions

The drill site geology is typical for southern Finland. A thin layer (0-20 m) of Quaternary sediments overlies the Precambrian bedrock. The bedrock comprises about 1.8 – 1.9 Ga age migmatitic rocks, i.e. mixtures of veined gneiss, mica and hornblende gneiss, amphibolite and

granitic intrusions. The lithological boundaries are mostly steep and subvertical (Figure 1). Due to thorough deformation and migmatization during the geological history of the area, the target formation structure is complex. Intact crystalline rock has very low porosity, less than 0.5 vol-%. Therefore, the fluid flow is constrained to brittle deformation structures, i.e., fracture and shear zones. At the surface level, such structures are revealed by several km long linear structures on topographic, geophysical and geological maps.

Geothermal gradient (rate of temperature increase with depth) is about 17 mK/m in the 2 km deep OTN-1 well, and corresponding heat flow is about 52 mWm^{-2}. It implies drill holes should be about 6 km deep to meet the 100°C temperature level.

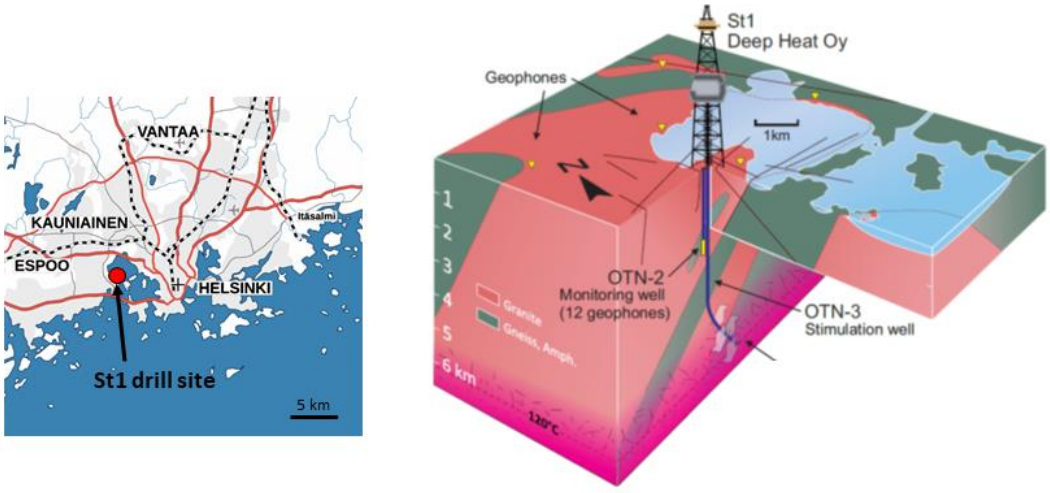

Figure 1. Location map of the St1 Deep Heat drill site (left panel), and a 3D diagram of the deep wells and simplified geology in the uppermost 6 km (right panel). Pink represents granitic rocks whereas green represents gneisses and amphibolites, respectively. Modified from Kwiatek et al. (2019).

3. Hydraulic stimulation, traffic light system and seismic reflectors

Hydraulic stimulation was carried out in the deep wells in 2018 and 2020 to improve hydraulic conductivity. In 2018 about 18,000 m^3 of fresh (tap) water was injected into OTN-3 in five 100-200 m long stimulation stages at 5.8 – 6.4 km depth (vertical depth 5.7 – 6.1 km). During stimulation, wellhead pressures, flow rates and induced seismicity were continuously monitored and recorded.

Regulating authorities required that a traffic light (TLS) system had to be applied in controlling the stimulation and seismicity. The TLS red light limit was set at magnitude M_L 2.1, meaning that occurrence of events bigger than this would imply stopping the stimulation. The injection induced seismicity, which comprised more than 50,000 microearthquakes with magnitudes below M_L 1.9, most of them below M_L 0.0 (Kwiatek et al., 2019, Leonhardt et al., 2020). Ground velocities were monitored in eastern Espoo and western Helsinki with up to 17 peak ground velocity (PGV) instruments installed in the terrain and some in the basements of buildings. The highest recorded PGV value was only 0.7 m/s. The stimulation produced three earthquake hypocenter swarms above the stimulated part of OTN-3.

Geological structures, i.e. hydraulically conductive fracture zones and lithological contacts of the reservoir were mapped with drill bit seismic (DSB) during hammer drilling of the deep wells and a VSP survey (vertical seismic profiling) in OTN-3 as well as downhole geophysical

logging of the wells. These studies revealed a major natural fracture/shear zone ('VSP reflector') dipping about 44° to ENE. The structure was then utilized in the design of the reservoir when OTN-2 was deepened to final depth of 6.2 km. The deepest part of OTN-2 was deviated to run along the fracture zone for about 1 km length. Finally, OTN-2 was stimulated in 2020 by injecting about 7000 m^3 of fresh water to the 1.3 km long open hole section of the well.

4. Hydraulic conductivity of the reservoir

Hydraulic conductivity of the reservoir was estimated from stimulation pressure and flow rate data. A major observation is that conductivity is pressure dependent due to elastic response of the fractured medium on increased pore pressure. At the highest applied wellhead pressures of 700 – 900 bar conductivity increased to about 10^{-9} … 10^{-8} m/s. Leak-off pressure of fractures is about 520 bar at 6 km. However, when the wellhead pressure was relaxed by about 200-300 bar, conductivity decreased by about one magnitude according to the stimulation pressure data. Pre-stimulation leak-off test data and post-stimulation long-term monitoring of shut-in pressures in OTN-3 allowed estimation of the low-pressure conductivity, which appears to be of the order of $5 \cdot 10^{-11}$ m/s. It is considered to represent the natural level of hydraulic conductivity in the reservoir.

The achieved EGS reservoir consists of the volumes stimulated from OTN-3 and the natural fracture zone intersected by OTN-3 and OTN-2. At present, the project proceeds with the installation of above ground heat plant equipment and instrumentation, followed by first test pumping to start in the first half of 2021.

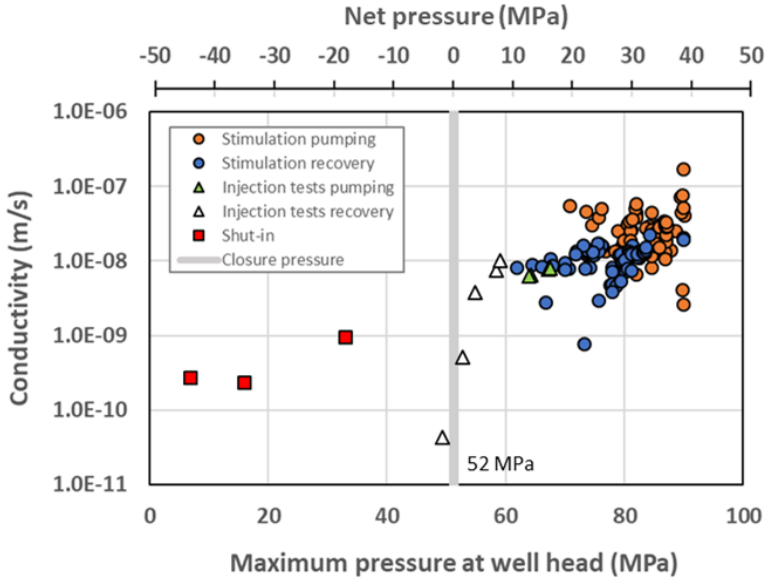

Figure 2. Hydraulic conductivity in OTN-3 well estimated from injection tests, stimulations and shut-in pressure data at 5.8 – 6.4 km depth (vertical depth 5.7 – 6.1 km). Net pressure indicates the difference between the applied overpressure and opening pressure of fractures (52 MPa). Data courtesy St1 Oy.

5. Discussion and conclusions

The St1 Deep Heat project has successfully drilled deep wells to 6 km depth level in crystalline rock. The project demonstrated that rock temperatures high enough for district heating purposes can be attained at the depth of 6 km. Further, the project achieved hydraulically stimulating

natural fractures at depth with considerable volumes of injection fluid. Stimulation was carried out without seismic events exceeding the earthquake magnitude limits set by regulating authorities. This is an encouraging signal for developing EGS methods and technologies for sustainable thermal power production, also in other areas of normal continental crust. The project generated extensive experience and data sets of the continental crust, deep drilling, hydrogeological properties and seismic response of the crystalline rock to stimulation.

References:

Kwiatek, G., Saarno, T., Ader, T., Bluemle, F., Bohnhoff, M., Chendorain, M., Dresen, G., Heikkinen, P., Kukkonen, I., Leary, P., Leonhardt, M., Malin, P., Martínez-Garzón, P., Passmore, K., Passmore, P., Valenzuela, S., Wollin, C., 2019. Controlling fluid-induced seismicity during a 6.1-km-deep geothermal stimulation in Finland. Science Advances, 5: eaav7224, doi.org/10.1126/sciadv.aav7224.

Leonhardt M, Kwiatek G, Martínez-Garzón P, Bohnhoff M, Saarno T, Heikkinen P, Dresen G. 2020. Seismicity during and after stimulation of a 6.1 km deep Enhanced Geothermal System in Helsinki, Finland Solid Earth Discussions https:// doi.org/10.5194/se-2020-139.

Thermodynamic constraints on assimilation of floor cumulates by superheated basaltic-andesitic melts in the Bushveld Complex, South Africa

R. Latypov[1], J. S. Heinonen[2]* and S. Chistyakova[1]

[1]School of Geosciences, University of the Witwatersrand, Johannesburg, South Africa
[2]Department of Geosciences and Geography, University of Helsinki, Helsinki, Finland
*Corresponding author e-mail: jussi.s.heinonen@helsinki.fi

Some portions of the Bushveld Igneous Complex in South Africa show circular depressions in the chamber floor (potholes) up to 100 m deep in which the overlying recharge melts seems to have devoured the pre-existing cumulate layers. Using thermodynamic modeling of phase equilibria (Magma Chamber Simulator, MCS), we examined the possibility of erosion of the floor cumulates – anorthosite and orthopyroxenite – by superheated (~15 °C above liquidus) basaltic-andesitic replenishing melts. Our preliminary modeling shows that the melts can completely absorb up to 4.5−8.5 wt.% of the floor cumulates without inducing crystallization in the melt, despite the melts having initial temperatures 110−260 °C lower than the liquidus temperatures of the cumulates. The assimilation process that formed the potholes appears to have been controlled by chemical dissolution rather than partial melting of the floor cumulates.

Keywords: Bushveld Complex, dissolution, thermodynamics, phase equilibria, modeling

1. Introduction

Assimilation is "an end-member mode of magmatic interaction in which an initial state (t_0) that includes a system of melt and solid wallrock evolves to a later state (t_n) where the two entities have been homogenized" (Heinonen et al., in press). Assimilation generally takes place via partial melting, when the difference in the liquidus temperature of the magma and the solidus temperature of the wall rock is large (>400 °C). There are, however, cases (e.g., layered intrusions) where inflowing magmas have assimilated the pre-existing floor cumulates, which have liquidus and solidus temperatures substantially higher than that of the magmas themselves. At issue is thus how does this process of assimilation take place?

The Bushveld Igneous Complex in South Africa contains extensive exposures of the cumulate layers formed by crystallization of basaltic to andesitic melts in a dynamic magma system (Fig. 1, insert). Some of the exposures show field evidence of the cumulate sequences formed by the crystallization of earlier magma pulses having been devoured (eroded and dissipated) by subsequent magmatic activity (Fig. 1). Since this process is not purely mechanical and cannot be triggered by the residual magma left after the formation of the cumulates – such magma should be saturated in the cumulate phases – recharge magmas of distinct composition must have been involved. The actual process is nevertheless poorly known and remains unconstrained.

2. Geological setting and background

The Bushveld Complex is the largest exposed mafic–ultramafic layered intrusion in the Earth's crust: it encompasses about a million km^3 of igneous rocks formed dominantly from primitive mantle-derived magmas that intruded the upper crust within an intracontinental rift about 2.05 billion years ago. The world's largest reserves of platinum-group elements are found in the complex, along with some notable Fe, Sn, Cr, Ti, and V deposits. The enormous size of the

complex is attributed to its formation from numerous magma pulses that successively replenished a large and long-lived magmatic system (e.g. Kruger, 2005).

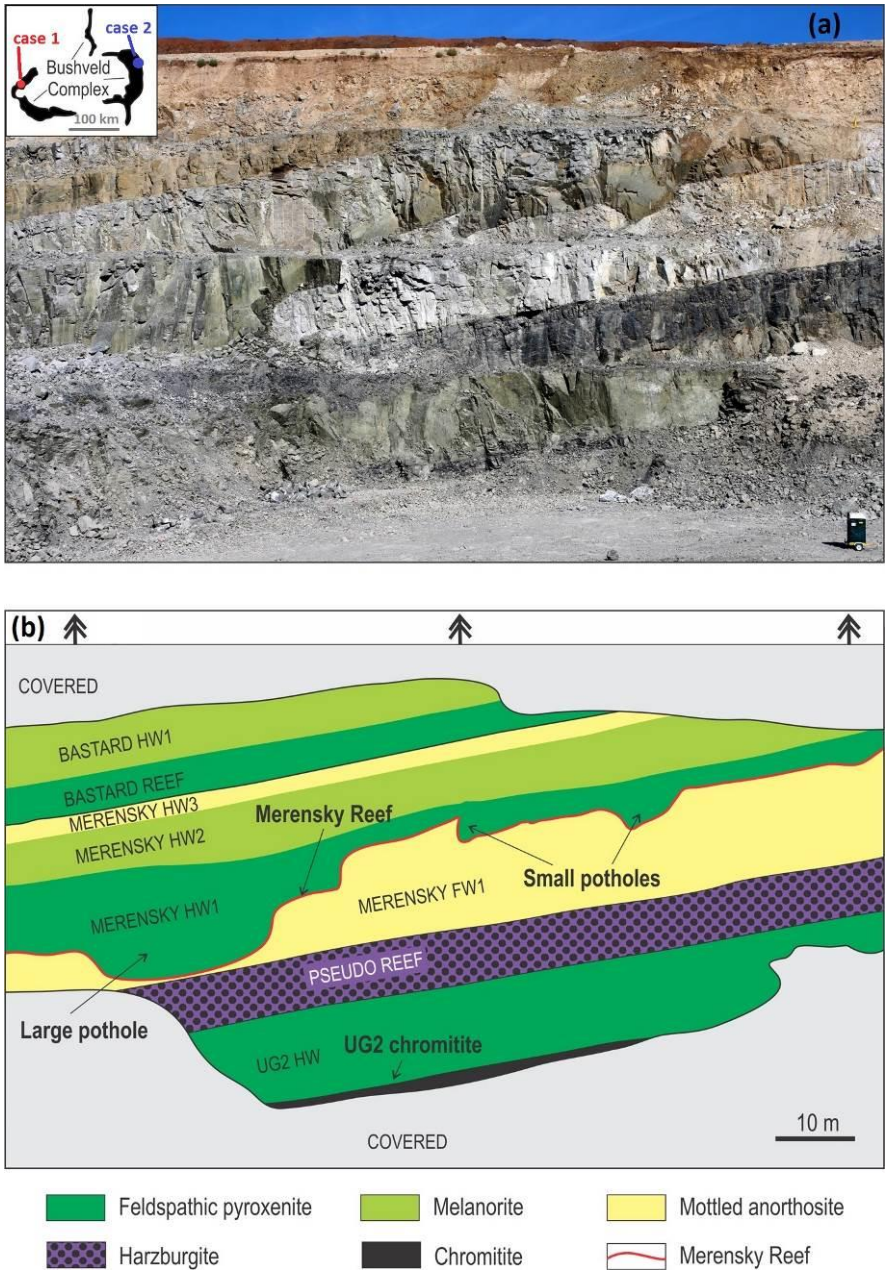

Figure 1. A photograph (a) and a schematic interpretation (b) of a cross-section through the part of the Upper Critical Zone in the wall of the open pit of the Pilanesberg Platinum Mine of the Bushveld Complex (case study 1). Note one large and two smaller potholes protruding into the mottled anorthosite underlying the mineralized Merensky Reef. Locations of the mine (case study 1) and case study 2 are shown in the inserted schematic map of Bushveld Complex in (a). Modified after Latypov et al. (2019).

All the major replenishment events are marked by regionally extensive unconformities, significant isotopic shifts and notable changes in whole-rock and mineral compositions.

Traditionally, such unconformities are attributed to erosion of the temporary floor of the chamber by new magma pulses (e.g. Campbell, 1986, Kruger, 2005, Latypov et al., 2015). It has been estimated that the total thickness of pre-existing cumulates that have been removed on a regional scale at the level of some replenishment events was in the range of 10 to 20 m (Latypov et al., 2015). One of the most spectacular manifestation of the erosive processes is potholes − roughly circular depressions in which some of the footwall rocks are lacking (Fig. 1).

In this study, we concentrate on two occurrences related to the Upper Critical Zone of the complex: 1) the erosion of anorthosites observed in the open pit of the Pilanesberg Platinum Mine, North-Western Bushveld Complex (Fig. 1; Latypov et al., 2019), and 2) the erosion of orthopyroxenites observed at Smokey Hills mine, Eastern Bushveld (Latypov et al., 2020).

3. MCS modeling – background and input

MCS is a thermodynamic model that can be used to compute the phase, thermal, and compositional evolution of a multiphase–multicomponent system of a fractionally crystallizing resident body of magma, linked wall rock, and recharge reservoirs (Bohrson et al., 2020). For the MCS models of this study (selected input and output given in Table 1), we used published and spatially relevant basaltic-andesitic melt compositions of Latypov et al. (2018 and 2020) as the parental melts that come into contact with the previously formed floor cumulates (average compositions of data published in Chistyakova et al., 2019). The floor cumulates were not considered as wall rock in the model but were rather homogenized with the magma as "stoped blocks". This approach reveals whether the bulk assimilation of stoped blocks induces crystallization or whether the magma remains undersaturated (i.e. is able to fully assimilate) the cumulate block. By iteration, we searched for a maximum mass of the stoped material that does not induce imminent crystallization in the melt. Based on earlier modeling (see Latypov et al., 2020), the initial temperatures of the melts were set to ~15 °C above liquidus. Two sets of models with the temperatures of the stoped cumulate blocks being either 1100 °C or 1200 °C were ran for both settings. The pressure was set to be 200 MPa (2 kbar).

Table 1. Results of the MCS modeling. See footnote for explanations.

Case 1

PM liquidus / initial T (°C)	Cumulate liquidus / initial T (°C)	Cumulate initial F (wt.%)	PM MgO & SiO_2 (wt.%)	Cumulate MgO & SiO_2 (wt.%)	**A MAX (wt.%)**
1256 / 1271	1390 / 1200	7.5	6.7 & 55	1.5 & 49	**4.5**
1256 / 1271	1390 / 1100	0.4	6.7 & 55	1.5 & 49	**3.5**

Case 2

PM liquidus / initial T (°C)	Cumulate liquidus / initial T (°C)	Cumulate initial F (wt.%)	PM MgO & SiO_2 (wt.%)	Cumulate MgO & SiO_2 (wt.%)	**A MAX (wt.%)**
1224 / 1239	1485 / 1200	18	7.0 & 54	20 & 53	**8.5**
1224 / 1239	1485 / 1100	2.5	7.0 & 54	20 & 53	**7.0**

Column explanations from left to right: 1) Parental melt liquidus and initial temperature (~15 °C above liquidus T); 2) Floor cumulate liquidus and initial temperature; 3) Melt content of floor cumulate at the initial temperature; 4) Parental melt MgO and SiO_2 contents; 5) Floor cumulate MgO and SiO_2 contents; 6) Maximum amount of assimilation of floor cumulate by parental melt without inducing crystallization.

4. MCS modeling – results

The amounts of assimilation predicted by our MCS modeling are presented in Table 1. In case study 1, the basaltic-andesitic melt can absorb 3.5−4.5 wt.% (relative to the mass of the parental melt) of anorthositic cumulate without inducing crystallization. In case study 2, the basaltic-andesitic melt can absorb 7.0−8.5 wt.% of orthopyroxenitic cumulate without inducing crystallization. Such masses are more than enough to explain the estimated relative masses of the magma and eroded cumulates based on field observations.

It is important to note that the amount of interstitial melt in the cumulates at the modelled temperatures is very small: 0.4−7.5 wt.% in case 1 and 2.5−18 wt.% in case 2. Even if heated to the initial temperatures of the respective recharge magmas, the cumulates would be dominated by solid instead of melt (26 wt.% in case 1 and 45 wt.% in case 2). This strongly suggests that, in case of pothole formation by bulk assimilation, the dominant process of assimilation was chemical dissolution rather than partial melting of the cumulates.

5. Implications and conclusions

Our MCS models show that it is thermodynamically feasible for the evolved melts to erode cumulates crystallized from earlier magma pulses by chemical dissolution. This has important implications for studies of layered intrusions: for example, if the described assimilation process is common, interpretations of magmatic evolution based on intrusion stratigraphy may be flawed due to gaps caused by recharge magma cannibalization of the cumulate layers. Effective cannibalization may also act as a homogenizer of magmatic signatures of different intrusive units. The limiting factor in the assimilation processes is probably not thermodynamic, but kinetic and/or mechanical. In order for the modeled dissolution to take place, the crystal-undersaturated (i.e. superheated) magma must have continuous access to fresh floor cumulate, which would likely require effective convection in the magma body. Future studies should concentrate on these aspects of the assimilation process.

References:

Bohrson, W.A., Spera, F.J., Heinonen, J.S., Brown, G.A., Scruggs, M.A., Adams, J.V, Takach, M.K., Zeff, G., Suikkanen, E., 2020. Diagnosing open-system magmatic processes using the Magma Chamber Simulator (MCS): part I–major elements and phase equilibria. Contrib. Mineral. Petrol., 175:104.

Campbell, I. H., 1986. A fluid-dynamic model for the potholes of the Merensky Reef. Economic Geology 81, 1118–1125.

Chistyakova, S., Latypov, R., Hunt, E.J., Barnes, S., 2019. Merensky-type platinum deposits and a reappraisal of magma chamber paradigms. Sci. Rep. 9:8807.

Heinonen, J.S., Iles, K., Heinonen A., Fred, R., Virtanen, V.J., Bohrson, W.A., Spera, F.J., in press. From Binary Mixing to Magma Chamber Simulator – Geochemical Modeling of Assimilation in Magmatic Systems. In: Masotta, M., Beier, C., Mollo, S. (Eds.). Crustal Magmatic System Evolution: Anatomy, Architecture and Physico-Chemical Processes. AGU Monograph.

Kruger, F., 2005. Filling the Bushveld Complex magma chamber: Lateral expansion, roof and floor interaction, magmatic unconformities, and the formation of giant chromitite, PGE and Ti–V-magnetitite deposits. Mineralium Deposita 40, 451-472.

Latypov, R. M., Chistyakova, S. Page, Yu., Hornsey A. R., 2015. Field evidence for the in situ crystallization of the Merensky Reef. Journal of Petrology 56, 2341–2372.

Latypov, R., Costin, G., Chistyakova, S., Hunt, E.J., Mukherjee, R., Naldrett, T., 2018. Platinum-bearing chromite layers are caused by pressure reduction during magma ascent. Nat. Comm. 9:462.

Latypov, R., Chistyakova, S., van der Merwe, J., Westraat, J., 2019. A note on the erosive nature of potholes in the Bushveld Complex. S. Afr. J. Geol. 122.4, 555−560.

Latypov, R., Chistyakova, S., Costin, G., Namur, O., Barnes, S., Kruger, W., 2020. Monomineralic anorthosites in layered intrusions are indicators of the magma chamber replenishment by plagioclase-only-saturated melts. Sci. Rep. 10:3839.

Natural seismicity in Russian Karelia

A.A. Lebedev[1] and N.V. Sharov[1]

[1]FGBUN FIC Karelian Research Centre, Russian Academy of Sciences, Institute of Geology, Petrozavodsk, Russia
E-mail: stayxalert@gmail.com

On the seismic division map of Russia (OSR-97) Karelia is shown as a zone of possible seismic intensity 5–7 with a recurrence period of 5000 years. Seismic activity is confined to the Kandalaksha-Dvina-paleorift and the Ladoga-Bothnian suture zone. The location of earthquake epicenters is demonstrated during monitoring of natural seismicity in 2017-2019.

Keywords: natural seismicity, seismic monitoring, Karelia, Fennoscandian Shield

1. General

Available seismostatistical data on the eastern Fennoscandian Shield are very limited. Therefore, when assessing the seismicity of the region, paleoseismological monitoring is also needed. Such a monitoring has been conducted in Russian Karelia.

On a map of Russia's seismic division, OSR-97 (Ulomov et al. 2000), Karelia is shown as a probable seismic intensity 5–7 earthquake zone with a recurrence period of 5000 years. Several earthquakes with a seismic intensity 4 occur in Northwest Russia during one decade, and earthquakes with a seismic intensity 5 take place every 30–50 years.

Before the 20th century, seismic events with earthquakes with a seismic intensity 7 were reported from the region. A summary catalog of historical and instrumental data on earthquakes in the Karelian region, compiled by B.A. Assinovskaya and A.A. Nikonov, contains evidence for 135 earthquakes that took place in 1542–2003 (Sharov, 2004). Fifty-two of them are based on macroseismic data and eighty three events were recorded instrumentally. The spatial distribution of earthquake epicenters in the region is irregular: Central Karelia is completely aseismic, but there are some seismic activity zones in Northern and Southern Karelia. The main zone, called the Kandalaksha zone, is confined to Kandalaksha Bay and its southwestern shore. This earthquake concentration zone is intersected by the NE-trending Kuusamo-Kandalaksha zone and other minor lineaments. The Kalevala and Topozero seismic activity zones were detected further south, and the Ladoga-Bothnian zone was revealed at the border with the St.Petersburg region.

The current tectonic movements of Fennoscandia's earth crust are controlled by three major factors: 1) horizontal compression from the diverging Mid-Atlantic Rift; 2) the inherited vertical arcuate isostatic uplift of the shield in general; 3) residual postglacioisostatic uplift (Sharov, 2017). The seismicity of Southeastern Fennoscandia in the area discussed with the coordinates 60°N 30°E–$67^\circ 5'$N 42°E is considered low and is, therefore, of little interest for scientists. Maps of earthquakes in Fennoscandia show scarce low-magnitude events in Karelia during an instrumental monitoring and historical time period (Uski et al., 2003; Sharov, 2004).

2. Monitoring network

The development of seismic networks and designing highly sensitive instruments in the past decade have enabled scientists to record low-magnitude events. To study the deep structure and seismic regime of Karelia, Institute of Geology scientists constructed a regional seismic

network in 1999. Quarry blasts were the main events recorded, the network was constantly updated, so that in 2015 the Karelian seismic network consisted of four wide-range seismic stations manufactured by *Güralp Systems*. KOS6 station is located 15 km from Kostamus, PITK station is located in Leppäsilta (Pitkäranta District) and PTRZ station is located in Petrozavodsk. PAAN station, located in Piäjärvi (Louhi District), began operating in 2016.

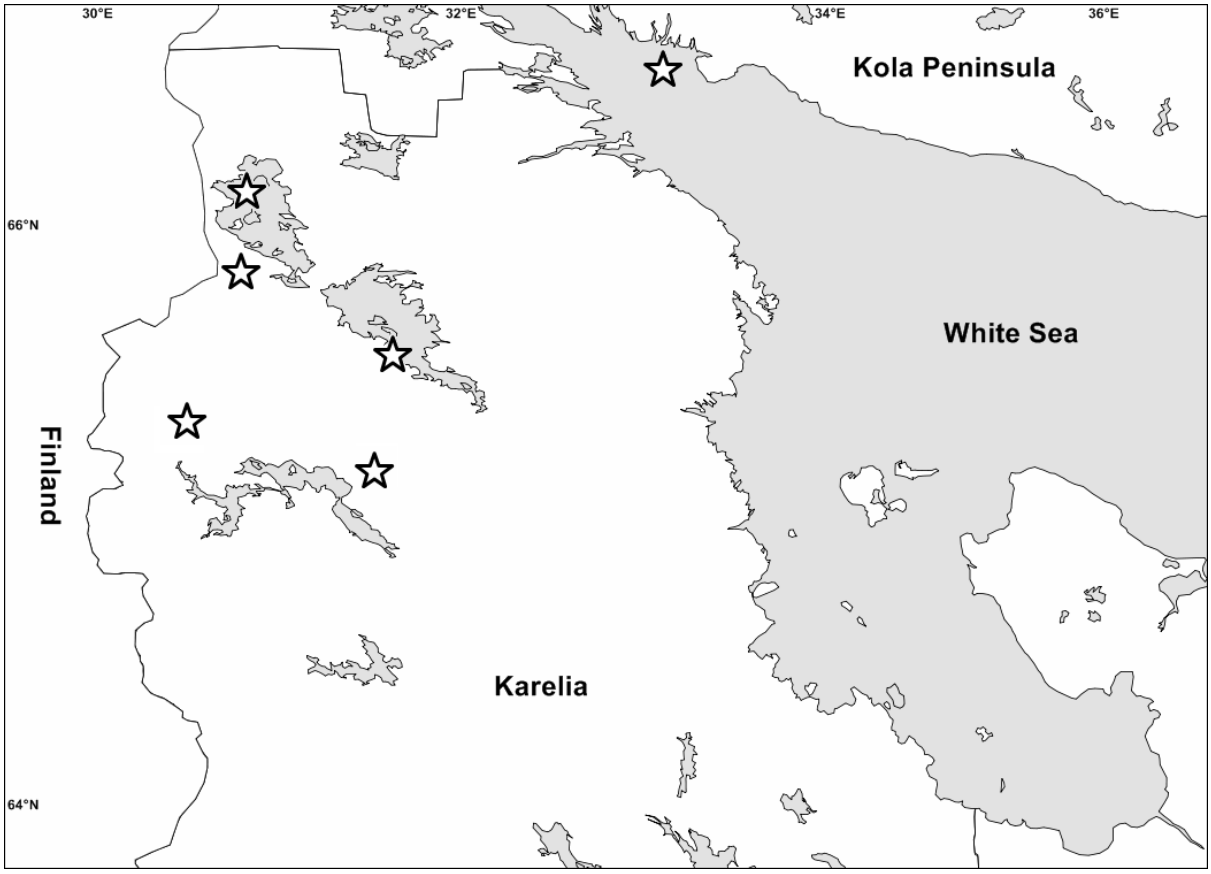

Figure 1. Location of earthquake epicenters during 2017-2019 registered by Karelian seismic network.

Karelian seismic network stations register mainly local blasts and local events near the border, in the Murmansk, Arkhangelsk, Leningrad and Vologda regions as well as in Finland and Sweden. In addition to local events, the Karelian seismic network register teleseismic events. Low-magnitude earthquakes occur in Karelia 1-2 times a year. During the continuous monitoring all of the events were registered in the north part of Karelia with magnitudes ML 1.5-2.3. The distribution of local earthquakes is shown in Figure 1, their characteristics are presented in Table 1.

Table 1. Bulletin of local earthquakes during 2017-2019.

YEAR	MONTH	DAY	H:M:S	LAT (N)	LON (E)	ML	CODE
2017	1	3	10:40:31.6	66.17	30.86	2.3	KOS6 PAAN AP0
2017	3	8	01:41:34.5	65.59	32.10	1.9	KOS6 PAAN AP0
2018	12	21	10:09:20.9	66.40	32.12	2.0	PAAN KOS6 AP0

2018	12	29	01:53:45.3	65.34	30.18	1.5	PAAN KOS6 PITK PTRZ
2019	1	27	02:35:13.8	65.36	30.43	1.6	KOS6 PAAN AP0
2019	5	21	16:50:39.3	65.97	30.64	1.6	PAAN KOS6 AP0

3. Conclusions

The region's seismic potential is much greater than that estimated earlier on the basis of short-term instrumental monitoring. Major seismogenerating zones and elevated seismic activity zones in the region are related to the newest large-scale structures, mainly the Kandalaksha graben and the Onega and Ladoga graben structures with signs of young tectonic activity. Available information for a period of no more than 400–500 years, a time too short for long-term estimates, the seismic potential of the main zones discussed above is estimated as follows: the Kandalaksha zone M = 6.5, the Onega zone about $M \geq 5.5$ and the North Ladoga zone $M \geq 5.5$.

Acknowledgements

The study was carried out under the state assignment of the Institute of Geology of the Karelian Research Centre RAS (No AAAA-A18-118020290086-1).

References:

Sharov, N.V., 2004. Deep structure and seismicity of the Karelian region and its margins. Petrozavodsk: Karelian Research Centre, Russian Academy of Sciences, 192-244.

Sharov, N.V., 2017. Lithosphere of Northern Europe: seismic data. Petrozavodsk: Karelian Research Centre, RAS, 173 p.

Ulomov, V.I., Strakhov, V.N., Shumilina, V.S., 2000. A set of maps of general seismic division of the Russian Federation. OSR-97. Scale 1: 8 000 000. M.: NPP. Tekart.

Uski M., Hyvönen, T., Korja, A., Airo, M.–L., 2003. Focal mechanisms of three earthquakes in Finland and their relation to surface faults, Tectonophysics, 363, 141–157.

Features of explosive seismicity in the Kostomuksha ore region

A.A. Lebedev[1] and I.A. Zueva[1]

[1]FGBUN FIC Karelian Research Centre, Russian Academy of Sciences, Institute of Geology, Petrozavodsk, Russia
E-mail: stayxalert@gmail.com

Technogenic seismicity dominates in the territory of Russian Karelia, which mainly includes active blasting operations. At the open pits of the Karelsky Okatysh 1-2 explosions are made per week. Seismic stations in Karelia permanently register events with magnitudes 1.5-2.5 in this area. The seismic data for the first half of 2018 were analyzed. The dependence of local magnitude (ML) on the total weight of explosives is plotted.

Keywords: Fennoscandian Shield, Karelia, magnitude, monitoring, industrial explosions

1. Summary

The territory of Russian Karelia is located in the northwest part of the East European Platform, in the southeastern part of the Fennoscandian shield. Seismicity in Fennoscandia, the highest in Northern Europe, is concentrated in several zones (Fjeldskaar et al., 2000). In Karelia three structural regions are distinguished (Sharov, 2004; Slabunov, 2008). Kostomuksha ore region is located on the border of eastern Finland and western Karelia.

Seismic monitoring of the southeastern part of the Fennoscandian shield is carried out by a network of four seismic stations: Petrozavodsk (PTRZ), Pitkyaranta (PITK), Kostomuksha (KOS6), Paanajarvi (PAAN). The largest quarries in Russian Karelia have been developed in the Kostomuksha ore region (Figure 1).

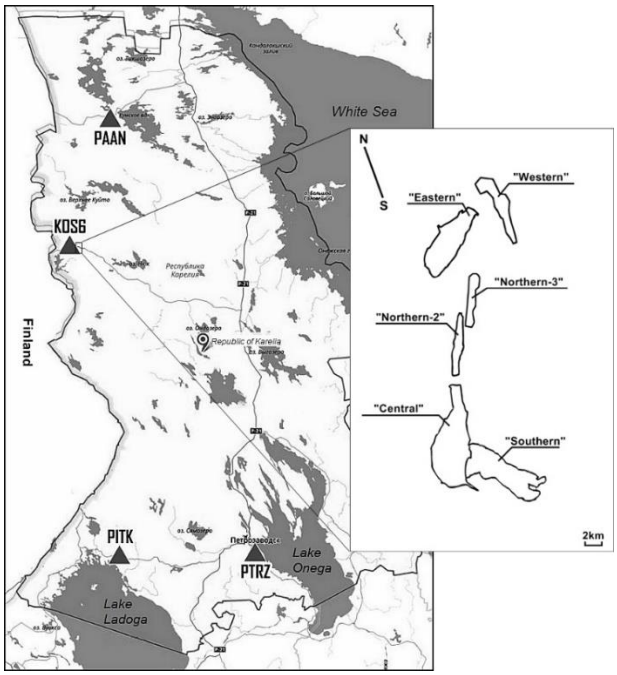

Figure. 1. Location of seismic stations in the territory of Russian Karelia and open pits of Karelsky Okatysh.

The marketable products of the company Karelsky Okatysh are non-fluxed iron ore pellets with an iron content of 65.5 % (Eilu et al. 2012; Gorkovets et al. 2015). The total weight of explosives reaches 100-1.250 tons. The dependence of the magnitudes on the total charges of short-delayed explosions at the open pits of the Karelsky Okatysh (the first half of 2018) is shown in Figure 2.

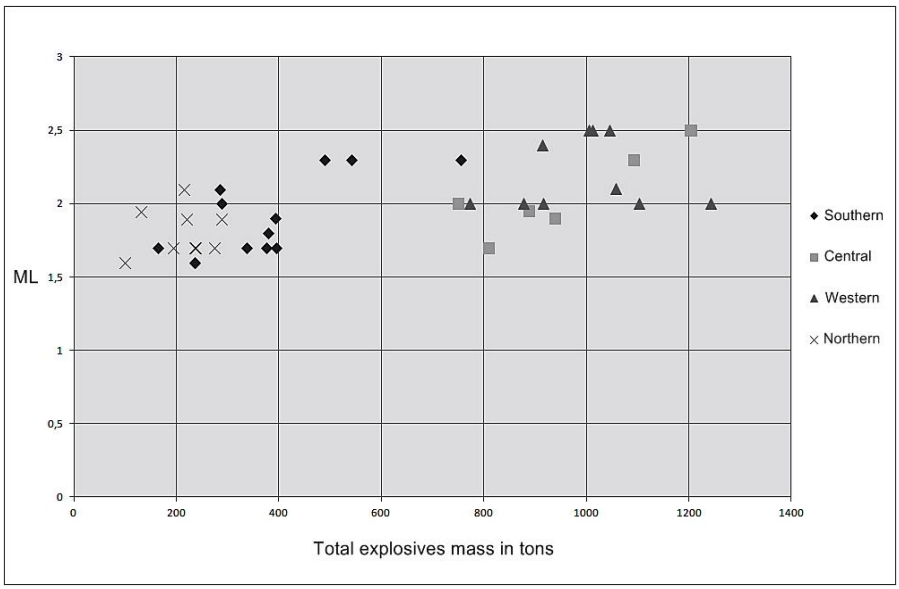

Figure. 2. Dependence of magnitude on the total weight of explosives of open pits of Karelsky Okatysh

The magnitude increases on average with an increase in the total charge at equal charges in the series. A scatter of points from the averaging curve is observed. Most blasting operations in the Kostomuksha ore region are carried out from 9:00-11:00 (UTC). More than 90 seismic events are recorded by Karelian seismic network in this area every year. The strongest and most frequent technogenic events with local magnitudes up to 2.5 are still observed.

This information will give an approach to a proper separation and identification of local earthquakes from industrial explosions in the study region.

Acknowledgements
The study was carried out under the state assignment of the Institute of Geology of the Karelian Research Centre RAS (No AAAA-A18-118020290086-1).

References:

Gorkovets V.Ya., Sharov N.V., 2015. Kostomuksha Ore Area (geology, deep structure and mineralogeny). Petrozavodsk: Karelian Research Centre, RAS, 2015. 322 p.,

Eilu, P., Boyd, R., Hallberg, A., Korsakova, M., Krasotkin, S., Nurmi, P. A., Ripa, M., Stromov, V. & Tontti, M. 2012. Mining history of Fennoscandia. Geological Survey of Finland, Special Paper 53, 19–32.

Fjeldskaar, W., Lindholm, C., Dehls, J.F., Fjeldskaar, I., 2000. Post-glacial uplift, neotectonics and seismicity in Fennoscandia. Quaternary Science Reviews, Vol. 19, 1413–1422.

Sharov N.V., 2004. Deep structure and seismicity of the Karelian region and its margins. Petrozavodsk: Karelian Research Centre, Russian Academy of Sciences, 365 p.

Slabunov A.I., 2008. Geology and geodynamics of the Archean mobile belts (on the example of the White Sea province of the Fennoscandian shield). Petrozavodsk, Karelian Scientific Center RAS, 296 p.

Geology field in The Helsinki Term Bank for The Arts and Sciences (Tieteen termipankki)

E. Lehtonen[1]

[1]PL 64 (Gustaf Hällströmin katu 2), 00014 Finland
E-mail: Elina.lehtonen@helsinki.fi

The Helsinki Term Bank for the Arts and Sciences (HTB, Tieteen termipankki in Finnish) is a multidisciplinary project, which aims to gather a permanent terminological database for all fields of research in Finland. Geology has been part of the HTB since 2018, but work is still unfinished and evolving. The geology field welcomes researchers from wide array of geology and geosciences who would like to contribute to term work.

Keywords: geology, geosciences, terminology

1. Introduction

The Helsinki Term Bank for the Arts and Sciences (HTB, Tieteen Termipankki in Finnish) is a research infrastructure project that was launched in 2012 (Enqvist et al. 2020). It is a multidisciplinary project, which aims to gather a permanent terminological database for all fields of research in Finland. Approximately a third of the scientific fields have so far joined (Enqvist et al. 2020). The project has created wiki-based website (http://tieteentermipankki.fi), which offers a collaborative and open environment for terminological work. All registered users can participate in the discussion about terms.

The data available for all users includes for example the term and its synonyms in Finnish, definition(s), pictures and term equivalents in other languages. The working method is a type of limited crowdsourcing, called niche-sourcing, in which the research community takes responsibility for the terminology work. The working method therefore supports open discussion of the terminology and democratic way to do term work. The goals of the project serve language policy and sociology of science as well.

An extensive Finnish research terminology database will help those researchers, translators, journalists and others who write about research and its results in the arts and sciences in Finnish. By gathering the scientific terminology in one place, the bank also improves the possibilities for multidisciplinary discussion and research. With periodical status and ISSN number, work in the HTB can be included in a list of publications and research data systems.

2. Background of the geology field

Geology field in the HTB started in August 2018 with the grant from the Kordelin Foundation as a part of Major cultural projects. Prior to this, the geophysics field had already been established, but it was not very active at the time geology field started.

The terminological work related to the geology field has included checking and updating some existing terms and producing new content based on already existing term databases, scientific articles and other suitable references. Researchers have also suggested some new definitions to some traditionally used terms and translation equivalents to terms that have not yet existed.

Currently there are a few active researchers who are doing terminological work in geology field, and at the moment E. Lehtonen is concentrating on terms related to the economic geology and environmental geology with the grant from the K. H. Renlund's foundation.

3. Case example

In 2020 Heinonen et al. (2020) wrote an article related to the solid layers of the Earth and their definitions. The article was written in co-operation between geologists and geophysicists, and the work showed that even very common concepts are not self-evident and such a debate is necessary as science and research progress. One outcome of the article was a suggestion that term "kivikehä" (rocksphere) should be used for the whole solid and silicate-dominated outer layer of the Earth instead of using it as a synonym for a lithosphere. This definition was also updated in the HTB with an attribute "suggested" and the discussion page of the concept page contains more information about the subject (Figure 1). This allows the discussion on the definition and use of the term to continue.

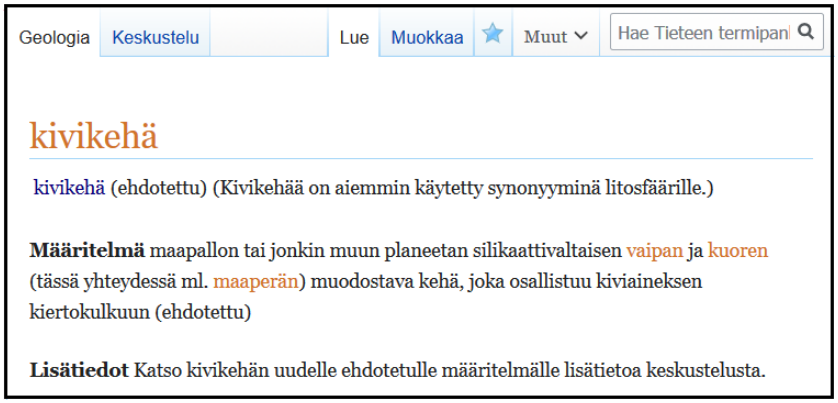

Figure 1. Example of a concept page representing the concept of "rock sphere" (kivikehä). Määritelmä = definition, lisätiedot = additional information.

4. What next?

Geological term work in the HTB has many potential uses. Updating and creating established terms in Finnish serves for example scientists, teachers from university levels to elementary schools, and journalists. In addition, the HTB offers interface and a possibility for discussion between different branches of sciences: for example the geology field has already collaborated with the art history field.

As geosciences are socially significant fields, term work in domestic languages should not be underestimated. Even though there are international definitions for many terms used in geosciences, the understanding and use of the terms can be unclear and variable even within the scientific community. With active and ongoing discussions related to terms, we can facilitate communication and prevent misunderstanding both within our academic community and between the geoscientists and other members of the scientific community and the society.

The geology field in the HTB welcomes researchers from wide array of geology and geosciences who would like to contribute to term work. If you are interested to know more, please contact the author.

References:

Enqvist, J., Pitkänen-Heikkilä, K., Onikki-Rantajääskö, T., 2020. Tieteen termipankki tiedeyhteisön työkaluna. Tieteessä tapahtuu 4, 26–32. (In Finnish)

Heinonen, J.S., Koivisto, E., Väkevä, S., Lehtonen, E., Öhman, T., 2020. Circular arguments: The structure and Finnish terminology of the Earth's interior. Geologi 71, 32–46. (In Finnish)

Imaging the Internal Structure along the Longitudinal Valley Fault System, Taiwan, Using Fault Zone Head Waves

T.-C. Lin[1, 2, 3], G. Hillers[2], S.-J. Lee[3] and S.-H. Hung[1]

[1]Department of Geosciences, National Taiwan University, Taiwan
[2]Institute of Seismology, University of Helsinki, Finland
[3]Institute of Earth Sciences, Academia Sinica, Taiwan
E-mail: tzu-chi.lin@helsinki.fi

Keywords: fault zone head waves, Longitudinal Valley fault system, bimaterial interface, synthetic seismograms, imaging the fault zone.

Introduction

In eastern Taiwan, the Longitudinal Valley between the Coastal and Central Ranges hosts a seismically active fault system. Many past catastrophic earthquakes highlight the need for an improved understanding of fault characteristics and mechanical properties in this tectonically active environment. However, identification of the main fault interfaces for detailed earthquake studies and hazard assessment is challenging. Here we apply a semi-automatic method to detect head waves, an emergent seismic wave in small-earthquake data collected by the Taiwanese seismic network in the northern part of the Longitudinal Valley fault system. Since FZHWs spend almost their entire path between source and receiver along the fault interface, imaging methods based on these phases should be able to provide high-resolution information on fault structure at seismogenic depths.

2. Data and Method

Seismic data from 87 stations of three Taiwanese seismic networks are used for this study, including the Taiwan Strong Motion Instrumentation Program (TSMIP), the Broadband Array in Taiwan for Seismology (BATS), and the Central Weather Bureau Seismic Network (CWBSN) (Figure 1). These stations are located along the 70 km long northern segment of the Longitudinal Valley Fault within some few kilometers on both sides of the fault. We focus on ~13,000 small-to-moderate earthquake seismograms recorded between 2012 to 2018. To this typical modern seismic "big" data set we apply a set of algorithms (Ross and Ben-Zion, 2014) to automatically detect and pick direct P and S waves, as well as potential head waves generated by earthquakes.

3. Picking FZHW and P phase

Earthquake phase detection and picking depends on a number of algorithmic tuning parameters that we could not easily transfer from previous studies along other major predominantly strike-slip faults. In a trial-and-error process we adapted the settings through tedious visual inspection of the automatically detected waveforms, adhering to the original algorithm philosophy of minimizing false detections. We converged to a set of robustly detected head waves and confirmed that the approach thus also works in this tectonically challenging environment (Figure 2). The events that excite these head waves are located along the west-dipping Central Range fault, which now suggests, for the first time, the existence of a considerable velocity contrast across that fault segment.

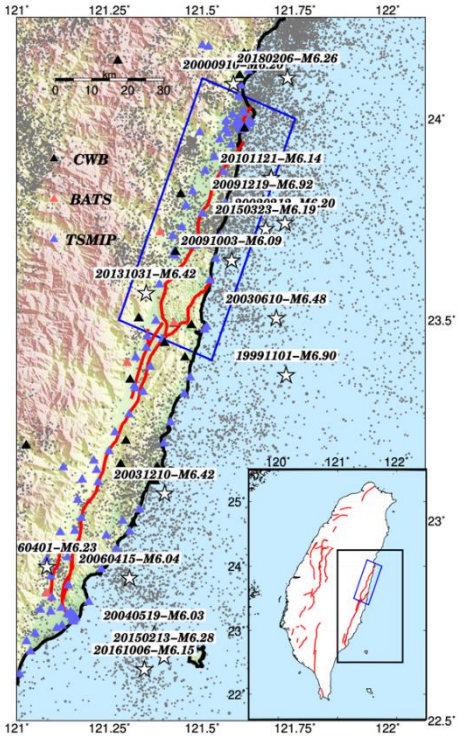

Figure 1. Map of the Longitudinal Valley fault zone study region. Triangles are seismic stations used for this study, including stations from the Taiwan Strong Motion Instrumentation Program (TSMIP, blue triangles), the Broadband Array in Taiwan for Seismology (BATS, red triangles), and the Central Weather Bureau Seismic Network (CWBSN, black triangles). Grey dots indicate the seismicity for $M_L > 3$ from 1990 to 2018. White stars represent $M_L > 6$ events from 1990 to 2019. Active faults in the Longitudinal Valley region are shown with red lines. The blue box indicates the area of the stations used in this study.

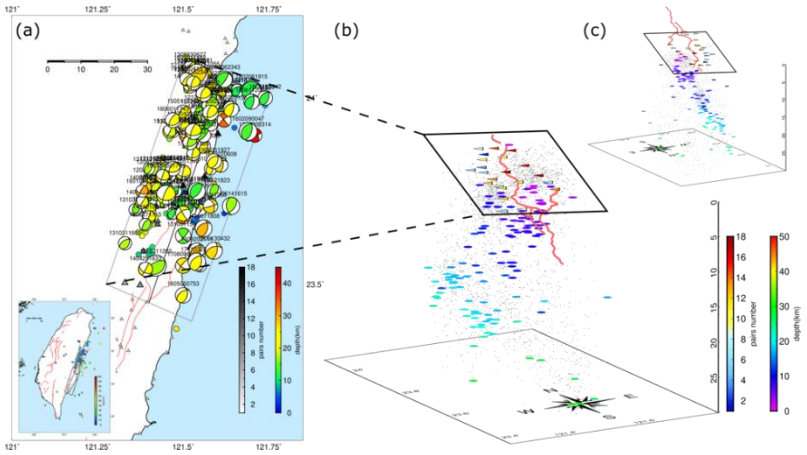

Figure 2. Summary of automatic [fault zone] head waves detections using data from stations in the vicinity of the Longitudinal Valley fault line. Coloured dots indicate events for which head waves have been detected. (a) Results in map view. The colored beach balls are 2012-2018 focal mechanisms from BATS CMT Catalog. (b) Results in a 3D perspective view from above the southwest corner, looking towards the northeast. (c) Similar to (b), but looking towards the southwest.

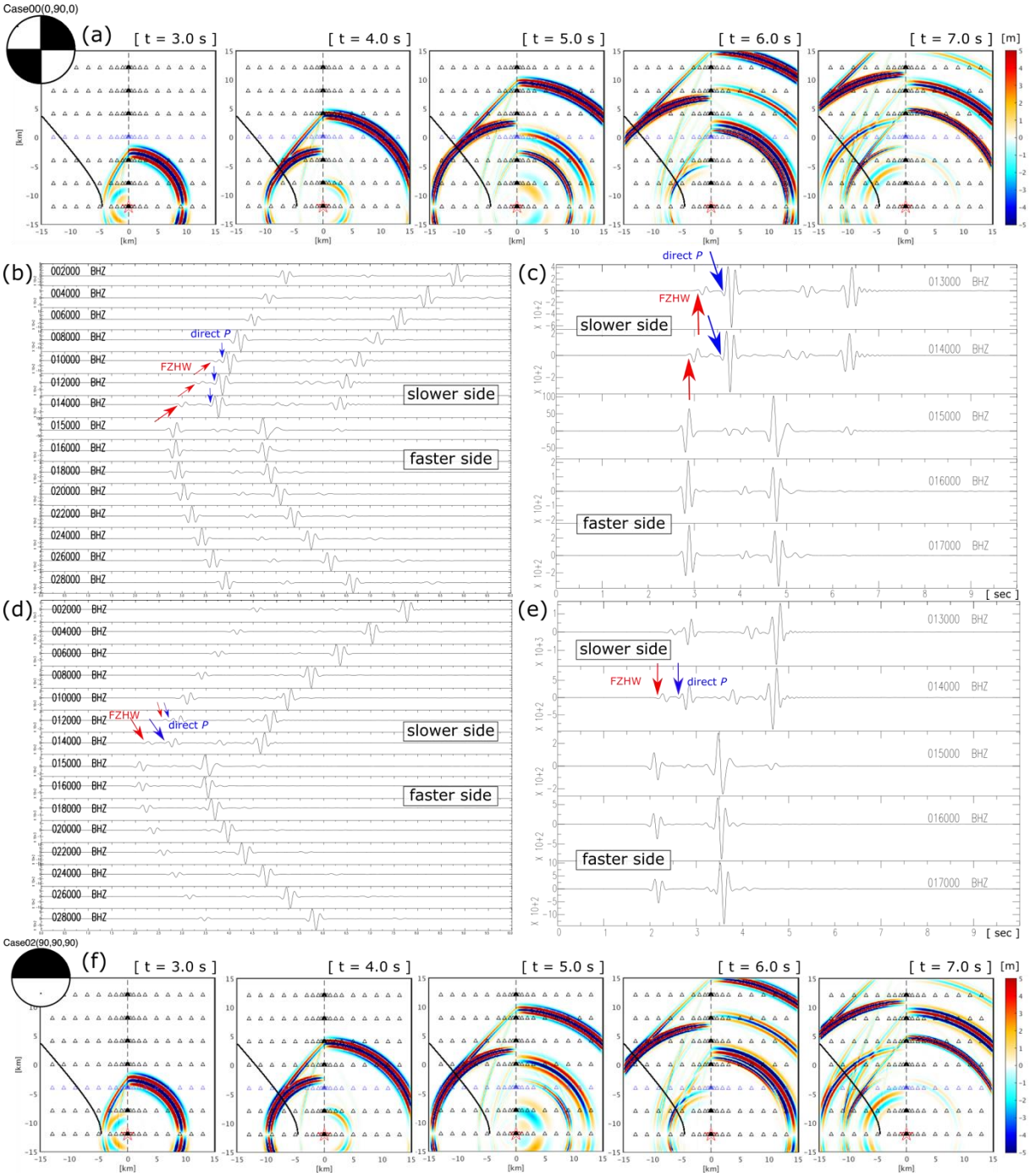

Figure 3. First motion polarity of fault zone head waves (FZHWs) and P waves generated by different focal mechanism. (a) Snapshots of the seismic wavefield at the surface with a strike-slip fault source at lapse times of t = 3.0 to 7.0 s. (b) Vertical component of synthetic velocity seismograms recorded by receivers at x = -13, -11, -9, -7, -5, -3, -1, 0, 1, 3, 5, 7, 9, 11, 13 km, y = 0.0 km, z = 0.0 km, shown as blue triangles in (a). Red and blue arrows indicate the first motion of FZHW and direct P wave, respectively. (c) Similar to (b) for receivers at x = -2, -1, 0, 1, 2 km, y = 0.0 km, z = 0.0 km. (d)-(f) Similar to (a)-(c), but with a high-angle thrust faulting mechanism (strike = 90°, dip = 90°, rake = 90°).

4. FZHW and direct P arrivals on synthetic seismograms

Ross and Ben-Zion (2014) built the algorithm to identify the direct P and FZHW phase by testing if P and FZHW picks have reversed polarity. It is directly applicable to detect head wave excited by a strike-slip source. However, the structure of the Longitudinal Valley fault system is complex, and the numerous small events exhibit a wide range of different source mechanisms. To understand the effect of a range of focal mechanism to the first motion polarity characteristics of the P wave and head wave, we use finite-difference simulations (Zhang and Chen, 2006; Zhang et al., 2012) to study P wave and head wave polarity relations for a set of systematically varying source mechanisms.

Figure 3 shows velocity record sections of the vertical component of motion for the numerical simulation with (a)-(c) a strike-slip source mechanism as a reference case; (d)-(e) a high-angle thrust faulting mechanism (strike = 90°, dip = 90°, rake = 90°). In both cases, as expected, stations on the faster side generally feature only simple P and S phase arrivals. In the strike-slip reference case stations near the fault on the slow side exhibit a first arrival that is an emergent phase with the polarity of the opposite side P wave, followed by a normally polarized P wave. This emergent phase is the head wave which propagates with the velocity of the faster medium and arrives before the direct P wave. However, for the high-angle thrust faulting and similar mechanism, the first motion of the head wave refracted along the interface has the same polarity of the direct P wave. The algorithmic choice of polarity reversal therefore rejects possible detections associated with a range of event mechanisms that result in same-polarity first motions, and that should therefore be adjusted for a more complete head wave detection set.

5. Summary

Conservative detection parameters adapted from previous studies performed in strike-slip environments yield a robustly detected set of head waves excited by events that are located within a thin volume along the west-dipping Central Range fault, which now suggests—for the first time—the existence of a consistent velocity contrast across that fault segment. A set of synthetic seismograms using a range of end-member fault mechanisms show head wave and P wave polarity relations that extend the typical first motion reversal associated with strike-slip events.

References:

Ross, Z. E., Ben-Zion, Y., 2014. Automatic picking of direct P, S seismic phases and fault zone head waves, Geophysical Journal International, 199(1), 368-381, doi: 10.1093/gji/ggu267

Zhang, W., Zhang, Z., Chen, X., 2012. Three-dimensional elastic wave numerical modelling in the presence of surface topography by a collocated-grid finite-difference method on curvilinear grids. Geophysical Journal International, 190(1), 358-378.

Zhang, W., Chen, X., 2006. Traction image method for irregular free surface boundaries in finite difference seismic wave simulation. Geophysical Journal International, 167(1), 337-353.

KEYNOTE. The Geocritical-Rock Physics and Fracture-Seismic Mapping of Permeability in the Brittle Lithosphere

P. Malin[1]

[1]Earth and Ocean Sciences, Duke University, Durham, NC
E-mail: malin@duke.edu

Over the past decades it has been shown that the Earth's brittle upper layers are in a constant state of mechanical failure. This paper summaries how this state has led to the observed characteristics of rock pores and fractures – the complex, variously connected void spaces in rock. The outcomes of this realization are two-fold: first is a new approach to understanding how fluid flow in rock can become channelized on all scales, resulting in a geocritical permeability field; second is the development of the Fracture Seismic method for mapping this field. FS uses the 3-D data collection method of Reflection Seismic, but in passive listening without sources. Such data has been found to contain episodic emissions from fluid filled voids, allowing the permeability field to be mapped.

Keywords: critical-state rock physics, void space, fluid flow, channels, passive seismic

1. Introduction

The movement of unbound fluids in the lithosphere has long been a prime example of a problem in complex-and-non-linear systems: difficult to observe and account for at depths beyond a few km. Beyond that point it is a fusion of multiphase chemistry and continuum-and-discontinuum mechanics, with a mix of pressures, temperatures, and deviatoric stresses. Commonly viewed either as a couple mechanical system or a structureless random process. The aim of this presentation is to bring something of a work-around past such deterministic and statistical approaches. It provides a third, more stochastic, perspective, and showing how this approach is grounded in observations and opens a way forward for further insights and practical applications. The Fracture Seismic (FS) method provides the way forward for the latter use.

Unbound fluids reside in pore spaces, the connections of which form the permeability field – the structures along which fluid-flow in rock takes place. Here the pores and their open connections are termed together as void space – be they gaps between grains, channels along grain boundaries, grain crossing cracks, veins, separations in bedding, fractures and fracture zones, or faults. Any place an unbound fluid can collect. In the lithosphere, such voids appear to conduct fluids in 3 different, overlapping, and heterogeneous regimes (Fig 1).

The insights that allow for this characterization come from studies of systems near transitions in their properties – in this case the way fluids flow through effectively solid rock. Generally known as critical state physics, here termed geocritical-rock physics, this approach is emerging in the description of lithospheric permeability - with original work done by Leary (1997, 1998, 2002), and others referenced in Bonnet et al. (2001). The models presented here are based on Leary and Malin (2021). An end-to-end description of FS is given by (Sicking and Malin 2019).

2. Geocritical Permeability

The right place to start describing the geocritical model is at the outcrop – in the case here, one that shows that there are places in the lithosphere where this description of permeability has not yet been investigated (Fig 2). As seen in 1-D images, it reveals the spatial attributes of

geocritical permeability: (i) channel with self-similar scaling, (ii) progression from numerous, small-scale, weak channels to large-scale, robust ones, and (iii) at least one channel that spans the full length of any sample. The largest, multiply connected channels naturally carry the bulk of the flow. Quantitatively, these attributes are described by the power law, $\mathbf{P(k)\sim 1/k^{\beta}}$, where $\boldsymbol{k}$ can be thought of as the number of channels per unit length, and $\boldsymbol{\beta}$ ranges from 0 to 2, the value observed for rocks in the brittle crust being 1 (e.g. Leary, 2002).

A further critical state permeability attribute, which relates void space and permeability populations, is found in long rock cores (Fig 3a). To a significant degree of correlation, void space is directly related to the logarithm of permeability, $\boldsymbol{\varphi \sim ln(\kappa)}$. Alternatively stated, the permeability field is an exponential function of void space: $\boldsymbol{\kappa \sim exp(\alpha\varphi)}$, where $\boldsymbol{\alpha}$ is a coupling constant. Thus, if $\boldsymbol{\alpha\varphi > 1}$ and $\boldsymbol{\varphi}$ has a normal population distribution, the resulting permeability field is lognormally distributed, with a few large channels dominating the flow structure.

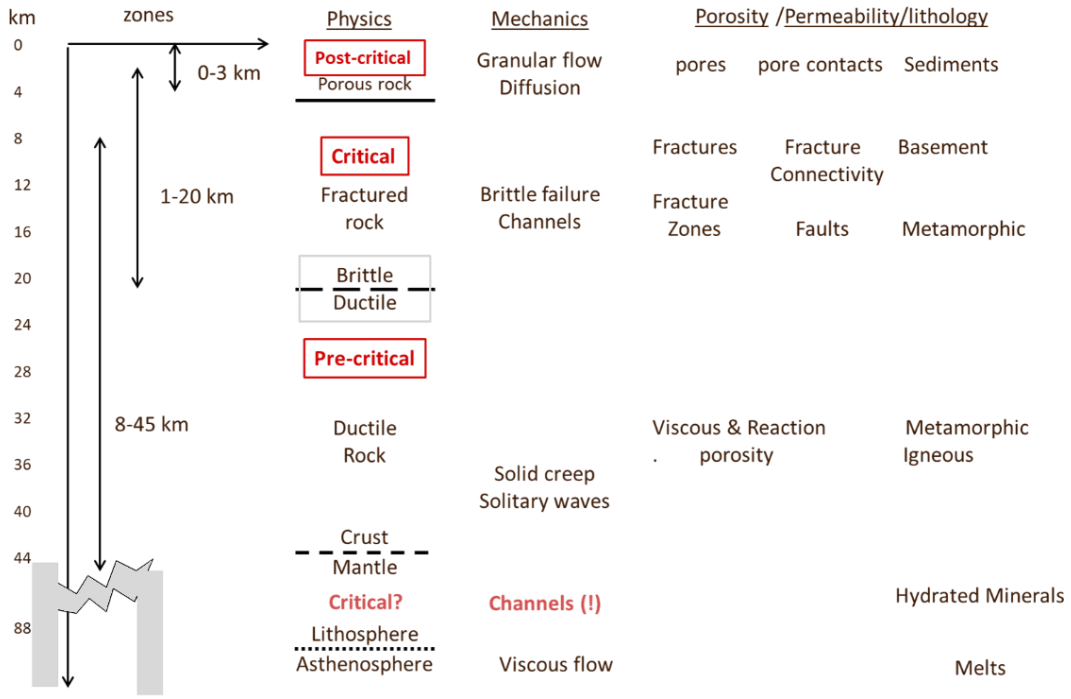

Figure 1. For the purposes of this discussion, permeability in the lithosphere is divided into 3 regimes, each of which have large lateral variation in depths, thicknesses, and internal heterogeneity. As explained in the text, the middle, critical, division is characterized primarily by flow in permeable channels. Flow in the overlying and underlying post-critical and pre-critical regimes appears more diffuse. The possible existence of critical-type flows at mantle depths in the lithosphere is also suggested by the channels shown in Fig 2.

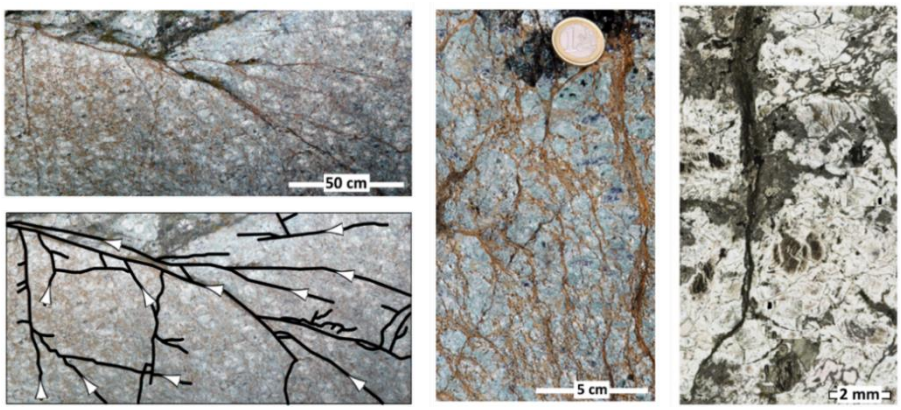

Figure 2. Erro-Tobbio meta-serpentinites in the Ligurian Alps of Italy. The mineral phases in connected void spaces indicate that these were formed at pressures of 2-2.5 GPa, essentially near the bottom of the lithosphere. Note the proliferation of short, closely spaced channels and the presence of at least one through-going channel. (Figure modified from Plumber et al., 2016.).

An equivalent, and perhaps more physically insightful, spatial characteristic of critical-state rock is its long-range correlation of fluid-flow related properties and mechanical behavior (Leary and Malin., 2020). In particular, the spatial correlation of natural and induced microearthquakes with magnitudes less than **M**~1 or so has been found to fall off as $\Gamma_{meq}(r) \sim 1/r^{1/2}$, r being the 1-D distance between events. This finding immediately links microearthquake seismicity back to the power law observed for critical-state rock, $\mathbf{P}(k)\sim 1/k$, and to the poroperm relation, $\kappa \sim exp(\alpha\varphi)$. The hypothesis being that **M**<1 seismicity is more controlled by the local permeability field, and not by the mechanics of faulting. It thus provides a physical basis for the Guttenberg-Richter law, $N\sim exp(a-bM)$, N being the number of events of magnitude greater than **M**, and a and b are constants. In essence, $a-bM$ is determined by $\alpha\varphi$.

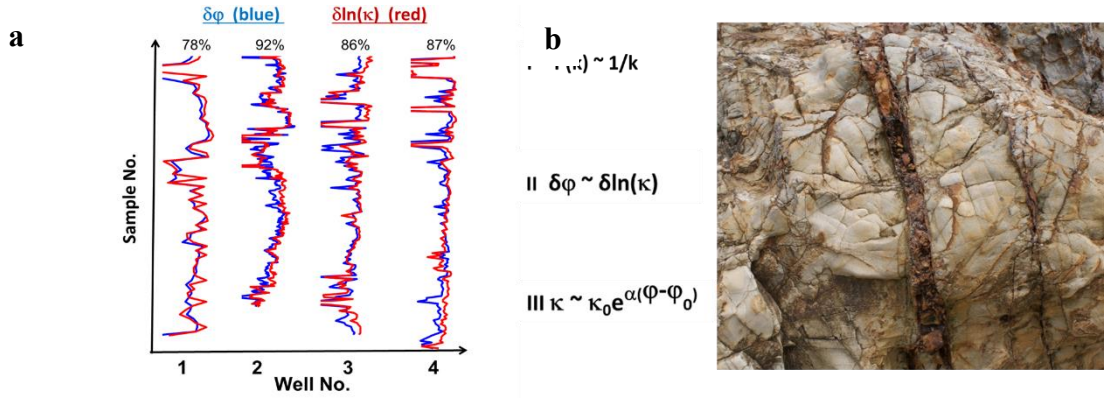

Figure 3. a. Plots of well-core void-space φ and the logarithm of permeability κ for 4 randomly chosen wells from a catalog of several hundred cores (Leary, 2002). The data are plotted with zero mean and normalized to unit variance. The correlation percentage between φ and $ln(\kappa)$ is shown above each well. **b.** The empirical relations that describe geocritical permeability and an outcrop illustration of them. (Photo by P. Leary)

The 3 relationships in Fig 3b work together to form the geocritical description of lithospheric permeability. The condition $\alpha\varphi > 1$ for lognormal flow can be seen from Rule III: $k \sim exp(a\varphi)$ can be expanded to $1+(\alpha\varphi)/1!+ (\alpha\varphi)^2/2!+(\alpha\varphi)^3/3!+\ldots$, which for $\alpha\varphi<1$ reduces to $\kappa \sim 1+(\alpha\varphi)$, implying that if φ is normally distributed so is κ, with no dominating channels. So what are the actual values of $a\varphi$ that corresponds to the rock shown in Fig 3b, and perhaps in some part, to the one in Fig 2? While the value for the latter is unknown, based on readily available borehole logs and cores, $\alpha\varphi$ appears to maintain a value of $3<\alpha\varphi<5$ for at least the upper quarter of the critical zone in Fig 1: roughly the top 6 km (Leary et al., 2017). To this depth, the quantitative relationships in Fig 3b can be used to calculate models that help reveal how they account for the observed physics of fluid flow (Fig 4). The modeling process helps to point out how the geocritical approach is different from that of, for example, an equivalent porous media (Lie and Mallison, 2015). It also shows why the FS mapping method described later in this abstract is essential for making practical use of the 3 relations in Fig 3b. (For a more complete discussion on that topic, see Malin et al., 2020.)

The initial modeling step is to the fill the model space with a normally distributed population of voids. The next step is the filtering of this population distribution so that it has a power law spatial distribution corresponding to $P(\mathbf{k})\sim 1/\mathbf{k}^{\beta}$, $0<\beta<2$, the choice of β determining the degree of channelization (Fig 4). These two steps point out that, without some way of anchoring the model to actual observations, the results will reflect the initial choice of void location and (random) starting value, with the possible number of model configuration equal to the number of model nodes for any one β value. The final step is selection of the value of $\alpha\varphi$.

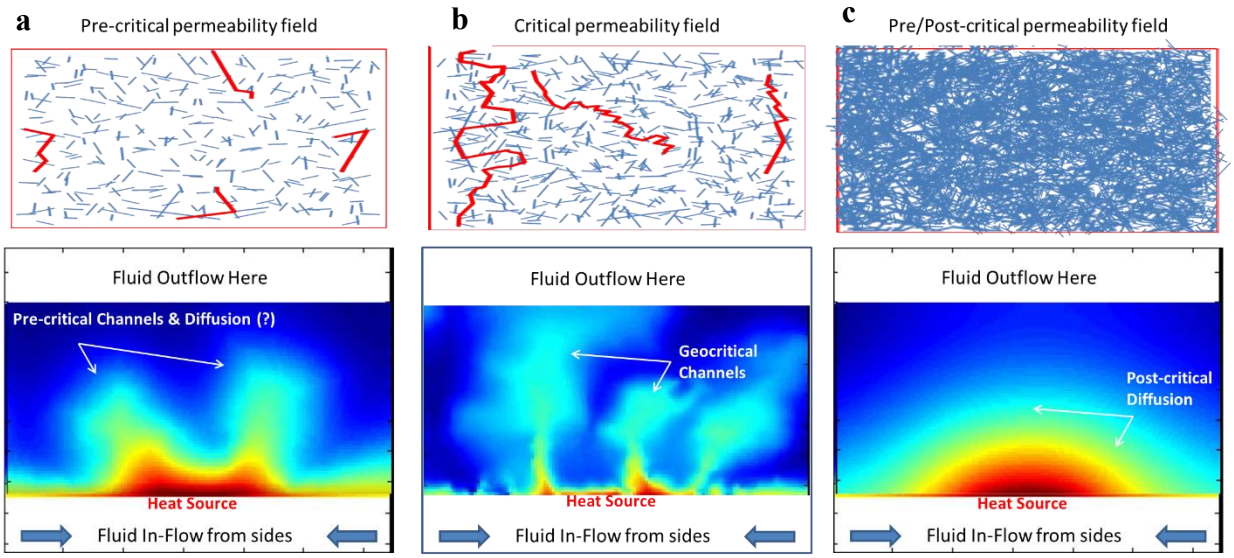

Figure 4. Geocritical flow modeling for different values of β and $\alpha\varphi$. Cool fluid begins flowing in from the lower sides of the model, heated by a source on the lower boundary, and flows upward. The flows shown are snap shots taken some time after the heated fluid begins rising. **a.** Represents the intermediate mixture of channelized, $\beta>0$, and diffusive, $a\varphi<1$, flow hypothesized here for the pre-critical regime in Fig 1. **b**. Illustrates $\beta\sim1$ and $a\varphi \sim4$, the channelized power-law and lognormal flow seen in brittle rock. **c**. For $\beta\sim0$ and $a\varphi<1$, this end member being equivalent to flow in a homogeneous porous medium. (Fig curtesy of P. Leary).

Application of this modeling approach to a specific site requires a calibration map consistent with the empirical rules in Fig 3b and that locates at least the main flow channels. In principle,

once shown to have the appropriate spatial and population characteristics, a geocritical-consistent permeability field can be built around the latter channels. While not resolving the actual locations of tributary channels, the model provides a stochastically robust forecast of its flow field. This is where Fracture Seismic Imaging enters the discussion.

3. Fracture Seismic Imaging

Fracture Seismic is an emerging void-mapping technology that has been demonstrated in Oil and Gas applications (e.g. Sicking and Malin 2019). More than a score of FS projects have been completed in both green and brown O&G fields. FS signals have been shown to be stress-and-fluid-pressure-change initiated elastic vibrations of fluid filled voids (Tary et al., 2013 a&b; Liang et al., 2017). Given the earth's constant tectonic, tidal, and fluid flow activity, episodes of these vibrations appear to be natural daily occurrences. They are also seen in much more powerful form in hydraulic stimulations. Recorded by passive monitoring with large 3-D seismic reflection layouts, but no controlled sources, these signals can be focused onto their sources with 1-way travel time signal processing (Fig 5). Like current 3-D Reflection Seismic, FS methods typically resolve feature with scale lengths >20-30 m.

Fig 6a illustrates how FS can be used to site successful wells at a O&G prospect with several pre-FS mapping dry wells. Based on FS data a test well was drilled, and a heavily fractured reservoir was found in the zone of high FS activity. From when this well was put on production and until April of 2019 it has produced 1.7 BCF gas.

Fig 6b shows two FS images of the progress of a hydraulic fracture stimulation in a shale gas field. Given the high amplitude and duration of the FS signals generated by the treatment it was possible to observe both the evolution and lateral extent of its apparent effectiveness. Initially the stimulation response rapidly progressed to one side of the treatment point, evidently coming to a stop before extending to the opposite side. Despite this difference, the FS signal intensity appears symmetrically distributed around the treatment well.

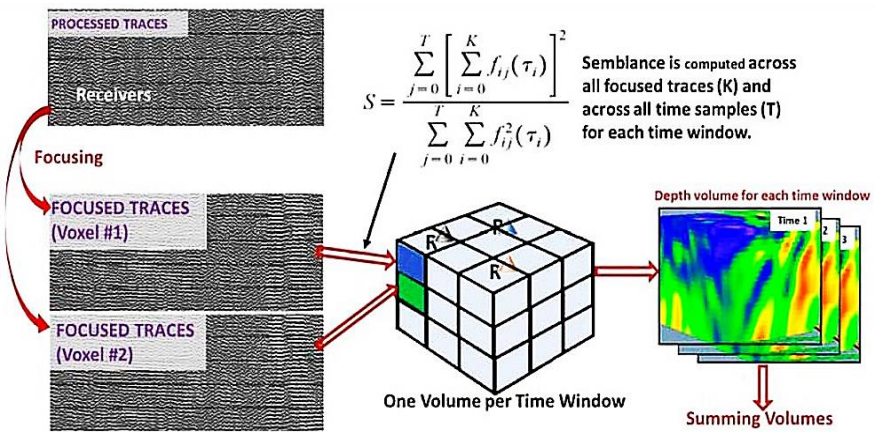

Figure 5. The processing scheme for mapping multi-receiver-and-time window ambient seismic data to their FS-source points. Numerous receiver-location versus observation-time sections are adjusted so that the travel time from a selected voxel is accounted for. The semblance for each is found, voxels emitting FS signals producing the highest values. Multiple time windows are added to produce the Fracture Seismic Image. (Fig from Sicking and Malin, 2019.)

a **b**

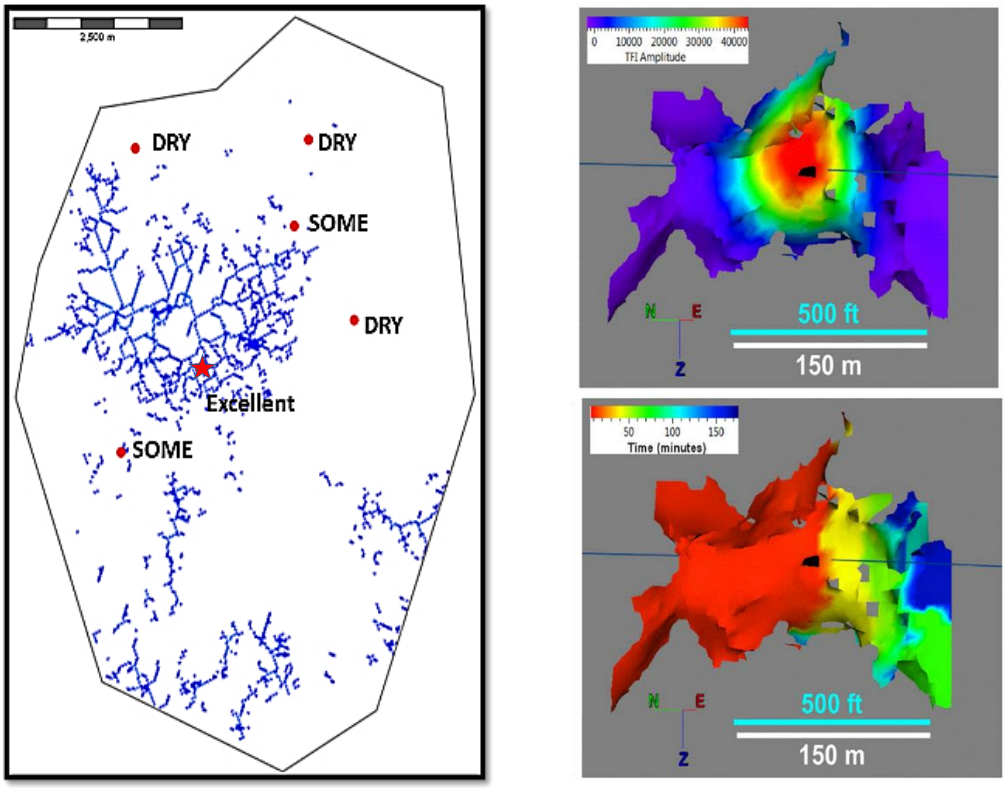

Figure 6. a. An O&G field FS map showing the natural permeability channels (the blue lines lie on the maximum semblance values). These channels may extend above and below the map. Red spots are dry or limited wells drilled before FS targeting, red star well using FSI. **b**. FS signals from a hydraulic stimulation stage. Upper shows the FS signal amplitude distribution. Lower the time evolution, the fractures to the left opening earlier than the fractures to the right side of the well. (**a** from Lacazette et al., 2013; **b.** from Sicking et.al., 2015).

FS observations show the kind of spatial and population distributions described by the geocritical approach to fluid flow (Fig 7a). They also locate flow channels with lengths greater than the minimum resolution of the collection method. Hence, an FSI map provides the large-scale framework on which a geocritical-permeability field model can be constructed to forecast fluid flow (Fig 7b) - the calibration points for the $\mathbf{P(}k\mathbf{)\sim1/}k^{\beta}$ and lognormal κ distributions.

The FS method has important implications for subsurface hazard mapping and monitoring. Two instances are in the evaluation of cap rock integrity (Fig 8a) and the potential for induced seismicity (Fig 8b). In the former case, the possible and actual creation of flow channels from an energy reservoir stimulation to an aquafer could be forecast and detected. Likewise, permeable zones that can conduct both high fluid-pressures and fluids to potentially active faults can be mapped ahead of time, avoiding inducing, or triggering a damaging earthquake.

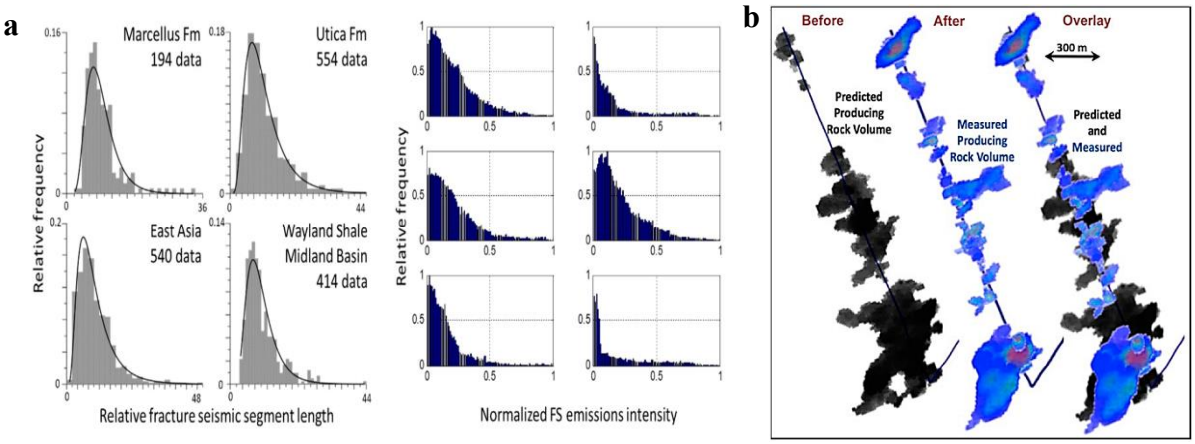

Figure 7. a. Population distributions of FSI image features. Left 4 panels show the results for main channel feature lengths for different O&G basins. Right 4 panels show results for relative FS signal amplitude during hydraulic stimulations. (Data are from Lacazette et al., 2013). **b.** Forecasting O&G well production before drilling. Left: Pre-drill, FSI intensity forecast of near-well production. Center: Map of the active FS voxels 2.5 years after drilling and production. Right: Overlay of the forecast map and the observed active FS voxels, showing that the production is coming from zones that were permeable before the well was drilled. Compare this to Figure 4b. (Figure modified from Sicking and Malin 2019 and Malin et al, 2020).

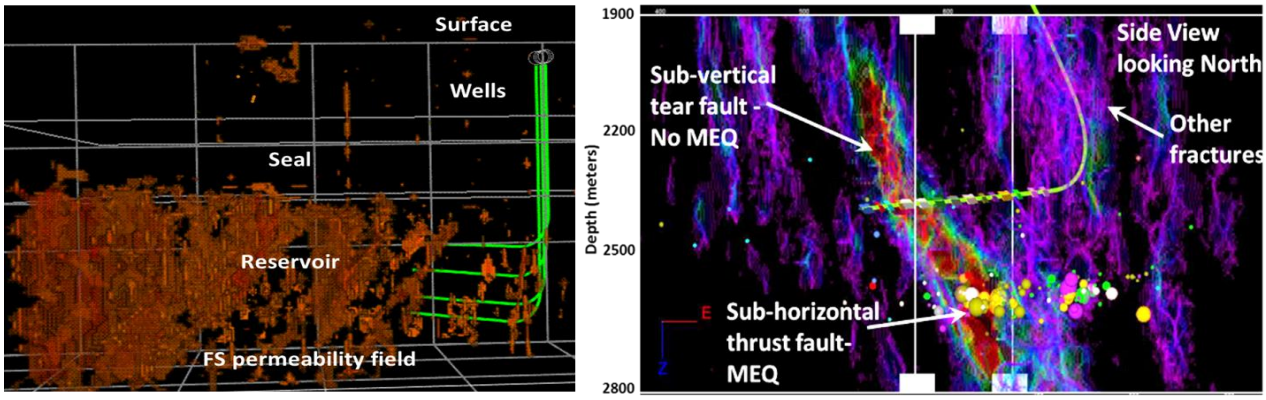

Figure 8. a. Block diagram view of FS signals from the hydraulic stimulation of four stacked 2000 m long lateral wells in a shale gas reservoir. The amber colored permeability field activated by the stimulation stops at the cap rock seal, indicating little communication with overlying strata. **b.** Seismicity induced on an underlying thrust fault by hydraulic stimulation of a permeable tear fault. (Fig **a** and **b** modified from Geiser et al., 2012 and Sicking and Malin 2010.)

In summary, geocritical-rock physics bring an observation-consistent approach to the mechanics of lithospheric permeability - in at least the limited range of environments studied so far. Much work remains to be done for a fuller accounting of current and other ones. Fracture Seismic methods hold a similar position, having been applied primarily to O&G fields. Efforts are underway to evaluate it for mapping geothermal resources and waste disposal, including

carbon sequestration. It remains to be seen how these seemingly promising development can be matured into a comprehensive description of the lithosphere's permeability field.

4. References

Bonnet, E., O. Bour, N. Odling, P. Davy, I. Main, P. Cowie, & B. Berkowit 2001 Scaling of fractures systems in geological media, Reviews of Geophysics, 39, 3 / August 2001 pages 347-383.

Geiser, P., A. Lacazette, J. Vermilye, 2012. Beyond "dots in a box": an Empirical View of Reservoir Permeability with Tomographic Fracture Imaging. First Break, 63-69.

Hunt, A. 2005 Percolation Theory for Flow in Porous Media, Lecture Notes in Physics book series LNP, volume 674 Springer.

Lacazette, A.; Geiser, P. Comment on Davies et al., 2012–Hydraulic fractures: How far can they go? Mar. Pet. Geol. 2013, 43, 516–518.

Leary, P. 1997 Rock as a critical-point system and the inherent implausibility of reliable earthquake prediction, Geophysical Journal International 131, 451-466.

Leary, P. 1998 Relating microscale rock-fluid interaction to macroscale fluid flow structure, in Faulting, Fault Sealing & Fluid Flow in Hydrocarbon Reservoirs, Jones G, Fisher Q & Knipe R eds, Geological Society Special Publication 147, London, 243-260.

Leary P., 2002, Fractures and physical heterogeneity in crustal rock, in J.A. Goff and K. Holliger, eds.: Heterogeneity of the Crust and Upper Mantle – Nature, Scaling and Seismic Properties, New York, Kluwer Academic/Plenum Publishers, p. 155-186.

Leary, P., P. Malin, T. Saarno, & I. Kukkonen 2017 Prospects for Assessing Enhanced Geothermal System EGS Basement Rock Flow Stimulation by Wellbore Temperature Data. Energies 2017, 10, paper no. 1979.

Leary P & Malin P 2020 Correlation function Γmeqr ~ 1/r½ coupling of microseismicity to permeability -- The basis for fluid flow seismic image targeting for geothermal production wells, Proceedings World Geothermal Congress 2021 Reykjavik, Iceland, 21-26 May 2021.

Leary, P., & P. Malin in press for 2021, Crustal reservoir flow simulation for k ~ expαφ poroperm media, Journal of Energy and Power Technology, Manuscript ID: jept-1122.

Liang, C., O. O'Reilly, 2017, E. Dunham, and D. Moos, Hydraulic fracture diagnostics from Krauklis-wave resonance and tube-wave reflections, GEOPHYSICS, VOL. 82, NO. 3 MAY-JUNE 2017; P. D171–D186, DOI: 10.1190/geo2016-0480.1.

Lie KA., Mallison B.T. 2015 Mathematical Models for Oil Reservoir Simulation. In: Engquist B. eds Encyclopedia of Applied and Computational Mathematics. Springer, Berlin, Heidelberg.

Malin, P., P. Leary, L. Cathles, C. Barton, 2020 Observational and Critical State Physics Descriptions of Long-Range Flow Structures. *Geosciences* 2020, *10*, 50.

Plümper, O., T. John, Y. Podladchikov, J. Vrijmoed, & M. Scambelluri 2016 Fluid escape from subduction zones controlled by channel-forming reactive porosity, Nature Geoscience 10,2 p150-156.

Sicking, C., P. Malin, 2019) Fracture Seismic: Mapping Subsurface Connectivity. Geosciences 2019, 9, 508.

Tary, J. B., M. Van der Baan, B. Sutherland, and D. W. Eaton (2014a), Characteristics of fluid induced resonances observed during microseismic monitoring, Journal of Geophysical Research, 119, 8207-8222.

Tary, JB, M. Van der Baan, DW. Eaton, (2014b), Interpretation of resonance frequencies recorded during hydraulic fracturing treatments Journal of Geophysical Research: Solid Earth 119 (2), 1295-1315.

Non-invasive Exploration technologies in the INFACT project: Examples from the reference sites

J. Nevalainen[1], J-P. Ranta[1], E. Kozlovskaya[1], M. Kirsch[2], L. Ajjabou[2] and R. Gloaguen[2]

[1]Oulu Mining School, University of Oulu, Finland
[2]Helmholtz-Zentrum Dresden-Rossendorf, Helmholtz Institute Freiberg for Resource Technology, Freiberg, Germany
E-mail: Jouni.nevalainen@oulu.fi

In this work, we present the selected results from the Innovative, Non-invasive and Fully Acceptable Exploration Technologies (INFACT) project, funded by Horizon 2020 research and innovation programme. We evaluated different geophysical data against the known geological and infrastructural challenges in two reference sites of INFACT, Sakatti (Finland) and Geyer (Germany). In addition, we evaluate how the technologies are performing to detect known exploration targets.

Keywords: Exploration, crust, Magnetics, Electromagnetism.

1. General

The Innovative, Non-invasive and Fully Acceptable Exploration Technologies (INFACT) project unites stakeholders of Europe's future raw materials security in its consortium and activities. INFACT is comprised of three main components: 1) Development and test of innovative, non-invasive exploration technologies, 2) Foundation of three reference sites for exploration technologies in the south-, central- and north Europe, 3) stakeholder engagement, education and policy reform. These actions are combined to reach each of the main areas in which the EU has the power to influence changes in its raw materials security.

Oulu Mining School is especially part in the technical and geological aspects of the project. This has included both technical work as well producing an out-reach material to increase the knowledge of exploration technologies for stakeholders and public.

Focusing on the technical aspect, our role in the INFACT has been further processing and evaluating the obtained data from the reference sites, mainly focusing on the north and central reference sites. In this work, we present selection of result to technical questions and how they have been answered at this stage. In addition, we discuss the differences between the state-of-art data and the data obtained by new technologies, evaluating the possibilities they bring.

2. The reference test sites and used exploration technologies

Here, we focus on the main exploration technologies used at the central and northern reference sites of INFACT. Both reference sites vary significantly from each other in terms of geology. The northern site is comprised of massive sulphide type Ni-Cu-PGE deposit (Sakatti), located in deep subsurface. It is currently under feasibility study. In addition to the deep massive sulphide, the quaternary deposits on top of the bedrock is highly conductive (Viiankiaapa mire area).

The central reference area is located near the city of Geyer, Germany. The area has a long mining history and the region is known for its deposits of tin, zinc, tungsten, molybdenum, copper, iron, silver and indium. The population is dense and the built infrastructure produces EM noise. Typical challenges for measurements in urban environment are fenced areas, buildings and other no-access areas in both for ground based and airborne measurements.

In 2018, at the northern and the central reference sites, magnetic data was obtained during airborne Electromagnetic survey (Geotech Ltd. VTEM-ET system) and airborne Full Tensor Magnetic Gradiometry (FTMG) data using Supracon® AG Ltd. Jessy Star system. (Supracon® AG, 2020). The latter data set is considered as a part of innovative technologies within INFACT. In addition, legacy datasets exist including AEM VTEM dataset (2009) from the northern reference site. Both geological and petrophysical information are available for verification of the technique with ground-truth data.

2.1 Magnetic method

The Total Magnetic field Intensity (TMI) measurements are routinely used in ground, airborne and borehole surveys. With a typical TMI instrumentation, the presence of magnetized rock can be detected within equipment detection limits. However, its modelling can be difficult due to the ambiguity problem associated with potential field methods. In addition, presence of a strong remanent magnetization component can make accurate modelling challenging, especially if no a-priori information about magnetization is available. Moreover, if the host rock is magnetic it may be an obstacle to the sharp lineation of the exploration target. Due to these obstacles, magnetic method is commonly used as an auxiliary method to support other geophysical exploration technique such as gravity and electro-magnetic surveys.

More information about magnetic properties of the subsurface can be obtained from measurements of all components of the magnetic field. In Full Tensor Magnetic Gradiometry (FTMG) measurements, all magnetic field gradients are obtained. They contain more information about the size, shape and particularly about magnetization direction of the magnetic rock mass. This full description of the magnetic field constrains the number of possible magnetic models, as the response of magnetic models need to satisfy all components of FTMG whereas in traditional TMI interpretation the magnetic model needs only to satisfy the general TMI field (Clark, 2014; Queitsch et al. 2019). In addition, FTMG can be used to extract information about possible presence of significant remanent magnetization (Clark, 2014).

After the millennia, SQUID (Superconducting QUantum Interference Devices) technology in highly sensitive magnetometers has been successfully adopted. With multiple SQUID sensors, it is possible to measure a full tensor of magnetic field gradient with excellent resolution. During last decade the FTMG have been successfully adopted in airborne measurements. This achievement has given magnetic method new opportunities for detailed subsurface modelling and hence new applications in exploration projects.

In the INFACT project, we evaluated the magnetic data in northern and central reference sites by comparing the differences between traditional magnetic TMI data and FTMG data obtained with Supracon® AG Ltd. Jessy Star systems SQUID sensors.

To demonstrate the increase of information with FTMG data we present a synthetic example of calculated TMI field and magnetic field gradients for four differently shaped and sized magnetic objects (Figure 1A). The shapes are a rectangle shaped prism (at NW), a sphere (NE), an L-shaped object (SW) and a triangle shaped object (SE). The objects are clearly visible in the TMI response. Note the different responses in the plots of magnetic gradient response presented below the TMI plot. In the Figure 1B, the same magnetic objects are present but with an added contact of two differently magnetized domains underneath them. Here, the shaped objects are not as visible as they were in Figure 1A but the gradient components immediately indicate the presence of anomalous objects in same locations than that in Figure 1A.

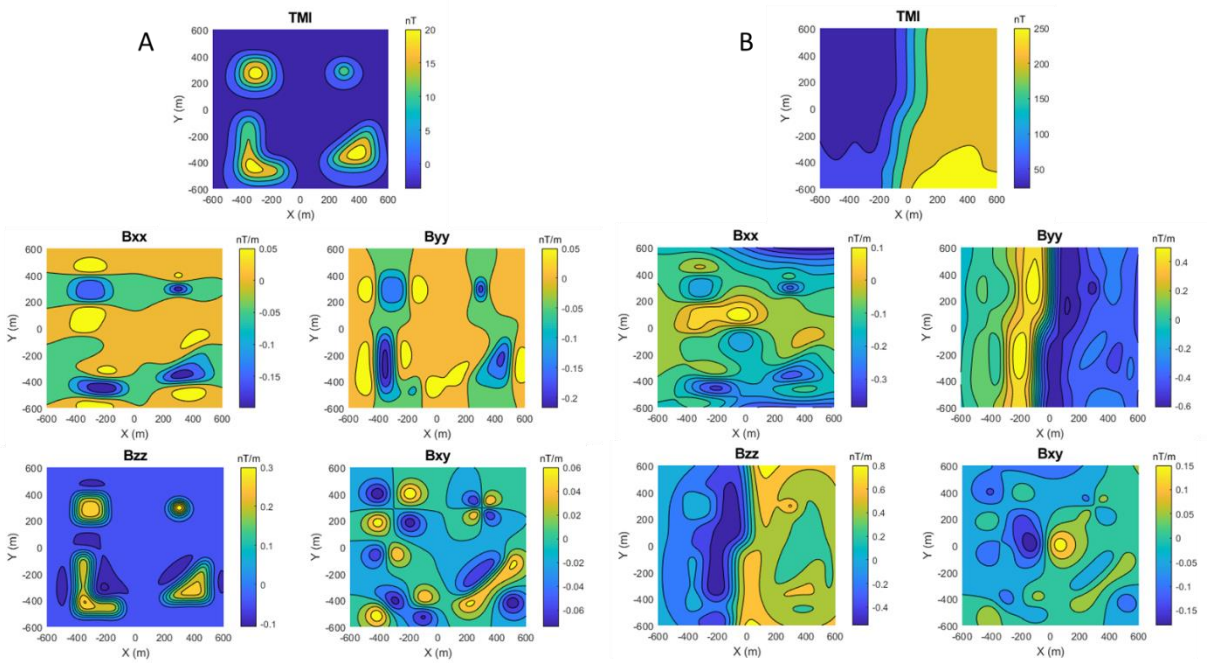

Figure 1. A: Calculated Total Magnetic field Intensity (TMI) and magnetic field gradients tensor components (Bxx, Byy, Bzz & Bxy) for magnetic bodies of different shape. The bodies are magnetized in the geomagnetic field similar to that in the Northern Finland. B: The same synthetic model elements than those in A but with a contact of two magnetic domains beneath the bodies. Note that coordinates are in NED system.

2.2 Modelling Airborne Electromagnetic data

As one of the most popular geophysical methods in mineral exploration, airborne electromagnetic survey was selected to be a part of the INFACT methods. AEM is very good for detecting buried electric conductors, both in large and small scales. The Geotech Ltd. VTEM-ET system represents a state-of-art technology.

The INFACT reference sites at Sakatti and Geyer are very different in terms of geology. The known conductive targets at Geyer are at shallower depth compared to the Sakatti, and the targets are smaller in size at Geyer. At Sakatti, the area is covered with conductive sedimentary layer due to the Viiankiaapa mire. There is also significant difference in EM noise between the areas. At Sakatti, the EM noise level is low for the whole site while in Geyer the EM noise is considerably higher and varies throughout the region.

In our work, we evaluated how the obtained data could be used to solve the problems mentioned above. In addition, we evaluated the obtained conductivity models from both the sites.

Conclusions & future development

The FTMG data gives detailed information about magnetic field at the INFACT reference sites and especially the magnetic fields behaviour between flight lines compared to TMI measurements. This allows a detailed delineation of interesting areas in mineral exploration. In addition, the generally increased resolution improves the mapping of the large-scale structures in more detail. In near future, we are to make a joint inversion of the five independent components of FTMG using Bayesian inversion as a general frame.

The electromagnetic data and models from north and central sites were analysed and evaluated against the site geological and EM-noise challenges. The research is in progress to increase the resolution and reliability of EM modelling by joint modelling of two different datasets.

Acknowledgements
This study has been done in the framework of EU Horizon 2020 funded INFACT project (webpage: https://www.infactproject.eu). This project has received funding from the European Union's Horizon 2020 research and innovation programme under grant agreement No 776487.

References:

Clark, D., 2014. Integrated magnetics: contributions to improved processing and interpretation of magnetic gradient tensor data, new methods for source location and estimation of magnetisation, and predictive magnetic exploration models. Doctoral thesis, Sydney, Australia: Macquarie University.

Hinze, W.J, von Frese, R.R.B., Saad, A.H., 2013. Gravity and Magnetic Exploration, Principles, Practices and Applications. Cambridge University Press. (Chapters 8, 9).

INFACT, 2020.The Innovative, Non-invasive and Fully Acceptable Exploration Technologies, Information webpage: < https://www.infactproject.eu/ >. This project has received funding from the European Union's Horizon 2020 research and innovation programme under grant agreement nº 776487.

Queitsch,M., Schiffler, M., Stolz, R., Rolf, C.,Meyer, M., Kukowski, N, 2019. Investigation of three-dimensional magnetization of a dolerite intrusion using airborne full tensor magnetic gradiometry (FTMG) data, Geophysical Journal International, Volume 217, Issue 3, June 2019, Pages 1643–1655, https://doi.org/10.1093/gji/ggz104.

Supracon® AG, 2020. Project information & Brochures. < http://www.supracon.com >

Structural evolution and melt formation within the southernmost Finland migmatitic belt

K. Nikkilä[1], P. Skyttä[2], A. Saukko[1] and O. Eklund[1]

[1]Geology and Mineralogy, Åbo Akademi University
[2]Department of Geography and Geology, University of Turku
E-mail: kaisa.nikkila@abo.fi

Southern Finland consist of belts of migmatitic infra- and supracrustal rocks. The southernmost migmatitic belt and Uusimaa belt have coeval and presumably similar tectonic histories, although it is proposed that they are separated by a terrane boundary. In this study, we investigated leucosomes, granitic intrusions and deformation history in the southernmost archipelago of Finland to clarify the relationship between the formation of the anatectic melts and deformation in the southernmost migmatitic belt. Further, we use this understanding to compare the southernmost migmatitic belt with the better-known Uusimaa belt. Results of our structural analysis indicate that the last migmatization events (at 1.84-1.81 Ga) affected all the rock types, and subvertical leucosome transportation took place during subhorizontal compression as in the Uusimaa belt. However, geochemistry (Saukko et al, 2021) and regional structural patterns show contrasting signatures between the belts.

Keywords: Southern Finland, migmatitic belt, granitic metatexite, deformation, shear zone, partial melts

1. Introduction

The Paleoproterozoic Svecofennian orogenic domain of Southern Finland consists of belts with strongly migmatized infra- and supracrustal rocks in upper amphibolite to granulite facies, with areas of less migmatized rocks in-between. The supracrustal rocks are approximately 1.90-1.88 Ga (e.g. Hopgood et al. 1983; Väisänen and Mänttäri, 2002; Skyttä et al. 2005), and the infracrustal rocks, here called granitic metatexites, are slightly younger ca.1.88 Ga (Hopgood et al. 1983; Saukko et al., 2021). Two tectonothermal events associated with migmatization are recognized: the older at 1.88-1.87 Ga (Skyttä et al., 2006) and the younger at 1.83–1.81 Ga, synchronous with regional folding and thrusting (e.g. Väisänen et al. 2002). NW-SE and NE-SW oriented shear zones are common in Southern Finland (e.g. Väisänen and Skyttä, 2007; Väisänen et al. 2002) and they were presumably active at 1.83–1.79 Ga (Väisänen and Skyttä, 2007), i.e. synchronous with and after the younger metamorphic peak.

The southernmost migmatitic belt is a 100 km long, E–W trending belt outcropping on the mainland and within the archipelago of the Gulf of Finland, south of the Uusimaa belt (Figure 1). The proportions of granitic and migmatitic supracrustal rocks vary in the southernmost belt so that the amount of granitic rocks increases southwards. Deformation zones crosscut the area in E-W and NE-SW orientations. The migmatization, melt transport, granites, and deformation zones are presumably related to each other. In previous publications, southernmost Finland is often included in the rest of the Southern Finland (e.g. Väisänen and Skyttä, 2007), although Jaanus-Järkkälä and Edelman (1983) discussed that a subduction zone may separate the southernmost migmatitic belt from Uusimaa belt. Regardless of several studies (e.g. Hopgood et al. 1983, Kurhila et al. 2011) the relationship between the southernmost belt and areas around it is ambiguous. Further, the relationship between the formations of anatectic melts, granites, and deformation in the southernmost migmatitic belt remains unclear. Bearing this in mind, the aim of this study is to understand the relationship between the formations of

anatectic melts, granitic magmatism, and structural evolution of the southernmost migmatitic belt, and further to look into the connection between the Uusimaa and the southernmost migmatitic belts. We place specific focus on understanding the role of major shear zones which may have acted both as melt pathways and as boundaries between geological domains.

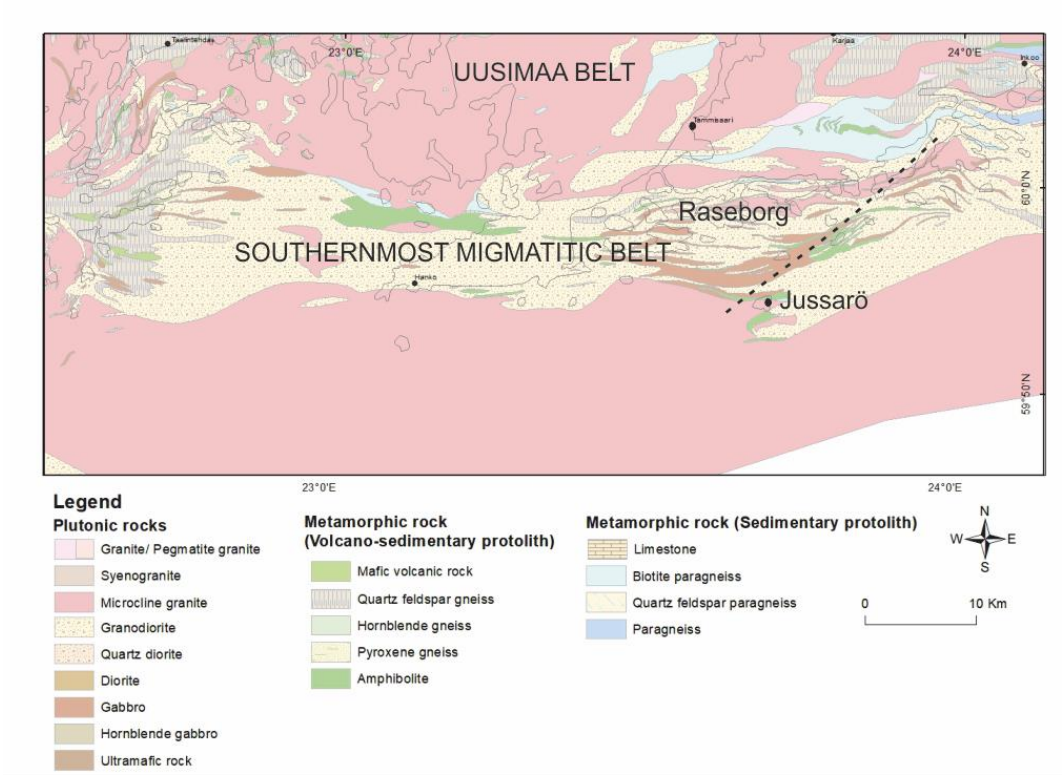

Figure 1. Simplified lithological map of the study area. The black dashed line indicate the location of the Barösund shear zone.

2. Materials and methods

This study is part of a larger project addressing the relationship between deformation, leucosomes and granitic magmatism. The utilized methods include field observations, geochemistry, geochronology of the granitic rocks, and structural analysis. In this study, we focus on the structural interpretations of the study area, arising from analysis of existing regional-scale datasets (geological and geophysical maps), complemented by detailed field investigations in selected key localities.

3. Results

The dominant structural trend, including foliation, within the southern migmatitic belt is E-W. Bedding (S0) is rarely visible, but if present, it is subparallel to first generation foliation (S1). Mafic layers, parallel to S1, have often been boudinaged and they may have melts in boudin necks, whereas felsic layers – probably metapsammitic rocks – were recrystallized in a ductile manner when S1 foliation was formed. It is likely that F1 folds and L1 formed during D1, but direct observations have not been made.

The second deformation event (D2) caused refolding of S1, and is associated with the development of a weak S2 foliation along F2 axial planes (Figure 2). However, S2 is not always present in the studied rocks. The (F2) folds are approximally upright, and have subhorizontal fold axes, with predominantly south-dipping axial surfaces. In some areas, mineral lineation

(L2) is parallel to the fold axes. Fold tightness varies regionally: folds are usually gentle to open and mineral lineations are parallel with the fold axes in the west. By contrast, folds are close to tight, similar or flexural slip –type folds, and the mineral lineations (L2) are moderately plunging in the east and centre of the study area (Raseborg/Jussarö). In mafic supracrustal formations, the lineation is strong and moderately plunging. The trend can vary in outcrop scale; thus, we propose that this is an earlier lineation (L1/L2) that was transposed during the folding.

NE-SW and E-W striking shear zones transect the study area and caused localised deflection of the main foliation and first and second generation folds, and likely caused the development of the third generation folds (F3). The E-W striking shear zones are 10-50 cm wide ultramylonitic to mylonitic zones with often dextral kinematics. The shear zones are common in the centre of the study area, where supracrustal rocks are present, often spatially associated with metalimestones. The NE-SW striking deformation zones are large-scale shear zones. In the study area, there are only a few in this direction but those shear zones can be tens to hundreds of meters wide. The largest shear zone is the Barösund shear zone, which is 500 m wide (Vehkamäki, 2019), oblique-slip shear zone with sinistral lateral component of deformation.

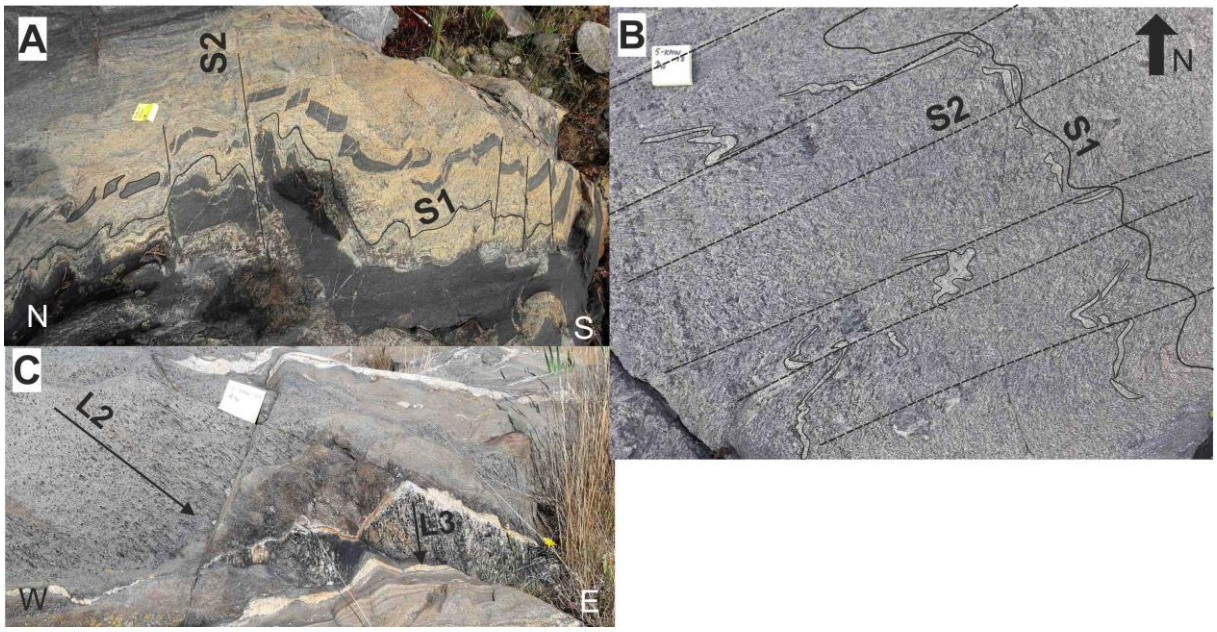

Figure 2. Structures in the migmatitic rocks. A) and B) Schistosity S1 has folded and partial melts has accommodated along axial planes (S2). C) The mineral lineation in the mafic layer (L2) plunge moderately to NE and mineral lineation in the leucosome (L3) plunge subvertically.

4. Infracrustal formations and two partial melting events

The infracrustal formations, granitic metatexites, intruded foliation-parallel (S1) in the supracrustal rocks between D1 and D2 around 1.88 Ga. The amount of granitic metatexites increases toward south, and they seem to locate stratigraphically below the volcano-sedimentary rocks. The first migmatization took place before F2 folding, thus the granitic metatexites can have caused the formation of the first partial melts at 1.88 Ga. The granitic metatexites have strong mineral lineation (L2), which varies locally, being subhorizontal in the west and subvertical in the east. The metatexites are mylonitic, especially close to the main deformation zones and in the eastern part of the study area, and they may be folded.

The granitic metatexites contain crystallised in situ melts that are proposed to represent the younger, 1.84-1.81 Ga migmatization event (Saukko et al. 2021). The leucosomes cross cut all formations, but some of these leucosomes were folded or boudinaged depending on their orientation with respect to the foliation in the surrounding bedrock. The texture of the leucosomes is massive and they do not have foliation; however, strong subvertical mineral lineation (L3) occurs in leucosomes parallel to the host-rock foliation. The character of L3 differs from lineations in the supracrustal formations suggesting later stage deformation. The leucosomes have also been emplaced along F2 axial planes in several rock types: metapsammitic, metavolcanosedimentary rocks and infracrustal rocks (metatexites), and in mafic rocks or dykes if present; regardless whether schistosity is present or not (Figure 2). We propose that the transportation of the leucosomes was active during the D3 at 1.84-1.81 Ga.

5. Conclusions/Summary

The preliminary results show that the granitic metatexites intruded parallel to the foliation of the supracrustal units between D1 and D2. The mylonitic granitic metatexites are located near NE-SW striking shear zones and they may have intruded coevally with the shearing, suggesting that the shear zones may have been active already around 1.88 Ga. Both rock types have been folded and deformed during D3, the last compression and melt transportation at around 1.84-1.81 Ga.

The last migmatization at 1.84-1.81 Ga was extensive and both supracrustal and infracrustal formations were migmatized. The accumulation of partial melts in the F2 axial planes, their deformation (folds or boudins) and the subvertical attitude of L3 indicate that melt transportation has been coeval with flattening and subhorizontal compression. It is also likely that transposition of the L1/L2 lineation took place simultaneously with the compression. Because the youngest melts, at 1.83-1.81 Ga, crosscut the mylonitic granitic metatexites in the south, we propose that the NE-SW striking shear zones were not active during the last melt transportation event, in the end of D3. Similar kind of crosscut relationship with the E-W striking shear zones and latest melts have not been found.

References:

Edelman, N., Jaanus-Järkkälä, M., 1983. A Plate tectonic interpretation of the Precambrian of the Archipelago of southwestern Finland. Geological Survey of Finland, Bulletin 325.

Hopgood, A. M., Bowes, D. R., Kouvo, O., Halliday, A. N., 1983. U-Pb and Rb-Sr isotopic study of poluphase deformed migmatites in the Svecokarelides, Southern Finland. In High grade metamorphism, migmatites and melting. Meeting of the Geochemical Group of the Mineralogical Society (pp. 80-92).

Kurhila, M., Mänttäri, I., Vaasjoki, M., Rämö, O. T., Nironen, M., 2011. U–Pb geochronological constraints of the late Svecofennian leucogranites of southern Finland. Precambrian Research, 190:1–4.

Saukko A., Nikkilä K., Eklund O., Väisänen M., 2021. Granites of southernmost Finland, this volume.

Skyttä, P., Käpyaho, A., Mänttäri, I., 2005. Supracrustal rocks in the Kuovila area, southern Finland: structural evolution, geochemical characteristics and the age of volcanism. Bulletin, Geological society of Finland, 77(2), 129.

Skyttä, P., Väisänen, M., & Mänttäri, I., 2006. Preservation of Palaeoproterozoic early Svecofennian structures in the Orijärvi area, SW Finland—Evidence for polyphase strain partitioning. Precambrian Research, 150(3-4), 153-172.

Vehkamäki, T. 2019. A multidisciplinary investigation of the Barösund Shear Zone area, southern Finland. Master's thesis, University of Turku. 65 p.

Väisänen M., Mänttäri, I. & Hölttä, P., 2002. Svecofennian magmatic and metamorphic evolution in southwestern Finland as revealed by U-Pb zircon SIMS geochronology. Precambrian Research, 116:1–2.

Väisänen, M. & Mänttäri, I., 2002. 1.90-1.88 Ga arc and back-arc basin in the Orijärvi area, SW Finland. Bulletin of the Geological Society of Finland, 74, 185-214.

Väisänen, M., & Skyttä, P. 2007. Late Svecofennian shear zones in southwestern Finland. GFF, 129(1), 55-64.

Magnetic inhomogeneities of the White Sea region crust

M. Nilov[1], L. Bakunovich[1], N. Sharov[1] and B. Belashev[1]

[1]Institute of Geology, FGBUN FIC, Karelian Research Center, RAS, Petrozavodsk, Russia
E-mail: mnilov@rambler.ru

The deep crustal structure of the White Sea region and the surrounding areas has been well described in the framework of individual case studies. There are also a number of models for the geological structure available. We propose a uniform assessment of magnetic sourcies responsible for the long wavelength magnetic features. Within the considered area, the Precambrian formations of the Fennoscandian Shield and the Russian Plate overlain by a sedimentary cover are represented. Large geological domains are separated by regional faults and suture zones. The study is based on a 1: 1,000,000 scale aeromagnetic field map.

Keywords: crust, magnetic anomalies, White Sea, Fennoscandia, modelling and interpretation.

1. General

The subject of the study is the White Sea basin and adjacent territories. Located at the junction of two large tectonic elements of the East European Craton, the Fennoscandian Shield and the Russian Plate, this region is constantly experiencing dynamic loads caused by the continuing uplift of the Fennoscandian Shield. Its original crustal structures formed in the Archean were partially transformed in the processes of Proterozoic rifting and subsequent tectonomagmatic activation. Studies of geodynamics, tectonics, and the evolution of the material composition of the lithosphere are relevant in the region. Its characteristic feature is the manifestation of kimberlitic magmatism, deposits of diamonds and other minerals. It is believed that the Arkhangelsk province, which ranks second in Russia in diamond mining after Yakutia, is far from exhausting its diamond potential. The geological research recently conducted here is aimed at finding hydrocarbons. The formulation and solution of theoretical and applied problems are facilitated by the study of the deep structure of the region (Sharov and Zhuravlev, 2019).

Long-term practice of studying the anomalous magnetic field has shown the presence of a regional component in its composition, which makes it possible to use it to study the deep structure of the earth's crust (Orliuk and Pashkevich, 2012; Pashkevich et al. 2014; Baluev et al. 2018). At present, there is enough complete data to construct a more detailed magnetic model of the earth's crust: a summary map of the total magnetic intensity (TMI) in digital form (Figure 1) with a sample of field values over a 1x1 km network.

2. Data processing

The modeling was carried out using the GIS "INTEGRO" software package containing the procedures necessary for calculating magnetic models based on 2D and 3D inversion (Cheremisina et. al. 2018). General data processing of the TMI data is made by using most common mathematical procedures. The basic procedure for extracting the contour of deep magnetic sources is the upward continuation procedure, which is a special form of wavelength filtering. In the Fourier domain, upward continuation is achieved using a simple exponential transform (Blakely, 1995), which reduces the high wavenumber content in the dataset and also reduces spatial resolution. Basically, it is a special form of low-pass filtering operation that allows for clean filtering with almost no unwanted effects.

Also we use the tilt derivative (TDR) procedure to define structural edge information for subsurface objects (Miller, H.G., Singh, V., 1994.).

3. The heat flow and the depth of the magnetic modelling

The possible depth of crustal magnetic modelling is always a discussion question. It has direct correlation to the intensity of the heat flow in the region. The area under consideration has a strong consistent Precambrian basement and available data indicate low values of heat flow no more than 50 mW*m^{-2} (Kukkonen et al. 1998; Tsibulua et al. 1992; Veikkolainen et al. 2017). Such low values make it possible to speak with confidence that minerals retain their magnetic properties up to the mantle cover, and give as an opportunity to iterpret magnetic susceptibility assignment throughout the all crust thickness.

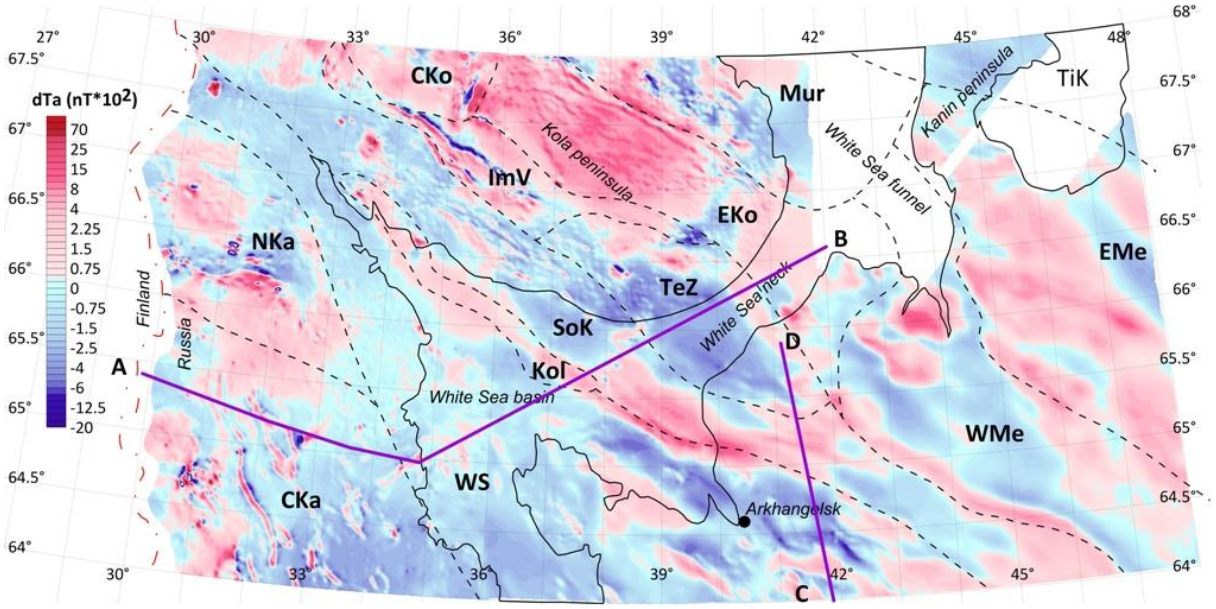

Figure 1. Colour image of the TMI data, with domain boundaries (see indexes in Table 1) and main regional profiles lines.

Table 1. Main geological domains of the White Sea region.

Label	Domain	Age
CKa	Central Karelian domain	Late Archaean
NKa	North Karelian domain	Late Archaean
WS	White Sea domain	Archaean
Kol	Kolvitskiy domain	Archaean
SoK	South Kola domain	Archaean
TeZ	Tersko-Zolotitskiy domain	Archaean
ImV	Imandra-Varzugskiy domain	Archaean
CKo	Central Kola domain	Early Archaean
EKo	East Kola domain	Early Archaean
Mur	Murmansk domain	Early Archaean
WMe	West Mezen' domain	Palaeozoic
EMe	East Mezen' domain	Palaeozoic
TiK	Timano-Kaninskiy domain	Palaeozoic

4. Conclusions

As a result, the models obtained make it possible to clarify the picture of the earth's crust, get new information about the deep structure of the region and the patterns of its evolution. The correctness of the results obtained was assessed by comparing it with the available geological and geophysical data and the complex models built on their basis. The spectral characteristics of regional anomalies made it possible to group them and make assumptions about the most probable source of the magnetic field disturbance. We assume that the sources of regional anomalies are confined to the "granite-metamorphic" and "granulite-basic" layers at depths from 10 km to the crust-mantle interface. A number of anomalies are confined not to individual bodies of a specific mineral and material composition, but to extensive permeable zones extending with root parts into the mantle.

The study was conducted under the Research Project AAAA-A18-118020290086-1 funded by the Russian Foundation for Basic Research under the Research Projects 20-05-00481 «Lithospheric structure and dynamics of the White Sea Region» and the scientific research of the Institute of Geology KRC RAS.

References:

Baluev, A. S., Brusilovskii, Yu. V., Ivanenko, A. N., 2018. The crustal structure of Onega-Kandalaksha paleorift identified by complex analysis of the anomalous magnetic field of the White Sea. Geodynamics&Tectonophysics 9 (4), 1293-1312.

Blakely, R.J., 1995. Potential Theory in Gravity and Magnetic Applications. Cambridge University Press, Cambridge, United Kingdom.

Cheremisina, Ye.N., Finkelstein, M.Ya., Lyubimova, A.V., 2018. GIS INTEGRO – import substitution software for geological and geophysical tasks. Geoinformatika. 2018, №3 pp. 8-17. (in Russian).

Kukkonen, I.T., Gosnold, W.D., Šafanda, J., 1998. Anomalously low heat flow density in eastern Karelia, Baltic shield: a possible palaeoclimatic signature. Tectonophysics 291 (1–4), 235–249.

Miller, H.G., Singh, V., 1994. Potential field tilt—a new concept for location of potential field sources. Journal of Applied Geophysics 32, 213–217.

Orliuk, M. I., Pashkevich, I. K., 2012. Deep sources of regional magnetic anomalies: tectonic types and relation with transcrustal faults. Geofizicheskiy zhurnal 34(4), 224—234 (in Russian).

Pashkevich, I. K., Sharov, N. V., Savchenko, A. S. Starostenko V. I., 2014. Three-dimensional geological-geophysical lithosphere model of the central part of the Karelian craton. Geofizicheskiy zhurnal № 6, T. 36, 2014. (in Russian).

Tsibulua, L. A., Levashkevich, V. G. 1992. Terrestrial Heat Flow in the Barents Sea Region. Apatity: KSC of the Russian Ac. Sct., 115p. (in Russian).

Sharov, N.V., Zhuravlev, A.V. 2019. Crustal structure of the White Sea and adjacent areas. Arctic: ecology and economy. No. 3 (35). pp. 62—72.

Veikkolainen, T., Kukkonen, I.T., Tiira, T., 2017. Heat flow, seismic cut-off depth and thermal modelling of the Fennoscandian Shield, Geophys. J. Int., 211, 1414–1427.

A preliminary assessment of hydrothermal alterations in the giant Kiruna IOA deposit, Kiruna, Sweden

L. Paolillo[1] and C. Giapis[1]

[1] Luossavaara-Kiirunavaara AB, Near Mine Exploration, FK9, 981 86 Kiruna, Sweden
E-mail: luca.paolillo@lkab.com

In this study we present a preliminary assessment of the nature and distribution of the hydrothermal alterations in the rhyolite-rhyodacite hanging wall of the Kiruna magnetite orebody.

Keywords: iron-oxide-apatite deposits, hydrothermal alteration, Kiruna deposit

1. Introduction

Iron-oxide-apatite (IOA) or Kiruna-type deposits are one of the main sources for iron worldwide. IOA deposits with economic importance exist in the Norrbotten region of northern Sweden. Kiruna is a world-class IOA deposit that is located, along with other orebodies, around the town of Kiruna and it has been mined by Luossavaara-Kiirunavaara Aktiebolag (LKAB) for over 120 years. The massive magnetite orebody, with more than 2,500 million metric tons, grading at 55-65% Fe and 0.05 to 5 wt % P, is hosted between Paleoproterozoic meta-volcanic rocks (ca. 1880 Ma, Bergman et al. 2001), also known as the Porphyry Group, of Svecokarelian age. The suggested age of the ore emplacement varies between 1874 ± 7 Ma and 1877 ± 4 Ma (Westhues et al. 2016). The mineralization occurs as a steeply dipping, NE striking, tabular body of about 5 km length and up to more than 100 meters thickness, between the lower andesite-trachyandesite footwall and the upper rhyolite-rhyodacite hanging wall (see also e.g. Westhues et al., 2016), with the contacts between the ore and the host rocks varying from sharp to ore veins to brecciation.

The ore formation of Kiruna-type IOA deposits in the Norrbotten region is still controversial, with different authors suggesting a magmatic (e.g. Troll et al. 2019), a sedimentary-exhalative (e.g. Parák, 1975), a hydrothermal origin (e.g. Hitzman et al. 1992) or magmatic-hydrothermal origin (e.g. Westhues et al. 2017). The description, classification, and spatial distribution of alterations around the Kiruna ore body might not only contribute to a better comprehension of its genesis and the evolution of the associated hydrothermal fluids but may also facilitate exploration around the deposit and in the wider region.

2. Methodology

Observations of alteration minerals, assemblages, textures, and styles are based on extensive core logging. XRF and ICP-MS whole rock geochemical data, as well as optical microscopy and microprobe data (e.g. Nordstrand, 2012) from internal reports, were used in order to corroborate the nature of mineral phases.

3. Results

Hydrothermal alteration is ubiquitous around the massive Kiruna magnetite orebody. Although, alterations are variable in extent and intensity along the orebody, consistent patterns can be observed in the hanging wall rocks.

Closest to the orebody a strong and pervasive albitization is common and can lead to an almost complete replacement of the host rock, giving it a whitish colour. This massive albite is generally cut by actinolite veins and/or overprinted by actinolite disseminations and

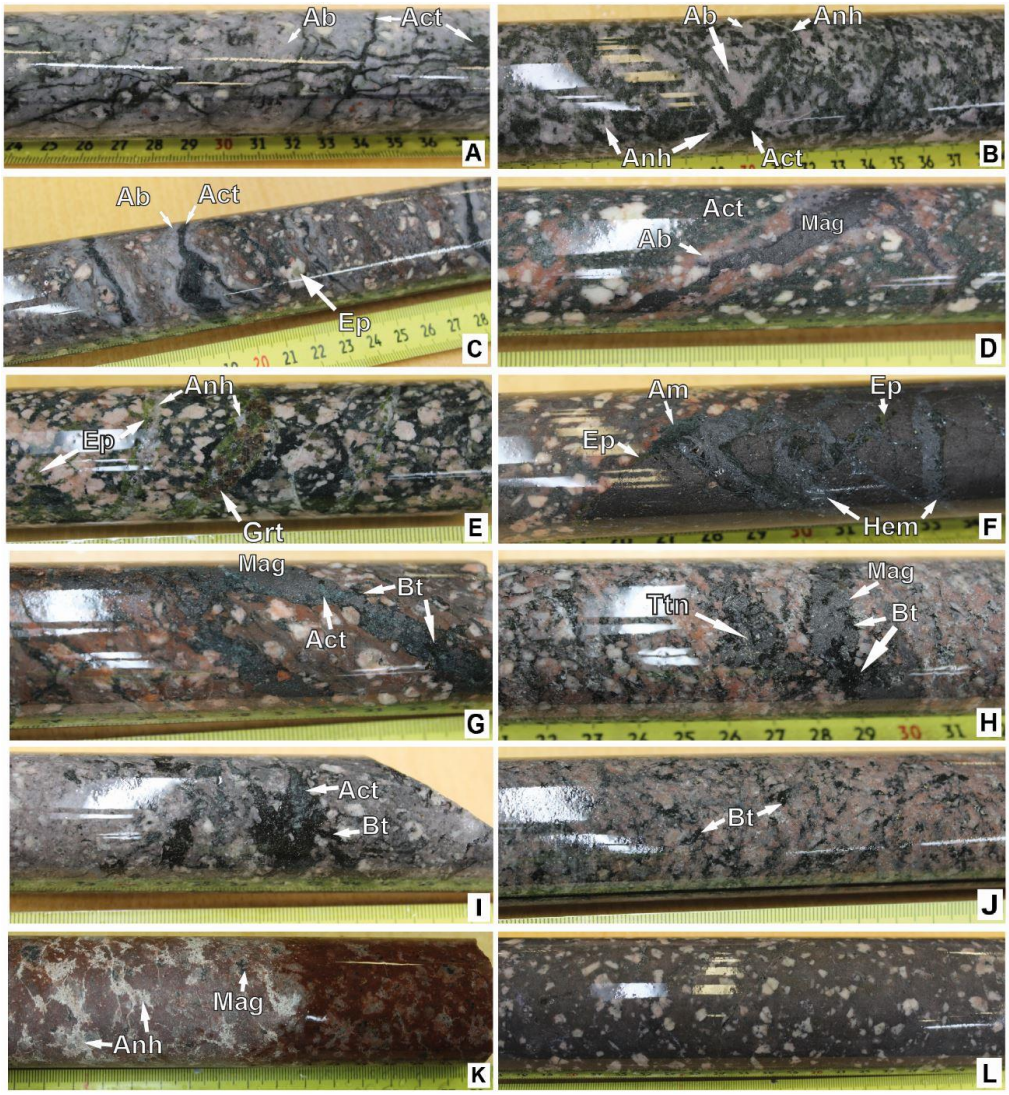

Figure 1. A. Strongly albitized rock cut by later actinolite (Act) veins. B. Almost completely albitized rock overprinted by a Na-Ca alteration consisting of actinolite ± albite (Ab). The Na and Na-Ca alteration have finally been overprinted by a Ca (± Fe) alteration visible here as anhydrite (Anh) veins (contain also garnet but not visible on picture). C. Na-Ca alteration consisting of actinolite veins with albite halos and locally epidote (Ep), replacing plagioclase phenocrysts. D) Magnetite (Mag) vein with albite halo (largely reddish due to hematite inclusions). Note how the albite halo dissolves the disseminated actinolite of the previous Na-Ca alteration. E. Ca (± Fe) alteration expressed by anhydrite-garnet-epidote veins cutting Na-Ca alteration dominated by actinolite and albite. F. Hematite (Hem)-amphibole (Amp)-epidote dominated veinlets of Ca-Fe alteration cutting massive magnetite vein related to the main magnetite orebody. G. Magnetite-actinolite ± biotite (Bt) vein in transitional environment between Na-Ca-Fe and K-Fe environment. H. Magnetite-biotite veins (± titanite (Ttn) traces) and disseminated biotite in matrix in K-Fe alteration environment. I. Biotite-actinolite patches disseminations in transitional environment from Na-Ca-Fe to K-Fe. J. Biotite disseminations in K (± Fe) alteration zone. K. Anhydrite patches ± magnetite disseminations in strong brick-red coloured rock in distal region from the ore body (half wet sample). L. Typical least altered hanging wall rock.

patches (Figure 1A and B). Further away from the ore, the actinolite veins become magnetite bearing and disseminated titanite can be found in the host rock. Incipient epidote replacement of plagioclase cores can be associated with this assemblage as well as disseminations of epidote in the groundmass. Locally, actinolite ± titanite ± epidote replacement of the host rock can be near total, resulting in a completely green colouration of the rock. Actinolite ± magnetite veins commonly display albite halos (Figure 1C). Distally from the ore, these veins evolve from actinolite dominant (Figure 1C) to magnetite dominant (Figure 1D) and eventually actinolite disappears at the expanse of biotite (Figure 1G). Albite halos, along these veins, decrease in intensity and extent within this evolution. Also, the disseminated actinolite gradually disappears at the expanse of biotite in more distal parts (Figure 1I). Proximally to massive magnetite, biotite commonly occurs together with magnetite in veins (Figure 1H), patches and/or disseminations. Further away from the orebody, magnetite veins completely disappear, but magnetite can be locally found as volumetrically minor disseminations. Generally, abundant disseminated biotite (Figure 1J) also faints out within several meters after the disappearance of significant magnetite occurrences. In these outer regions, biotite and actinolite are commonly at least partially affected by a weak, late chlorite alteration.

In proximal regions to the main orebody, it is common to observe anhydrite veins with red-brownish to yellowish garnets (Figure 1E) cutting the actinolite ± albite alteration assemblage (Figure 1B). These veinlets commonly contain minor amounts of epidote, specular hematite and sometimes traces of acicular, dark green amphibole (Figure 1F). Abundant anhydrite disseminations seem to be linked to the occurrence of these anhydrite dominated veinlets (Figure 1B). Also, the above-mentioned epidote disseminations appear to be the most pronounced in assemblages containing these veinlets.

Beyond the biotite altered zone, hydrothermal alteration assemblages can still be significant but appear to be less systematic. The rocks are largely characterized by a variably strong brick-red coloration due to Fe-oxide (hematite) inclusions in feldspars. In this area, it is also common to find anhydrite patches and disseminations, often associated with magnetite (Figure 1K) ± biotite ± pyrite and chalcopyrite. In rare occasions, biotite can be affected by sericite. The presence of hydrothermal K-feldspar has not been univocally proven so far.

4. Discussion

Alteration mineral assemblages associated with the Kiruna orebody suggest an evolution from a proximal Na-alteration (albite) to a Na-Ca (actinolite ± albite ± epidote ± titanite) to a Na-Ca-Fe (actinolite – magnetite ± albite) to a K-Fe (biotite ± magnetite) alteration in more distal regions from the ore body (Figure 2). A Ca ± Fe alteration consisting of abundant anhydrite with garnet ± epidote ± specular hematite and rare dark green amphibole can be observed mainly cutting/overprinting the Na-Ca alteration (probably retrograde alteration). A Ca-Fe-K (actinolite-magnetite ± biotite) alteration might be distinguished as a transition between the Na-Ca-Fe and K-Fe alteration zones, but further investigation is needed in order to determine whether it is a separate alteration (actinolite – biotite paragenesis) or rather a replacement of actinolite by biotite. All alterations show a rather continuous transition between each other and are, regarding the mineralogy and spatial distribution, in good agreement with alterations observed in other IOA-IOCG deposits world-wide (e.g. Barton 2013 and references therein, Corriveau et al. 2016; Warren et al. 2016). The extent and intensity of alterations in Kiruna can vary and locally more distal alterations can directly overprint more proximal alterations (e.g. biotite ± magnetite overprinting massive albite). Apart from hematite inclusions giving a brick-red colour to the rock in more distal regions, lower temperature and slightly more acidic alterations (e.g. Barton, 2013; Corriveau et al. 2016) seem to be poorly developed in Kiruna. Hydrothermal alterations in the footwall of the Kiruna orebody are generally more pervasive

and less clear spatial distributions can be observed in comparison with the hanging wall. Future work will, among other things, focus on getting a better understanding of the alterations in the footwall.

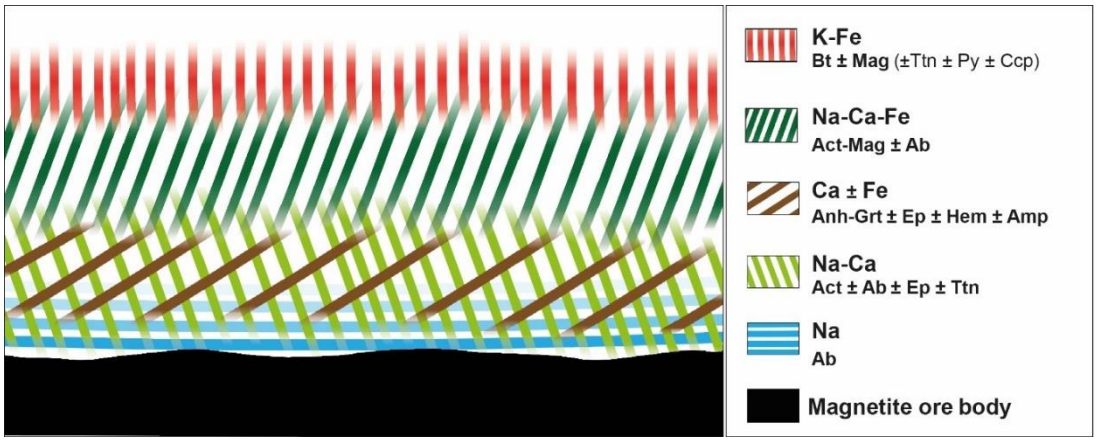

Figure 2. Simplified alteration model for the hanging wall rocks of the Kiruna IOA deposit.

5. Conclusion

Hydrothermal alterations in the hanging wall rocks of the Kiruna Fe deposit display a systematic zonation in mineral assemblages. The most proximal regions to the ore are typically dominated by a strong Na alteration, grading into a Na-Ca, Na-Ca-Fe and K-Fe alteration with increasing distance from the ore. A Ca ± Fe alteration frequently overprints the Na-Ca alteration. These observations are in good agreement with findings from other studies on alterations in IOA-IOCG systems throughout the world.

References:

Barton, M. D., 2013. Iron oxide (-Cu-Au-REE-P-Ag-U-Co) systems. In Treatise on Geochemistry: Second Edition (pp. 515-541). Elsevier Inc.

Bergman, S., Kübler, L., Martinsson, O., 2001. Description of regional geological and geophysical maps of northern Norrbotten County (east of the Caledonian orogen): Sveriges Geologiska Undersökning.

Corriveau, L., Montreuil, J. F., Potter, E. G., 2016. Alteration facies linkages among iron oxide copper-gold, iron oxide-apatite, and affiliated deposits in the Great Bear magmatic zone, Northwest Territories, Canada. Economic Geology, 111(8), 2045-2072. (Geological Survey of Sweden), Ba Series 56, 110 p.

Day, W. C., Slack, J. F., Ayuso, R. A., Seeger, C. M., 2016. Regional geologic and petrologic framework for iron oxide ± apatite ± rare earth element and iron oxide copper-gold deposits of the Mesoproterozoic St. Francois Mountains terrane, southeast Missouri, USA. Economic Geology, 111(8), 1825-1858.

Hitzman, M.W., Oreskes, N., Einaudi, M.T., 1992. Geological characteristics and tectonic setting of Proterozoic iron-oxide (Cu-U-Au-REE) deposits: Precambrian Research, v. 58, p. 241–287.

Nordstrand, J., 2012. Mineral chemistry of gangue minerals in the Kiirunavaara iron ore. Unpublished.

Parák, T., 1975, Kiruna iron ores are not "intrusive magmatic ores of the Kiruna type": Economic Geology and the Bulletin of the Society of Economic Geologists, v. 70, p. 1242–1258.

Troll, V. R., Weis, F. A., Jonsson, E., Andersson, U. B., Majidi, S. A., Högdahl, K., Nilsson, K. P., 2019. Global Fe–O isotope correlation reveals magmatic origin of Kiruna-type apatite-iron-oxide ores. Nature communications, 10(1), 1712.

Westhues, A., Hanchar, J.M., Whitehouse, M.J., Martinsson, O., 2016. New constraints on the timing of host-rock emplacement, hydrothermal alteration, and iron oxide-apatite mineralization in the Kiruna district, Norrbotten, Sweden: Economic Geology and the Bulletin of the Society of Economic Geologists, v. 111, p. 1595–1618.

Westhues, A., Hanchar, J. M., LeMessurier, M. J., Whitehouse, M. J., 2017. Evidence for hydrothermal alteration and source regions for the Kiruna iron oxide–apatite ore (northern Sweden) from zircon Hf and O isotopes. Geology, 45(6), 571-574.

Application of the Group Method of Data Handling for the analysis of petrophysical and geophysical data

I.A. Ponomarenko[1] and O.M. Muravina[1]

[1]Voronezh State University, Voronezh, Russia
E-mail: kochuma@yandex.ru

The paper discusses examples of the use of a modern statistical method for processing geophysical data - the Group Method of Data Handlin (GMDH). The results of using GMDH for the purpose of a comprehensive analysis of petrophysical parameters, determination of the porosity coefficient from logging data and taking into account the terrain relief during the interpretation of aeromagnetic prospecting are presented.

Keywords: Group Method of Data Handling, petrophysics, well logging data, aeromagnetic prospecting, influence of the relief

1. General

The Group Method of Data Handling (GMDH) is a method of data analysis based on inductive modelling. It allows to explore multicomponent systems and is able to reveal hidden relationships between elements, including non-linear ones. Algorithms GMDH allow to create and test many variants of mathematical models and determine the model equation of optimal complexity. Generation of models is performed combinatorically based on the support function. The best model is selected according to the minimum values of external criteria. External criteria are calculated based on data that is not involved in the procedure for determining the structure and parameters of the model (Ivakhnenko (1988)). The nature of the GMDH algorithms allows us to consider it as an alternative to multilevel neural networks (Fernández et al. 2010).

In the last decade, the Department of Geophysics of Voronezh State University has been actively conducting research aimed at studying the possibility of MGDH for analyzing geological and geophysical information. Below are some examples of the method application (Muravina et al. 2018).

2. Complex analysis of petrophysical data

Petrophysical information is an important part of knowledge in the course of geological and geophysical interpretation, on the basis of which the transition from physical to geological model of the environment is carried out. To perform the identification analysis of the MGDH, a sample of data on density, electrical resistivity, and magnetic susceptibility of rocks representing magmatic, volcanogenic-sedimentary, and metamorphic formations widespread within the Voronezh Crystalline Massif (VCM) was formed. The sample size was 224 samples. For each group, mean values and standard deviations of density(σ) and logarithms of electrical resistivity ($\log \rho$) and magnetic susceptibility ($\log \varkappa$) were calculated. In Figure1,,a shows the summary point diagrams of the distribution of the averaged values of these parameters. As can be seen from the figure, for most rocks, rather significant differences were revealed in the aggregate statistical characteristics of petrophysical parameters, which was a prerequisite for the subsequent analysis by the Group Method of Data Handling (Muravina et al. 2019a).

As a result, complex quasilinear model equations were obtained connecting the average density values with the logarithm of resistivity and the logarithm of magnetic susceptibility:

$$\bar{\sigma} = a_0 + a_1 \overline{\log \rho} + a_2 \overline{\log \varkappa} + a_3 \overline{\log \rho} \cdot \overline{\log \varkappa}, \quad (1)$$

The correspondence between the experimental and model values of the average density values is shown in Figure 1,b. The results obtained will be used in the procedure of complex inversion of geophysical fields when studying the structure of the upper part of the earth's crust.

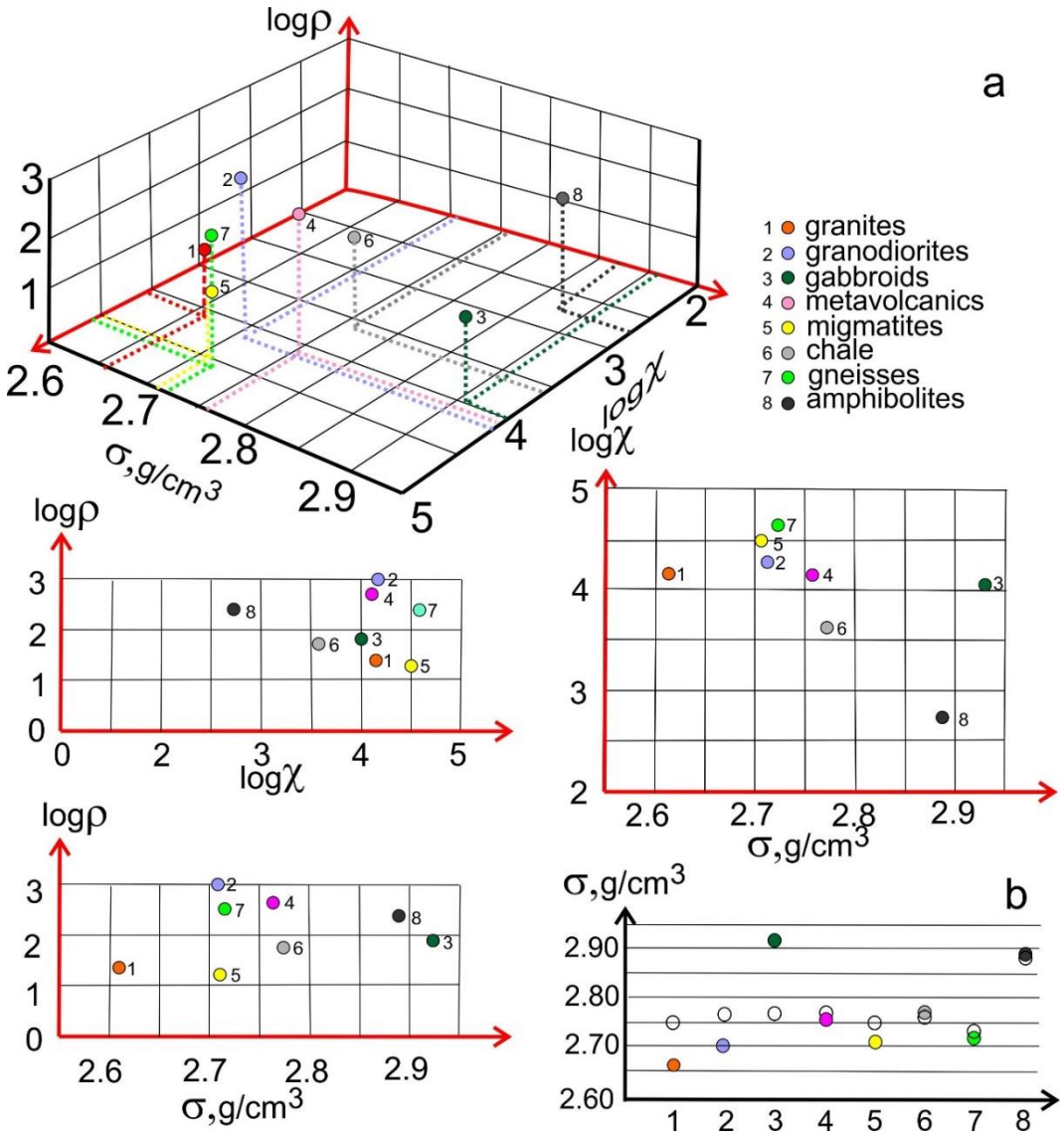

Figure 1. The results of the complex analysis of petrophysical data: a – summary point diagrams of distribution of averaged values of petrophysical parameters of crystalline rocks of VKM; b – the results of identification modelling. Coloured circles - experimental data, off-coloured - model data.

3. Estimation of the porosity coefficient from logging data

Here is an example that demonstrates the capabilities of GMDH for estimating the porosity coefficient of a productive formation from logging data. As the initial data, the results of

laboratory analysis of the core on 14 samples were used. For the formation of the training sequence, the averaged values of the porosity of the reservoir core were used (Muravina et al. 2019b).

As a result, a polynomial dependence was obtained, which makes it possible to calculate the porosity coefficient (Kp) according to the data of four gradient probes of different lengths (GZ1, GZ2, GZ3, GZ4) and gamma-ray logging (GK): Kp = f (GZ1, GZ2 , GZ3, GZ4, GK) The correspondence of the experimental values of the porosity coefficient is shown in Figure 2.

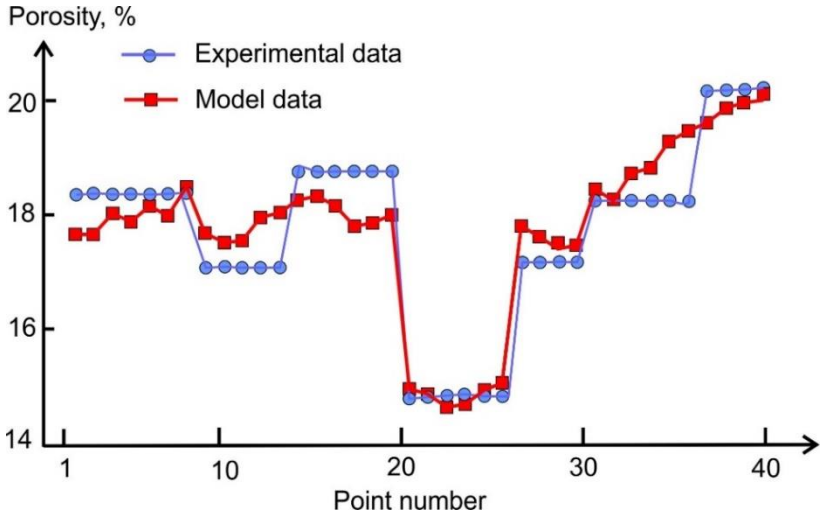

Figure 2. Correspondence of the experimental and model values of the porosity coefficient.

4. Assessment of the relief influence during aeromagnetic studies over volcanogenic formations

In conditions of a highly dissected relief, with a high degree of lateral heterogeneity of the magnetic properties of the rocks in the upper part of the section, it is practically impossible to obtain acceptable estimates of the topographic correction within the framework of simplified model concepts. The reasons for this are: a lack of reliable petrophysical information, inaccuracy in setting the relief near the point of calculation, the use of a “flat” Earth model, etc.The traditional statistical method for assessing the anomalous relief effect is based on identifying the relationship between the ΔT field and the elevations of the relief H. However, in difficult physical and geological conditions, the closeness of the linear correlation directly between ΔT and H can be very low. The solution can be more effective when using the Empirical Mode Decomposition (EMD) (Huang et al. 1998) method in combination with GMDH (Dolgal et al. 2017). At the first stage, the discrete values of ΔT and H are decomposed into empirical mode functions (IMF). Then GMDH is used to determine the total component of the magnetic field (δTrf), that is most closely related to the IMF of the relief (Hiassat et al. (2004)). Let us give an example of using the proposed method when taking into account the influence of the relief on the results of aeromagnetic survey carried out in difficult physical and geological conditions of the Norilsk region (Dolgal et al. 2020). As a result of identification modeling, the low-frequency components of the magnetic field were established, due to the influence of the relief, and then the model of the relationship between the total magnetic component δTrf and the components of the relief of heights H4, H3, H1 was calculated. The quality of the correlation dependence is shown in Figure 3.

Calculations based on practical examples have shown that the proposed method for determining δTrf is consistent with the results of calculating the topographic correction by

solving the direct problem (Dolgal et al. 2020), but it is less laborious, does not require a priori information about the magnetic properties of rocks and heights of survey flights, and automatically takes into account the spheroidism of the Earth.

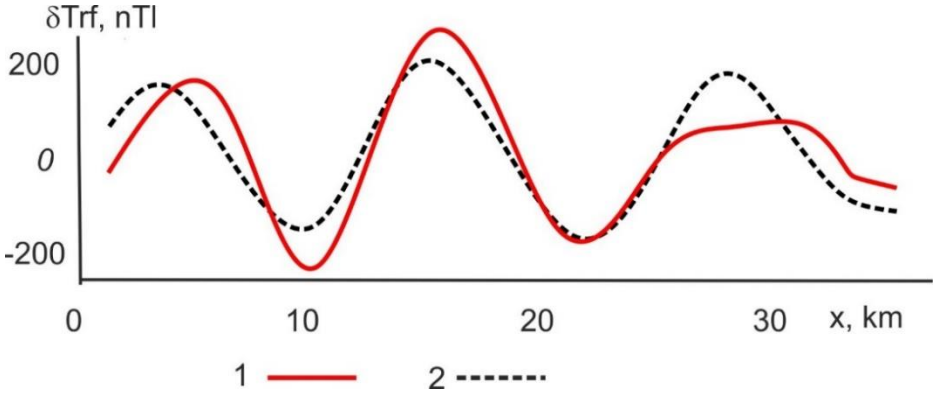

Figure 3. Results of identification modelling of low-frequency components of the magnetic field: b - experimental (1) and model (2) values of the total component δTrf.

5. Conclusions

The presented materials indicate that the modern technology of statistical analysis of geophysical data developed by the authors is applicable to the widest range of geophysical and petrophysical studies. Practical implementation of the proposed approaches makes it possible to increase the reliability of interpretation of geophysical data and their geological information content.

The research was supported by the RFBR, grants No 19-05-00336; 19-05-00654 and 20-05-00190.

References:

Dolgal, A. S., Krivolutskaya N.A., Muravina, O. M., Ponomarenko, I. A., 2020. Accounting the effect of terrain relief during aeromagnetic surveying within large magmatic provinces, Geofizika, (4), 2-8.

Dolgal, A. S., Muravina, O. M., Hristenko, L. A., 2017. The reduction of the magnetic field within development areas of the plateau-basalts. European Association of Geoscientists & Engineers, 16th International Conference on Geoinformatics - Theoretical and Applied Aspects, 1, 1-5.

Fernández, F. H., Lozano, F. H., 2010. GMDH Algorithm Implemented in Intelligent Identification of a Bioprocess. In ABCM Symposium series in Mechatronics, Vol. 4, 278-287.

Hiassat, M., Abbod, M. F., Mort, N., 2004. Using Genetic Programming to Improve the Group Method of Data Handling in Time Series Prediction. Statistical Data Mining and Knowledge Discovery. Chapman&Hall/CRC, 282-293.

Huang, N. E., Shen, Z., Long, S. R., Wu, M. C., et al., 1998. The empirical mode decomposition and the Hilbert spectrum for nonlinear and non-stationary time series analysis. Proceedings of the Royal Society of London. Series A: mathematical, physical and engineering sciences, 454, 903-995.

Ivakhnenko, A. G., 1988. Self-Organizing Methods in Modelling and Clustering: GMDH Type Algorithms. In Systems Analysis and Simulation I, Springer, New York, 86-88.

Muravina, O. M., Chernyshova, M. N., Zhavoronkin, V. I., 2019. Identification analysis of ultramafic-mafic intrusions of the mamonsky complex voronezh crystalline massif. Vestnik KRAUNTs. . Nauki o Zemle, No 3, 89–98.

Muravina, O. M., Davudova, E. I., Ponomarenko, I. A., 2019. Possibility of identification of modeling in complex analysis geological and geophysical data. In Practical and Theoretical Aspects of Geological Interpretation of Gravitational, Magnetic and Electric Fields, Springer, Cham, 157-162.

Muravina, O. M., Glaznev, V. N., Mints, M. V. 2018. 3D-density model of the Earth crust for central part of the East-European platform. In Lithosphere 2018 – Tenth symposium on structure, composition and evolution of the lithosphere, 81-86.

United Nations and Subcommittee on Geodesy

M. Poutanen[1]

[1]Finnish Geospatial Research Institute FGI
E-mail: markku.poutanen@nls.fi

In this article we describe the development of a globally-coordinated approach to establish geodesy as a permanent component within the United Nations. During last five years, since the 2015 UN General Assembly adoption of the resolution on a Global Geodetic Reference Frame for Sustainable Development (A/RES/69/266), a permanent Subcommittee has been established, and finally leading in 2020 establishment a Global Geodetic Centre of Excellence. Considering the importance of geodesy in geosciences, current development is very welcome, in which Member States will commit themselves to maintain the global geodetic infrastructure. Education, outreach and supporting developing countries are as well goals of this effort. Current roadmap shows the way to reach the goal, but there is still a long way to go.

Keywords: geodesy, United Nations, reference frames, sustainable development

1. Introduction

In 2013, the United Nations Committee of Experts on Global Geospatial Information Management (UN-GGIM) requested the formulation of a resolution to strengthen the Global Geodetic Reference Frame GGRF. This lead very quickly to a proposal, supported almost 50 UN Member States, Finland among them. In February 2015 the United Nations General Assembly adopted the resolution on a Global Geodetic Reference Frame for Sustainable Development (A/RES/69/266, 2015), recognizing the importance of a globally coordinated approach to geodesy.

The UN-GGIM decided to formulate and facilitate a resolution for a global geodetic reference frame and established a working group on the Global Geodetic Reference Frame (GGRF). The task of the working group was to formulate the resolution and prepare a roadmap for GGRF for sustainable development according to the UN GA resolution. Without commitment by Member States, the Global Geodetic infrastructure will be in danger of degradation over time and consequently gradually lose its required accuracy and fundamental role in societal and scientific applications. This can happen due to aging infrastructure, insufficient coordination and financing, and diminishing human capacity.

At the UN-GGIM sixth session in New York in August 2016, the UN-GGIM endorsed the GGRF Roadmap and decided to elevate the GGRF working group to a permanent sub-committee on geodesy (UN GGRF, 2020).

The GGRF roadmap addresses each of the key areas of action described in the UN General Assembly resolution:

Data sharing: Development of geodetic standards and open geodetic data sharing are required to enhance and develop the GGRF.

Education and capacity building: Appropriate geodetic skills and educational programs are essential for the development, sustainability and utilization of the GGRF.

Geodetic infrastructure: A more homogeneous distribution of geodetic infrastructure is needed to develop and utilize an accurate GGRF.

Communication and outreach: It is imperative to develop communication and outreach programmes that enable the GGRF to be more visible and understandable to society.

2. Roadmap to the future

At its seventh session in 2017, UN-GGIM adopted decision 7/103, in which it endorsed the formal establishment and composition of the Subcommittee on Geodesy. The vision for the Subcommittee is to provide "an accurate, accessible and sustainable global geodetic reference frame to support science and society" (UN GGRF, 2020). On August 9 2019, Member States of the UN-GGIM commended the Subcommittee on Geodesy on the revised proposal to establish a Global Geodetic Centre of Excellence (GGCE) under the auspices of the United Nations.

German's proposal to host the Centre of Excellence at the UN Campus in Bonn was accepted by the UN-GGIM Committee of Experts in 2020 (UN GGRF, 2020). The role of the Centre is to assist in sustaining the GGRF by implementing operational paragraphs of UN General Assembly resolution 69/266. The Centre will

- Enhance global cooperation and coordination across Member States and relevant geodetic stakeholders to maximise the benefit of ongoing geodetic efforts, ensure coherence, and avoid duplication of effort.
- Strengthen geodetic infrastructure
- Assist Member States in making their geodetic data Findable, Accessible, Interoperable and Reusable in line with standards, policies and conventions.
- Support education, training and capacity building
- Improve communication and raise awareness

Currently, detailed planning of structure, governance and implementation of the GGCE is going on. Aim is to get plans ready for endorsement in the next UN-GGIM meeting in 2021.

One important link will be current geodetic infrastructure and services provided by the International Association of geodesy (IAG) services (Poutanen and Rozsa, 2020). The purpose of GGCE and SCoG is to sustain already existing geodetic infrastructure, not duplicate it. It means that the role of the IAG must be strong and visible in these plans. Considering the importance of geodetic observations and infrastructure in all Earth-exploring disciplines, it is very welcomed to have the globally coordinated structure where the Nations are committed.

Modern society is more and more dependent on accurate and up-to-date reference frames, reliable geodetic observations and geodesy-related applications. Development within the UN will be beneficial for whole field of geosciences. Sustainability, education, knowledge transfer and improving geodetic infrastructure in developing countries will also have substantial global consequences. Current situation with institute or organization level funding with arbitrary changes will not be sufficient and secure anymore in the future.

References:

A/RES/69/266, 201.5 https://undocs.org/en/A/RES/69/266

Poutanen, M., Rózsa, S., 2020. The Geodesist's Handbook 2020. Journal of Geodesy, **94(11)**, 109. https://doi.org/10.1007/s00190-020-01434-z

UN GGRF, 2020. https://www.unggrf.org/

Influence of Pulsed Magmatic Activity, Latent Heat, and Partial Melting on the Strength of the Continental Crust

A.M. Rantanen[1], D.M. Whipp[1], J.S. Heinonen[2], L. Kaislaniemi[1] and M. Putz[1]

[1]Institute of Seismology, Department of Geosciences and Geography, University of Helsinki
[2]Geology and Geophysics Research Programme, Department of Geosciences and Geography, University of Helsinki
E-mail: aleksi.m.rantanen@helsinki.fi

Magmatism causes changes in crustal strength which may influence tectonics and how the continental crust deforms. We present a model for estimating the reduction in crustal strength caused by magmatic intrusions. The model uses a finite difference solution to a 2D heat conduction equation. Increased temperatures and melting of the surrounding rock reduce the integrated crustal strength, which is evaluated by calculating the changes in the crustal strength envelopes as a function of time. The purpose of the model is to study how different intrusion and crustal compositions, such as changes in rheology, melting temperatures, and other material properties, effect the integrated crustal strength. In general, we find that the initial strength reduction is significant when the intruding magma has much higher temperature than the solidus temperature of the surrounding rock. However, it is also possible that the crustal strength can increase after the magma cools down and solidifies for intrusions that are more mafic than the host rock.

Keywords: Arc magmatism, Partial melting, Latent heat, Crustal strength, Rock rheology, Numerical modelling

1. Introduction

In subduction zones, the strength of the crust can be affected by plutonism in the volcanically active areas. The intruding magma heats and melts the surrounding crustal rock, which decreases the effective viscosity of the rock and the integrated crustal strength while the crust cools. The strength of the rock is determined by the deformation mechanism that requires the smallest differential stress, and increased heat decreases the viscous strength of the rock. When the rock is partially molten its shear strength is reduced to almost zero. However, when the rock cools and solidifies, its rheology and other material properties will play a larger role in the total crustal strength. These changes in strength will affect how the crust deforms and where faults and shear zones are formed.

2. Model Design

The effect of plutonism on integrated crustal strength are calculated using a finite difference solution to the 2D thermal heat transfer equation coupled to a series of 1D crustal (visco-plastic) strength envelopes (Figure 1). The rhyolite-MELTS software (Gualda et al. 2012) is used to calculate melt fractions for felsic, intermediate, and mafic compositions at different temperatures and pressures. The reduction in viscosity (strength reduction from melting) from partial melting is calculated using a viscosity model for a solid with fluid-filled pores (Schmeling et al., 2012).

Different example scenarios run for this paper are shown in Table 1. The cool case and hot case scenarios were run with and without including latent heat, and the effect of different intrusion compositions/rheologies was studied. Also, a scenario with the same rheologies between the hot and the cool case, and a scenario where the rheologies for the intrusions are appropriate for the chemistry of the intruding material, were considered. The total simulation

time was 50 Ma, and the period of pulsed magmatic activity lasted for 10 Ma. The total input volume during this time was approximately 12,000 km^3.

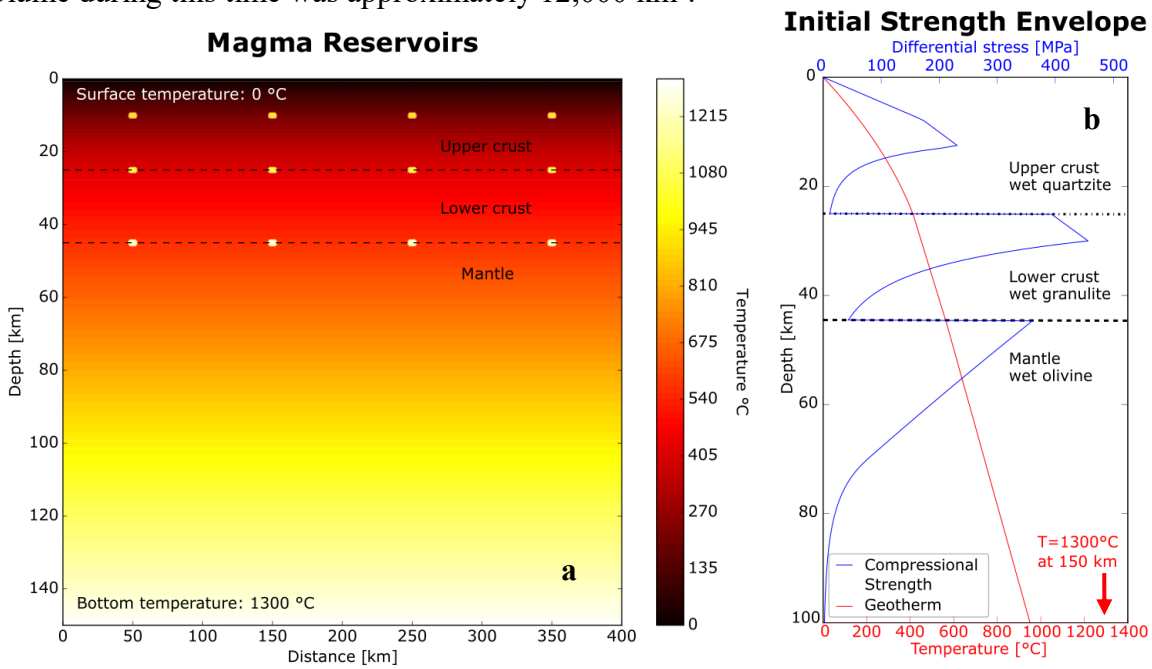

Figure 1. Thermal and strength envelope model design. (**a**) The scale of the profile is 150 km by 400 km, and temperatures reach from 0 °C to 1300 °C from the surface of the model to the base of the model. The small rectangles are the approximate positions of the magma chambers that are placed periodically in the model. (**b**) The initial geotherm is the red curve and the initial strength envelope is the blue curve. The strength of the crust is determined by the smallest amount of differential stress the rock can withstand, and the deformation mechanism by which this deformation happens is either frictional plastic (brittle behaviour) or viscous (ductile behaviour). Crust deforms in the linear portions of the strength envelope by frictional plastic deformation mechanism and curved portions deform by viscous deformation mechanism. The rheologies used in the flow law for viscous deformation are wet quartzite, wet granulite, and wet olivine, for the upper crust, the lower crust, and the mantle respectively.

Table 1. Parameters for the intrusions for different magmatic scenarios. Cool case intrusions have compositions with lower melting temperatures, initial temperatures, and melt fractions compared to the Hot case intrusions. Both Cool case and the Hot case are run with and without latent heat.

Group	*Depth [km]*	*Composition*	*T [°C]*	*Melt [%]*
Cool Case	10	Wet Felsic	750	30
	25	Wet Intermediate	772	35
	45	Dry Basalt	1250	40
Hot Case	10	Wet Basalt	960	40
	20	Wet Basalt	1035	50
	45	Dry Basalt	1278	60

3. Results

The temperature development during the first 10 Ma increases rapidly, after which the crust starts to cool (Figure 3, c). The largest strength reduction corresponds to the peak mean crustal temperatures (Figure 3, d). At the time of peak crustal strength decrease, the region within 15–20 km of the magma reservoirs can have strength decreases up to 50–100 %.

The pulsed magmatism in the first 10 Ma of the simulations reduces crustal strength by 30–40%, followed by a gradual increase in strength as the intrusions cool (Figure 2, c). The rheologies in these runs between the hot and the cool cases were kept the same. The peak strength reduction in the cool case runs with and without latent heat are almost the same, because the intrusions are not hot enough to melt the country rock. The latent heat run for the hot cases show a larger difference in strength reduction, since the intruding material can melt the surrounding rock. This melting and crystallization keep the crustal temperatures higher for a longer time. The peak strength decrease for the cold case runs are approximately 33% and for the hot case runs 37–40%.

The increase in crustal temperatures and the corresponding integrated strength reduction is initially much higher when hot mafic material intrudes a more felsic crust, but crustal strength may actually increase once the intrusions cool (Figure 2, b). Because mafic magmas are rheologically stronger than the country rock when cooled to the same temperature, the integrated crustal strength can increase once the intrusions cool. Conversely, in cases where felsic magma, with high heat production and a weak rheology, intrudes a rheologically stronger crust, the long-term crustal strength decrease can be larger after the magmatic activity has ceased, compared to the case with hotter basaltic intrusions.

4. Conclusions

Based on our experiments, we draw the following conclusions:

- The reduction in integrated strength at the peak of crustal temperatures can be even 30–40 % depending on the composition and temperature of the intrusions. The strength reduction around the intrusions (15–20 km) can be 50–100 %
- Mafic intrusions can decrease crustal strength significantly because of their higher intruding temperatures. It is possible however that these intrusions will ultimately increase crustal strength due to changes in the crustal bulk composition when the materials have cooled down.
- If intrusion temperatures are much higher than the solidus temperatures of the surrounding rocks, latent heat can keep crustal temperatures high for a long time. This effect is negligible however, if the intrusion temperatures are low or if the country rock solidus temperatures are high.

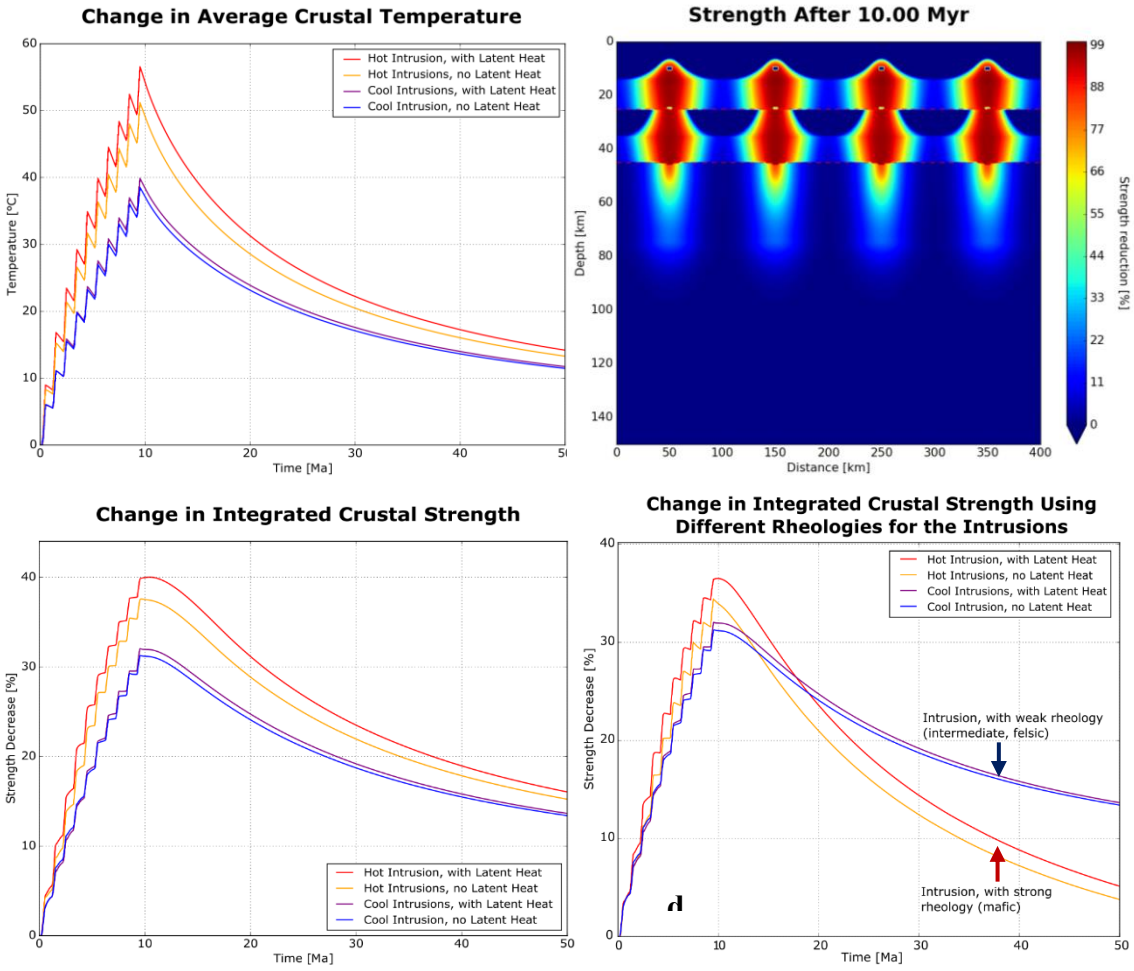

Figure 2. (**a**) Change in average crustal temperature as a function of time for the hot and cool magmatic scenarios. (**b**) Crustal strength reduction at the time of the peak crustal temperatures, which corresponds to 10 Ma. The strength reduction at 15–20 km distance is over 50 %. Close to the intrusions the strength decrease is close to 100 %. (**c**) Integrated crustal strength decreases as a function of time using same rheologies for cool and hot intrusions. Crustal melting is not significant for the cooler intrusions, but the latent heat and no latent heat cases for the hot intrusions show a difference. As the country rock melts, the temperatures remain higher for a longer time, which causes a larger drop in integrated crustal strength. (**d**) Integrated crustal strength decrease using different rock strengths depending on the compositions of the intrusions. Felsic and intermediate intrusions are weaker than mafic intrusions. Here the cooler intrusions cause a larger drop in integrated crustal strength compared to the mafic intrusions, after the magma reservoirs start to cool down.

References:

Gualda, G.A.R., Ghiorso, M.S., Lemons R.V., Carley T.L., 2012. Rhyolite-MELTS: A modified calibration of MELTS optimized for silica-rich, fluid-bearing magmatic systems. Journal of Petrology, 53, 875-890.

Schmeling, H., Kruse, J.P., Richard, G., 2012. Effective shear and bulk viscosity of partially molten rock based on elastic moduli theory of a fluid filled poroelastic medium. Geophysical Journal International, 190, 1571-1578.

A network to study the induced seismicity related to the Otaniemi deep geothermal power plant

A.E. Rintamäki[1], G. Hillers[1], T.A.T. Vuorinen[1], K. Galvin[1], J. Keskinen[1], T.-C. Lin[1], T. Luhta[1], T. Oksanen[1], J. Pownall[1], P. Seipäjärvi[1], G. Taylor[1], C. Tsarsitalidou[1], A. Voutilainen[1] and D. Whipp[1]

[1]Institute of Seismology, University of Helsinki, PL 68 (Pietari Kalmin katu 5), 00014 Helsingin yliopisto
E-mail: annukka.rintamaki@helsinki.fi

The development of a geothermal power plant at the border between Espoo and Helsinki resulted in high levels of induced seismicity in 2018 and 2020. The induced seismicity associated with the two stimulations were monitored by seismic networks of more than 100 permanent and short-term instruments. The measurements yielded two two high quality data sets that are suitable for a wide range of analysis techniques and allow detailed characterization of subsurface processes related to geothermal operations.

Keywords: induced seismicity, deep geothermal energy, seismology, structural geology, Fennoscandian shield, Helsinki capital region

1. Introduction

The risk of induced seismicity is an integral part of deep geothermal heat extraction. Pore pressure changes, thermal contraction and chemical reactions can induce earthquakes when fluids are circulated trough fractures or pipes at depth of several kilometers in the Earth's crust (e.g. Majer et al. 2007). The most apparent risk is related to geothermal power plants using the enhanced geothermal system (EGS) technology, where the permeability of a hot rock volume is increased in a reservoir stimulation by injecting pressurised fluids to open a fracture network. This increases the efficiency of heat extraction.

A deep geothermal power plant in Otaniemi can be considered a pilot project in many ways. It is the first geothermal power plant in Fennoscandia to use the EGS technology, and the geothermal wells are the deepest in the world (Ader at al. 2019). Production at the Otaniemi power plant is scheduled to start in 2021. Earlier stages of the power plant development include two reservoir stimulations in 2018 and 2020. The two stimulation induced tens of thousands of small earthquakes combined (Kwiatek et al. 2019, Hillers et al. 2020, Veikkolainen et al. 2020). Both stimulations were monitored by the Institute of Seismology (ISUH) and the operating company St1 Deep Heat Oy in parallel, and there are two high-resolution seismic data sets.

EGS stimulations are scientific natural earthquake laboratories on the intermediate scale between rock laboratories and in-situ tectonic deformation regions. The Otaniemi data sets allow us to study how the pressure, rate and volume of injected fluid and the ambient geological conditions of the Fennoscandian shield affect the properties of induced seismicity. In-depth understanding of the physical processes that induce earthquakes can help improve monitoring of the seismic risk related to deep geothermal power plants. The significance of induced seismicity may increase in the near future as several geothermal systems are currently being planned throughout the Fennoscandian shield, e.g. in Tampere and Turku, and the Otaniemi geothermal power plant will probably keep producing small earthquakes during its anticipated 30 to 40 year run time.

2. Stimulations, monitoring networks and induced seismicity data sets

The first stimulation of the Otaniemi power plant in June–July 2018 lasted 49 days and entailed the injection of over 18 million litres of tap water into an open section at the bottom of the first ~6 km well (Kwiatek et al. 2019). The seismic response was monitored by the operator with 24 borehole seismometers and in parallel by the ISUH with eight permanent and 100 short-period instruments (Figure 1a). The short-period network was arranged as six 4–25 seismometer arrays and 10 single stations mostly within a 6 km radius of the power plant.

Using near-real-time data of the seismic response the operator was able to adapt the pumping parameters to allow energy stored in the reservoir to dissipate. This approach helped limit the magnitude of induced earthquakes below local magnitude (M_L) 2.1 set as an upper limit in the environmental permit (Ader et al. 2019, Kwiatek et al. 2019). However, thousands of earthquakes up to M_L 1.8 were induced (Kwiatek et al. 2019, Hillers et al. 2020).

The second geothermal well was finished during the spring of 2020 and the second stimulation was conducted 6–24 May 2020 (Veikkolainen et al. 2020). The second stimulation was monitored with a dense network of 23 permanent and semi-permanent seismometers operated by the ISUH and St1, and 116 short-period seismometers deployed by the ISUH (Figure 1b). Our aim was to build on and improve the design of the 2018 short-period network. The network aperture was increased to ~23 km to increase the resolution of seismic source inversion. The seismometers were arranged as 19 arrays with 3–17 seismometers each to increase the signal-to-noise ratio around the edges of the network. 83 induced earthquakes up to M_L 1.2 were detected in January–September 2020 in ISUH routine analysis using data from 10 of the operator's borehole seismometers and 11 ISUH permanent stations (Veikkolainen et al. 2020).

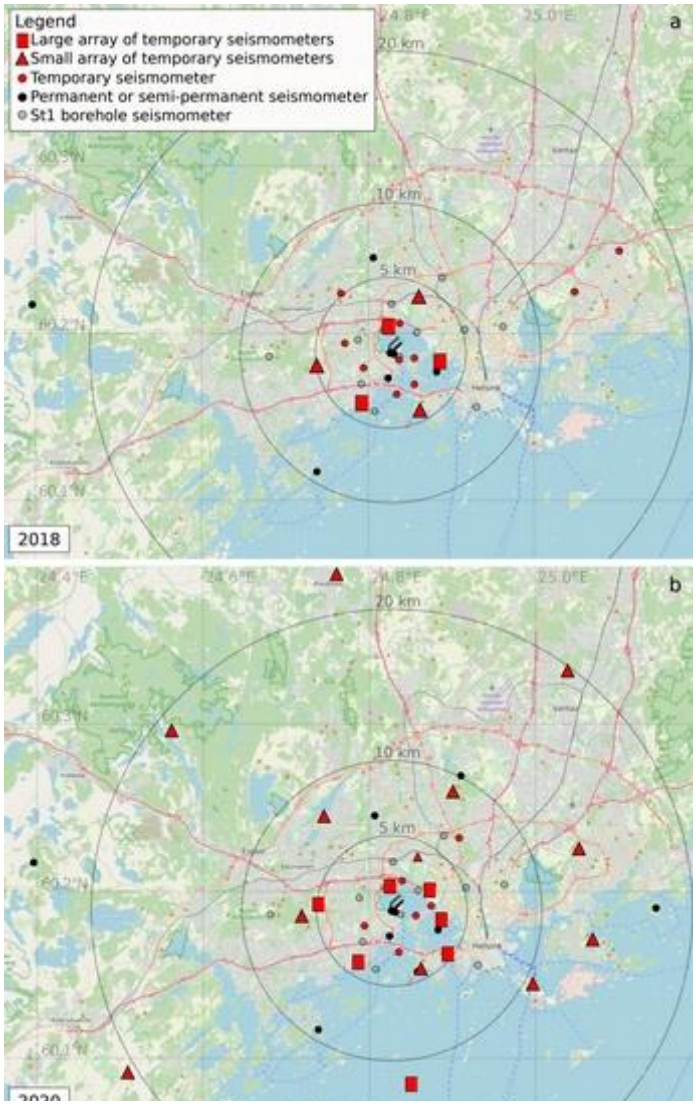

Figure 1. Comparison of the 2018 (a) and 2020 (b) seismic networks around the Otaniemi power plant. The network aperture and the number of arrays was increased significantly from 2018 to 2020. The circles with 5 km, 10 km and 20 km radii are centred around the Otaniemi power plant. Projections of the geothermal wells are plotted as a dark grey and lighter grey line originating in Otaniemi.

3. Initial results

The 2018 and 2020 measurements produced high-quality data sets that are suitable for various types of analyses techniques. First results of the Otaniemi 2018 induced seismicity distribution display three separate, dense clusters that are elongated parallel to the maximum principal stress axis (Kwiatek et al. 2019, Hillers et al. 2020). A deviation from the Gutenberg-Richter distribution was observed above M_L 1.5 indicating an absence of large enough structures in the stimulated volume to facilitate a larger earthquake (Ader et al. 2019, Kwiatek et al. 2020). Further analysis of the ISUH data sets is expected to reveal more details about the spatial, temporal and magnitude distribution of the seismicity and the distribution of seismic risk in Otaniemi.

Our goal is to use the Otaniemi induced seismicity data and surface geological background knowledge to investigate the applicability of the available knowledge to understanding geothermal reservoirs in the Fennoscandian shield at 6–8 km depth. To investigate seismic wave interactions with local scale structures, we conducted detailed field mapping of brittle and brittle-ductile structures in Elfvik, ~2 km north of the injection site, where an array of seismometers was located in both 2018 and 2020.

Seismic waveforms excited by a M_W 4.1 mining induced earthquake in Kiruna in ~1000 km distance on 18 May 2020 recorded at some of the 2019–2020 short term stations are shown in Figure 2. High signal-to-noise ratio (SNR) waveforms result from quality seismometer installations on outcropping bedrock. Installations in loose sediments or insufficient coupling result in noisy waveforms. The data management of the 2019–2020 measurement campaign led to overall very few acquisition gaps during the simulation. The data set is also quite complete some months before and after the stimulation, as indicated by the data availability plot of the 70 short term instruments (Figure 3).

Hillers et al. (2020) inverted earthquake source mechanisms of fourteen large events from the 2018 data set using the software package *Focmec* (Snoke, 2003) that finds double-couple focal mechanisms based on observed P- and S-wave velocities and amplitude ratios. This first analysis revealed dominant thrust faulting mechanisms. Further analysis of ~150 events with *Grond*, a probabilistic moment tensor inversion tool (Heimann et al., 2018) yields compatible results and confirms an overwhelming dominance of the reverse mechanisms with a few exceptions of strike-slip events (Figure 4).

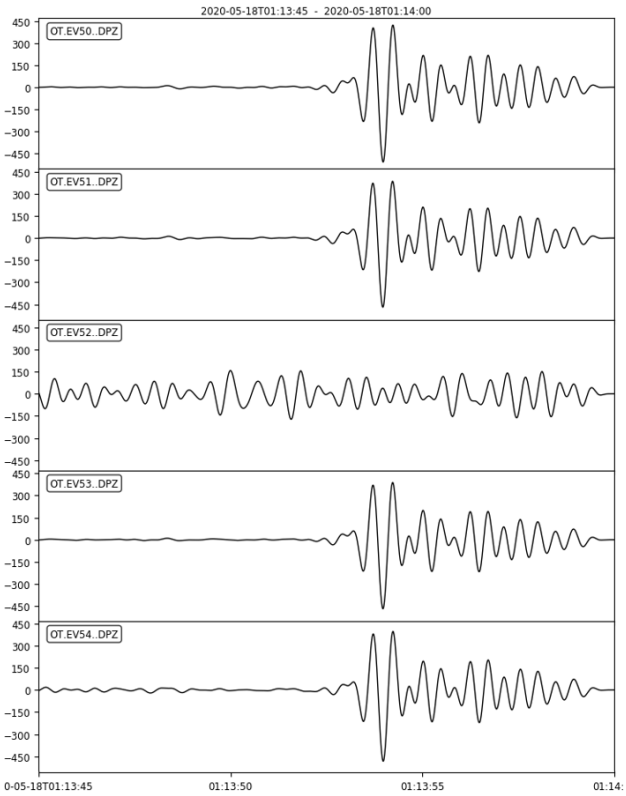

Figure 2. Vertical component waveforms of the Kiruna M_W 4.1 mining induced earthquake on selected short-period seismometers. Waveforms demonstrate excellent data quality in most of the stations. Installations in loose sediments (e.g. EV52) produce noisy waveforms.

7. Conclusions

Two highlight quality and versatile data sets of induced seismicity have been collected in 2018 and 2019–2020. These data sets can be used to analyse features of induced seismicity

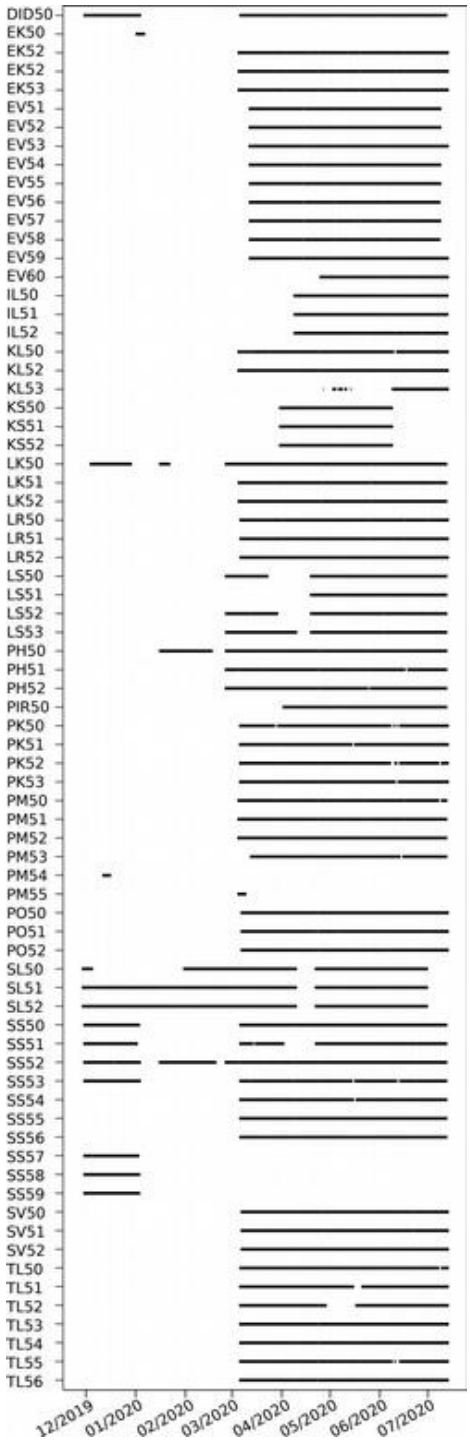

Figure 3. Data availability of 70 DATACUBE3 seismometers of the 2019-2020 network deployment.

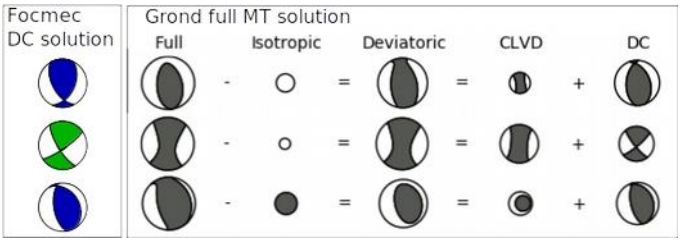

Figure 4. Source mechanisms of three selected M_L induced events from the 2018 dataset. Double-couple solutions inverted using polarity picking and Focmec (Hillers et al., 2020) are shown on the left and full moment tensor solutions and their decompositions of the same selected events inverted using Grond are shown on the right.

in the Fennoscandian shield. The versatility of the data sets allows the use of several different kinds of analysis techniques for a comprehensive description of subsurface processes and detailed features of the seismicity.

References:

Ader, T.; Chendorain, M.; Free, M.; Saarno, T.; Heikkinen, P., Malin, P. E., Leary, P., Kwiatek, G., Dresen, G., Bluemle, F., Vuorinen, T., 2019 Design and implementation of a traffic light system for deep geothermal well stimulation in Finland. Journal of Seismology, https://doi.org/10.1007/s10950-019-09853-y

Heimann, S.; Isken, M.; Kühn, D.; Sudhaus, H.; Steinberg, A.; Vasyura-Bathke, H.; Daout, S.; Cesca, S.; Dahm, T. 2018. Grond - A probabilistic earthquake source inversion framework. V. 1.0. GFZ Data Services. https://doi.org/10.5880/GFZ.2.1.2018.003

Hillers, G., Vuorinen, T. A. T., Uski, M. R., Kortström, J. T., Mäntyniemi, P. B., Tiira, T., Malin, P. E., Saarno, T., 2020. The 2018 geothermal reservoir stimulation in Espoo/Helsinki, southern Finland: Seismic network anatomy and data features. Seismological Research Letters 91 (2A): 770-786.

Kwiatek, G., Saarno, T., Ader, T., Bluemle, F., Bohnhoff, M., Chendorain, M., Dresen, G., Heikkinen, P., Kukkonen, I., Leary, P., Leonhardt, M., Malin, P., Martínes-Garzón, P., Passmore, K., Passmore, P., Valenzuela, S., and Wollin, C. 2019. Controlling fluid-induced seismicity during a 6.1-km-deep geothermal stimulation in Finland. Science Advances, 5: eaav7224, doi: 10.1126/sciadv.aav7224

Majer, E. L., Baria, R., Stark, M., Oates, S., Bonner, J., Smith, B., Asanuma, H., 2007. Induced seismicity associated with Enhanced Geothermal Systems. Geothermics 36, 185 – 222.

Veikkolainen, T., Uski, M., Voutilainen, A., Vuorinen, T., Oinonen, K., Kortström, J., Luhta, T., Mäntyniemi, P., Tiira, T. 2020. Seismisyys Espoon Otaniemen syväreikähankkeen viimeistelyvsiheessa. Seismologian instituutti, Helsingin yliopisto, Raportti T-102.

Granites of southernmost Finland

A. Saukko[1], K. Nikkilä[1], O. Eklund[1] and M. Väisänen[2]

[1]Åbo Akademi University, Geology and mineralogy, Geohouse, Akademigatan 1, FI-20500 Åbo, Finland
[2]Department of Geography and Geology, FI-20014 University of Turku, Finland
E-mail: anna.saukko@abo.fi

Migmatitic granites are common in the Svecofennian bedrock of southern Finland. We have studied the southernmost granite-migmatite belt in Finland and found that the granites there differ from the other Svecofennian granites. This is important for a better understanding of the processes that took place during the Svecofennian orogeny.

Keywords: granite, migmatite, Svecofennian orogeny, southernmost Finland

1. Geological overview of the southern Svecofennian domain

The bedrock in southern Finland consist of east-west trending zones that formed in varying metamorphic conditions during the 1900-1800 Ma Svecofennian orogeny. Partial melting during the orogeny resulted in belts of migmatite and leucogranite. Studies of leucogranite plutons in the Uusimaa belt (e.g., Kurhila et al. 2011) and the link between granites and migmatites in the Turku area (Väisänen et al. 2002; Johannes et al. 2003) have improved our understanding of partial melting during the ca 1830-1810 Ma metamorphic peak.

The southernmost Svecofennian granite-migmatite belt only outcrops in the southern archipelago of Ingå, Raseborg, Hanko and Kimitoön municipalities. Its connection to the rest of the Svecofennian domain has not been extensively investigated, although Edelman and Jaanus-Järkkälä (1983) proposed that a former subduction zone separates the southern archipelago of Finland from the rest of the Svecofennian domain. The presence of E-W and NE-SW shear zones, including the large Barösund shear zone (Vehkamäki, 2019) and many smaller shear zones (Nikkilä et al. 2021) shows that large crustal movements have taken place, and may indicate that the area is a distinct unit. As the southernmost directly observable part of the Svecofennian domain, the granite-migmatite belt may contain evidence of processes that occurred closer to the plate margin and, thus, contribute to a more detailed picture of the Svecofennian orogeny.

In this study, we describe the mineralogical and geochemical composition and radiometric age data of the different granitoid rocks that occur in the southernmost Svecofennian granite-migmatite belt. We also present geochemical and geochronological data from some leucosomes in the area to compare them to the granites, but do not focus on partial melting or migmatites in this study.

2. Rock types in the southernmost Svecofennian granite-migmatite belt

On the mainland and in the inner archipelago of southernmost Finland, the bedrock is dominated by migmatised supracrustal rocks of volcanogenic and sedimentary origins, now appearing as amphibolites and metapsammites. In addition to partial melting, the supracrustal rocks have also been affected by fluids, and K-feldspar megacrysts crystallised in different supracrustal layers after the rocks were formed. Some even-grained granodiorites also occur as large dikes and small plutons on the Hanko peninsula. In the outer archipelago, migmatised

supracrustal rocks and even-grained granodiorites are less common but deformed and migmatised feldspar megacryst-bearing granites and leucogranites are abundant.

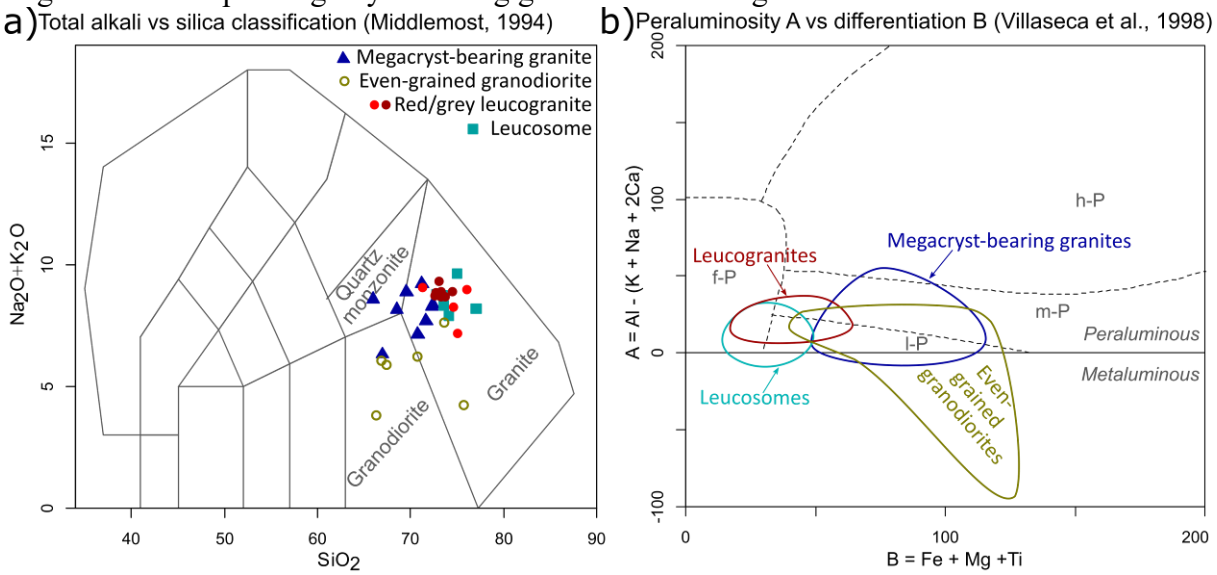

Figure 1. a) Geochemical rock type classification of the different granitoids in southernmost Finland. b) In the B-A plot (Villaseca et al. 1998), the even-grained granodiorites and deformed megacryst-bearing granites are low to moderately peraluminous, indicating they may have formed through partial melting of metaigneous rocks and possibly greywackes. The position of leucosomes and leucogranites suggests that they are partial melting products of the megacryst-bearing granites. As no rocks plot into the h-P or upper parts of the f-P field, metapelitic rocks were not a major contributing source.

3. Deformed and partially melted megacryst-bearing granites

Among the supracrustal rocks in the archipelago, migmatised feldspar megacryst-bearing granites occur as approximately layer-parallel intrusions. To the south, the granite appears to form a more extensive area, constituting the main rock type of the southernmost islets, but their true extent remains undetermined due to the scarcity of islands. The megacryst-bearing granites are deformed, appearing mylonitic close to shear zones. Leucosomes are common, showing that the granites were partially melted. We classify the migmatite as a granitic metatexite, because the proportion of leucosome is generally low and the megacryst-bearing granite still displays some original textures.

Petrographically, the feldspar megacrysts are the most distinctive feature of the deformed granites. The megacrysts are perthitic orthoclase crystals, which have undergone some microclinitisation. The matrix consists of quartz, strongly sericitized plagioclase, perthitic orthoclase, and some microcline. Biotite is present as a minor phase and appears in two distinct types: an unaltered euhedral type, and an altered Ti-rich type that has broken down into ilmenite, K-feldspar, and quartz.

Geochemically, the rocks are granites and granodiorites (Figure 1a), but whether their current composition is similar to the original composition is unknown. Partial melting likely affected the composition at the melting sites, but we do not know how pervasive the changes were in less-melted areas. Fluid activity may also have altered the chemical composition after crystallisation, similarly to the fluid-induced changes to the supracrustal rocks in the area.

U-Pb isotope analyses of zircon from megacryst-bearing granites reveal that most zircons crystallised at around 1880 Ma (Figure 2), although a few zircons show a younger age at around 1825 Ma. We assume that the older age represents the intrusion age and note that it is coeval

with or slightly younger than leucosomes in inner archipelago amphibolites, which Bredenberg (2019) dated to around 1890 Ma. The younger age corresponds to the partial melting event that occurred in the granites during the late stages of the Svecofennian orogeny.

4. Even-grained granodiorites

Even-grained granodiorites occur as grey-coloured plutons and large dikes cross-cutting the supracrustal metatexites on the Hanko peninsula. Apart from the absence of feldspar megacrysts, the mineral composition is similar to the megacryst-bearing granites. Geochemical similarities are notable as well: the granodiorites are less peraluminous than the megacryst-bearing granites, but have a similar spread in silica content, so that some of them are more accurately granites (Figure 1 a). The low peraluminosity suggests they formed through partial melting of metaigneous rocks (Figure 1 b), which is in accordance with the field observation that they appear similar to leucosomes in amphibolites. Our even-grained granodiorite sample yielded and intercept age of 1875±9 Ma. Thus, the even-grained granodiorites are approximately coeval with the megacryst-bearing granites.

5. Leucogranites

Leucogranites are mainly located offshore to the south and west of Hanko peninsula. They commonly contain partly assimilated rafts of the megacryst-bearing granites and supracrustal rocks, indicating formation through anatexis of those rocks. Leucogranites located close to deformed megacryst-bearing granites are red in colour and contain fewer dark minerals than supracrustal-associated leucogranites, which tend to be greyer in colour. Thus, the red leucogranites likely formed through anatexis of megacryst-bearing granites, whereas the grey leucogranites are a product of partial melting of old supracrustal rocks.

The leucogranites primarily consist of K-feldspar, plagioclase, and quartz. As in the megacryst-bearing granites, microcline has partly replaced orthoclase and plagioclase, and the minor phase biotite appears in the same two types. Some of the grey leucogranites contain magnetite flecks surrounded by light haloes of quartz and feldspar. As similar flecks are found in supracrustal metatexites in the area, they were likely inherited from the supracrustal protoliths. Protolith composition also affected the accessory mineral composition: zircon is scarce in the red leucogranites, but more common in the grey leucogranites.

Geochemically, the leucogranites are very similar to the leucosomes we analysed. The leucogranite and leucosome peraluminosities in comparison to the granitic metatexite (Figure 1 b) support the argument that both leucosomes and leucogranites were partially formed through partial melting of the older granite.

Radiometric dating shows that the leucogranites crystallised during a relatively long time between 1850 and 1820 Ma. Ages of leucocratic in-source dikes from granitic and supracrustal metatexites overlap with the youngest ages in leucogranites, indicating that the partial melting and granite accumulation event was long-lived.

6. Conclusions

Three distinct granitoids formed in southernmost Finland during the Svecofennian orogeny. The oldest granites intruded supracrustal rocks at around 1880 Ma and are now seen as deformed potassium feldspar megacryst-bearing granites, or granitic metatexites. An anatectic event in the supracrustal rocks occurred at approximately the same time. Plutons and dikes of homogeneous even-grained granodiorite that may be a partial melting product of amphibolites also crystallised at the same time.

Another episode of partial melting occurred in the same area later, at around 1850-1810 Ma. Before this second partial melting event took place, potassium feldspar megacrysts

crystallized in the supracrustal rocks that had already produced melt in the earlier partial melting event, rendering them more susceptible to melting. The intrusive megacryst-bearing granites also partially melted, producing granitic leucosomes poor in mafic minerals. Partial melts from all source lithologies accumulated into leucogranites containing varying amounts of the parent rocks as partially assimilated remnants.

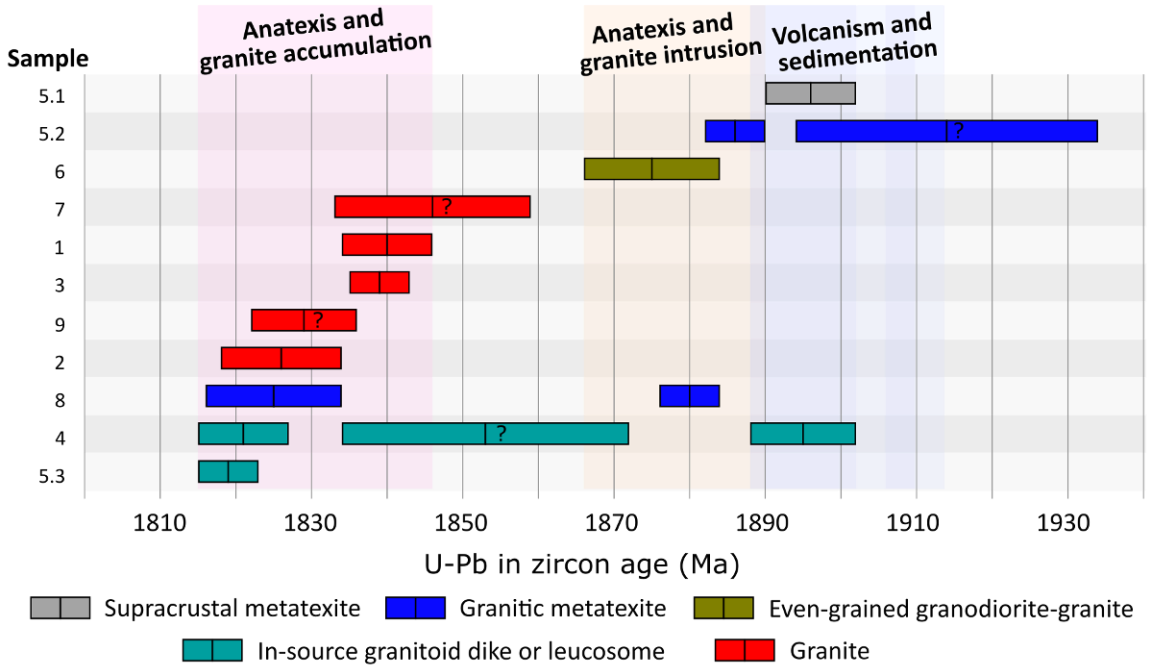

Figure 2. SIMS-analysed U-Pb in zircon ages of leucogranites (1,2,3,7 and 9), in-source granitoid dikes (4 and 5.3), granitic metatexite (5.2 and 8), supracrustal metatexite (5.1), and even-grained granodiorite (6) in the Hanko-Ekenäs area. The shaded areas represent the different phases of Svecofennian magmatism that we have identified in the area.

References:

Bredenberg, E., 2019. Tonalit migmatit i Södra Finland – åldersbestämning och petrografisk analys. Master's thesis, Åbo Akademi University. 48 p.

Edelman, N., Jaanus-Järkkälä, M., 1983. A Plate tectonic interpretation of the Precambrian of the Archipelago of southwestern Finland. Geological Survey of Finland, Bulletin 325. 33 p.

Johannes W., Ehlers, C., Kriegsman, L. M., Mengel, K., 2003. The link between migmatites and S-type granites in the Turku area, southern Finland. Lithos, 68(3–4):69–90.

Kurhila M., Mänttäri, I., Vaasjoki, M., Rämö, O. T., Nironen, M., 2011. U–Pb geochronological constraints of the late Svecofennian leucogranites of southern Finland. Precambrian Research, 190(1–4):1–24.

Middlemost, E. A. K., 1994. Naming materials in the magma/igneous rock system. Earth Science Reviews 37:(3–4):215–224.

Nikkilä, K., Skyttä, P., Saukko, A., Eklund, O., 2021 Structural evolution and melt formation within the southernmost Finland migmatitic belt. This abstract volume.

Vehkamäki, T. 2019. A multidisciplinary investigation of the Barösund Shear Zone area, southern Finland. Master's thesis, University of Turku. 65 p.

Villaseca, C., Barbero, L., Herreros, V., 1998. A re-examination of the typology of peraluminous granite types in intracontinental orogenic belts. Transactions of the Royal Society of Edinburgh, Earth Sciences 89(2): 113-119.

Väisänen M., Mänttäri, I., Hölttä, P., 2002. Svecofennian magmatic and metamorphic evolution in southwestern Finland as revealed by U-Pb zircon SIMS geochronology. Precambrian Research, 116(1–2):111–127.

Earth-Space Research Ecosystem: scientific and industry collaboration platform

E.I. Tanskanen[1], J. Tammi[2], J. Pulliainen[3], H. Koivunen[4] and E2S team

[1]Sodankylä Geophysical Observatory, University of Oulu
[2]Metsähovi Radio Observatory, Aalto University
[3]Finnish Meteorological Institute
[4]Finnish Geospatial Research Institute in the National Land Survey of Finland
E-mail: Eija.Tanskanen@oulu.fi

Earth-Space Research Ecosystem (E2S) is a new infrastructure on national infrastructure road map aiming to improve space situational awareness. E2S forms on Tähtelä and Metsähovi sites covering measurements from ground and atmosphere to near-Earth and deep space. The infrastructure includes continuous observatory-quality data for over 100 years as well as cutting-edge instruments and analysis methods for monitoring environmental patterns and trends. Basic functions of our high-tech society need to be protected against natural hazards from extraterrestrial and terrestrial origins. Improved know-how on GPS disturbances is needed for better guaranteeing the safety of our society. This presentation will give details of the infrastructure and propose how FIN-EPOS and E2S infrastructures best complement each other and can work together towards safer society.

Keywords: lithosphere, crust, upper mantle, Fennoscandia, Helsinki

Array-derived rotational motion of induced earthquakes

G. Taylor[1], G. Hillers[2] and T. A.T. Vuorinen[2]

[1]Ocean Environment Team, UK Hydrographic Office, Taunton, United Kingdom
[2]Institute of Seismology, University of Helsinki, Helsinki, Finland
E-mail: gregor.hillers@helsinki.fi

Keywords: induced earthquakes, crust, Helsinki, rotational motion

A proportional relationship exists between the translational acceleration and the vertical rotation rate induced by horizontally-polarised S-waves. In an homogeneous elastic medium, the waveform of SH-waves recorded perpendicular to the propagation direction will differ from that of the rotation rate by a factor of 2c, where c is the local phase speed. The propagation direction will usually, though not always perfectly, align with the back-azimuth of the seismic source.

In this study, we apply wavefield gradiometry at several arrays of translational seismometers to estimate vertical rotation rates for 204 induced earthquakes that occurred during the 2018 stimulation of the Espoo/Helsinki geothermal reservoir (Figure 1). The three 25- and three 4-station arrays are located at hypocentral distances of 6-9 km, with the events varying in magnitude from M0.0 to M1.8, at depths betweeen 4.8 and 6.3 km. Our estimates of vertical rotation rates are supported by the very high data quality that provide clean records of horizontal displacement variations. The rotation rates vary between 10^{-7} – 10^{-9} rad/s, indicating that array-derived rotation (ADR) estimates have a similar sensitivity as more specialised instruments, such as portable rotational sensors. Compared to horizontal component S-wave delay-and-sum beamforming our ADR estimates of earthquake back-azimuth are more consistent with the direction of the grat-circle back-azimuth.

However, both approaches show site-specific consistent deviations from great-circle propagation, indicating heterogeneous velocity structure (Figure 2), with the array-derived measurements able to resolve velocity variations over the 100 m aperture of the seismic arrays. We hightlight the results at the Elfvik array site that show a remarkable agreement of the ADR derived propagation direction pattern and the location and trend of geologically mapped shear bands. We measure apparent S-wave speeds of ~6 km/s, consistent with steep incidence angles and high propagation velocities in the crystalline rocks of the Fenno-Scandian Shield. The reliable measurement of rotation rates as small as 10^{-9} rad/s obtained from small and micro-earthquakes suggests that arrays of translational sensors can play an integral role in providing observations of rotational motion in weak-motion seismology. Although bespoke six-component rotational sensors are required to resolve rotational motion around the vertical and horizontal axes, the robust estimates of vertical rotational motion demonstrated in this study are capable of contributing to better inversions of moment tensors and thus improved source mechanism estimates of natural and induced earthquakes.

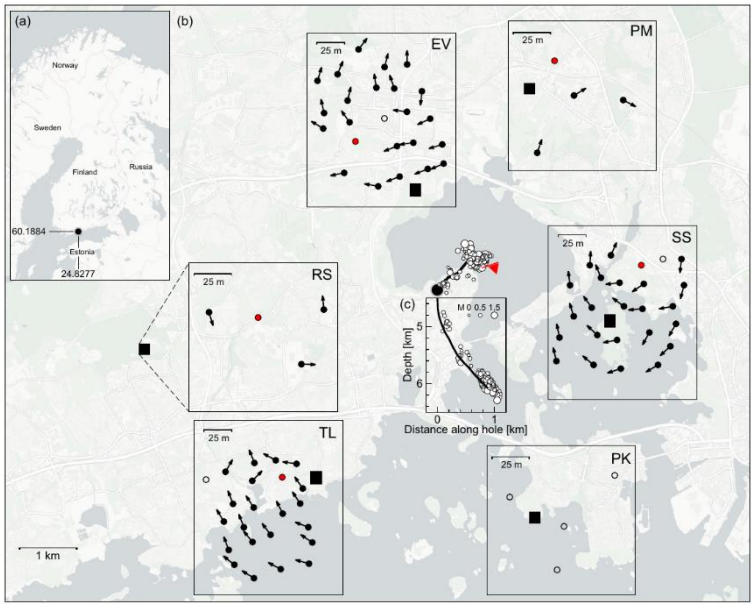

Figure 1. (a) Location of the study area in southern Finland. The coordinates indicate the wellhead. (b) Map of the study area. The central black circle marks the wellhead, the attached line shows the borehole trajectory between 4.8 and 6.1 km depth, and the white circles are epicenters of the analyzed earthquakes. The red flag marks the largest event. Solid black rectangles indicate array locations (not to scale). The corresponding station distributions are shown in the insets, and the arrows visualize an example rotational motion pattern obtained for the largest event. The red circles show the reference station, and the open circles indicate missing data for this event. EV, PM, SS, PK, TL, and RS abbreviate the locations Elfvik, Pajamäki, Seurasaari, Poliisin kesäkoti, Toppelund, and Rudolf-Steiner school Espoo, respectively. (c) Depth cross-section of the borehole trajectory and seismicity.

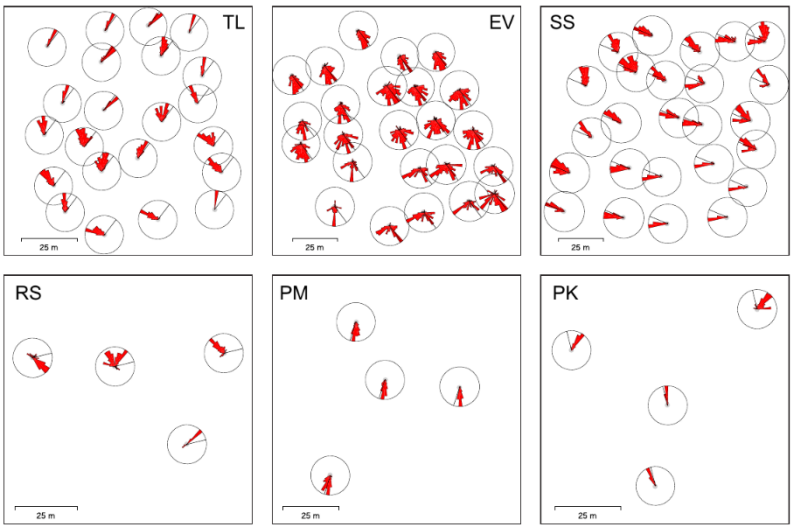

Figure 2. The rose diagrams show the station-by-station misfit between the observed propagation direction estimated by the rotational method and the event back-azimuth. The black line in the rose diagram indicates the mean event back-azimuth of all 204 events at that station.

Seismic surface wave focal spot imaging

C. Tsarsitalidou[1], B. Giammarinaro[1], G. Hillers[1], P.Boué[2] and L.Stehly[2]

[1] University of Helsinki, Institute of Seismology, Finland
[2]ISTerre, CNRS, Université Grenoble Alpes, Grenoble, France
E-mail: christina.tsarsitalidou@helsinki.fi

The present study explores a seismic surface wave imaging method based on the correlation of seismic ambient noise data recorded by dense seismic arrays. Its resolution power in the case of an elastic multi-layered half-space medium is studied using numerical simulations based on the Green's function solver AXITRA. We show results of the first application of the method to data provided by the US Transportable Array (TA).

Keywords: ambient noise, seismic surface wave imaging, array seismology

1. Introduction

Converging surface wave fields create a large-amplitude feature at the origin referred to as focal spot. Its properties are governed by local medium properties and have long been used in medical imaging approaches such as passive elastography (Catheline et al., 2013). Modern dense seismic arrays consisting of many hundreds of sensors now allow the application of noise correlation-based focal spot imaging in seismology (Hillers et al., 2016). The high- and low-frequency resolution limit of the method is governed by the array inter-station distance and the aperture of the array, respectively. Since the maximum surface-wave sensitivity depth is related to the wavelength (0.5λ), in the case of the TA and for periods between 80-300s, the method can extend the imaging to the depth range of 150-700 km. Here, we present numerical experiments, which investigate the resolution properties of the focal spot method and the potential limits of data applications, together with initial results of the method applied to the TA, a large-N seismic array, for the period of 100s.

2. Numerical Studies

Focal spot imaging is based on the correlation of diffuse isotropic wavefields. We perform numerical experiments using an equivalent time-reversal approach (Derode et al. 2002) to synthesize Rayleigh waves focal spots in an elastic half-space from Green's functions computed with the AXITRA solver (Cotton and Coutant, 1997). This study explores different cases such as multi-layered elastic media. Simulations are performed using a 85x85 grid with an inter-station spacing of 8m. The Rayleigh wave speed is set as 2 km/s near the surface and increases with depth. Time-reversal mirrors are set at the surface at 12 km distance from the origin. Example focal spots of the nine vertical (Z), radial (R), and transversal (T) component combinations are shown in Figure 1, left. Results are fitted for frequencies between 2 and 15 Hz to theoretical expressions describing the near-field surface wave Green's tensor developed by Haney et al. (2012) using a non-linear least square methods. An example of this fitting process is presented for the components ZZ and ZR in Figure 1, right, which are parametrized by the Bessel functions of order zero and one,

$\varphi_{zz} \propto J0\left(\frac{\omega r}{c_R}\right)$ and $\varphi_{ZR} \propto -J1\left(\frac{\omega r}{c_R}\right)$, respectively. The distance of the first zero crossing as a proxy for the spot size is equal to (3/8)λ and (3/5)λ for the J0 and J1 functions (Abramowitz

and Stegun, 1965) and thus allow estimates of the local wavelength for a specific frequency. This allows to reconstruct the dispersion curves for the studied medium. Systematic departures from perfect conditions are implemented to test the fidelity of the obtained estimates for anisotropic wave field energy and interfering body waves.

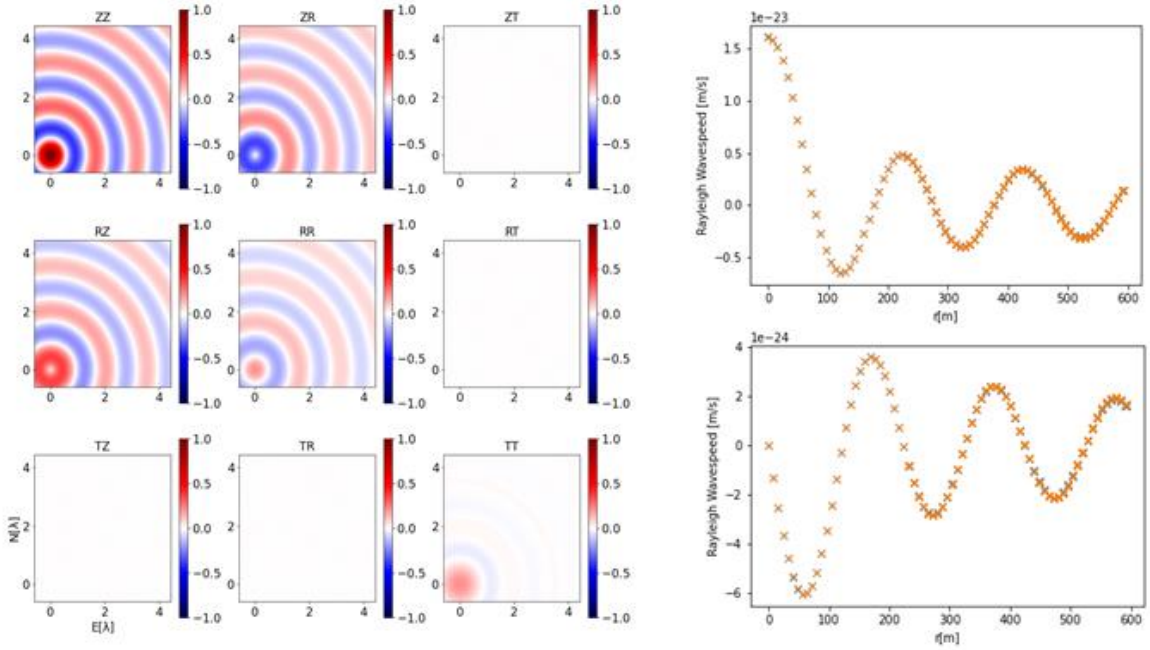

Figure 1. Left: Nine component simulated focal spots obtained in a multi-layered elastic medium at 10Hz. Axis are normalized using the theoretical wavelength λ for Rayleigh waves in the upper layer. Right: Upper and lower figures show the simulated amplitude distribution (blue crosses) for the ZZ and ZR components, respectively, and the perfect match with the Bessel-function parametrization (orange crosses).

3. Application to seismic data

Our initial analysis of data from 600 stations located at the west part of the US with inter-station distance of 60 km suggests that we can reconstruct experimental Rayleigh-wave focal spots between 80 s and 300 s period. The first step in obtaining empirical focal spots is the pre-processing of the three-component daily noise records for one year (BHZ, BHE, BHN). Decimation at 1Hz and deconvolution is applied to single-station data, followed by a bandpass filter in the range of (2-330s). Normalization techniques are applied to 4-h segments, first spectral whitening in the range of (2.85-340s) followed by time-domain standard-deviation clipping and tapering. For each station pair, we compute the cross-correlations between the three components (Z, E, N) and then rotate the ZEN to the ZRT system (Lin et al. 2008). In Figure 2, the zero-lag amplitude distribution or focal spot is plotted for a reference station at the origin that acts as the virtual source and all other array stations are receivers. The near circular shape with the center located on the reference station is maintained for the ZZ, ZR and RZ components. A first interpretation of these results imply that we can obtain Rayleigh-wave phase velocity values to a depth of 200 km.

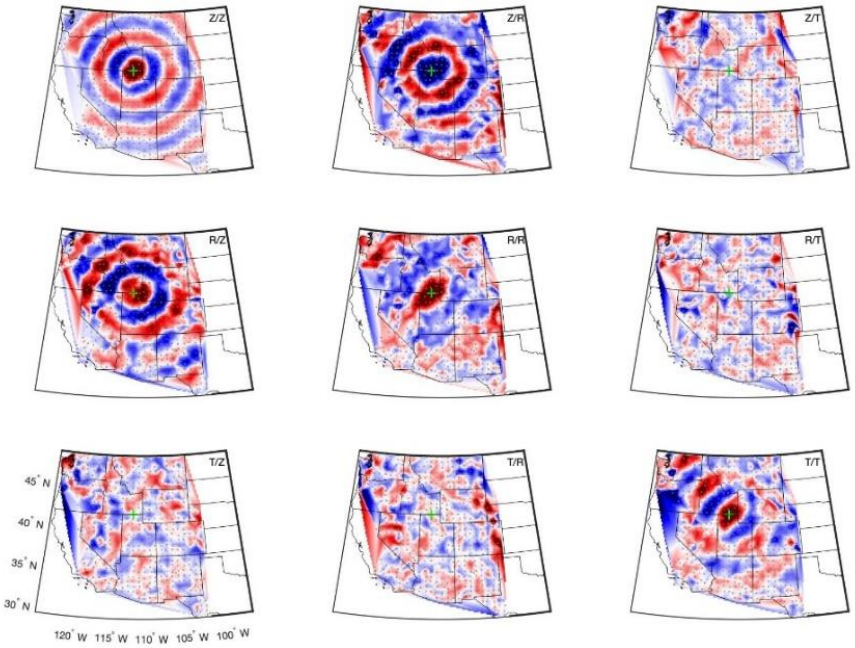

Figure 2. Focal spots at 100s for a reference station.

References:

Abramowitz, M., Stegun, I.A., 1965. Handbook of Mathematical Functions, 1057 pp.

Catheline, S., Souchon, R., Rupin, M., Brum, J., Dinh, A. H., Chapelon, J.-Y., 2013. Tomography from diffuse waves: Passive shear wave imaging using low frame rate scanners. Applied Physics Letters, 103(1), 014101. https://doi.org/10.1063/1.4812515.

Cotton, F., Coutant, O., 1997. Dynamic stress variations due to shear faults in a plane-layered medium. Geophysical Journal International, 128(3), 676-688. https://doi.org/10.1111/j.1365-246X.1997.tb05328.x

Derode, A., Larose, E., Tanter, M., de Rosny, J., 2002. Recovering the Green's function from field-field correlations in an open scattering medium (L). The Journal of the Acoustical Society of America, 113(6), 2973. https://doi.org/10.1121/1.1570436.

Haney, M. M., Mikesell, T. D., van Wijk, K., Nakahara, H., 2012. Extension of the spatial autocorrelation (SPAC) method to mixed-component correlations of surface waves. Geophysical Journal International, 191(1), 189–206. https://doi.org/10.1111/j.1365-246X.2012.05597.x

Hillers, G., Roux, P., Campillo, M., Ben-Zion, Y., 2016. Focal spot imaging based on zero lag cross-correlation amplitude fields: Application to dense array data at the San Jacinto fault zone. Journal of Geophysical Research: Solid Earth, 121(11), 8048–8067. https://doi.org/10.1002/2016JB013014

Lin, F.-C., Moschetti, M. P., & Ritzwoller, M. H., 2008. Surface wave tomography of the western United States from ambient seismic noise: Rayleigh and Love wave phase velocity maps. Geophysical Journal International, 173(1), 281–298. https://doi.org/10.1111/j.1365-246X.2008.03720.x.

Comparing geochemical characteristics of a gold-only and a base metal-rich orogenic mineralization from the Central Lapland Greenstone Belt, northern Finland

M. Vasilopoulos[1], F. Molnár[2], H. O'Brien[2] and Y. Lahaye[2]

[1]University of Oulu
[2]Geological Survey of Finland
E-mail: mikael.vasilopoulos@student.oulu.fi

In this article we compare the geochemical characteristics of two different types of orogenic mineralization: the Hirvilavanmaa (Au-only) and the Naakenavaara (Cu-Co-Ni-Au) deposits from the Central Lapland Greenstone Belt. We use in situ multi- and single collector LA-ICP-MS analytical techniques to study the trace element and sulfur isotope characteristics of sulfides and boron isotope composition of tourmaline from these two deposits. The trace element and sulfur isotope characteristics of sulfides together with the boron isotope composition of tourmaline prove to be effective in discriminating between these two different types of mineralization in the CLGB. Trace element contents of pyrite also record multiple mineralizing events in the base metal-rich Naakenavaara deposit.

Keywords: orogenic gold, pyrite, trace elements, sulfur isotopes, tourmaline

1. Introduction

The Paleoproterozoic Central Lapland Greenstone Belt (CLGB) is the largest mafic-volcanic dominated province in Finland and one of the most important metallogenic belts in the Fennoscandian shield. More than 60 orogenic Au deposits and occurrences have been discovered in the CLGB, with most of them being spatially associated with the east-west trending Sirkka Shear Zone (SiSZ; Eilu et al. 2007). The SiSZ is a complex shear zone involving several parallel faults and fault segments and reaching up to 2 km in width (Patison, 2007). Among the orogenic deposits found along the SiSZ, several are also enriched in base metals (Cu, Co, Ni) in addition to Au. A second major structure of significance in the CLGB is the NNE-trending Kiistala Shear Zone (KiSZ). The KiSZ hosts several Au-only deposits, including the Suurikuusikko Au deposit, which is currently the largest Au producer in Europe. In this study, we investigate the mineralogical and geochemical characteristics of the Hirvilavanmaa and Naakenavaara deposits that are spatially associated with these two major structures and represent the two main types of Au mineralization in the CLGB: orogenic Au-only mineralization and base metal-rich orogenic Au mineralization. The Hirvilavanmaa Au-only deposit is the closest discovered deposit to the intersection of the SiSZ and the KiSZ (Figure 1). Naakenavaara is situated just 5 km south of the Hirvilavanmaa deposit (Figure 1) and is an example of atypical base metal-rich orogenic mineralization.

In order to understand the hydrothermal processes that led to the different metal associations in the Hirvilavanmaa and Naakenavaara deposits we applied in situ multi- and single collector LA-ICP-MS analytical techniques to study sulfur isotope and trace element characteristics of sulfide minerals and boron isotope characteristics of tourmaline from these deposits.

2. Geological setting

The CLGB is part of the larger Karasjok-Kuusamo-Lake Onega belt that extends from northern Norway to the Russian Karelia (Hanski and Huhma 2005). The CLGB comprises several supracrustal formations of volcanic and sedimentary origin that were deposited between 2.44 Ga and 1.92 Ga (Lahtinen et al. 2005; Köykkä et al. 2019). The supracrustal rocks of the CLGB were intruded by 2.44-2.05 Ga mafic-ultramafic intrusive rocks, 1.92-1.88 Ga felsic porphyritic rocks, and 1.88-1.80 Ga syn- to post orogenic granitoids (Köykkä et al. 2019). The Paleoproterozoic development of the CLGB started with the eruption of intermediate-composition to felsic volcanic rocks of the Salla Group. The volcanic formations

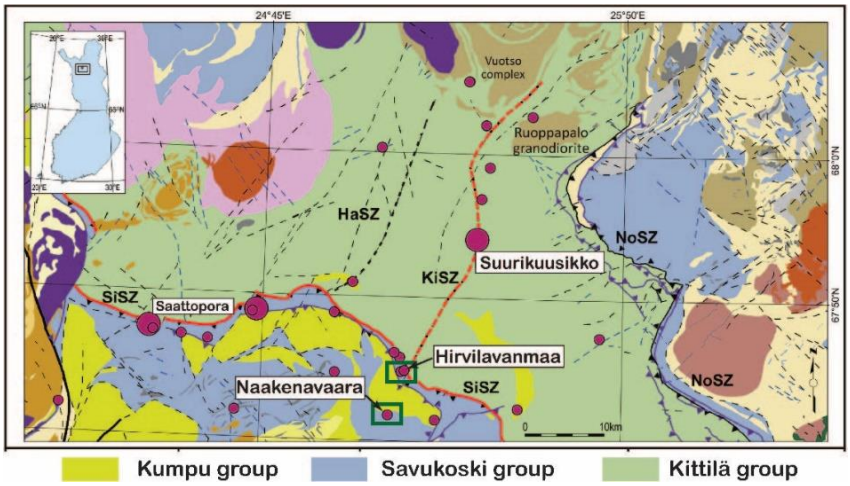

Figure 1. Location Map of the CLGB showing the position of the Hirvilavanmaa and Naakenavaara deposits. The continuous red line represents the Sirkka Shear Zone (SiSZ), whereas the dashed red line represents the Kiistala Shear Zone (KiSZ). Modified after Molnár et al. (2018).

of the Salla Group were followed by crustally contaminated komatiites and mafic lavas of the Kuusamo Group and by siliciclastic sediments, flood basalts, carbonate rocks, and pelitic sediments of the Sodankylä Group. These sedimentary formations were succeeded by fine-grained sediments, phyllites and black schists of the Savukoski Group. Basaltic volcanic rocks, chemical sediments and ophiolitic mantle rocks of the allochtonous Kittilä Suite are in tecnonic contact with the volcanosedimentary formations of the previously mentioned groups. Uppermost in the stratigraphy are quartzites and conglomerates of the Kumpu Group that lie unconformably on top of earlier rocks.

The CLGB underwent deformation and metamorphism in several stages during the 1.92-1.77 Ga Svecofennian orogeny (Patison, 2007). The central part of the CLGB that hosts most of the discovered Au deposits, was metamorphosed in greenschist facies conditions.

3. Geology and mineralogy of the Hirvilavanmaa and Naakenavaara deposits

The Hirvilavanmaa Au-only deposit is hosted by altered metakomatiites and mafic metavolcanic rocks. Hulkki and Keinänen (2007) recognized a sequence of alteration including four major stages: (1) regional hydration that formed talc and chlorite, (2) albitization, (3) silicification together with pyritization and (4) carbonatization. The latter two alteration stages were closely related to Au mineralization, which is associated with several generations of quartz-carbonate-albite veins (Figure 2). Pyrite is the most dominant sulfide with minor chalcopyrite also being present. Accessory minerals include hematite, magnetite, rutile and

pyrrhotite. Native gold is present mostly as inclusions and fracture fillings in pyrite (Figure 2) and locally in vein quartz and carbonate. The resource estimate for Hirvilavanmaa is 0.11 Mt of ore grading at 2.9 ppm Au (Scan Mining 2002).

The mineralization at Naakenavaara is hosted by altered phyllite, graphite phyllite and sericite schists and is characterized by zones with different metal enrichments. Host rocks are brecciated by quartz-carbonate-albite veins. Albitization of the host rocks precedes the mineralizing events. The most abundant sulfides are chalcopyrite and pyrrhotite followed by pyrite; in the Co-rich zones pyrite and pyrrhotite are typically more abundant than chalcopyrite (Figure 2). Gersdorfite is present in Ni-rich parts of the deposit. There is no observable microscopic gold in the studied samples. No resource estimates have been calculated for Naakenavaara.

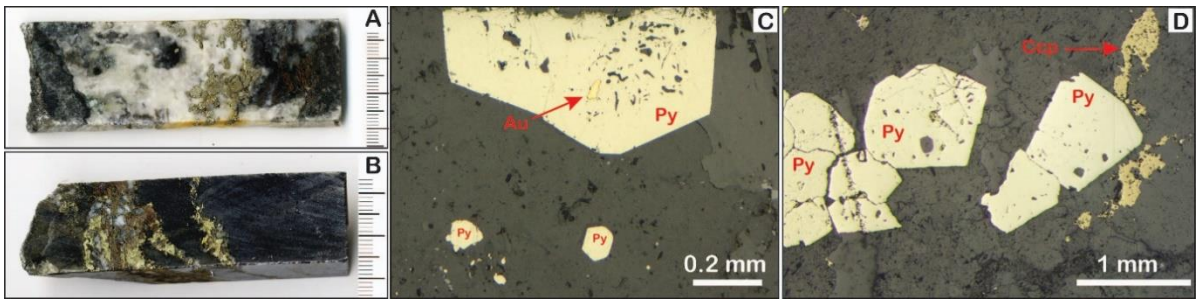

Figure 2. Photographs and photomicrographs from mineralized parts of the Hirvilavanmaa and Naakenavaara deposits. A) Mineralized drill core sample from Hirvilavanmaa. B) Mineralized drill core samples from Naakenavaara. C) Photomicrograph showing a gold inclusion in pyrite in a mineralized sample from the Hirvilavanmaa deposit. D) Photomicrograph from a cobalt-rich part of the Naakenavaara deposit showing pyrite with pyrrhotite and chalcopyrite inclusions.

4. Analytical results

Sulfides from the Hirvilavanmaa deposit show light $\delta^{34}S$ values with a median of +1.2 ‰. On the other hand, sulfides from Naakenavaara show a significantly heavier $\delta^{34}S$ signature with a median value of +9.9 ‰ (Figure 3).

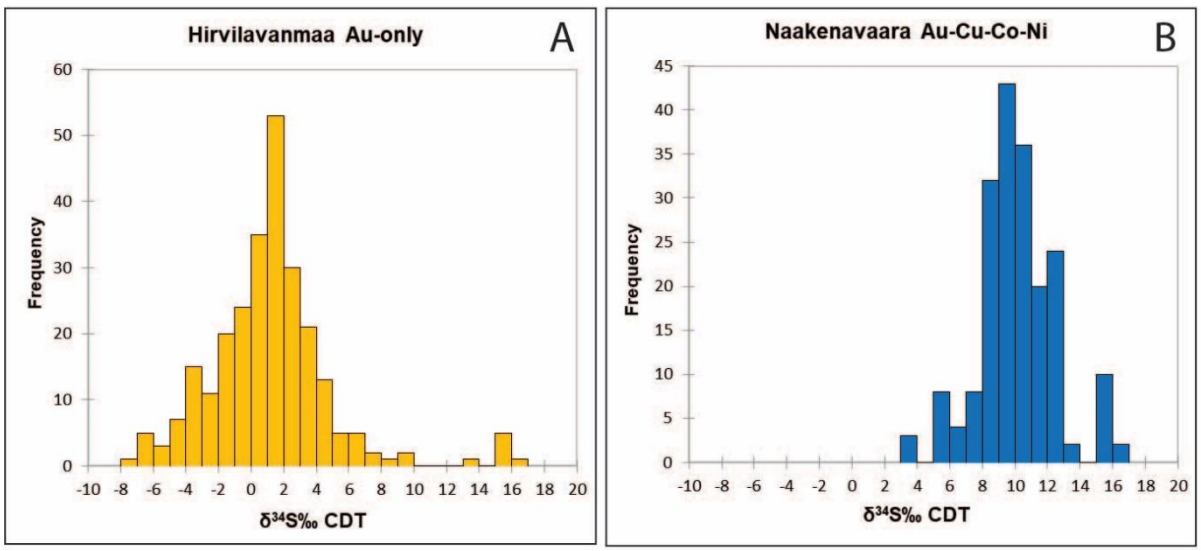

Figure 3. Results of sulfur isotope analyses from pyrite, pyrrhotite and chalcopyrite from the Hirvilavanmaa (A) and Naakenavaara (B) deposits.

At Hirvilavanmaa, tourmaline associated with sulfides in mineralized zones has higher $\delta^{11}B$ ‰ (median -5.8) compared to tourmaline from barren zones (median -8.5). Tourmaline from Naakenavaara shows even lower δ11B ‰ values with a median of -9.4.

Pyrite trace element characteristics from the two occurrences show notable differences. Pyrite from the Au-only Hirvilavanmaa deposit has higher Ni, Cu, Au, V, Te, and Hg concentrations whereas pyrite from the polymetallic Naakenavaara occurence is significantly more enriched in Co, As, and Se. Furthermore, pyrite from zones with different metal enrichments at Naakenavaara have different trace element signatures. Pyrite generations distinguished by their Co/Ni ratios also show systematic variation in other trace element contents such as Cu, V, Mn, Ag, Te. Bi, Sb, W, and As.

5. Conclusions

Trace element and sulfur isotope characteristics of sulfides together with boron isotope composition of tourmaline prove to be effective in discriminating between these two different types of mineralization in the CLGB. Results indicate that fluids of different origins and characteristics were responsible for the Au-only and Au-base metal mineralization in the studied deposits. Strongly contrasting $\delta^{34}S$ ‰ values of sulfides from Hirvilavanmaa and Naakenavaara indicate different sources of S. Multiple mineralizing events in the base metal-rich Naakenavaara deposit are recorded in trace element characteristics of pyrite, showing similar trends to other base metal-rich Au deposits from northern Finland such as the Juomasuo and Hangaslampi Au-Co deposits from the Paleoproterozoic Kuusamo belt (Vasilopoulos et al. 2019).

References:

Eilu, P., Pankka, H., Keinänen, V., Kortelainen, V., Niiranen, T. & Pulkkinen, E. 2007. Characteristics of gold mineralisation in the greenstone belts of northern Finland. Geological Survey of Finland, Special Paper 44, 57−106.

Hulkki H., Keinänen V. 2007. The alteration and fluid inclusion characteristics of the Hirvilavanmaa gold deposit, Central Lapland Greenstone Belt, Finland. Geological Survey of Finland, Special Paper 44, 137-153

Köykkä J., Lahtinen R., Huhma H. 2019. Provenance evolution of the Paleoproterozoic metasedimentary cover sequences in northern Fennoscandia: age distribution, geochemistry, and zircon morphology. Precambrian Research 331, 105364

Lahtinen, R., Korja, A., Nironen, M., 2005. Paleoproterozoic tectonic evolution. In: Lehtinen, M., Nurmi, P.A., Rämö, O.T. (Eds.), Precambrian Geology of Finland: Key to the Evolution of the Fennoscandian Shield. Elsevier, Amsterdam, pp. 481−532.

Molnár, F., Middleton, A., Stein, H., O'Brien, H., Lahaye, Y., Huhma, H., Pakkanen, L., Johanson, B., 2018. Repeated syn- and post- orogenic gold mineralization events between 1.92 and 1.76 along the Kiistala Shear Zone in the Central Lapland Greenstone Belt, northern Finland. Ore Geology Reviews 101, 936-959.

Patison, N.L. 2007. Structural Controls on Gold Mineralisation in the Central Lapland Greenstone Belt. Geological Survey of Finland, Special Paper 44, 107–124.

Scan Mining Oy 2002. Press release 09/09/2002

Vasilopoulos, M., Molnár, F., O'Brien, H., Lahaye, Y., Ranta, J-P. 2019. Sulphide trace element, sulphur isotope and hydrothermal alteration studies in the Juomasuo and Hangaslampi Au-Co deposits, Kuusamo belt, northeastern Finland. Life with Ore Deposits on Earth: 15th Biennial SGA Meeting, Glasgow, Scotland, August 27-30, 2019. Conference proceedings, Volume 4, 1704-1707

Metamorphic zones in SW Finland: monazite and zircon U-Pb dating of leucosomes in paragneisses

T. Vehkamäki[1], M. Väisänen[1], M. Kurhila[2], H. O'Brien[2],
P. Hölttä[2] and J.-K. Syrjänen[1]

[1]Department of Geography and Geology, FI-20014 University of Turku, Finland
[2]Geological Survey of Finland, FI-02151 ESPOO
E-mail: tetave@utu.fi

The Central Svecofennian Arc Complex (CSAC) and the Southern Svecofennian Arc Complex (SSAC) show different ages of peak metamorphism: ~1.88 Ga in the CSAC and ~1.83 Ga in the SSAC. In the present project we study the age of the metamorphism in SW Finland. We have collected two samples. Of these the Eurajoki leucosome zircons were > 1.92 Ga, i.e.,inherited, but monazites show two populations: ~1.83 Ga and ~1.7 Ga. The zircons from the Rauma leucosome yielded two populations: ~1.86 Ga and ~1.83 Ga. The monazites show ages of ~1.83 Ga and ~1.7 Ga. We interpret that the ~1.86 Ga zircons represent the older metamorphism and the 1.83 Ga zircon and monazite group to represent the younger metamorphism. The 1.7 Ga group is unusual and needs further investigation.

Keywords: Paragneiss, U-Pb, Geochronology, Svecofennian orogeny, southern Finland

1. Introduction

At 1.92-1.77 Ga, the present day central and southern Finland was affected by the Svecofennian orogeny (Gorbatschev & Bogdanova, 1993; Lahtinen et al., 2005). In Finland, the orogen is divided in two inferred terranes: The Central Svecofennian Arc Complex (CSAC) and the Southern Svecofennian Arc Complex (SSAC). These are shown in Figure 1.

A key difference between these is the age of the peak metamorphism. In the southernmost part of the CSAC, the Pirkanmaa belt, the metamorphism peaked at c. 1.88 Ga, while in the SSAC the highest metamorphic temperatures were reached at c. 1.83 Ga. This difference is shown in Figure 1.

It is not known whether the age of peak metamorphism changes sharply or gradually across the terrane boundary.

We have started a project to determine the age of metamorphism in the CSAC and SSAC. We will perform U-Pb zircon and monazite geochronology from leucosomes in paragneisses sampled from the Pirkanmaa belt in the north to the Åland archipelago in the south. Here we present some of our preliminary results from the Rauma region where we have gathered two samples denoted as the Eurajoki leucosome and the Rauma leucosome.

2. Methods

Zircons and monazites were separated by crushing, panning, heavy liquid, magnetic separating and hand picking. Grains were BSE-imaged with the SEM at the Department of Physics and Astronomy at the University of Turku. The U-Pb dating was carried out with the TM AttoM High Resolution ICP-MS in the Finnish Geosciences Research Laboratory at the Geological Survey of Finland, Espoo.

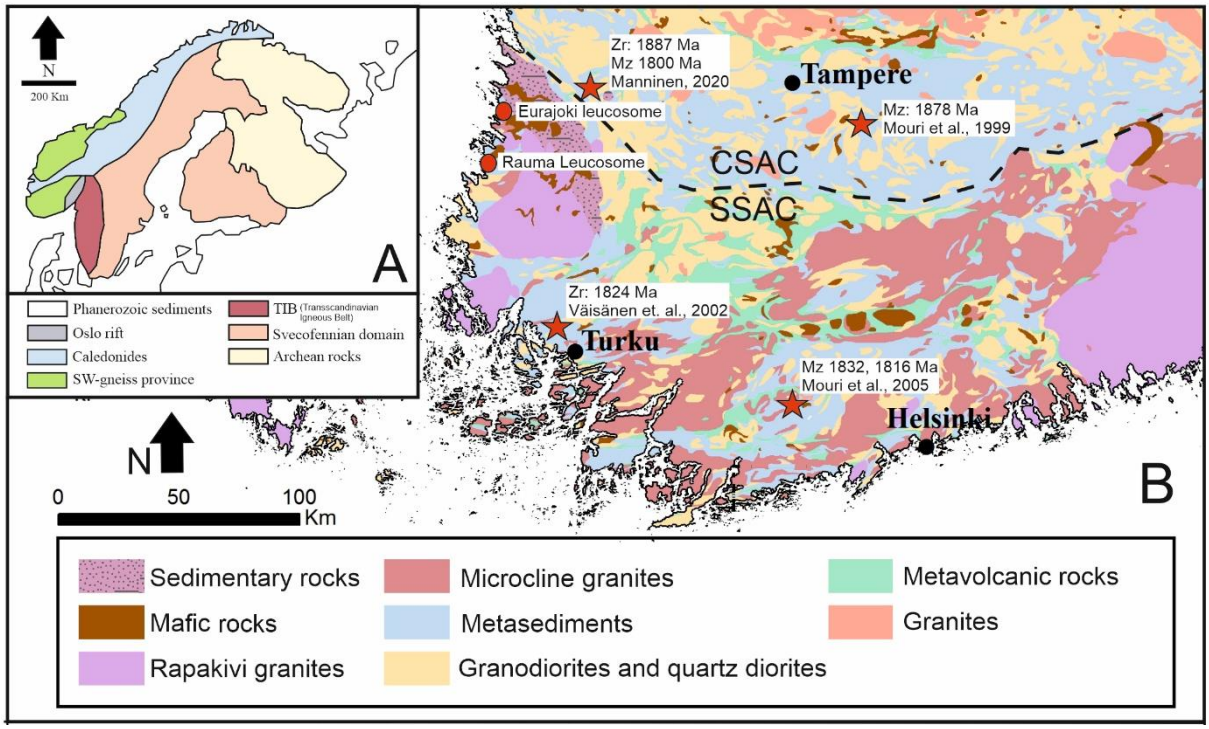

Figure 1. A: Simplified geological division of Fennoscandia. B: Simplified geological map of South Finland with selected previous U-Pb age determinations indicated by red stars. Sample locations of this study are indicated by red circles. Modified from Nironen et al., (2016). CSAC= Central Svecofennian Arc Complex, SSAC= Southern Svecofennian Arc Complex, Mz= monazite, Zr= zircon.

3. Results

Eurajoki Leucosome

The zircons of the sample show only Archean 2.7-2.6 Ga and Paleoproterozoic 2.1-1.92 Ga ages. These are therefore interpreted to be inherited.

The monazites show two concordant populations. The older one contains six analyses and has a concordia and $^{207}Pb/^{206}Pb$ ages of ~1.83 Ga. The younger population of 13 analyses yields a concordia age of ~1.7 Ga with a similar weighted average $^{207}Pb/^{206}Pb$ age.

Rauma Leucosome

The zircons yield two distinct populations. The older concordant population consist of four grains and has a U-Pb concordia age of ~1.86 Ga with a similar weighted average $^{207}Pb/^{206}Pb$ age. The younger age comprises only one analysis and yields a concordia age of ~1.83 Ga and a similar $^{207}Pb/^{206}Pb$ age.

The monazite ages show two populations. The older one contains 14 analyses and has concordia and weighted average $^{207}Pb/^{206}Pb$ ages of ~1.83 Ga. The younger population comprises 11 analyses and yields a concordia age of ~1.7 G with a similar weighted average $^{207}Pb/^{206}Pb$ age.

4. Discussion

We have analysed both monazites and zircons from the leucosomes in the migmatitic paragneisses. It is assumed that the anatectic melting of water- and aluminium-rich metasediments and their subsequent crystallisations occur during the peak temperature. Therefore, leucosomes are the best rock type for dating ancient high-T metamorphic events.

Zircon is a very robust mineral and has a high closure temperature (Corfu et al., 2003). It crystallises readily from the magma but may retain its U-Pb composition during the later metamorphism. Not even melting completely destroy zircon and their U-Pb system. This is proven by abundant inherited zircon populations that are often present in the Svecofennian rocks, including this study. Monazite has a lower closure temperature and recrystallises more readily in subsequent metamorphism (Kohn, 2017). This can be seen in the behaviour of the two minerals in Manninen (2020), where zircon yielded an age of 1885 Ma and monazite 1800 Ma. In that case the zircon was inferred to represent the melt formation and the monazite the later hydrothermal metamorphic event.

The oldest age group of ~1.86 Ga was found in zircon from the Rauma leucosome but the same age was not found from monazite of the either sample. This age represents the oldest metamorphism so far found in S-Finland and it is older than the previous findings (Hölttä et al., 2020). The ~1.86 Ga. period contains magmatism in the SSAC (Mänttäri et al. 2006; Väisänen et al., 2012; Nevalainen et al., 2014). The absence of ~1.86 Ga ages in monazites is most likely due to its readiness to recrystallise: the ~1.86 Ga monazites, if they ever existed, have been reset by later thermal events.

The ~1.83 Ga age is present in zircon from the Rauma leucosome and the Rauma and Eurajoki monazites. This age group represents the well-documented 1.83 Ga peak metamorphism in the SSAC, which resulted in formation of large volumes of anatectic melts (Väisänen & Hölttä 1999; Mouri et al., 2005; Kurhila et al., 2010). The later high T- low P-metamorphism was not able to destroy all the evidence from an earlier thermal event in the zircons, but no older monazites are present in the samples.

The ~1.7 Ga concordant age group, present in both Eurajoki and Rauma monazites is the most surprising result and the previously published youngest monazite ages from southern Finland are much older (Hölttä et al., 2020). The reason for these young monazites remains to be solved.

The preliminary data does not give a clear answer to the variation of the peak metamorphic ages between the CSAC and the SSAC: The ~1.83 Ga age group fits perfectly with the known c. 1.83 Ga age for the late-orogenic event in the SSAC and would therefore indicate a sharp change in the age of the peak metamorphism. The presence of the ~1.86 Ga ages, however, complicates the matter. The nature of the age difference between the two terranes depends whether the ~1.86 Ga age group represents the oldest metamorphism in the SSAC or the onset of the younger 1.83 Ga metamorphism.

References:

Corfu, F., Hanchar, J.M., Hoskin, P.W., Kinny, P., 2003. Atlas of zircon textures. Reviews in Mineralogy and Geochemistry, 53, 469–500.

Gorbatschev, R., Bogdanova, S., 1993. Frontiers in the Baltic Shield. Precambrian Research, 64, 3–22.

Hölttä, P., Huhma, H., Lahaye, Y., Mänttäri, I., Lukkari, S., O'Brien, H., 2020. Paleoproterozoic metamorphism in the northern Fennoscandian Shield: age constraints revealed by monazite. International Geology Review, 62, 360–387.

Kohn, M., J., 2017. Titanite petrochronology. Reviews in Mineralogy and Geochemistry, 83, 419–441.

Kurhila, M., Andersen, T., Rämö, O.T., 2010. Diverse sources of crustal granitic magma: Lu–Hf isotope data on zircon in three Paleoproterozoic leucogranites of southern Finland. Lithos, 115, 263–271.

Lahtinen, R., Korja, A., Nironen, M., 2005. Paleoproterozoic tectonic evolution. Developments in Precambrian Geology, 14, 481–531.

Manninen, J., 2020. Structural control of the orogenic gold deposits in Kullaa, SW Finland. MSc thesis, University of Turku, Department of Geography and Geology, 81p.

Mänttäri, I., Talikka, M., Paulamäki, S., Mattila, J., 2006. U–Pb ages for tonalitic gneiss, pegmatitic granite, and diabase dyke, Olkiluoto study site, Eurajoki, SW Finland. Posiva Working Report 2006–12, 18 p.

Mouri, H., Korsman, K., Huhma, H., 1999. Tectono-metamorphic evolution and timing of the melting processes in the Svecofennian Tonalite- Trondhjemite Migmatite Belt: an example from Luopioinen, Tampere area, southern Finland. Geological Society of Finland Bulletin, 71, 31–56.

Mouri, H., Väisänen, M., Huhma, H., Korsman, K., 2005. Sm–Nd garnet and U–Pb monazite dating of high-grade metamorphism and crustal melting in the West Uusimaa area, southern Finland. GFF, 127, 123–128.

Nevalainen, J., Väisänen, M., Lahaye, Y., Heilimo, E., Fröjdö, S., 2014. Svecofennian intra-orogenic gabbroic magmatism: a case study from Turku, southwestern Finland. Bulletin of the Geological Society of Finland, 86, 93-112.

Nironen, M., Kousa, J., Luukas, J., Lahtinen, R., (Eds.). 2016. Geological Map of Finland: Bedrock 1: 1,000,000. Geological map of Finland.

Väisänen, M., Hölttä, P. 1999. Structural and metamorphic evolution of the Turku migmatite complex, southwestern Finland. Bulletin of the Geological Society of Finland, 71, 177-218.

Väisänen, M., Mänttäri, I., Hölttä, P., 2002. Svecofennian magmatic and metamorphic evolution in southwestern Finland as revealed by U-Pb zircon SIMS geochronology. Precambrian Research, 116, 111–127.

Väisänen, M., Eklund, O., Lahaye, Y., O'Brien, H., Fröjdö, S., Högdahl, K. and Lammi, M., 2012. Intra-orogenic Svecofennian magmatism in SW Finland constrained by LA-MC-ICP-MS zircon dating and geochemistry. GFF, 134, 99–114.

Modelling geotherms of the Wiborg rapakivi batholith in southeastern Finland in light of seismic data

T. Veikkolainen[1], T. Luhta[1] and I.T. Kukkonen[2]

[1]Institute of Seismology, Department of Geosciences and Geography, University of Helsinki, P.O. Box 68, FIN-00014 University of Finland
[2] Geology and Geophysics Research Program, Department of Geosciences and Geography, University of Helsinki, P.O. Box 68, FIN-00014 University of Finland
E-mail: toni.veikkolainen@helsinki.fi

This article analyzes the thermal and seismic properties of crust in the Wiborg rapakivi batholith. The area is also crossed by BALTIC, KOKKY, and SOFIC seismic profiles. Surface outcrops reveal a high radiogenic heat production (3.6 ± 1.2 μWm^{-3}) yet thermal modelling implies that this is limited to the upper crust (0...10 km) which is used in our three-layer model to approximate the depth extent of the batholith. The mantle heat flow constraint 12 ± 3 mWm^{-2} derived for the entire shield from xenolith data requires that heat production in the middle crust is 0.5 μWm^{-3} and in the lower crust (30...41 km) 0.3 μWm^{-3}. Seismicity takes place in distinct near-surface swarms within the batholith, mostly in its western part and along the coast of Gulf of Finland. Seismic cutoff depth is likely to represent a rheological transition towards a lithology with a higher gabbro-anorthosite concentration.

Keywords: heat flow, heat production, seismicity, rapakivi, crust

1. Introduction

The 1.65-1.63 Ga Wiborg rapakivi batholith (WRB) is the largest rapakivi area within the Fennoscandian shield. It is a product of intraplate anorogenic magmas, which intruded into the deeply eroded 1.8-1.95 Ga Svecofennian crust (Rämö and Haapala, 1995). The exceptionally strong crustal differentiation in the area is related to the bimodal magmatism, with felsic rocks originating from the lower crust and mafic rocks from the mantle.

The original tectonic interpretation of WRB derives from the BALTIC seismic profile crossing the area. It suggests that the rapakivi massif is a plate, about 10 km thick (Janik, 2010). The KOKKY (Kokkola-Kymi) profile based on quarry blasts of years 2012-2013 terminates at the eastern part of the batholith, although this part is too short to allow an in-depth geological interpretation including the determination of Moho depth (Tiira et al. 2020). New information of the structure of rapakivi area is being obtained from the SOFIC profile, which runs parallel to the south coast of Finland from Turku archipelago to Ylämaa. More than one third of the line, 120 km, is located on the rapakivi area.

2. Heat production and thermal models

Altogether 93 outcrop samples of Finnish lithogeochemical data show that WRB has a high heat production (3.6 ± 1.2 μWm^{-3}). No data from Russian side are available. Internal variation of heat production is little but contrasts to other nearby Finnish areas are sharp (Veikkolainen and Kukkonen, 2019).

Upper crustal heat production is an important parameter in thermal modelling, and various techniques have been applied in the calculation of geotherms. In WRB, it is not desirable to assume an exponential decrease of heat production by depth (Rybach and Cermák, 1987) because heat production is more or less dependent on rock type. A layered model with each layer representing a mixture of rock types is more useful, as layer boundaries are often visible in seismic cross-sections, and the mean heat production within a layer can be adjusted

by varying the proportions of different rocks. For thermal conductivity λ, a temperature dependence can be assumed from Equation 1:

$$\lambda = \lambda_0 \left[1/(1+bT) + c(T+273.15K)^3\right] \quad (1)$$

Here T is temperature [°C], λ_0 (2.9 $Wm^{-1}K^{-1}$) is thermal conductivity [$Wm^{-1}K^{-1}$] at the reference temperature of 25 °C and b (0.0008 K^{-1}) is a pre-selected empirical parameter, which depends on the lithology but is generally considered to be near the value 0.001 in crust. The factor c, representing radiative heat transfer, can be considered zero in typical crustal temperatures which do not exceed 800 °C (Kukkonen and Peltonen, 1999). Using constant heat production H within each layer, but temperature-dependent λ (Equation 1), steady-state temperature T at a depth of z can be solved using Equation 2:

$$T(z) = (1/b)\left\{(1+bT_0)\exp\left[\left(\frac{b}{\lambda_0}\right)\left(q_0 z - \frac{Hz^2}{2}\right)\right] - 1\right\} \quad (2)$$

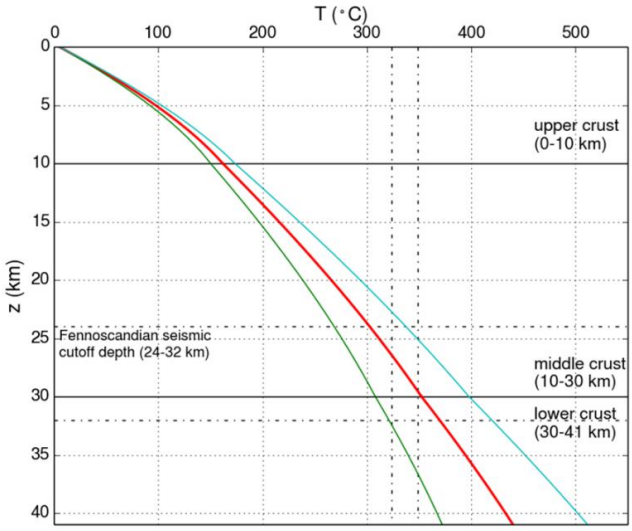

Figure 1. Geotherms corresponding to the three-layered model of crust of the rapakivi area. Red curve represents the situation with Q0 = 60.3 μWm^{-3}, green curve that with Q_0 = 57.3 μWm-3 and cyan curve that with Q_0 = 63.3 μWm^{-3}. Temperature-dependent thermal conductivity (Equation 2) and fixed heat production constraints are used for all layers. Dashed lines show the depth and temperature range of seismic cutoff depth in Fennoscandia (Veikkolainen et al. 2017).

We assume here T_0 = 5 °C and q_0 ~60 mWm^{-2}. For our purpose, a one-dimensional model in a three-layered crust is sufficient. For the upper layer (0...10 km) we can assume a mixture of rapakivi granites and gabbro-anorthosites with a very strong granitic dominance. Using H = 3.5 μWm^{-3} means that 3.3% of upper crust is gabbro-anorthosites and the rest is rapakivi granites. For the middle crust (10...30 km), we use H = 0.5 μWm^{-3} and for lower crust (30...41 km) H = 0.3 μWm^{-3} in line with the increasing content of mafic rocks.

Variation of surface heat flow between our models is produced to meet the fixed heat production constraints and the Moho heat flow, which is bound to be in the xenolith-derived

range 9...15 mWm^{-2} (Kukkonen and Peltonen, 1999). Using these constraints, three models with different surface heat flow values are generated (Figure 1).

The uncertainty over the Moho temperature in our models is ~70 °C, even though the surface heat flow variation is only ±3 mWm^{-2} between models. Although the uncertainty over λ_0 is also large, fortuitously it only affects the shape of geotherms, rather than heat flow, which is controlled by layer thicknesses and heat production within each layer.

3. Seismicity

Earthquake data in this study originates from the FENCAT catalogue (Ahjos and Uski, 1992; updates online), maintained by the Institute of Seismology of the University of Helsinki. FENCAT data can be fetched using the online search tool (https://www.seismo.helsinki.fi/EQ-search/query.php). To find out FENCAT data limited to the Finnish side of WRB, we used the 1 : 1 000 000 bedrock map of Finland, available for download at the Hakku service of the Geological Survey of Finland (https://hakku.gtk.fi). Earthquakes on the Russian side were not abundant, and could be assigned to the rapakivi area by using geological maps in literature (e.g. Rämö and Haapala, 1995; Karell et al. 2014).

Earthquakes within WRB are typically very shallow, with depths of 5 km or less. All of them have depths within the upper crust in our thermal models. In the last year, they have taken place in coastal towns of Kotka (4 events) and Hamina (4 events), but also in Kouvola (2 events) and Pyhtää (1 event). Seismicity is swarm-type and the best-studied examples of it derive from Anjalankoski (Uski et al. 2006) and Kuusaanlampi (Smedberg et al. 2012) areas of Kouvola. Nearly 200 events can be assigned to the same swarm in Kuusaanlampi area in December 2011 – January 2012. The majority of them was only detected by a temporary local network, not by the national network. The strongest earthquakes detected in WRB are related to the Kuusaanlampi swarm and they have magnitudes M=3.0 (December 1, 2011) and M=2.9 (December 22, 2011). On the Russian side of the batholith, a notable swarm has been located east of Wyborg. The middle part of the batholith is almost devoid of earthquakes.

In the first half of June 2019, five earthquakes ($0.9 \leq M \leq 1.8$) took place in Kouvola. Thereafter, an array of semi-permanent and temporary seismic stations has been operating in the area. Its data are expected to shed further light on active faults in the northwestern part of the batholith, in particular the Kuusaanlampi fault. For a map of earthquakes and heat production in WRB, see Figure 2.

4. Conclusions

Our thermal models favor the hypothesis of strong concentration of rapakivi granites in the upper crust. The estimated thickness of this layer is in agreement with results from forward ray tracing of BALTIC (Janik, 2010), KOKKY (Tiira et al. 2020) and SOFIC (analysis underway) profiles. Seismicity takes place where rapakivi granites dominate over rigid intermediate and mafic rocks, which are more prominent beneath.

In WRB, new seismic events often take place in same swarms where previous events have been found, because the rapakivi structure is already fractured and less resistant to stress. Geotherms suggest that in WRB, seismic cutoff takes place where crustal temperature is less than 200 °C. The range of 300-400 °C typically assigned for brittle-ductile transition in granitic lithology (Blanpied et al. 1991) does not apply, probably because the interface of granitic and gabbro-anorthositic rocks is closer to the surface.

The Wiborg rapakivi batholith, due to its sufficiently large size and internal homogeneity within its seismogenic zone, turns out to be a good natural test environment for swarm-type seismicity in Finland and beyond. However, due to the general rarity of seismic events there, a longer observation period and the deployment of temporary research networks will be required

to understand some features such as the apparent absence of seismicity in the middle part of the batholith and the extent of active faults.

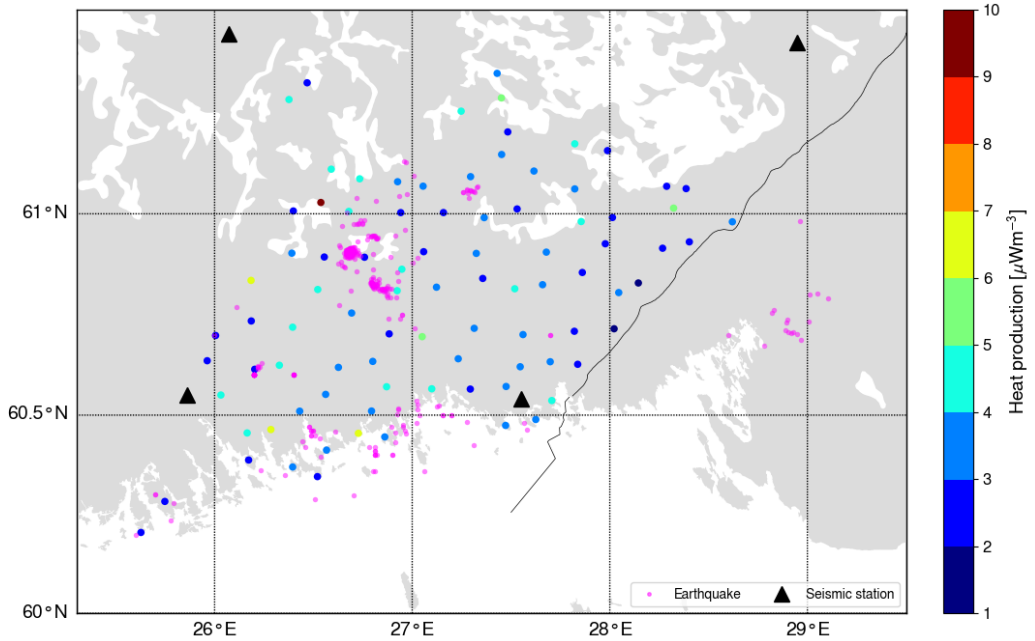

Figure 2. Earthquakes and heat production in the Wiborg rapakivi batholith. Data from the Ahvenisto, Onäs and Suomenniemi satellite intrusions are included. Locations of seismic stations within the batholith and adjacent areas are also visible.

References:

Ahjos, T., Uski, M., 1992. Earthquakes in northern Europe in 1375-1989. Tectonophysics 207, 1-23.

Blanpied,M.L., Lockner, D.A., Byerlee, J.D., 1991. Fault stability inferred from granite sliding experiments at hydrothermal conditions. Geophysical Research Letters, 18, 609-612.

Janik, T., 2010. Upper Lithospheric Structure in the Central Fennoscandian Shield: Constraints from P- and S-Wave Velocity Models and V_P/V_S Ratio Distribution of the BALTIC Wide-Angle Seismic Profile. Acta Geophysica 58, 543-586.

Karell, F., Ehlers, C., Airo, M.-L., 2014. Emplacement and magnetic fabrics of rapakivi granite intrusions within Wiborg and Åland rapakivi granite batholiths in Finland. Tectonophysics, 614, 31-43.

Kukkonen, I.T., Lahtinen, R., 2001. Variation of radiogenic heat production rate in 2.8–1.8 Ga old rocks in the central Fennoscandian shield. Physics of the Earth and Planetary Interiors 126, 279-294.

Kukkonen, I.T., Peltonen, P., 1999. Xenolith-controlled geotherm for the central Fennoscandian Shield: implications for lithosphere–asthenosphere relations. Tectonophysics 304, 301-315.

Rybach, L., Cermák, V., 1987. The depth dependence of heat production in the continental lithosphere, derived from seismic velocities. Geophysical Research Letters, 14, 311-313.

Rämö, O.T., Haapala, I., 2005. Rapakivi granites. In: Lehtinen, M., Nurmi, R.A., Rämö, O.T., 2005 (Eds.). Precambrian Geology of Finland - Key to the Evolution of the Fennoscandian Shield, Elsevier, 553-562.

Smedberg, I., Uski, M., Tiira, T., Komminaho, K., Korja, A., 2012. Intraplate earthquake swarm in Kouvola, south-eastern Finland, EGU General Assembly, Vienna, Austria, April 22-27, EGU2012-8446.

Tiira, T., Janik, T., Skrzynik, T., Komminaho, K., Heinonen, A., Veikkolainen, T., Väkevä, S., Korja, A., 2020. Full-Scale Crustal Interpretation of Kokkola-Kymi (KOKKY) Seismic Profile, Fennoscandian Shield. Pure and Applied Geophysics, 177, 3775-3795.

Uski, M., Tiira, T., Korja, A., Elo, E., 2006. The 2003 earthquake swarm in Anjalankoski, south-eastern Finland. Tectonophysics, 422, 55-69.

Veikkolainen, T., Kukkonen, I.T., 2019. Highly varying radiogenic heat production in Finland, Fennoscandian Shield. Tectonophysics, 750, 93-116.

Veikkolainen, T., Kukkonen, I.T., Tiira, T., 2017. Heat flow, seismic cut-off depth and thermal modeling of the Fennoscandian Shield, Geophysical Journal International, 211, 1414-1427.

The effects of assimilation on sulfide saturation and the formation of norite-hosted Cu-Ni deposits in the Duluth Complex, Minnesota

V. J. Virtanen[1], J. S. Heinonen[1], N. Barber[2] and F. Molnár[3]

[1]Department of Geosciences and Geography, University of Helsinki, Helsinki, Finland
[2]Department of Earth Sciences, University of Cambridge, Cambridge, UK
[3]Geological Survey of Finland, Espoo, Finland
E-mail: ville.z.virtanen@helsinki.fi

In this contribution, we use thermodynamically constrained geochemical models to study how black shale assimilation affected sulfide saturation and norite-hosted Cu-Ni deposit formation in the Duluth Complex (DC), Minnesota. These models show in unprecedented detail how progressive assimilation changes the chemical composition of the magma leading to earlier and increased sulfide saturation compared to pure fractional crystallization. The models indicate that at least half of the S in the wall-rock black shale must partition to the assimilated partial melt to form the norite-hosted Cu-Ni deposits. Against the general consensus, sulfide saturation seems to occur at temperatures too low for FeS sulfide melt formation, which explains the dominantly low-grade disseminated sulfide deposits in the DC.

Keywords: Sulfide saturation, Duluth Complex, Cu-Ni deposit, Magma Chamber Simulator

1. Introduction

Sulfide saturation is a process which occurs when the sulfur (S) content in a melt exceeds the amount that can be dissolved, and as a result, a liquid or solid sulfide phase forms. In addition to the absolute S content of the melt, composition and temperature (T) of the silicate melt affect the timing and degree of sulfide saturation (Smythe et al. 2017), and hence control the formation and grade of base metal (e.g., Cu and Ni) sulfide deposits.

In continental settings, mantle-derived magmas are typically sulfide undersaturated at the time of intrusion or extrusion. As these magmas cool and crystallize, they eventually reach sulfide saturation, and sulfides start to form in cotectic proportions. Such cotectic proportions are rarely high enough to form economical sulfide deposits. Accordingly, with few exceptions, all the economically important magmatic Cu-Ni deposits worldwide formed as magmas assimilated wall-rocks (Lesher, 2019).

Assimilation of S-bearing wall-rocks can directly increase the S content of the melt, but sulfide saturation can be further intensified by changes in the major element composition of the assimilating melt. Until recently, only the compositional effects of assimilating bulk wall-rocks or putative partial melts could be tested by simplified chemical mixing models. Consequently, the detailed effects of assimilation on sulfide saturation are largely unknown.

The Magma Chamber Simulator (MCS) is a thermodynamically constrained modelling tool designed especially for fractionally crystallizing (FC) magmas experiencing open system processes such as assimilation and/or magmatic recharge (Bohrson et al. 2014, Bohrson et al. 2020). Heat and mass balance between the magma, wall-rock, and possible recharge magmas are accounted for and phase equilibria are modelled accordingly. This provides a sophisticated approach for assimilation, where its continuous effect on compositional evolution of the magma can be monitored. Both major and trace elements (and isotopes) can be tracked within the different reservoirs in the model (Bohrson et al. 2020, Heinonen et al. 2020). Hence, the MCS

can provide new detailed insight into how assimilation-fractional crystallization (AFC) lead to formation of sulfide deposits.

We studied the differences in the silicate melt's ability to dissolve S during FC and AFC using the MCS and the sulfide saturation model of Smythe et al. (2017). Due to the lack of thermodynamic data on sulfides, S was modelled with the MCS trace element protocol (Heinonen et al. 2020). These models show in detail how assimilation of a progressively melting wall-rock effectively reduces the amount of S required for sulfide saturation. This together with excess S assimilated from the wall-rock leads to early sulfide saturation and an increased amount of sulfide precipitation in the magma.

2. Geological settings

The Duluth Complex (DC), Minnesota, is a 1.1 Ga composite mafic layered intrusion hosting some of the largest known Cu-Ni deposits in the world (Miller et al. 2002, Figure 1). All of the deposits are situated at the proximity of the footwall contact of the intrusions (Figure 1). Troctolitic cumulates host some 70% of the deposits consisting mostly of disseminated sulfides. The remaining 30% of the deposits consist of semi-massive to disseminated sulfides and are hosted by noritic rocks as well as footwall rocks and xenoliths. Based on S isotopes, it has been estimated that approximately 75% of the S in some of the deposits derived from the adjacent Paleoproterozoic Virginia Formation (VF) black shale, which contains 6000 ppm S on average (Ripley 1981, Rao and Ripley 1983, Figure 1).

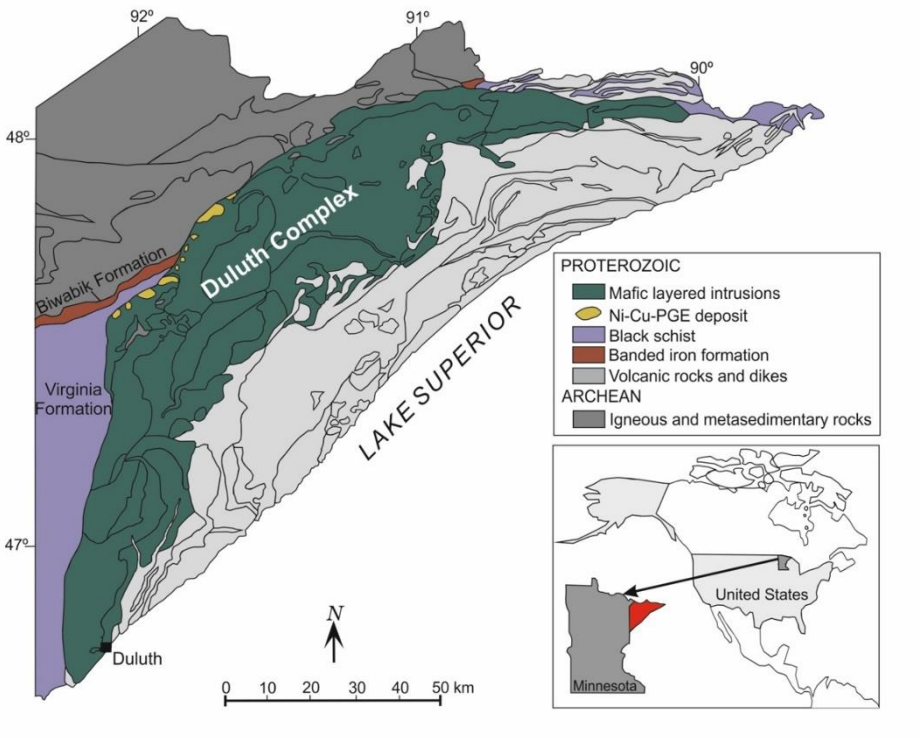

Figure 1. The geological map showing the Duluth Complex and the adjacent rocks.

3. The MCS and sulfide saturation model results

In the MCS models, we used composition of a cogenetic basalt from the North Shore Volcanic Group (Figure 1) as the parental magma for the DC intrusions. We set the initial oxygen fugacity to ΔFMQ -2 and tested different H_2O contents (dry to 2.25 H_2O) for the parental magma. The

modelled cumulate stratigraphies show that the amount of troctolitic cumulates (*sensu lato*) positively correlates with the H_2O content of the magma (Figure 2). Comparison with the natural cumulate from a DC intrusion (Severson et al. 1996) reveals that the magma must have been hydrous (≥ 1 wt.% H_2O) to produce the dominantly troctolitic cumulates (Figure 2).

The parental melt with 1 wt.% H_2O was used for the AFC models. The VF black shale (Figure 1) wall-rock was preheated to 600 °C and the initial wall-rock magma mass ratio was 0.5. In this model, norites replace troctolites after assimilation of ~20 wt.% (relative to parental melt) of wall-rock partial melts (Figure 2). The magma assimilates 38 wt.% of wall-rock partial melts in total until the T of the magma is too low for further assimilation. The subsequent FC produces first noritic (*sensu lato*) cumulates before the formation of anorthositic troctolite (Figure 2).

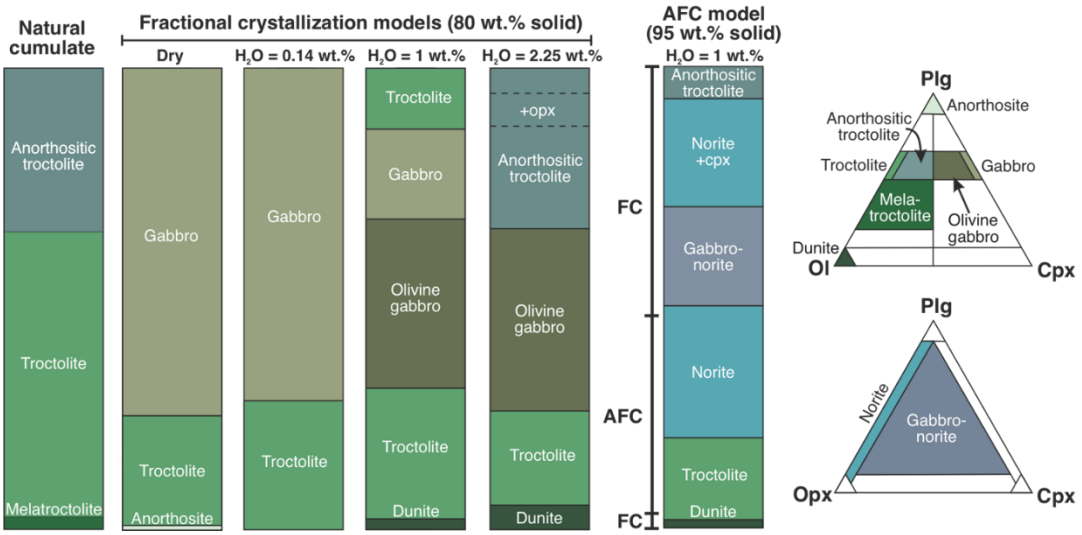

Figure 2. Natural cumulate stratigraphy (Severson et al. 1996) from the Duluth Complex compared with the cumulate stratigraphies produced after 80 wt.% of fractional crystallization (FC) in the models with different initial parental melt H_2O contents. The cumulate sequence (95 wt.% relative to the parental melt) formed in the assimilation fractional crystallization (AFC) model for the parental melt with 1 wt.% H_2O is shown on the right.

Sulfide saturation models for the parental melt with 1 wt.% H_2O and 800 ppm S experiencing FC and AFC are compared to show the effect of assimilation on S content at sulfide saturation (SCSS) in the magma. The initial S content in the wall-rock is 6000 ppm. The FC model reaches SCSS when ~27 wt.% of the melt has crystallized and T is ~1145 °C. When assimilation begins in the AFC model, the SCSS decreases rapidly relative to FC due to decreasing FeO and increasing H_2O content in the magma (Figure 3). In the model, where S is compatible (D^S = 100) to the residual wall-rock, the magma reaches SCSS at ~13 wt.% solids and T of ~1140 °C (Figure 3). When S is equally compatible to wall-rock residual and assimilated partial melt, the SCSS of the magma is reached at ~8 wt.% solids and T of ~1150 °C (Figure 3). If S is completely incompatible to the residual wall-rock (D^S = 0.001), the magma reaches SCSS when ~5 wt.% of the system has solidified and the T is ~1150 °C (Figure 3). In all cases, the T at SCSS is lower than the solidus of an FeS sulfide melt (~1190 °C). The maximum proportion of black-shale derived S in the magma is ~6 wt.% with D^S = 100, ~74 wt.% with D^S = 1, and 78 wt.% with D^S = 0.001.

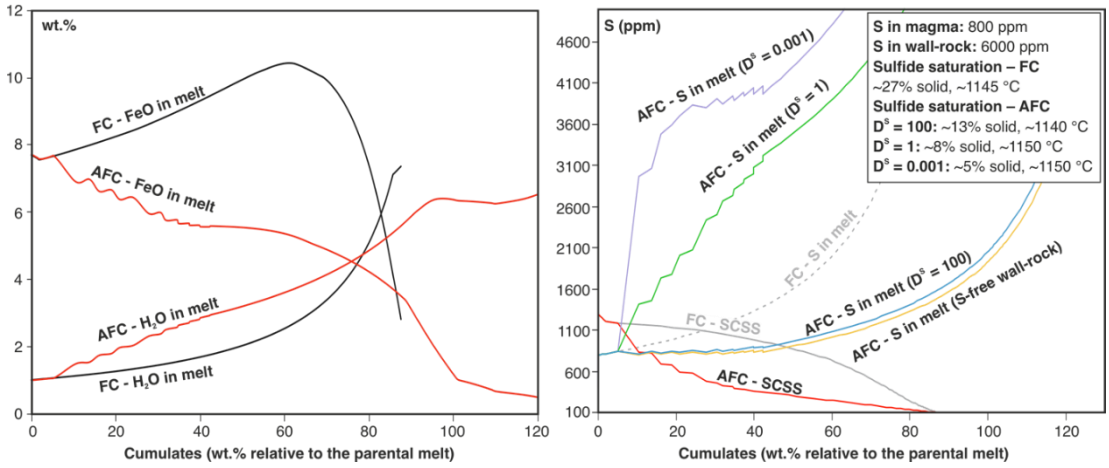

Figure 3. On the left, fractional crystallization (FC) and assimilation fractional crystallization (AFC) models for FeO and H_2O contents of the Duluth Complex parental magmas with 1 wt.% H_2O. On the right, S content at sulfide saturation (SCSS) are shown for the same models. The partition coefficients for S (D^S) are relative to wall-rock residual.

4. Conclusions

Our models show that the troctolitic cumulates of the DC likely formed by FC of a hydrous magma, whereas the formation of the noritic rocks requires >20 wt.% assimilation of partial melts from the VF black shale. To meet the isotopic criteria of ~75 wt.% black-shale derived S in the norite-hosted DC Cu-Ni deposits, at least half (wall-rock $D^S \leq 1$) of the VF S must partition to the assimilated partial melt. In all the models, SCSS is reached at T lower than FeS solidus indicating that only minor Cu-rich residual sulfide melt could have formed in the DC magmas. Coalescence of solid sulphides is ineffective, which is compatible with the dominantly low-grade Cu-Ni deposits.

References:

Bohrson, W.A., Spera, F.J., Ghiorso, M.S., Brown, G.A., Creamer, J.B., Mayfield, A., 2014. Thermodynamic Model for Energy-Constrained Open-System Evolution of Crustal Magma Bodies Undergoing Simultaneous Recharge, Assimilation and Crystallization: the Magma Chamber Simulator, J. Petrol., 55, 1685-1717.

Bohrson, W.A., Spera, F.J., Heinonen, J.S., Brown, G.A., Scruggs, M.A., Adams, J.V, Takach, M.K., Zeff, G., Suikkanen, E., 2020. Diagnosing open-system magmatic processes using the Magma Chamber Simulator (MCS): part I–major elements and phase equilibria. Contrib. Mineral. Petrol., 175:104, 29 pages.

Heinonen, J.S., Bohrson, W.A., Spera, F.J., Brown, G.A., Scruggs, M.A., Adams, J.V., 2020. Diagnosing open-system magmatic processes using the Magma Chamber Simulator (MCS): part II–trace elements and isotopes. Contrib. Mineral. Petrol., 175:105, 21 pages.

Lesher, C.M., 2019. Up, down, or sideways: emplacement of magmatic Fe-Ni-Cu-PGE sulfide melts in large igneous provinces. Can. J. Earth Sci. 56, 756–773.

Miller, J.D. Jr., Green, J.C., Severson, M.J., Chandler, V.W., Hauck, S.A., Peterson, D.M., Wahl. T.E., 2002. Geology and mineral potential of the Duluth Complex and related rocks of northeastern Minnesota. Minnesota Geological Survey Report of Investigations, 58, 207 pages.

Rao, B.V., Ripley, E.M., 1983. Petrochemical Studies of the Dunka Road Cu-Ni Deposit, Duluth Complex, Minnesota. Econ. Geol., 78, 1222–1238.

Ripley E.M., 1981. Sulfur Isotopic Studies of the Dunka Road Cu-Ni Deposit, Duluth Complex, Minnesota. Econ. Geol., 76, 610–620.

Severson, M.J., Patelke, R.L., Hauck, S.A., Zanko, L.M., 1996. The Babbitt Copper-Nickel Deposit Part C: Igneous Geology, Footwall Lithologies, and Cross-Sections. Univ. of Minnesota TR-91/21c, 68 pages.

Smythe, D.J., Wood, B.J., Kiseeva, S., 2017. The S content in silicate melts at sulfide saturation: New experiments and a model incorporating the effects of sulfide composition. Amer. Miner., 102, 795–803.

U-Pb zircon dating of igneous rocks in the Salo area, SW Finland

M. Väisänen[1], J. Kara[1], H. Penttinen[1], Y. Lahaye[2], H. O'Brien[2] and P. Skyttä[1]

[1]Department of Geography and Geology, FI-20014 University of Turku, Finland
[2]Geological Survey of Finland, FI-02150 Espoo, Finland
E-mail: markku.vaisanen@utu.fi

The bedrock of the Salo area in SW Finland is mainly occupied by granitoids. We dated five granitoids and two mafic volcanic rocks with single zircon method. The granitoids fall in two age groups, 1.86–1.85 and 1.83–1.82 Ga. Mafic plutonic rocks occur in both age groups. The volcanic rocks are 1.90 and 1.89 Ga in age. Further, the samples display two periods of metamorphic zircon growth at 1.86 and 1.83 Ga, synchronous with the granitoid magmatism.

Keywords: U-Pb, zircon, granitoids, metamorphism

1. Introduction

The Svecofennian bedrock in the Salo area in SW Finland defines a 30x40 km wide rhomboidal-shaped map area dominated mainly by plutonic rocks intercalated by minor migmatitic paragneisses, mafic volcanic rocks and calcareous gneisses. In the northern part, the granitoids are granites, granodiorites and minor quartz diorites, while the southern part is occupied by the porphyric Perniö granite (Figure 2).

Opposing to the surrounding areas, the Salo area is characterised by gently-dipping structures, including common isoclinal recumbent folds within paragneisses and volcanic rocks. These folds are intruded by subhorisontal sheets of granitoids (Figure 1; Aho et al. 2014).

Figure 1. Subhorisontal supracrustal rocks and granitoids along the E18 motor way road cut in the Salo area.

In this project we performed age determinations on different igneous rocks across the study area. Some previous zircon results are presented in Penttinen et al. (2016) and Penttinen (2019), which are shown in Figure 2. In this contribution we present additional seven zircon age determinations. The analyses were performed in the Finnish Geosciences Research Laboratory at the Geological Survey of Finland, Espoo, using the LA-MC-ICP-MS method, except for the Paimio gabbro and granodiorite samples which were analysed with the LA-SC-ICP-MS method.

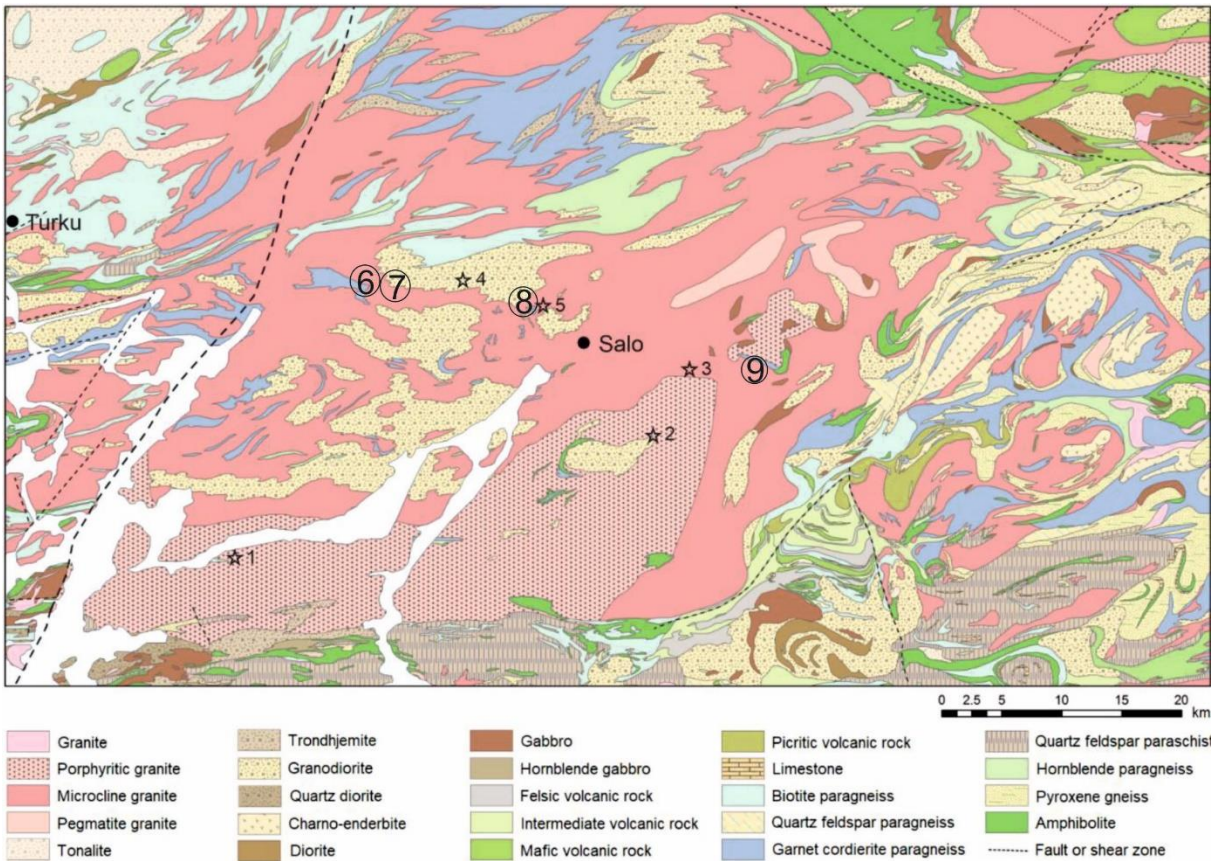

Figure 2. Geological map of the Salo area, modified after Bedrock map of Finland, DigiKP and Penttinen (2019). Sampling locations indicated: 1) Perniö granite, Pungböle (c. 1.84 Ga; Kurhila et al. 2005), 2) Perniö granite, Kistola (c. 1.85 Ga; Kurhila et al. 2010), 3) Muurla granite (1.82 Ga; Penttinen 2019) and Muurla gabbro (c. 1.83; Väisänen et al. 2014), 4) Hiittenmäki granite (c. 1.86 Ga; Penttinen et al. 2016, Penttinen 2019), 5) Hurtinmäki granite (c. 1.85 Ga; Penttinen et al. 2016, Penttinen 2019), 6) Paimio granodiorite and gabbro (this study), 7) Ilttula granite (this study) 8) Hurtinmäki mafic volcanic rock (this study), 9) Kruusila mafic volcanic rock, Kruusila granite and Kruusila pegmatite (this study).

2. Results

Seven U-Pb zircon age determinations are presented. The sampling locations are shown in Figure 2 and the results are summarized in Table 1.

3. Discussion

The oldest igneous rocks in the Salo area are the two dated volcanic rocks from Hurtinmäki and Kruusila, 1.89 and 1.90 Ga, respectively. The latter is the oldest volcanic rock so far discovered in Southern Svecofennia (cf. Kara et al. 2018). The plutonic rocks are of two ages, 1.86–1.85 and 1.83-1.82 Ga. The 1.83-1.82 Ga granites resemble the common migmatising granites in southern Finland (e.g. Ehlers et al. 1993, Skyttä & Mänttäri 2008, Kurhila et al. 2010). However, the Perniö granite in the southern part of the area seems to be slightly older (Figure 2). Previously found 1.86–1.85 Ga magmatism in southern Finland has occurred as minor dykes

and sills (Väisänen et al. 2012; Nevalainen et al. 2014; Kara et al. 2020). Therefore, the Salo area rather resembles the Ljusdal batholith in central Sweden where 1.86 Ga granitoids are common (Högdahl et al. 2008).

Table 1. Overview of the age results of this study.

Sample name	ID/Figure 2	Rock type	Setting	Age (Ga)
Paimio	6	Granodiorite	Plutonic	1.86 Ga
Paimio	6	Gabbro	Rounded enclaves in granodiorite	1.86 (core), 1.83 (rim)
Ilttula	7	Granite	Dyke along fold axial surface	1.81
Hurtinmäki	8	Intermed.-mafic volcano-sedim. rock	banded	from 2.1 to 1.91 (inherited) 1.89 major cluster 1.86 & 1.83 younger populations
Kruusila	9	Mafic volcanic rock	layered	1.92 (inherited); 1.90 major group 1.86 & 1.83 younger populations
Kruusila	9	Granite	Subhorisontal sheet	1.82
Kruusila	9	Pegmatite	Steeply crosscutting dyke	1.82

A conspicuous feature is the lack of evidence for the 1.88 Ma magmatism in the area, which is after all the main crustal growth period in the Svecofennian orogen (e.g. Korsman et al. 1999). The rhomboidal shape of the Salo area resembles a pull-apart basin evoking a question whether the area originally formed by extension of older Svecofennian orogeny (see the orogenic collapse model of Lahtinen et al. 2005 and the retreating subduction zone model of Hermansson et al. 2008).

Two younger ages (1.86 and 1.83 Ga) found in the older rocks are interpreted to be metamorphic. The 1.86 Ga metamorphic age has not previously been found but it is very logical regarding the amount of 1.86 Ga granitoids in the area. The 1.83-1.82 Ga metamorphic age is comparable to other lateorogenic ages elsewhere in southern Finland (Väisänen et al. 2002, Mouri et al. 2005). Both 1.86 and 1.82 Ga metamorphic events also have corresponding magmatic events. Both thermal pulses also contain mafic magmatism, exemplified by the Paimio gabbro (this study) and the Muurla gabbro (Väisänen et al. 2014). The connection of mafic magmatism and metamorphism suggests that the mafic magmatism together with radioactive decay (Kukkonen and Lauri 2009) is a possible heat source for high heat flow needed for melting.

References:

Aho, R., Kauti., T., Penttinen, H., Skyttä, P., Väisänen, M., 2014. A multi-disciplinary approach to unravel the tectonic setting of the bedrock in the Salo area, SW Finland. In: Lithosphere 2014 Symposium, November 4-6, 2014, Turku, Finland. Institute of Seismology, University of Helsinki, Report S-62, 1-4.

Bedrock of Finland – DigiKP200. Digital map database [Electronic resource]. Geological Survey of Finland [accessed 5.11.2015].

Ehlers, C., Lindroos, A., Selonen, O., 1993. The late Svecofennian granite-migmatite zone of southern Finland—a belt of transpressive deformation and granite emplacement. Precambrian research, 64, 295-309.

Hermansson, T., Stephens, M. B., Corfu, F., Page, L. M., Andersson, J., 2008. Migratory tectonic switching, western Svecofennian orogen, central Sweden: Constraints from U/Pb zircon and titanite geochronology. Precambrian Research, 161, 250-278.

Högdahl, K., Sjöström, H., Andersson, U. B., Ahl, M., 2008. Continental margin magmatism and migmatisation in the west-central Fennoscandian Shield. Lithos, 102, 435-459.

Kara, J., Väisänen, M., Heinonen, J. S., Lahaye, Y., O'Brien, H., Huhma, H., 2020. Tracing arclogites in the Paleoproterozoic Era–A shift from 1.88 Ga calc-alkaline to 1.86 Ga high-Nb and adakite-like magmatism in central Fennoscandian Shield. Lithos, 372, 105663.

Kara, J., Väisänen, M., Johansson, Å., Lahaye, Y., O'Brien, H., Eklund, O., 2018. 1.90-1.88 Ga arc magmatism of central Fennoscandia: geochemistry, U-Pb geochronology, Sm-Nd and Lu-Hf isotope systematics of plutonic-volcanic rocks from southern Finland. Geologica Acta, 16, 1-23.

Korsman, K., Korja, T., Pajunen, M., Virransalo, P., GGT/SVEKA Working Group, 1999. The GGT/SVEKA transect: structure and evolution of the continental crust in the Paleoproterozoic Svecofennian orogen in Finland. International Geology Review, 41, 287-333.

Kukkonen, I. T., Lauri, L. S., 2009. Modelling the thermal evolution of a collisional Precambrian orogen: High heat production migmatitic granites of southern Finland. Precambrian Research, 168, 233-246.

Kurhila, M., Andersen, T., & Rämö, O. T., 2010. Diverse sources of crustal granitic magma: Lu–Hf isotope data on zircon in three Paleoproterozoic leucogranites of southern Finland. Lithos, 115, 263-271.

Kurhila, M., Vaasjoki, M., Mänttari, I., Rämo, T., Nironen, M., 2005. U-Pb ages and Nd isotope characteristics of the lateorogenic, migmatizing microcline granites in southwestern Finland. Bulletin of the Geological Society of Finland, 77, 105-128.

Lahtinen, R., Korja, A., Nironen, M., 2005. Paleoproterozoic tectonic evolution. In: Developments in Precambrian Geology, 14, 481-531.

Mouri, H., Väisänen, M., Huhma, H., Korsman, K., 2005. Sm-Nd garnet and U-Pb monazite dating of high-grade metamorphism and crustal melting in the West Uusimaa area, southern Finland. GFF, 127, 123-128.

Nevalainen, J., Väisänen, M., Lahaye, Y., Heilimo, E., Fröjdö, S., 2014. Svecofennian intra-orogenic gabbroic magmatism: a case study from Turku, southwestern Finland. Bulletin of the Geological Society of Finland, 86, 93-112.

Penttinen, H., 2019. Svecofennian granitic magmatism in the Salo area, SW Finland − in situ U−Pb age determinations on zircon and monazite. Master's Thesis, University of Turku, Finland, 90 p.

Penttinen, H., Kara J., Väisänen, M., Lahaye, Y., O'Brien H., 2016. 1.86 Ga granites in the Salo area, SW Finland. 32nd Nordic Geological Winter Meeting, 13-15.1.2016, Helsinki, Finland. Bulletin of the Geological Society of Finland, Special Volume, 167-168.

Skyttä, P., Mänttäri, I., 2008. Structural setting of late Svecofennian granites and pegmatites in Uusimaa Belt, SW Finland: Age constraints and implications for crustal evolution. Precambrian Research, 164, 86-109.

Väisänen, M., Eklund, O., Lahaye, Y., O'Brien, H., Fröjdö, S., Högdahl, K., Lammi, M., 2012. Intra-orogenic Svecofennian magmatism in SW Finland constrained by LA-MC-ICP-MS zircon dating and geochemistry. GFF, 134, 99-114.

Väisänen, M., Mänttäri, I., Hölttä, P. 2002. Svecofennian magmatic and metamorphic evolution in southwestern Finland as revealed by U-Pb zircon SIMS geochronology. Precambrian Research, 116, 111-127.

Väisänen, M., Simelius, C., O'Brien, H., Kyllästinen, M., Mattila, J., 2014. Late Svecofennian mafic magmatism in southern Finland. In: Lithosphere 2014 Symposium, November 4-6, 2014, Turku, Finland. Institute of Seismology, University of Helsinki, Report S-62, 107-110.

Numerical Modelling of Oblique subduction in the Southern Andes region

Y. Wang[1] and D. Whipp[1]

[1]Institute of Seismology, Department of Geosciences and Geography, University of Helsinki
E-mail: yijun.wang@helsinki.fi

The Southern Andes has been an ideal region to study strain partitioning behavior due to the variable nature of its subduction geometry and variations in the structural and mechanical properties of the continental crust. The Liquine-Ofqui Fault Zone, located in the central Southern Andes, is characterized by the presence of a set of margin-parallel and margin-oblique faults that accommodate oblique plate convergence, and is a region where previous analog models have captured this faulting behavior. Here, we use numerical geodynamic models to reproduce the results of these analog experiments and expand on them using equivalent models scaled to natural dimensions. Our experiments reproduce results similar of the earlier analog models (at both scales) and confirm that the displacement field in the LOFZ can be related to a southward decrease in crustal strength.

Keywords: lithosphere, crust, Andes, strain partitioning, numerical modeling, geodynamics

1. Background

Along the plate margin between the subducting Nazca plate and the South American plate (Figure 1), the strain partitioning behavior varies from north to south, while the plate convergence vector shows little change. The study area for this work, the Liquine-Ofqui Fault Zone (LOFZ) (Figure 1), lies between 38ºS to 46ºS in the Southern Andes around 100 km inland from the trench. This region has been characterized as an area bounded by margin-parallel strike-slip faults that creates a forearc sliver, the Chiloe block (Herve, 1976). It is also located on top of an active volcanic zone, the Southern Volcanic Zone (SVZ) (Lopez Escobar et al., 1995). This area is notably different from the Pampean flat-slab segment directly to the north of it (between latitude 28º S and 33º S), where volcanic activity is absent, and slip seems to be accommodated completely by oblique subduction (Siame et al., 2005).

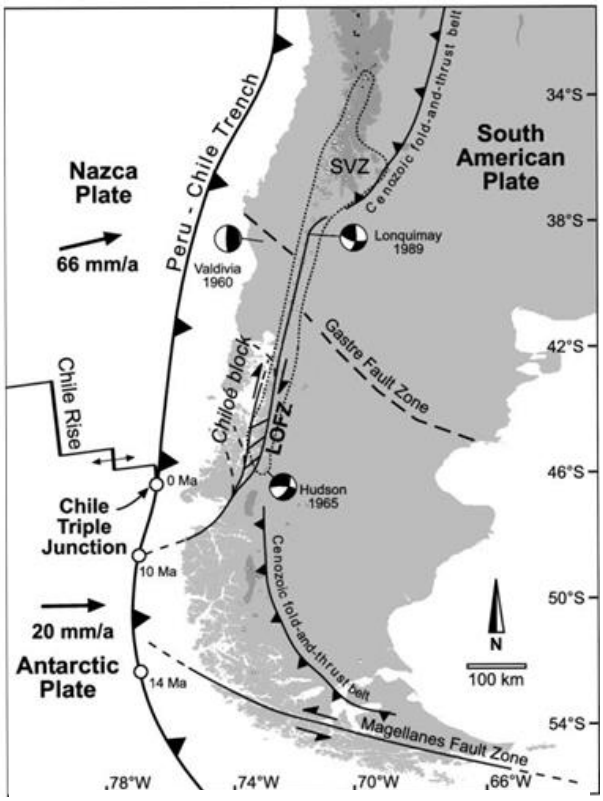

Figure 4. Plate convergence geometries and other key structures including the study area Liquine-Ofqui Fault Zone (LOFZ). Adapted from Rosenau et al., (2006).

Seismicity in central LOFZ is spatially correlated with NE trending margin-oblique faults that are similar to the structure of SC-like kinematics described by Hippertt (1999). This network of faults encloses sigmoid-shaped domains that are less deformed and rotated, which could accommodate regional simple shear

(Melnick et al. 2006a; Rosenau et al. 2006; Hernandez-Moreno et al., 2014). The margin-oblique faults and rhomb-shaped domains have also been captured in analog experiments by Cembrano et al. (2005) and Eisermann et al. (2018) and Eisermann et al. (2018) relates the change in GPS velocity at the northern end of LOFZ to a decrease in crustal strength southward possibly caused by the change in subduction dip angle.

2. Numerical modeling

This project uses DOUAR (Braun et al. 2008), a numerical geodynamic modelling program, to explore the formation of the complex fault system in the LOFZ in relation to strain partitioning in the Southern Andes. To test the possibility to reproduce analog modelling results with numerical models, we implement the numerical versions of the analog models from Eisermann et al. (2018), which we refer to as the MultiBox experiments and equivalent models at the scale of the natural system, which we refer to as the NatureBox models. We also create simplified models of the LOFZ, the Natural System models, to compare the model displacement field with deformation pattern in the area.

3. Results and Conclusions

Our numerical model results replicate the general findings from MultiBox experiments of Eisermann et al. (2018). We observe the formation of NW trending margin-oblique faulting in the central deformation zone, which creates rhomb-shaped blocks together with the margin-parallel faults (Figure 2). More strain is accommodated in the stronger part of the model, where the strain prefers to settle on a few larger shear zones, whereas in the weaker part of the model, the strain is more distributed and tends to localize on smaller faults.

In contrast to the MultiBox or NatureBox models, the margin-oblique faults and rhomb-shaped domains accommodating strain are not present in the Natural System models irrespective of a difference in crustal strength along strike. This raises the question about the formation of the complex fault system in both the analog models and our MultiBox/NatureBox numerical models and suggests factors other than an along-strike strength gradient should be tested in the future.

References:

Braun, J., Thieulot, C., Fullsack, P., DeKool, M., Beaumont, C., Huismans, R., 2008. DOUAR: A new three-dimensional creeping flow numerical model for the solution of geological problems. Physics of the Earth and Planetary Interiors, 171(1-4):76–91.

Cembrano, J., Gonzalez, G., Arancibia, G., Ahumada, I., Olivares, V., Herrera, V., 2005. Fault zone development and strain partitioning in an extensional strike-slip duplex: A case study from the Mesozoic Atacama fault system, Northern Chile. Tectonophysics 400 (1e4), 105e125.

Herve, M., 1976. Estudio geologico de la falla Liquine-Reloncavı en la area de Liquiñe: Antecedentes de un movimiento transcurrente (Provincia de Vadivia), Actas Congr. Geol. Chil. I, 1(B), 39 – 56.

Hippertt, J., 1999. Are S-C structures, duplexes and conjugate shear zones different manifestations of the same scale-invariant phenomenon, J. Struc. Geol., 21, 975 – 984, doi:10.1016/S0191- 8141(99)00047-4.

López-Escobar, L., Cembrano, J., Moreno, H., 1995. Geochemistry and tectonics of the Chilean southern Andes Quaternary volcanism (37 – 46S), Rev. Geol. Chile, 22(2), 219 – 234.

Rosenau, M., Melnick, D., Echtler, H., 2006. Kinematic constraints on intra-arc shear and strain partitioning in the Southern Andes between 38°S and 42°S latitude. Tectonics 25 TC4013 10.1029/2005TC001943

Siame, L. L., Bellier, O., Se´brier, M., Araujo, M., 2005. Deformation partitioning in flat subduction setting: Case of the Andean foreland of western Argentina (28S – 33S), Tectonics, 24, TC5003, doi:10.1029/2005TC001787.

The thickness of the Earth's crust in the territory of Republic of the Niger according to the stochastic interpretation of the gravity field

I.A. Yacouba[1] and V.N. Glaznev[1]

[1]Voronezh State University, Voronezh, Russia
E-mail: yibrahimabdou@yahoo.fr

In this article we describe the method of generalizing the data of terrestrial gravity survey and satellite gravimetric measurements in order to create a generalized digital model of the field for the territory of Republic of the Niger. The resulting composite gravity anomalies map was used to estimate the thickness of the Earth's crust based on stochastic field models with random sources in the horizontal layer. The resulting map of the Moho border depth is compared with the data of the CRUST1 model.

Keywords: gravity field, stochastic interpretation, Earth's crust, Republic of the Niger

1. Introduction

In the territory of Republic of the Niger and the surrounding countries of West Africa, there were virtually no deep seismic soundings aimed at studying the structure of the crust and the depth position of the crust-mantle boundary. Generalized data on the structure of the lithosphere, obtained from the results of seismological tomography and receiver function analysis, for example Begg et al. (2009), Globig et al. (2016), Jessell et al. (2016), Laske et al. (2013), Pasyanos et al. (2014), allowed making very approximate models of the structure of the earth's crust for the study area. The available data of gravimetric interpretation of satellite gravity data are also not highly accurate in determining the depth of the Moho boundary Bagherbandi and Sjoberg (2012), Reguzzoni et al. (2013), Tedla et al. (2011). The proposed work examines the methods and results of estimates the model thickness of the Earth's crust for the territory of the Republic of the Niger in the absence of detail data from deep seismic soundings of the crust and weak land gravimetric study.

The purpose of this article is to compile ground and satellite data of the gravity field intended to study the Earth's crust in the conditions of incomplete original geological and geophysical information. The task of the subsequent interpretation of the detected gravity anomalies is to create an updated pattern of thickness of the Earth's crust of the territory of Republic of the Niger, for which to date several significantly different variants of the crust structure are known. Gravity data will form the basis for a detailed study of the geological structure of the upper crust, as shows in Glaznev et al. (2015), Mints et al. (2020), and the identification of the links of its geological features with the location of the main minerals that play an important role in the economy of Republic of the Niger.

2. Data

The regional survey of the gravitational field in the Territory of Republic of the Niger was carried out in the mid-sixties by French geophysicists Rechenmann and Louis (1966). The survey was carried out on a system of profiles with a link to the system of reference geodesic and gravimetric points. In total, more than 14,500 observations were made with the accuracy of the field approximately 0.1 mGal. The total error of the survey was no more than 0.5 mGal,

which allowed to build a map of gravitational anomalies in the Bouguer reduction for the studied territory in a scale of 1000,000. These mapping materials were used by us to create a digital model of the anomalous gravitational field of the territory. The data of observations were digitized in the ArcGIS system, which allowed to compile a consolidated catalog of gravitational field observation points in geographical coordinates.

Because the main focus of our research is the territory of Republic of the Niger, the most reasonable is the use land gravity data and data from gravity model EGM2008, Pavlis et al. (2012), for the surrounding territories. This composite synthetic model of the gravity field in the Bouguer reduction served as the basis for the tasks of regional gravimetric modelling. The digital gravity model was built from a composite synthetic model for a regular network with a spatial resolution of 5 km. At the interpolation stage of the consolidated materials of the survey, the harmonic averaging of the data was used in the relatively narrow buffer zone of the surveys, so that there were no sharp-gradient field jumps at the boundaries of areas with different data representation. The gravity field scheme is shown in Figure 1.

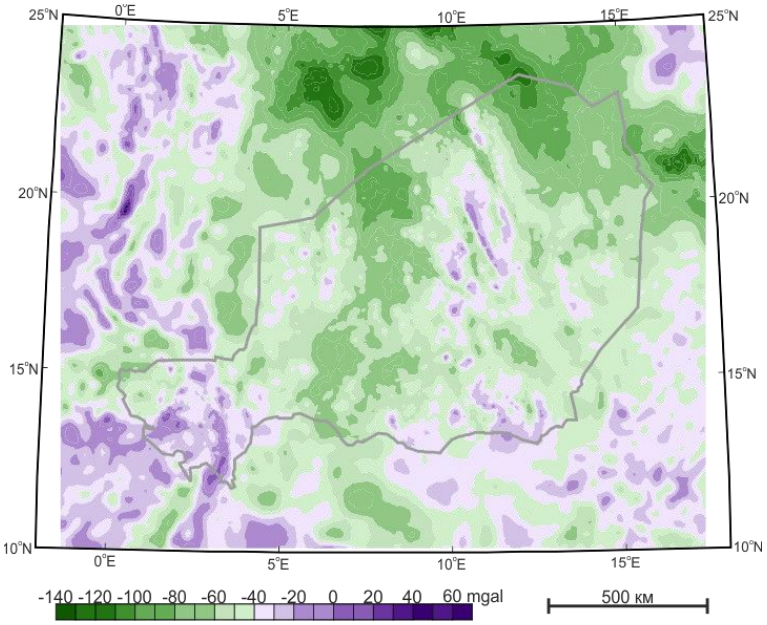

Figure 1. Scheme of the gravity field in the Bouguer reduction for study area.

3. Method

The thickness of the Earth's crust was assessed using the autocorrelation functions of the gravity field. In a three-dimensional case, for the arbitrary random isotropic distribution of singular sources in a horizontal layer with some symmetrical uncorrelated density distribution, the expression of the normalized autocorrelation function of the random gravitational field generated by such a model is known Glaznev (2003), Glaznev et al. (2014). This expression has the form of:

$$\boldsymbol{B_N(\tau, h, H) = \frac{2hH}{H-h}\left(\frac{1}{\sqrt{4h^2+\tau^2}} - \frac{1}{\sqrt{4H^2+\tau^2}}\right)}$$

Here *h* and *H* are the depth to the upper and lower boundary of the layer, and the τ is the correlational function argument for the average circumference of the gravity field.

To estimate the thickness of the Earth's crust in a sliding window (300 by 300 km), a two-dimensional autocorrelation function of the gravity field was calculated and compared with the theoretical model of the correlation function. An example of this interpretation for one site of

the map is presented in Figure 2, which shows the calculated two-dimensional normalized autocorrelation function of the field and the actual estimate of the thickness of the earth's crust on the criterion of the minimal differences between calculated and theoretical correlation functions. Of course, the results of the stochastic interpretation should be considered as an appropriate assessment of the depths of the upper and lower boundaries within the accepted model.

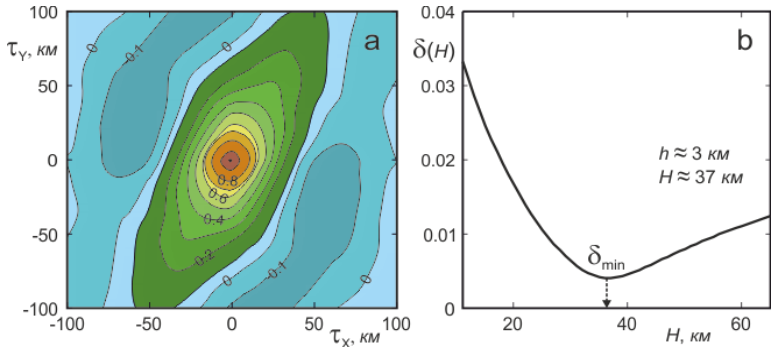

Figure 2. An example of a stochastic estimates of the thicknesses of the Earth's crust: (a) a two-dimensional normalized autocorrelation function of the gravity field, calculated in a sliding window; (b) a type of cross-section function δ (*H*) to estimate the depth of the bottom boundary of the *H* layer, at a given size of its upper limit *h*.

4. Results and discussion

According to the proposed method, the gravitational field of the research area (with partial exit outside the allocated site) for 130 provisions of the sliding window of calculations was processed. The shifting position of the sliding window was half its width - 150 km. With the relatively isotropic distribution of the field, the calculation of the circumference of the auto-correlation function, or one-dimensional projection of this function in the direction with a minimum correlation radius, allows to obtain meaningful estimates of the depth of the Moho boundary within the accepted model. However, in some cases, the calculated two-dimensional autocorrelation function demonstrated significant anisotropy of the original gravity field in the current window, which does not allow to reliably estimate the depth of the model layer.

The constructed scheme of the thicknesses of the Earth's crust, compared with the results of previous work to determine the thickness of the earth's crust, demonstrates significant differences in the models of the crust, especially in the eastern part of the region. The statistical analysis of the received estimates of the Earth's crust thickness and the averages elevations shows some trend of communication between these parameters, which allows us to conclude a partial isostatic compensation for large blocks of the region's crust. The analysis of data on the crust thickness and the scheme of surface geological and tectonic elements of the study territory allowed to map out the connection between the geodynamic evolution of the crust with the position of the Moho boundary.

5. Conclusions

The synthetic model of the gravitational field in the Bouguer reduction serves as a reliable basis for solving the problems of regional gravimetric modeling. The results of the stochastic interpretation of the gravity field of the region allowed to obtain estimates of the Earth's crust thicknesses of the studied territory within the accepted model of the layer with the random distribution of density heterogeneities. Comparison of the received estimates of the crust thickness with the data of the model CRUST1 (Figure 3) demonstrates a significant discrepancy

of the latters for the study area. The analysis of new data on the Earth's crust thickness allowed us to identify the features of the deep structures of the lithosphere blocks identified with large elements of the geological and tectonic scheme of the territory of Republic of the Niger.

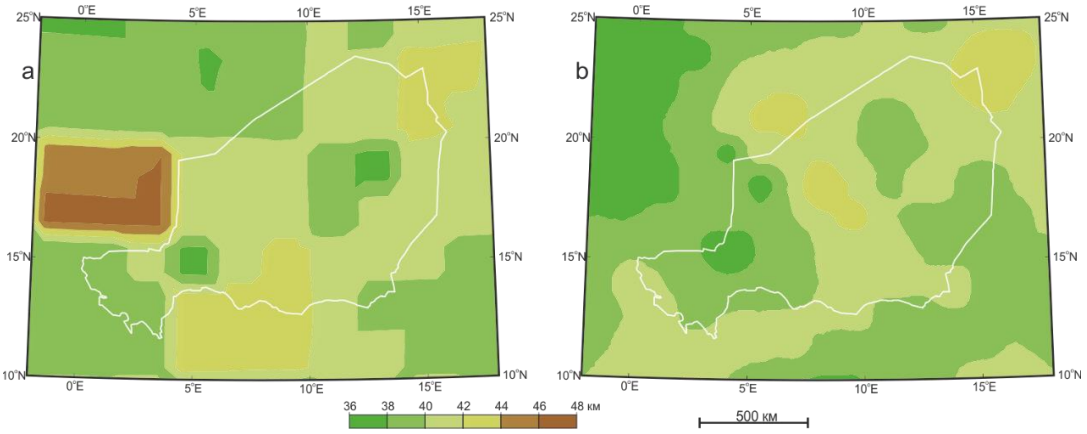

Figure 3. Estimates of the thickness of the earth's crust: (a) the CRUST1 model, Laske et al. (2013); (b) our results of the stochastic interpretation of the gravity field. Schemes are given in a single color scale.

References:

Bagherbandi, M., Sjoberg, L.E., 2012. Modelling the density contrast and depth of the Moho discontinuity by seismic and gravimetric–isostatic methods with an application to Africa, J. of Afr. Earth Sci., 68, 111–120.

Begg, G.C., Griffin, W.L., Natapov, L.M., O'Reilly, S.Y., Grand, S.P., O'Neill, C.J., Hronsky, J.M.A., Djomani, Y.P., Swain, C.J., Deen, T., Bowden, P., 2009. The lithospheric architecture of Africa: seismic tomography, mantle petrology and tectonic evolution, Geosphere, 5(1), 23–50.

Glaznev, V.N., 2003. Complex geophysical models of the Fennoscandian lithosphere, Apatity, «K&M». 252 pages. (in Russ.).

Glaznev, V.N., Mints, M.V., Muravina, O.M., Raevsky, A.B., Osipenko, L.G., 2015. Complex geological–geophysical 3D model of the crust in the southeastern Fennoscandian Shield: Nature of density layering of the crust and crust–mantle boundary, Geodyn. & Tectonophys., 6(2), 133-170.

Glaznev, V.N., Muravina, O.M., Voronova, T.A., Holin, V.M., 2014. Assessment of the gravity-active layer of the Earth's crust of the Voronezh crystalline massive, Proc. of Voronezh St. Univ., Ser.: Geol., 4, 78–84. (in Russ.).

Globig, J., Fernandez, M., Torne, M., Verges, J., Robert, A., Faccenna, C., 2016. New insights into the crust and lithospheric mantle structure of Africa from elevation, geoid, and thermal analysis, J. Geophys. Res., Solid Earth, 121. 5389–5424.

Jessell, M.W., Begg, G..C., Miller, M.S., 2016. The Geophysical Signatures of the West African Craton, Precam. Res., 274(3), 3-24.

Laske, G.., Masters, G.., Ma, Z., Pasyanos, M., 2013. Update on CRUST1.0 - A 1-degree Global Model of Earth's Crust, Geophys. Res. Abstr., 15, 2658.

Mints, M.V., Glaznev, V.N., Muravina, O.M., Sokolova, E.Yu., 2020. 3D model of Svecofennian Accretionary Orogen and Karelia Craton based on geology, reflection seismics, magnetotellurics and density modelling: Geodynamic speculations, Geoscience Frontiers, 11(3), 999-1023.

Pavlis, N.K., Holmes, S.A., Kenyon, S.C., Factor, J.K., 2012. The development and evaluation of the Earth Gravitational Model 2008 (EGM2008), J. Geophys. Res., Solid Earth, 117, B04406.

Pasyanos, M.E., Masters, G., Laske, G., Ma, Z., 2014. LITHO1.0: An updated crust and lithospheric model of the Earth, J. Geophys. Res., Solid Earth, 119, 2153–2173.

Rechenmann, J., Louis, P., 1966. Mesure gravimetriques dans le Niger orienta. Années 1963 - 1964 – 1965, Rap. Off. de la Rech. Sci. et Tech. Outre–Mer, Paris, 83 pages.

Reguzzoni, M., Sampietro, D., Sanso, F., 2013. Global Moho from the combination of the CRUST2.0 model and GOCE data, Geophys. J. Int., 195(1), 222–237.

Tedla, G.E., Meijde, M., Nyblade, A.A., Meer, F.D., 2011. A crustal thickness map of Africa derived from a global gravity field model using Euler deconvolution, Geophys. J. Int., 18, 1-9.

Forward and inverse modelling of terrestrial cosmogenic nuclides to detect past glaciations

L. Ylä-Mella[1], I. Kukkonen[1] and D. Whipp[2]

[1] Geology and Geophysics Research Program, Department of Geosciences and Geography, University of Helsinki
[2] Institute of Seismology, Department of Geosciences and Geography, University of Helsinki
E-mail: lotta.yla-mella@hotmail.com

Terrestrial cosmogenic nuclides can be used date to exposed surfaces. The concentration of the nuclides increases with exposure time and decreases with depth. In theory, samples from a depth profile can be used to detect also earlier exposure and coverage periods such as during and between previous glaciations. We tested this theory using artificial samples whose concentrations were calculated with a forward model, and then used an inverse model to attempt to detect past glaciation histories. Our results show that it is possible to detect past glaciations if the constraints set for the inverse solutions are strict enough (i.e. limited duration of glaciation and small dating uncertainty) or when sampling with a depth profile is used.

Keywords: cosmogenic nuclides, glaciation, forward model, inverse model

1. Introduction

Glaciations have shaped landscapes through the history of Earth. Glacial periods have occurred frequently, however, from a geological point of view, we often have information only from the latest glaciation. The reason is that the glaciers erode the bedrock and can remove the traces left by the earlier glaciations (Benn and Evans, 2014). Terrestrial cosmogenic nuclide (TCN) dating can be a key to find out more about the past glacial history. The conditions of the past can be used to predict events in the future, and that can be beneficial for example in storage of nuclear waste. Therefore, we need to know what has happened before.

2. Background

TCN dating is based on the number of reaction products in minerals caused by the bombardment of cosmic rays. Thus, the number of formed isotopes is proportional to the duration of the exposure (Dunai, 2010). The most important nuclides in terrestrial applications are ^{3}He, ^{21}Ne, ^{22}Ne, ^{10}Be, ^{26}Al and ^{36}Cl because of their low occurrence in geological materials and their abundance in accessible minerals and rocks (Dunai, 2010). The number of atoms produced also depends on other things than the production path such as altitude, magnetic field, vegetation and snow coverage (Gosse and Phillips, 2001). The production rate also decreases with depth because the cosmic rays are attenuated by the bedrock. The attenuation is caused when the rays interact with atoms in rocks and lose their energy (Dunai, 2010). The flux of cosmic rays is not constant; it varies both spatially and temporally (Beer et al., 2002). The age determination with cosmogenic nuclides usually refers to the dating of either exposure or burial age. To find both the exact exposure age and the erosion rate, the measurements must be done at least with two nuclides (Dunai, 2010).

During the Pleistocene, Finland experienced many glaciation cycles. Johansson et al. (2011) presents the most important ones. During the Saalian stage glaciation in the Middle Pleistocene (ca. 130 ka) whole Finland had was covered with ice. Later, during the several Weichselian glaciations in the Late Pleistocene, the glacial coverage was not as extensive, and

as a result Lapland has experienced more glaciations than southern Finland. The most important ones in southern Finland are First Mid-Weichselian (ca. 75-60 ka), Second Mid-Weichselian (ca. 50-35 ka) and Late Weichselian (ca. 25-10 ka). Southernmost Finland did not experience the Second Mid-Weichselian. Although Finland has experienced several glaciations, the landscape was shaped particularly by the Late Weichselian glaciation (Ehlers and Gibbard, 1996).

3. Modelling

A forward model is used to predict the nuclide concentrations of a depth profile after certain exposure history (Figure 1). During an exposure period, the concentration is increasing, but production rate attenuates with depth. During the glaciation the glacier prevents the reaction between rays and bedrock, so new nuclides are not produced, but there is decay of existing nuclides. The forward model is designed to be used with exposure histories that can contain several glaciation periods.

The inverse model predicts an exposure history based on the nuclide concentrations of a sample. It tests which the range of exposure histories that could produce similar concentrations within certain limits. If the concentrations are similar to the sample concentrations, the tested glaciation history is accepted as one of the possible solutions.

A simplified glaciation history (inset in Figure 1) used as a reference has one glaciation 25 to 10 ka ago and two exposure periods from 35 to 25 ka ago and 10 to 0 ka ago. If the reference scenario includes erosion, it is implemented as a removal of surface concentrations at the end of the glaciation. We consider several possible glaciation histories, which were selected randomly. Each had to contain at least one glaciation and one exposure period, and the maximum of exposure periods was set to four. It was also required that the minimum duration of a glaciation-exposure period is at least 500 years.

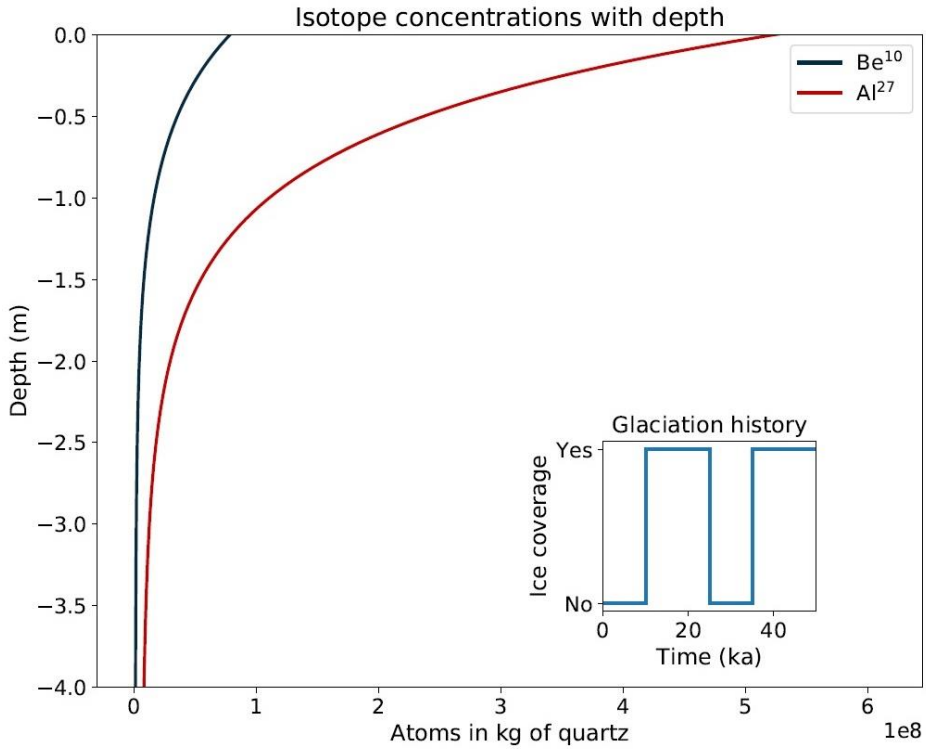

Figure 1. ^{10}Be and ^{26}Al concentrations as a function of depth with the glaciation history of two exposure periods (inset figure). Total exposure time is 20 ka. The concentration of ^{26}Al is

higher than ^{10}Be concentrations, and they both decrease rapidly with depth.

4. Results

The simplest tested case was one infinite glaciation. The reference model had the deglaciation at 10 ka. The inverse model found the best fit at 10.0 ka. The sampling depth did not affect to the best fit.

With more complicated cases there does not appear to be a clear pattern. When erosion is included, the total exposure time was recovered by the inversion, but the deglaciation could not be dated. This applies for samples from the surface as well as below surface. Overall, better solutions were found when there were more constraints for the inverse model.

The model results show more promise if there were more samples from multiple depths (Figure 2). Depth profiling improved the estimation of the amount of erosion and the total exposure duration compared a case with only one surface sample. However, the number of accepted solutions was low, so the result is a bit uncertain.

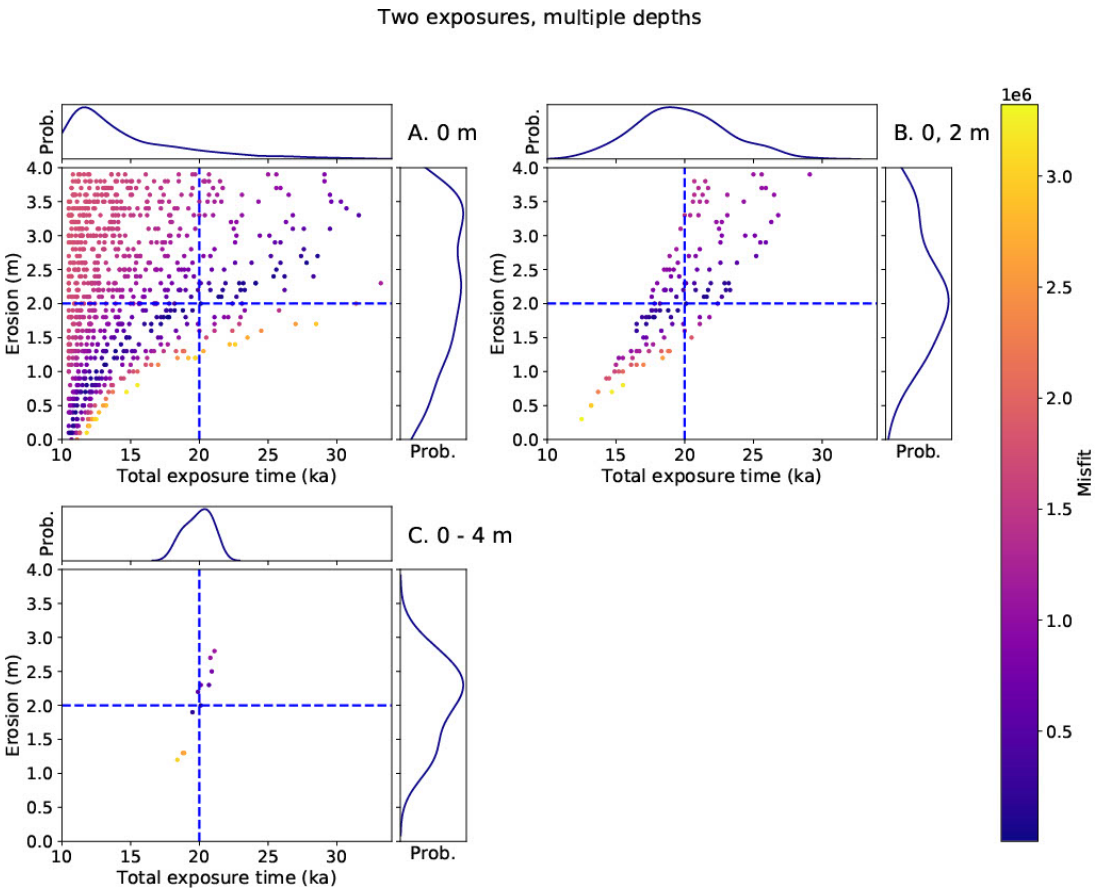

Figure 2. Erosion and total exposure time when there is A. one sample from the surface, B. two samples from surface and 2.0 m depth and C. five samples from surface to 4.0 m depth. Blue dashed lines are expected values of the parameter. Fewer models are accepted when sampling depth is increased.

5. Conclusions

This study aimed to determine whether if terrestrial cosmogenic nuclides could be used to study past glacial histories based on the nuclide concentrations. The concentrations were modelled with a forward model that took into account the exposure history of the rock and the erosion

during the glaciation. Then an inverse model was used to find out possible glaciation histories that fit in the artificial samples, which were based on the forward model. The past histories were detected if the constraints for the inverse model were strict enough, for example if the ending time of the last glaciation was tied. If there were no constraints, the past glaciations could not be detected. However, we found that when a depth profile was used in sampling, we were able to limit the possible range of accepted models and provide more accurate results than using just one sample. In the future the models should be tested together with real samples.

References:

Beer, J., Muscheler, R., Wagner, G., Laj, C., Kissel, C., Kubik, P. W., Synal, H.-A., 2002. Cosmogenic nuclides during Isotope Stages 2 and 3. Quaternary Science Reviews, 21(10):1129–1139.

Begg, G.C., Griffin, W.L., Natapov, L.M., O'Reilly, S.Y., Grand, S.P., O'Neill, C.J., Hronsky, Benn, D. I., Evans, D. J. A., 2014. Glaciers & Glaciation. Routledge.

Dunai, T. J., 2010. Cosmogenic Nuclides: Principles, Concepts and Applications in the Earth Surface Sciences. Cambridge University Press.

Ehlers, J., Gibbard, P. L., 1996. Quaternary and Glacial Geology. J. Wiley & Sons, Chichester; New York.

Gosse, J. C. and Phillips, F. M. (2001). Terrestrial in situ cosmogenic nuclides: Theory and application. Quaternary Science Reviews, 20(14):1475–1560.

Johansson, P., Lunkka, J. P., Sarala, P. (2011). The Glaciation of Finland. In Developments in Quaternary Sciences, volume 15, pages 105–116. Elsevier